

Geodätisch-geophysikalische Arbeiten in der Schweiz

(Fortsetzung der Publikationsreihe
«Astronomisch-geodätische Arbeiten in der Schweiz»)

herausgegeben von der

Schweizerischen Geodätischen Kommission
(Organ der Akademie der Naturwissenschaften Schweiz)

Achtundsiebzigster Band
Volume 78

**GPS Based Dynamic Monitoring of Air
Pollutants in the City of Zurich**

Philippe Kehl

2009

Adresse der Schweizerischen Geodätischen Kommission:

Institut für Geodäsie und Photogrammetrie
Eidg. Technische Hochschule Zürich
ETH Hönggerberg
CH-8093 Zürich, Switzerland

Internet: <http://www.sgc.ethz.ch>

ISBN 978-3-908440-22-2

Redaktion des 78. Bandes:
Dr. Ph. Kehl, J. Müller-Gantenbein, Prof. Dr. A. Geiger
Druck: Print-Atelier ADAG, Zürich

VORWORT

Die Thematik der zunehmenden Umweltbelastung durch Schadstoffe in der Atmosphäre gewinnt zunehmend an Aktualität. Der vorliegende Bericht zeigt auf, wie geodätisches Fachwissen und geodätische Methodologien im Bereich des Umweltmonitoring mit Blick auf den Klimaschutz eingesetzt werden können.

Im Rahmen eines Projektes am Departement Bau, Umwelt und Geomatik der ETHZ hat Herr Kehl in Zusammenarbeit mit dem IAC (Institute of Atmospheric and Climate Sciences, ETHZ) eine Machbarkeitsstudie zur dynamischen, lokalen Umweltdatenerfassung durchgeführt. Das zu Grunde gelegte Konzept und dessen Realisierung ermöglichten eine Beurteilung der Luftqualität in Echtzeit. Die Datenanalyse trägt zur Vertiefung des Verständnisses für die Zusammenhänge zwischen Verkehrsemissionen und städtischer Luftqualität bei.

Herr Kehl hat sich den folgenden drei Forschungsthemen gewidmet:

Dem dynamischen Echtzeit-Monitoring der Luftqualität,
der satellitengestützten Positionierung (GPS) des Messsystems in urbaner Umgebung und
dem Einfluss der Emissionen des Strassenverkehrs auf die Luftqualität in der Stadt Zürich.

Zur Beurteilung der Luftqualität dienten die Messungen der Konzentrationen der Luftschadstoffe Stickoxide (NO und NO₂), Feinstaub und Ozon (O₃). Zur quantitativen Erfassung der Konzentrationen musste ein mobiles, autonomes Messsystem entwickelt und konstruiert werden. Der Einsatz auf dem Dach eines Trams der VBZ im operationellen Betrieb, die Temperatur- und Feuchtebedingungen sowie die mechanischen Beanspruchungen stellten besondere Ansprüche an die Konstruktion und bauliche Ausführung der Messplattform. Zusätzlich waren gewisse Randbedingungen in Bezug auf Stromverbrauch und Betriebslogistik zu beachten.

Die Messkampagnen erfolgten auf drei die Stadt durchquerenden Tramstrecken. In den Kampagnen erwiesen sich das Mess- und Positionierungssystem, das Übertragungssystem und die online Computerverarbeitung als funktionstüchtig. Die Messungen wurden in Echtzeit über das Mobilfunknetz (GPRS/GSM) übertragen.

Die auf geodätischen Methoden basierende Raum/Zeit-Kollokation erlaubte es, aus den sowohl in der Zeitachse als auch in der Ortsachse dispers vorliegenden Daten ein kohärentes Raum/Zeit Bild der Schadstoffkonzentrationen zu berechnen. Damit hat Herr Kehl gezeigt, dass an Hand repetitiver, mobiler Messungen eines einzelnen Gerätes der Zustand der Luft mit hoher zeitlicher und örtlicher Auflösung beurteilt werden kann.

Mit dieser Arbeit hat Herr Kehl ein weites Feld für die Anwendung geodätischer Methodologien erschlossen. Die systematische Aufarbeitung der Problemstellungen und ihrer Lösungswege, sowie das entwickelte generische, autonome Umweltmonitoring System bilden eine solide Basis für zukünftige Weiterentwicklungen.

Der Schweizerischen Akademie für Naturwissenschaften danken wir für die Übernahme der Druckkosten.

Prof. Dr. Hans-Gert Kahle
Institut für Geodäsie und Photogrammetrie
ETH Zürich

Prof. Dr. Alain Geiger
ETH Zürich
Präsident der SGK

PREFACE

La thématique de la pollution de l'atmosphère par des substances nocives est brûlante d'actualité. Le travail présenté montre comment les connaissances et les méthodes de la géodésie peuvent contribuer au domaine du monitoring de l'environnement et plus précisément à la protection du climat.

Dans le cadre d'un projet au Département de la construction, de l'environnement et de la géomatique de l'EPFZ, en partenariat avec l'IAC (Institute of Atmospheric and Climate Sciences, ETHZ), Monsieur Kehl a réalisé une étude de faisabilité sur l'acquisition de données environnementales dynamiques à petite échelle.

Le concept sous-jacent ainsi que sa réalisation ont permis une évaluation de la qualité de l'air en temps réel. L'analyse des données contribue à l'approfondissement de la compréhension des processus entre les émissions dues au trafic et de la qualité de l'air en ville.

Monsieur Kehl s'est consacré aux trois thèmes suivants:

Le monitoring dynamique en temps réel de la qualité de l'air, le positionnement satellitaire d'un système de mesure dans un environnement urbain ainsi que sur l'influence des émissions du trafic routier sur la qualité de l'air en ville de Zürich.

Cette évaluation de la qualité de l'air s'est basée sur des mesures de la concentration de polluants comme l'oxyde d'Azote (NO et NO₂), la poussière fine et l'ozone (O₃). Afin de permettre l'acquisition quantitative des différentes concentrations, un système de mesure spécial, mobile et autonome a dû être développé et construit.

Le système a été déployé sur le toit d'un tramway de la VBZ. La mise en service pour une exploitation opérationnelle, en tenant compte des contraintes météorologiques et mécaniques, engendrait des exigences particulières au niveau de la conception de la plateforme de mesure. De plus, certaines conditions comme la consommation d'énergie ainsi que de logistique étaient à considérer avec une attention particulière.

Les campagnes de mesures ont été réalisées sur trois voies de tramway qui traversent la ville. Lors de ces campagnes, les systèmes de mesure, de positionnement, de communication et de traitement informatique en ligne ont été fonctionnels. Les mesures étaient transmises en temps réel via le réseau de téléphonie mobile (GPRS/GSM).

La mise en oeuvre de méthodes géodésiques basées sur la collocation spatio-temporelle a permis le calcul d'une image dans le temps et l'espace de la concentration de polluants cohérente à partir de données dispersées dans le temps et dans l'espace. A partir de cela, Monsieur Kehl a démontré qu'à partir de mesures récoltées par un système unique de mesure mobile, il est possible de monitorer et d'évaluer l'état de l'air avec une haute résolution en temps et en position.

Avec ce travail, Monsieur Kehl a ouvert un vaste champ d'application des méthodes géodésiques. L'étude systématique de la problématique, les voies de recherches des solutions ainsi que le développement générique du système autonome de monitoring de l'environnement forment une base solide pour des développements futurs.

Nous remercions l'académie des sciences naturelles pour la prise en charge des frais d'impression.

Prof. Dr. Hans-Gert Kahle
Institut de Géodésie et Photogrammétrie
ETH Zürich

Prof. Dr. Alain Geiger
ETH Zürich
Président de la CGS

FOREWORD

Increasing interest is put onto the topic of pollution of the atmosphere by noxious substances. This study shows how the geodetic know-how and the geodetic methodologies can contribute to the environmental monitoring in view of the protection of the climate. In the frame of a project of the department of civil and environmental engineering and geomatics, ETHZ, and with the partnership of the IAC (Institute of Atmospheric and Climate Sciences, ETHZ) mister Kehl has realized a feasibility study on the dynamic acquisition of environmental data at small scales.

His concept and realisation enables the evaluation of the air quality in real-time. The developed methods for the analysis of data contribute to the comprehension of the processes and will elucidate the relation between traffic emission and air pollution in a city.

Mister Kehl has focussed on the following three research topics:

The dynamic monitoring in real time of the air quality,
the positioning by satellites in urban environment, and
the impact of traffic emissions onto air quality in Zurich.

To evaluate the air quality the concentrations of pollutants such as nitrogen oxides, particulates, and ozone have been measured. To this end a mobile and autonomous measurement system had to be developed and constructed. After first tests the system was installed on the rooftop of a tram in the city of Zurich. The power consumption, temperature, humidity, and the mechanical and operational constraints made high demands on the design of the system

The measurement campaigns were carried out on three tram lines crossing the city. The measuring and positioning systems as well as the communication and the data treatment proved to perform very well. Measurements were transmitted online by mobile communications.

Space-time collocation based on geodetic methodologies allowed retrieving a coherent space-time picture of the pollutant's concentration from dispersed data in space and in time. With this Mr. Kehl has shown that it is possible to determine the state of the atmosphere with high temporal and spatial resolution by only one mobile measurement system.

With his work, Mr. Kehl has opened a wide field of applications of geodetic methods. The systematic study and the description of solutions, as well as the development of a generic autonomous monitoring system form a solid basis for future developments.

We are grateful to the Swiss Academy of Sciences for financing the printing costs.

Prof. Dr. Hans-Gert Kahle
Institute of Geodesy and Photogrammetry
ETH Zurich

Prof. Dr. A. Geiger
ETH Zurich
President of SGC

Abstract

Despite the decrease in road traffic emissions air pollutant concentrations of nitrogen dioxide, particulates and ozone often exceed the limit values at urban sites in Switzerland.

This project aimed at providing a dynamic and real-time assessment of ambient air quality and at improving the understanding of the interaction between road traffic emissions and urban air quality. It is designed as a feasibility study for dynamic air-pollution measurements in the local scale.

Three research topics were being pursued in this thesis: air quality monitoring, satellite based positioning (GPS) of a measurement system in an urban environment and the influence of road traffic emissions on the air quality in the city of Zürich.

The data analysed are based on the autonomous operation of a measuring system on a tram in regular service. A dedicated measurement system was built to measure the concentrations of the three most relevant air pollutants in Zürich. These are nitrogen oxides (NO and NO₂), aerosol particles (particulate matter) and ozone (O₃). Nitrogen oxides and ozone are measured using the standard techniques involving chemiluminescence of NO and UV absorption of O₃, respectively. Particulates are measured using a diffusion charging particle sensor which suits the requirements for space, a short measurement period and resistance against vibrations. Furthermore meteorological parameters (temperature, humidity and pressure) were measured.

The tram was equipped with the measurement system. During two measurement campaigns in spring/summer 2005 and winter/spring 2005/06 the tram travelled on three different tram tracks, which cross the city in north-south or east-west direction. They represent the various characteristics of an urban environment, such as busy places and parts of the city without private road traffic. The measurements were being transferred in real-time using mobile communication technologies (GSM, GPRS). A web site was being updated in real-time with the position of the tram on a map, the measurements and the operating state of the measurement system and its sensors.

GPS was used for precise positioning and timing. Urban sites often degrade navigation accuracy and availability. Therefore, a suitable receiver was evaluated and techniques to provide precise and reliable positioning data were developed. The latter involves filtering and projective map-matching to exclude faulty positions and determine precise positions. Furthermore, standard position-time relations for the tram were determined to interpolate GPS outages, which last a few seconds up to a few dozens of seconds.

A dispersion modelling study was carried out for a 3.3 km² area in the inner city of Zürich using a state-of-the art numerical dispersion model. This involved the models NEMO (emissions from traffic), GRAMM (meteorology) and GRAL (dispersion) from the

Institute of Internal Combustion Engines and Thermodynamics of the Graz University of Technology.

The feasibility of dynamic and real-time measurements and its limitations were shown by carrying out two measurement campaigns lasting 18 and 20 weeks in spring/summer 2005 and winter/spring 2005/06.

The analysis of the measurements clearly show varying concentrations of air pollutants along the tram track as well as characteristic hot-spots at busy places.

* * *

Zusammenfassung

Trotz der Abnahme der Emissionen des Strassenverkehrs werden die Grenzwerte der Luftschadstoffe Stickoxide, Partikel (Feinstaub) und Ozon in städtischen Gebieten in der Schweiz oft überschritten.

In diesem Projekt soll eine dynamische Beurteilung der Luftqualität in Echtzeit ermöglichen. Zudem soll das Verständnis für die Zusammenhänge zwischen Verkehrsemissionen und städtischer Luftqualität erweitert werden. Das Projekt ist als Machbarkeitsstudie für eine dynamische und kleinräumige Umweltdatenerfassung konzipiert.

Drei Forschungsrichtungen werden in dieser Arbeit verfolgt: Monitoring der Luftqualität, die satellitengestützte Positionierung (GPS) eines Messsystems in urbaner Umgebung sowie der Einfluss der Emissionen des Strassenverkehrs auf die Luftqualität in der Stadt Zürich.

Die analysierten Daten stammen von einem autonomen Messsystem. Es wurde auf einem Tram betrieben welches im normalen Betrieb gefahren wurde. Das Messsystem wurde speziell für diese Aufgabe gebaut und misst die drei Luftschadstoffe welche für Zürich bedeutsam sind. Es sind dies Stickoxide (NO und NO_2), Feinstaub und Ozon (O_3). Standardtechnologien wurden zur Messung der Stickoxide und des Ozons gewählt. Die Messprinzipien basieren auf der Chemilumineszenz von NO beziehungsweise der UV-Absorption von O_3 . Feinstaub wird mittels eines sogenannten *diffusion charging particle sensors* gemessen. Dieser entspricht den Anforderungen an Platz, Reaktionszeit und Unempfindlichkeit gegenüber Vibrationen. Zudem wurden meteorologische Parameter erfasst (Temperatur, Feuchte und Luftdruck).

Ein speziell angepasstes Tram wurde mit dem Messsystem ausgerüstet und fuhr dann während zwei Messkampagnen im Frühling/Sommer 2005 und im Winter/Frühling 2005/06 auf drei Tramstrecken. Die Tramstrecken durchkreuzen die Stadt in Nord-Süd beziehungsweise Ost-West-Richtung. Die Linie führt entlang verschiedenartiger Orte welche die Stadt gut repräsentieren. Dazu zählen verkehrsstarke Plätze und Strassen aber auch Fussgängerzonen.

Die Messungen wurden in Echtzeit über das Mobilfunknetz (GPRS/GSM) übertragen. In einer Internetapplikation (auf einer Webseite) konnten die Messungen in Echtzeit mitverfolgt werden. Eine Karte zeigte die aktuelle Position des Trams und daneben die aktuellen Messwerte sowie diverse Zustandsanzeigen der Messgeräte und des Messsystems.

Zur präzisen Positionierung und als Zeitreferenz wurde GPS gewählt. In städtischen Gebieten ist die satellitengestützte Navigation oft eingeschränkt. Ein geeigneter GPS-Empfänger wurde bestimmt und Techniken zur weiteren Verbesserung der Genauigkeit

und Zuverlässigkeit wurden entwickelt. Mittels Filteralgorithmen und einem projektiven Mapmatching-Verfahren konnten fehlerhafte Positionen erkannt beziehungsweise korrigiert werden. Um GPS-Ausfälle zu überbrücken wurde eine Methode entwickelt, die fehlenden Positionen zu interpolieren. Dazu wurden die Geometrie der Tramlinie und der bekannte (gemessene) Relation zwischen Position des Trams und der Zeit verwendet.

Eine Ausbreitungssimulation für Stickoxide wurde in einem 3·3 km²-Gebiet ausgeführt. Ein modernes, numerisches Ausbreitungsmodell wurde verwendet. Dazu gehörten die Modelle *NEMO* (Verkehr und Emissionen), *GRAMM* (Meteorologie) und *GRAL* (Ausbreitung) des *Institutes für Verbrennungsmotoren und Thermodynamik* der *Technischen Universität Graz*.

Die Machbarkeit von dynamischen Luftschadstoffmessungen wurde durch zwei Messkampagnen gezeigt. Sie dauerten 18 Wochen im Frühling/Sommer 2005 und 20 Wochen im Winter/Frühling 2005/06.

Die Analyse der Messungen zeigt deutlich variierende Schadstoffkonzentration entlang der Tramlinie. Die höchsten Konzentrationen korrelieren deutlich mit verkehrsreichen Strassen und Plätzen.

* * *

Acknowledgements

I would like to express my gratefulness to the many people and organisations who rendered this research project possible. Their support and contributions during the research and during writing up the dissertation are greatly appreciated.

The project was conducted under grants from the *Department of Civil, Environmental and Geomatic Engineering (D-BAUG)* of the ETH Zürich.

- * I am appreciative and thankful to my doctoral advisor Prof. Dr. Hans-Gert Kahle and my co-examiners Prof. Dr. Alain Geiger and Prof. Dr. Johannes Stähelin who came up with the original project idea. I thank them for their continual support, their contributions and their encouragement.
- * The collaboration with the public transport of Zürich (*Verkehrsbetriebe Zürich, VBZ*) was extraordinarily fruitful and valuable for this project. I am especially thankful to the support of many persons at the VBZ offices and at the *Depot 8* workshop/depot without whom the measurement campaigns would not have been possible. In particular I like to thank Ueli Frick, Harry Bruggmann, Walter Spörri, Marco Piller, Christoph Dubler, Urs Leemann, Hansjörg Fink, Hans Rindlisbacher and Christian Fischer.
- * I am thankful to several people for their valuable support and contribution at various stages of the project: Prof. Dr. Kay W. Axhausen, Prof. em. Dr. Heinrich Brändli, Dr. Bruno Neininger and Silvia Rossinelli.
- * I am very grateful to Dr. Dietmar Oetzl and Prof. Dr. Peter Sturm, TU Graz, who kindly provided the programmes (models) and the support to carry out the dispersion modelling study. Mr. Oetzl's patience and expertise are greatly appreciated.
- * I thank several organisations who provided data, pictures and information which were valuable for this project: BAFU/EMPA, VBZ, Tagesanzeiger, UGZ, J.-M. Zogg/uBlox AG, Cabtronix AG and Sunrise AG.
- * I thank my colleagues at the Geodesy and Geodynamics Lab at the ETH Zürich for their amity and support: Anna Somieski, Dr. Beat Bürki, Jrene Müller-Gantenbein, Dr. Marc Troller, Michael Müller and Oliver Heller.
- * And last but not least I thank Aretha, B. B., Beth, Bob (2x), the Duke, Endo, Ernest, Frank, Heidi, the huskies, James, Janis, John, Kari, Kutti, Mani, Mary, Melanie, Nick, Norah, Otis, Paul, Peter, Regina, Serge, Sophie and many others. Thank you for the music (especially when I had the blues).

Philippe Kehl, Zürich, July 2007

Contents

1	Introduction	1
2	Scientific Theory	3
2.1	Air pollution & emission sources	3
2.1.1	Nitrogen oxides	4
2.1.2	Ozone	5
2.1.3	Conversion between ppb and mass per volume units	6
2.1.4	Particulate matter	8
2.1.5	Smog	9
2.1.6	Ambient air quality standards and legislation	12
2.1.7	Air quality trends for Zürich	13
2.2	Global positioning system (GPS)	19
2.2.1	GPS constellation	19
2.2.2	Measurement principle	21
2.2.3	Sources of errors and accuracy	22
2.2.4	GPS in urban areas	23
2.2.5	Co-ordinate transformation	26
3	Measurement System	27
3.1	The measurement platform	27
3.2	The measurement system	29
3.3	Environmental sensors & measurement principles	31
3.3.1	Nitrogen oxides sensor	31
3.3.2	Ozone sensor	31
3.3.3	Particle sensor	33
3.3.4	Meteorological sensors	33
3.4	Positioning sensor & time reference	34
3.5	Power supply & control	35
3.6	Computer & data logger	37
3.7	Telemetry	38
4	Measurement Campaigns & Data Processing	41
4.1	Tram operation and tram lines	41
4.2	Measurement campaigns	44
4.2.1	Campaign #1	44
4.2.2	Campaign #2	45
4.2.3	Real-time visualisation of the measurements	47
4.3	Data post-processing	49
4.3.1	Database	50
4.3.2	Environmental measurements	50

4.3.3	GPS measurements	50
4.3.4	Map-matching and interpolation	52
4.3.5	Georeferencing	55
4.4	Permanent stations data	60
5	Data Analysis & Results	63
5.1	Overview over the available data	63
5.1.1	Raw time series	63
5.1.2	Daily mean values	65
5.2	Data quality assessment	67
5.3	Data analysis & discussion	69
5.3.1	Comparison of daily mean values	69
5.3.2	Comparison of monthly mean values	72
5.3.3	Limit value exceedances	76
5.3.4	Comparison of tram measurements at the UGZ permanent station	77
5.3.5	Summer 2005	81
5.3.6	Winter 2006	98
5.4	GPS performance analysis	106
6	Emission & Dispersion Modelling	111
6.1	Introduction	111
6.2	Modelling approach	112
6.3	Geometrical data	114
6.3.1	Topography (elevation model)	114
6.3.2	Buildings	114
6.4	Emission modelling	115
6.4.1	Overview	115
6.4.2	Input data	115
6.4.3	Results	118
6.5	Meteorological modelling (wind field simulations)	120
6.5.1	Overview	120
6.5.2	Classification of weather situations	120
6.5.3	Calculation	124
6.5.4	Analysis	126
6.6	Dispersion modelling	131
6.6.1	Calculation	131
6.6.2	Results analysis	133
6.7	Comparison with measurements	141
6.7.1	Summer 2005	142
6.7.2	Comparison with the NABEL permanent station	144
6.7.3	Winter 2006	145
7	Conclusions	147
	Bibliography	151

Abbreviations & Names

A	ampères
AC	see VAC
ADT	average daily traffic [vehicles/day], see JDTV
AGL	above ground level
ASL	above (mean) sea level
BAFU	Bundesamt für Umwelt, federal agency for the environment
BUWAL	Bundesamt für Umwelt, Wald und Landschaft, see SAEFL
CET	central European time
CI	confidence interval
CPU	central processing unit, also a computer
DC	see VDC
DEM	digital elevation model
DHM25	Digitales Höhenmodell 25m, Swiss 25 m grid DEM
DOP	dilution of precision
DST	daylight saving time
ECEF	earth-centred earth-fixed
EMPA	Eidgenössische Materialprüfungs- und Forschungsanstalt (federal institute for materials sciences & technology)
FSB	front side bus
FSF	Free Software Foundation
GCC	GNU compiler collection
GIS	geographic information system
GGL	Geodesy and Geodynamics Lab, ETH Zürich
GNU	GNU is not Unix, see FSF
GPRS	general packet radio service
GPS	global positioning system (see also NAVSTAR-GPS)
GRAMM	Graz mesoscale model (to simulate 3d wind fields)
GRAL	Gral lagrangian model, a pollutant dispersion model
GSM	global system for mobile communication
IP	Internet protocol
JDTV	jahresdurchschnittlicher (JD) täglicher Verkehr (TV), see ADT.
NABEL	Nationales Beobachtungsnetz für Luftfremdstoffe (national air pollution monitoring network)
NaN	not a number
NAVSTAR-GPS	Navigation system with timing and ranging GPS
NEMO	network emission model
MOSFET	metal-oxide-semiconductor field-effect transistor
OS	operating system
ppb(v)	parts per billion by volume
PBL	planetary boundary layer

PCB	printed circuit board
PDOP	position DOP
PM	particulate matter
POSIX	portable operating system interface
PTFE	polytetrafluoroethylene (also known as Teflon™)
RAIM	receiver-autonomous integrity monitoring
RDBMS	relational database management system
RF	radio frequency
RH	relative humidity
SAEFL	Swiss agency for the environment, forests and landscape, see BUWAL
SQL	structured query language
Swisstopo	Bundesamt für Landestopographie (federal office of topography)
SV	satellite vehicle
TCP	transport control protocol
TSP	total suspended particles
UGZ	Umwelt und Gesundheitsschutz Zürich (office for environment and health protection)
UTC	universal time coordinated
UV	ultraviolet radiation (400–1 nm wavelength)
V	volts
VAC	volts alternate current
VBZ	Verkehrsbetriebe Zürich (the public transport operator in Zürich)
VDC	volts direct current
VOC	volatile organic compounds
WGS84	world geodetic system 1984

* * *

1

Introduction

Anthropogenic air pollution became a problem for our society as a consequence of the industrialisation in the 19th century. During that time coal was increasingly used to fulfill the energy demand of the society. This led to increased concentrations of anthropogenic pollutants in the atmosphere (in particular sulphur dioxide and particles). At the beginning of the 20th century air pollution disasters happened where the air pollution caused a dramatic increase in mortality during winter smog periods. Nowadays the demand in fossil fuel is unbroken and air pollution has remained a serious problem. Today air quality problems in urban areas are connected with road traffic emissions. Traffic and road transport belong to the main emission sources of nitrogen oxides (NO_x) and particulate matter (such as PM_{10}) in cities, and it is likely to remain an important source of air pollutants in the future [Krzyzanowski et al., 2005].

Despite the decrease in road traffic emissions in the last decades (see section 2.1.7) air pollutant concentrations of nitrogen dioxide, particulates and ozone still often exceed the limiting values at urban sites in Switzerland.

This project aimed at providing a dynamic and real-time assessment of ambient air quality. For this purpose, the following problems needed to be solved.

I. A mobile measurement system was constructed. A tram (or streetcar, see below) was chosen as a platform circulating on roads in Zürich. The exact position of the instruments (environmental sensors) was determined by means of satellite navigation (GPS, the global positioning system). The measurement system has been proven capable of real-time air pollutant monitoring.

II. In order to study the relations *between air pollutant concentrations and ambient air pollution*, the line of the tram was selected to cover streets of different vehicle densities. The measurement system allowed to monitor air pollutant concentrations on streets in Zürich in a quasi two-dimensional way (i.e. position of the measurement along the tram track and time of the measurement). The data set was also used to assess the strength and weakness of mobile monitoring system compared to a fixed monitoring system.

III. The measurements of nitrogen oxides (NO_x) were compared to a state-of-the-art numerical urban dispersion model. This involved the models *NEMO*, *GRAMM* and *GRAL* from the *Institute of Internal Combustion Engines and Thermodynamics* of the *Graz University of Technology*.

Remarks on the nomenclature of the measurement platform: Previous articles published on this project call the measurement platform a *streetcar* [Kehl et al., 2005, 2006b, 2007]. This refers to the American word for *a commuter vehicle that operates on rails in city streets* [Oxford University Press, 1999]. The British word for *a passenger vehicle powered by electricity conveyed by overhead cables, and running on rails laid in a public road* is *tram* [Oxford University Press, 2006a]. Both words mean the same vehicle. It turned out, however, that *tram* is more widely understood than *streetcar* among English speaking colleagues [a poll among a handful of colleagues at a social evening at a conference]. The author's preference for *tram* comes from the Swiss German expression (*das Tram*). These are the reasons why the word tram is used in this text rather than the word streetcar, which was used in earlier publications.

The thesis contains the following chapters:

Chapter 2: Scientific Theory summarises the basics of air pollution and satellite navigation required to understand this research project.

Chapter 3: Measurement System contains the description of the measurement system.

Chapter 4: Measurement Campaigns & Data Processing summarises the approach to carry out the measurements and the postprocessing of the raw measurement data.

Chapter 5: Data Analysis & Results deals with the data analysis and validation and discusses the results.

Chapter 6: Emission & Dispersion Modelling contains the study of modelled air pollutant concentrations and compares these with the measurements.

* * *

2

Scientific Theory

2.1 Air pollution & emission sources

Atmospheric air pollution originates from anthropogenic emission of chemicals into the atmosphere. The following factors can cause anthropogenic air pollution.

Release of primary air pollutants from the source. Many of these emissions are produced from the use of fossil energy sources (petroleum, coal, natural gas). The anthropogenic emission sources connected to energy consumption include motorised road traffic (or combustion engines in general), domestic heating, industrial processes and construction industry.

Transport and conversion in the ambient air depend on the kind of compound and the weather.

The ambient air concentration of air pollutants at a certain site and its effect on human beings and the environment depend on the emission source strengths, transport and dilution.

Problems of different scopes are distinguished in atmospheric chemistry. *Local-scale* problems are the pollution in a city. An example of a *regional-scale* problem is summer smog which is observed over a wide area. *Global-scale* problems have universal impacts independent from the location of the emissions.

Local-scale air pollution takes place in the planetary boundary layer (PBL). The PBL is the lowest part of the atmosphere. The depth and the structure is mainly influenced by the buoyancy induced by the surface heat balance and the winds in the free troposphere lying above. The turbulence in the PBL influences the transport, mixing and dispersion of pollutants. These processes are described in more detail in section 2.1.5 and in chapter 6.

In this work the air pollution at a local scale (i.e. the city of Zürich) is the subject of interest. In Zürich, the emissions from road traffic and domestic heating are the dominant sources of air pollutants. The degree of pollution (i.e. the ambient air concentration of pollutants), however, is influenced by regional and to a lesser extent global anthropogenic activities.

The primary anthropogenic pollutants include nitric oxide (NO), carbon monoxide (CO), sulphur dioxide (SO₂) and volatile organic compounds (VOC). High concentrations of these substances can be found at the origin, i.e. near to the emission sources.

Secondary air pollutants, such as nitrogen dioxide (NO₂) and ozone (O₃), are formed through chemical reactions in the ambient air. Photochemical smog is an example of the result of these processes in conjunction with certain weather (see section 2.1.5).

Besides of these gaseous substances emissions of suspended particulate matter contribute to air pollution as well.

The three major air pollutants measured in this thesis and monitored in the city of Zürich are nitrogen oxides (see section 2.1.1), ozone (see section 2.1.2) and particulate matter (see section 2.1.4).

The following sections describe emission sources, the chemical and meteorological mechanisms and the effects of the air pollution that are important in the scope of this project. Detailed information on the chemical properties of the compounds described in this chapter can be found in various textbooks on (inorganic) chemistry.

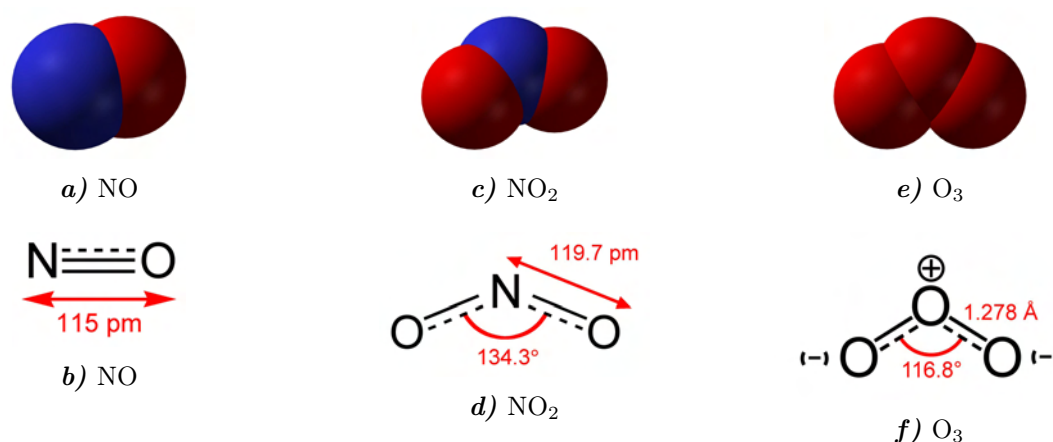


Figure 2.1: The chemical structure of the discussed gaseous pollutants: nitric oxide (**a**, **b**), nitrogen dioxide (**c**, **d**) and ozone (**e**, **f**). The upper row shows 3d visualisations of the molecules (blue balls are nitrogen atoms and red balls are oxygen atoms). The bottom row shows 2d diagrams of the molecules which indicate the size and geometry of the compounds, the connection of the atoms and, for the O₃ dipole (**e**, **f**) the polarity.

Figures source: public domain

2.1.1 Nitrogen oxides

In the scope of this work the focus lies on two compounds from the group of nitrogen oxides. These are nitric oxide (NO) and nitrogen dioxide (NO₂) (see figure 2.1a/b and 2.1c/d, respectively).

Combustion at high temperatures ($> 1000^\circ\text{C}$) forms NO from atmospheric oxygen (O_2) and atmospheric nitrogen (N_2) (reaction 2.1). Lightning is a natural source of NO. The use of internal combustion engines and the industrialisation has increased the emission of anthropogenic NO in the atmosphere. NO appears as a colourless gas.



In the atmosphere NO is oxidised in the air to NO_2 , mainly by oxidising with O_3 (see reaction 2.4).

NO_2 appears as a brown gas. The sum of NO and NO_2 is called NO_x .

According to EU classification¹, NO is *toxic* and *corrosive*. This classification described NO_2 as *highly toxic*.

NO_2 is transformed to nitric acid (HNO_3) in the troposphere by reaction with hydroxyl radicals (OH) during the day and by conversion to nitrate (NO_3) during night.

This leads to acid rain and because of the nitric part to an eutrophication of soils. This is the reason why inhalation of NO_2 affects the pulmonary functions, particularly in asthmatics and increases the allergic inflammatory reactions in airways [WHO, 2004]. The long-term effects are a reduction in lung function and an increased probability of respiratory symptoms.

2.1.2 Ozone

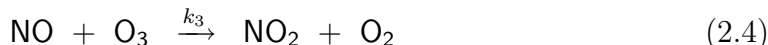
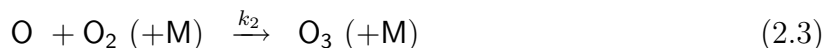
Ozone was discovered in 1839 in Basel, Switzerland, by C. F. Schönbein. He was able to show the existence of Ozone in the ambient air in 1885. Ozone obtained only little scientific attention until the first half of the 20th century. Then the spatial distribution and the temporal variation of ozone concentration were explored. It was not until the end of World War II when it was discovered that ozone is formed by (tropospheric) air pollution and elevated ozone concentrations have a significant negative impact on vegetation. At the beginning of the 1970s the complex mechanisms of ozone formation from the precursors nitrogen oxides and organic gases were understood [Staehelin, 2003].

Stratospheric ozone protects life on Earth's surface from harmful UV radiation. In the lower levels of the atmosphere, however, it is a harmful air pollutant that affects life and the environment. It is a strong oxidant that can have adverse effects on pulmonary functions, provoke lung inflammatory reactions and in general has adverse effects on respiratory symptoms. WHO [2004] furthermore states that long-term exposure can reduce the lung function development. The vulnerability of children is generally higher than the one of adults. Ozone also significantly reduces agricultural crop yields.

Ozone is a secondary air pollutant. It is formed in the atmosphere from precursors. The most important precursors are nitrogen oxides, volatile organic compounds (VOC) and carbon monoxide (CO).

¹Council Directive 67/548/EEC of 27 June 1967 on the approximation of laws, regulations and administrative provisions relating to the classification, packaging and labelling of dangerous substances.

The photolysis of nitrogen dioxide (NO_2) leads to the production of ozone (O_3) and in the reverse reaction to the reformation of NO_2 [Staehelin, 1999, chap. 3] (see figure 2.2).



NO_2 it is excited by light ($h\nu$) leading to photolysis (reaction 2.2). Nitric oxide (NO) and atomic oxygen (O) are produced. The rate of the reaction (k_1) is proportional to the concentration of NO_2 ($[\text{NO}_2]$) and depends on the intensity of radiation (sun light, altitude of the sun). Atomic oxygen reacts very quickly with molecular oxygen (O_2) to ozone (reaction 2.3). The rate of the reaction is k_2 . Finally ozone reacts very fast with NO to form NO_2 (reaction 2.4). The rate is k_3 .

Since the first reaction depends on radiation (sun light) the three reactions form an equilibrium (equation 2.5) during the day that depends on the intensity of sunlight. Since all three reactions are very fast equilibrium appears within minutes. This equilibrium is called photo-stationary state (see figure 2.3).

$$K = \frac{k_1}{k_3} = \frac{[\text{NO}][\text{O}_3]}{[\text{NO}_2]} \quad (2.5)$$

The photo-stationary state does not lead to a photochemical net production of O_3 . For net photochemical ozone production, the presence of VOCs or carbon monoxide (CO) is required (see figure 2.3). The mechanism proceeds via a radical chain (orange part in figure 2.3). The reactive OH radical is formed mainly by photolysis of ozone. OH radicals react very quickly with most gaseous trace gases, leading to peroxy radicals, which can react with NO , forming NO_2 . Ozone is subsequently formed by reactions (2.2) and (2.3). The most important termination of the radical chain reaction in polluted air is the reaction of OH with NO_2 . It limits the turnover rate of the chain reactions.

2.1.3 Conversion between ppb and mass per volume units

All gaseous pollutant sensors used in this project measure the volume per volume (ppbv) concentration of the pollutant in a gas (the air). The output is therefore the percentage of pollutant molecules of all molecules in the ambient air. The readings are in ppb(v) which is parts per billion by volume. One ppb(v) is one volume of gaseous pollutant per 10^9 volumes of ambient air.

The limit values, however, are given in units of mass per volume, e.g. $\mu\text{g}/\text{m}^3$, (see section 2.1.6) and the readings are converted into this unit. This is done according to the measurement recommendations issued by the Swiss government [BUWAL, 2004] which use the same approach as the respective EU legislation.

The conversion is done using the following formula based on the ideal gas law:

$$C_i = x_i \cdot \frac{p \cdot M_i}{T \cdot R} \quad (2.6)$$

Where:

- C_i : mass concentration of the gas i in $\mu\text{g} \cdot \text{m}^{-3}$
- x_i : molar concentration of the gas i in ppb
- p : atmospheric pressure in Pa ($= \text{kg} \cdot \text{m}^{-1} \cdot \text{s}^{-2}$)
- T : absolute ambient air temperature in K
 $T = \vartheta + 273.15$ where ϑ is the temperature in $^{\circ}\text{C}$
- R : the gas constant, $R = 8.314472 \text{ J} \cdot \text{mol}^{-1} \cdot \text{K}^{-1}$
- M_i : molar mass of the gas in $\text{kg} \cdot \text{mol}^{-1}$

The molar masses of the compounds NO, NO₂ and O₃ are:

$$M_{NO} = 30.006 \text{ g/mol} \quad M_{NO_2} = 46.005 \text{ g/mol} \quad M_{O_3} = 47.997 \text{ g/mol}$$

For locations below 1500 m ASL the legislation [BUWAL, 2004, p. 22] specifies to use $p = 1013.25 \text{ hPa}$ and $T = 293.15 \text{ K}$ ($\vartheta = 20^{\circ}\text{C}$). This leads to the conversion factors described in table 2.1. There is no conversion factor for NO_x. The sum of either c_{NO} and c_{NO_2} or x_{NO} and x_{NO_2} is c_{NO_x} and x_{NO_x} , respectively.

Pollutant		Conversion factor	
Nitric oxide	NO	1.25	1.24738
Nitrogen dioxide	NO ₂	1.91	1.91247
Ozone	O ₃	2.00	1.99528

Table 2.1: Conversion factors to convert concentration readings in ppb to $\mu\text{g}/\text{m}^3$. The first value is the official value from [BUWAL, 2004] and the second value is calculated to three more digits.

2.1.4 Particulate matter

Particulate matter, also known as aerosols and hereafter called PM, are very small organic and inorganic compounds suspended in the air. They are classified by their aerodynamic diameter and grouped into PM₁₀ (diameter less than 10 μm), PM_{2.5} (diameter less than 2.5 μm) and PM₁ (diameter less than 1 μm) (see table 2.2). In the human health field, these groups are called coarse particles (PM₁₀), fine particles (PM_{2.5}) and ultra-fine particles (PM₁). Furthermore primary and secondary particles are distinguished.

Primary fine particles are directly emitted from combustion sources. They typically aggregate to or with larger particles (and so form secondary PM_{2.5}) or act as fog and cloud nuclei. The lifetime of primary fine particles is typically less than one hour. Tailpipe

emissions from road transport are accountable for up to 30% of fine PM in urban areas [Krzyzanowski et al., 2005]. Secondary PM_{2.5} is also formed from transformations of gases to particles. This includes the oxidation of NO_x to nitric acid mentioned in section 2.1.1. Diesel engines and wood stoves directly emit primary fine particles and diesel engines in addition NO_x which forms secondary fine particles.

Coarse particles (PM₁₀ and larger) include particles from wind-blown dust, sea salt and some pollen (or fragments of pollen) and spores. In cities dust is mainly traffic generated. Wear from tyres, break linings and the road as well as re-suspended road dust is the most important source of coarse particles in cities [Krzyzanowski et al., 2005].

Due to the aerodynamic properties fine particles settle less quickly than coarse particles. Particles larger than PM₁₀ are less likely to enter the human respiratory tract and are not considered harmful [Krzyzanowski et al., 2005]. Smaller particles, however, are inhaled and, especially ultra-fine particles, may enter deep into the bronchial tubes. Of particular danger are emissions from diesel engines and to a lesser extent break linings wear because these particles often contain substances that are suspected to be cancerous and heavy metals. Scientifically assured are the following facts [WHO, 2004]: Short-term exposure effects are lung inflammation reactions, respiratory symptoms and adverse effects on the cardiovascular system. The more severe long-term exposure effect are the increase in lower respiratory symptoms, the reduction in lung function in children and adults, the increase in chronic obstructive pulmonary disease and the reduction in life expectancy (mainly due to cardiopulmonary mortality and probably to lung cancer).

The Swiss NABEL monitoring (see also section 2.1.6) network started measuring PM₁₀ in 1997. Before total suspended particles (TSP) was measured. This included, mainly depending on wind speed and direction, also particles larger than 10 µm.

Class	Diameter	Nomenclature
PM ₁₀	≤ 10.0 µm	coarse particles
PM _{2.5}	≤ 2.5 µm	fine particles
PM ₁	≤ 1.0 µm	ultra-fine particles

Table 2.2: Size classes of particulate matter (PM). Note that concentration declarations for PM_i include all particles with a diameter smaller or equal i µm whereas the nomenclature usually refers to the respective interval (e.g. coarse particles are particles with a diameter larger than 2.5 and smaller or equal 10 µm). The terms for the particle classes given here are used in the human health field.

2.1.5 Smog

The Oxford English dictionary [Oxford University Press, 2006b] defines *smog* as *fog or haze intensified by smoke or other atmospheric pollutants*, a blend of *smoke* and *fog* that originates in the early 20th century.

There are two types of this kind of air pollution: the classic smog, also known as London fog and the photochemical smog, also known as Los Angeles smog. The two types and their origin are described in the following two sections.

Classic smog (a.k.a. London fog)



© TA-Bild / R. Oeschger

Figure 2.4: A view towards south of the smog in the city Zürich (foreground). The lake and the Üetli ridge dissolve in the haze (background).

Industrialisation reached a huge dimension in Great Britain, and later in continental Europe, and the United States in the early 20th century. The large amounts of coal burning to satisfy the energy demand of growing urban agglomerations lead to high levels of smoke and sulfur dioxide in ambient air.

The connection of health or mortality and increased concentrations of poisonous substances in the ambient air were first described in the beginning of the third decade of the 20th century, e.g. by Haldane [1931], as Nemery et al. [2001] point out.

The *London smog incident of 1952* [Logan, 1952] (also referred to as the *Big Smoke*) caused extra death of thousands. The dramatic increase of mortality lasted 9 weeks from November 1952 to January 1953. It is generally the first smog event referred to in books about health effects of air pollution. Hence the alias *London smog* for the classic smog. However, the cited article already mentions two earlier events where smog was determined to be the reason for increased mortality.

The *Meuse Valley fog of 1930* in Belgium is believed to be the first documented air pollution disaster ever, Nemery et al. [2001] subsume. In December 1930 a thick smog

developed in the 20 km long, narrow valley of the river Meuse between Liège and Huy. Pollutants from the heavily industrialised region started accumulating in the valley. After two days hundreds of people started to have severe respiratory signs and symptoms and more than 60 people died in the following three days until the smog period ended and the air cleared up. The event had a big impact on both, the scientific community [Batta et al., 1933; Firket, 1936] and the public.

A similar episode in the heavily industrialised *Donora, Pennsylvania*, United States in 1948 caused 20 extra deaths.

Nowadays the effects of smog periods and the thickness of the fog in winter are not that severe anymore (due to changed energy sources and effective air quality standards). But the limit values of primary air pollutants (nitrogen oxides, particulate matter) are still frequently exceeded during certain weather conditions. See figure 2.4 for a picture of a smog day in Zürich.

Smog weather conditions arise at high-pressure weather which favours surface inversions² preventing vertical ventilation. As a consequence cold air reservoirs are formed in the lowlands which leads to, usually very stable, inversions. Emissions at ground level can then hardly dilute. The pollutants are trapped in the inversion and accumulate over time if the weather condition prolongs for several days. The concentrations of particulate matter and nitrogen oxides raise steadily usually beyond the limit values. Eventually a smog dome results from this process. changes in weather conditions, such as fronts, terminate periods of inversions lasting several days in winter.

Photochemical smog (a.k.a. Los Angeles smog)



Photo by D. Iliff. Edited and reproduced under the terms of [GNUFDL, 2002].

Figure 2.5: View from the Hollywood Hills (foreground) to downtown Los Angeles (background) on a late afternoon. Air pollution (i.e. the photochemical smog; also Los Angeles smog) is clearly visible.

The main problem of the photochemical smog are very high ozone concentrations. Ozone is formed in a photochemical reaction as described above (section 2.1.2). Hence the name photochemical smog for this kind of smog.

²The increase of air temperature with height (temperature inversion). The opposite is more common.

In areas of high population density there is a very pronounced diurnal variation of the ozone concentration (see figure 5.12a and b on page 82). During the night ozone is removed from the air by dry deposition and by chemical reactions with NO (mostly emissions from traffic) (see reaction 2.4 on page 6). This happens below the (low) nocturnal inversion layer which commonly occur during fair weather in summer. Above ozone is stored. In the morning of the following day the inversion layer slowly dissolves. The ozone formed during the previous days is then mixed down into the previously “cleaned” air. This results in a steep increase of the ozone concentration during the morning. At noon regeneration of ozone from local and regional emissions (precursors) starts. The diurnal maximum is then reached earlier or later in the afternoon, depending on the weather conditions.

The pronounced diurnal variation of the ozone concentration is characteristic for cities located in valleys, such as Zürich or Los Angeles. The nocturnal inversion are particularly stable in a valley. The vertical exchange through the inversion lid is almost completely stopped. If the weather conditions prolong for several days, the concentrations in the reservoir layer above the inversion increase from day to day. As a consequence the morning rise of the ozone concentration and the maxima in the afternoon increase (see figure 5.12 on page 180). Eventually a smog situation arises.

This phenomenon and its negative effects on plant life and human health was first found in Los Angeles in the 1940s. A sour haze that irritated the eyes was observed. In the 1950s it was found that ozone is the main component of the photochemical smog. Very high concentrations up to several hundreds of $\mu\text{g}/\text{m}^3$ were observed until the 1970s. New emission standards introduced at that time reduced ozone’s precursors and with that the exorbitantly high ozone concentrations which diffuses the sunlight (see figure 2.5). During such periods particulates are accumulated as well.

2.1.6 Ambient air quality standards and legislation

The Swiss environmental law of 1984 (*Bundesgesetz über den Umweltschutz*, [USG, 1983]) has two aims.

1. To protect men, animals, plants and their biocoenosis against harmful or irritating influence.
2. To permanently conserve the natural live resources in general and the biodiversity and the soil fertility, in particular.

Based on this law a clean air regulation (*Luftreinhalte-Verordnung*, [LRV, 1985]) was issued in 1985. It aims at the same goals as above in connection with air pollution. The most important goals are:

1. The precautionary limit of emissions that pollute the air.
2. Requirements for fuel.
3. The maximum acceptable ambient air concentrations (rlimit values, see table 2.3).
4. The procedure in case air pollutant concentrations are excessive.

In the EU the *National Emission Ceilings* (NEC) for certain atmospheric pollutants are regulated by the directive 2001/81/EC (NECD)³ and its daughter directives.

The United States, for example, have a limit value for PM₁₀ and PM_{2.5} where the legislation of Switzerland and the EU only specifies limits for PM₁₀. There are ongoing discussions on setting up limit values for ultra-fine particles (PM₁, aerodynamic diameter < 1 µm). They contribute little to the mass concentration but they dominate the number concentration and as such may have a dominant affect on health (see also section 2.1.4).

A Swiss national air pollution monitoring network was started in the late 1970s. Today the NABEL (*nationales Beobachtungsnetz Luft*) network consists of 16 permanent stations spread over Switzerland. It is operated by the federal organisations BAFU and EMPA. It achieves the requirement for the monitoring of air pollutants as demanded by the LRV. The long lasting measurements allow the control of the success of the measures against air pollution. See the section 2.1.7. However, also cantons and several cities operate air quality monitoring networks as required by the LRV.

2.1.7 Air quality trends for Zürich

Series of measurements of many years are suitable to assess the efficiency of the air quality legislation. The NABEL station in Zürich (see figure 4.1 on page 42) provides extensive measurements from more than the last two decades. The assessments for individual pollutants are described in the following paragraphs.

Further details on a yearly assessment of the current air quality in Switzerland as well as updates of the past time series can be found in the yearly report on the NABEL permanent monitoring network, e.g. [BAFU, 2006b].

Sulphur dioxide

The time series of measurements of the NABEL station in Zürich shows that the ambient air concentrations of SO₂ decreased strongly since the middle of the 1980s (figure 2.6). The annual averages decreased by roughly a factor of six. This success is the result of governmental regulations that limited the the content of sulphur in fuel, the substitution of coal for domestic heating and the improved monitoring and adjustment of combustion plants.

Nitrogen oxides

The ambient air concentrations of nitrogen oxides have decreased since the 1980s (figure 2.6). However, the goal of the clean air regulation [LRV, 1985] has not yet been reached. At many locations the limit values are still exceeded considerably. The introduction of a catalytic converter in new gasoline vehicles was an important measures to reduce the concentrations of nitrogen oxides. The catalytic converter reduces emissions of pollutants

³http://eur-lex.europa.eu/LexUriServ/site/en/oj/2001/l_309/l_30920011127en00220030.pdf

Pollutant	avg.	Switzerland	EU 2005/10	U.S.A.	WHO
NO₂	1/2 h	100 95% / a			
	1 h		200 18 / a		200
	24 h	80 1 / a			
	annual	30	40	100	40
PM₁₀	24 h	50 1 / a	50 ¹ 7 / a	150 1 / a	
	annual	20	² 20	50	
O₃	1/2 h	100 98% / m			
	1 h	120 1 / a	³ 180	240	
	8 h		⁴ 120 25 d / a	160	120
	AOT40		⁵ 18k May–July		
SO₂	1/2 h	100 95% / a			
	1 h		350 24 / a		
	3 h			1 310 1 / a	
	24 h	100 1 / a	125 3 / a	365 1 / a	125
	annual	30	⁶ 20	79	50
CO	1 h			40 k 1 / a	30 k
	8 h		10 k	10 k 1 / a	10 k
	24 h	8 k 1 / a			
other limited substances include...	annual	Pb (500 ng/m ³) & Cd (1.5 ng/m ³) in PM ₁₀ ; Pb (100 µg/m ² /d), Cd (2 µg/m ² /d), Zn (400 µg/m ² /d) & Tl (2 µg/m ² /d) in dust deposit (200 mg/m ² /d)	Benzene (5 µg/m ³) + Pb (500 ng/m ³) in PM ₁₀	Pb (1 500 ng/m ³) in PM ₁₀ (quart. average); PM _{2.5} 65 µg/m ³ (daily, 98%), 15 µg/m ³	

All values are in µg/m³. Official values given in ppb were converted to µg/m³.
n / a means that *n* exceedances per year are permitted.
n % / a (or m) means that *n* % of the averaged values must be below the limit for each year (or month).

¹EU2005 allows 37 exceedances of this limit.

²EU2005 specifies 40 µg/m³ as the limit.

³EU2005, 180 µg/m³ is the information threshold, there is a warning threshold at 240 µg/m³ for three consecutive hours.

⁴EU2010, replaces the above 1 h limit.

⁵EU2010, limits the total ozone exposition during growing periods (May–July, e.g. crops and forests) to 18 000 µg/m³·h in 2010 and to 6 000 µg/m³·h in 2020.

⁶annual as well as winter (Oct–Mar) maximal allowed concentration

Sources: DMU National Environmental Research Institute, Denmark (<http://www.dmu.dk>, retrieved July 2007) and LRV [1985, p. 84f].

Table 2.3: Air quality standards (limit values) in Switzerland, the EU, the U.S.A. and the WHO guideline values in µg/m³ (converted where necessary according to section 2.1.3). Arithmetic average periods and statistical definitions are given.

by oxidising hydrocarbons to CO₂ and H₂O and, to a lesser extent, converting nitrogen oxides to N₂ and O₂. Nowadays almost all cars are equipped with three-way catalytic converters.

However, the concentrations could increase again if more diesel cars without denox catalytic converters are introduced or if kilometres travelled of heavy duty transport vehicles continues to increase. Another concern relates to the proportion of NO₂ to NO_X in vehicle exhaust. It appears that modern exhaust technology causes to increase the NO₂ fraction and therefore NO₂ did not decrease in the same amount as NO_X [Hueglin et al., 2006].

Volatile organic compounds

As a result of the propagation of the catalytic converters in transport vehicles volatile organic compounds (VOC) concentrations have decreased strongly since the 1990s as well.

Particulate matter

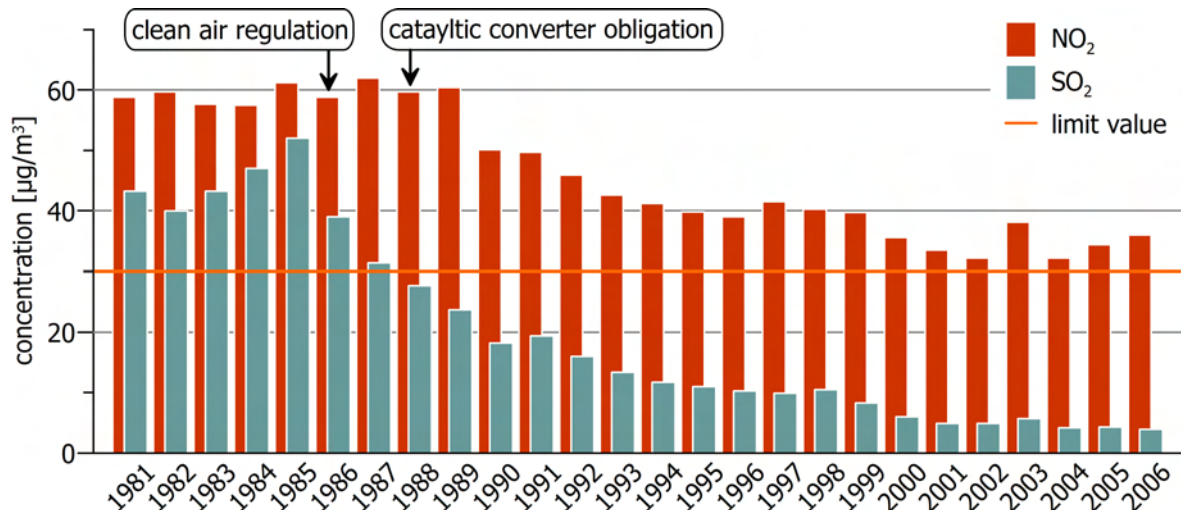
The ambient air concentrations have also decreased for particulate matter in the last two decades (figure 2.7). However, all limit values are still exceeded at moderately polluted sites. More effort is needed to meet the air quality standards of the clean air regulation [LRV, 1985]. Particular attention should be paid to diesel cars.

The exceptionally high maximum daily average and large number of daily maxima exceedances in the year 2006 (see figure 2.7b) is mainly related to two distinct smog periods in January and February 2006 (compare figure B.10 on page 178).

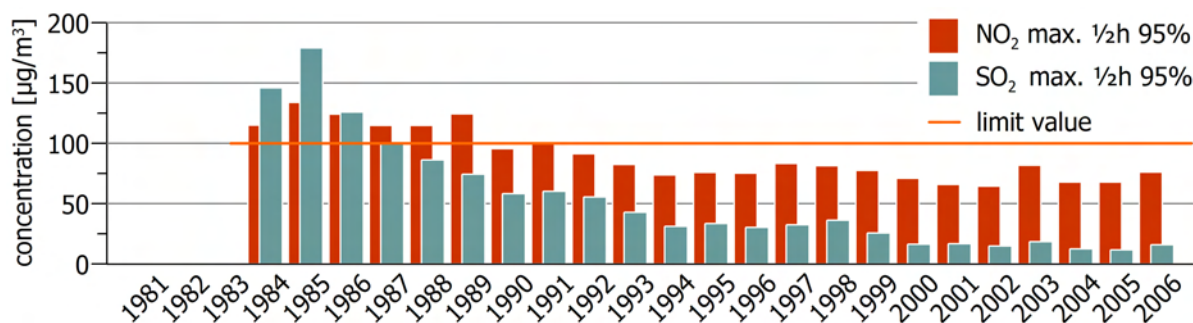
Ozone

Ozone annual mean values steadily increased until the late 1990s at the NABEL station in Zürich. This is caused by the decrease in NO emissions, which first destroys ozone close to the emission source. However, only high ozone concentrations are relevant for the environment. High (summer) values depend on ozone precursor emission strength and meteorology (see e.g. year 2003 in figure 2.8b and c).

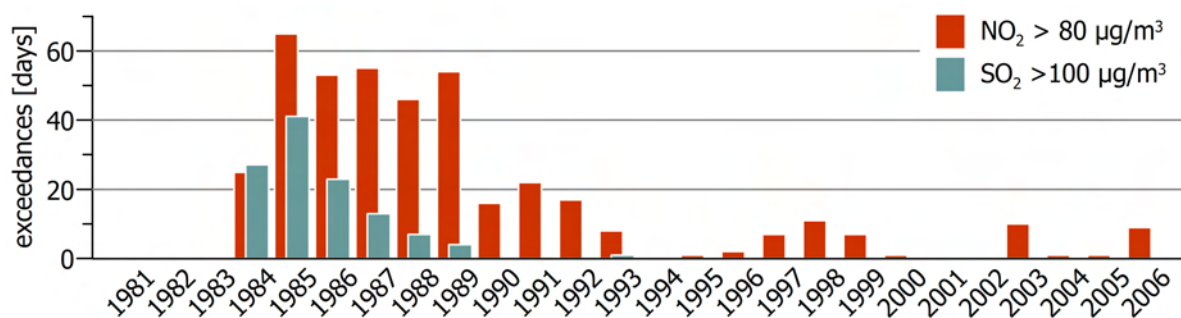
Despite the decrease in the concentration of precursor substances (mainly NO_X and VOC) the peak ozone concentrations did not change significantly, and air quality standards are exceeded repeatedly (see figure 2.8 and [Ordóñez et al., 2004]). The concentrations of precursor substances have also been significantly reduced in the surrounding countries. Therefore, it is surprising that the ozone maxima concentrations did not decrease. This is a current research topic. There is evidence that this is a northern hemisphere pollution problem and that the amount of ozone transported to Europe has increased [Ordóñez et al., 2007].



a) annual average (the limit value is for both, NO₂ and SO₂, at 30 $\mu\text{g}/\text{m}^3$)

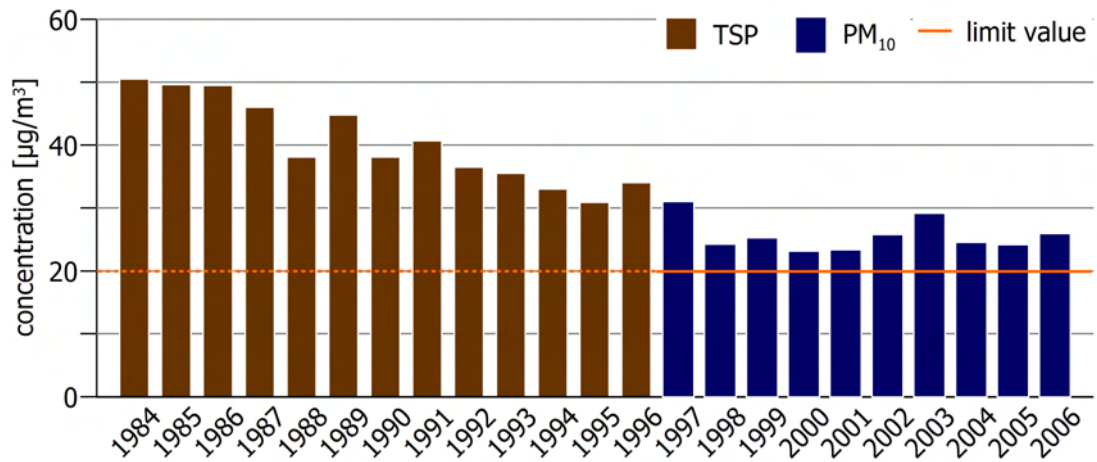


b) maximum 1/2h 95% value (the limit value is at 100 $\mu\text{g}/\text{m}^3$)

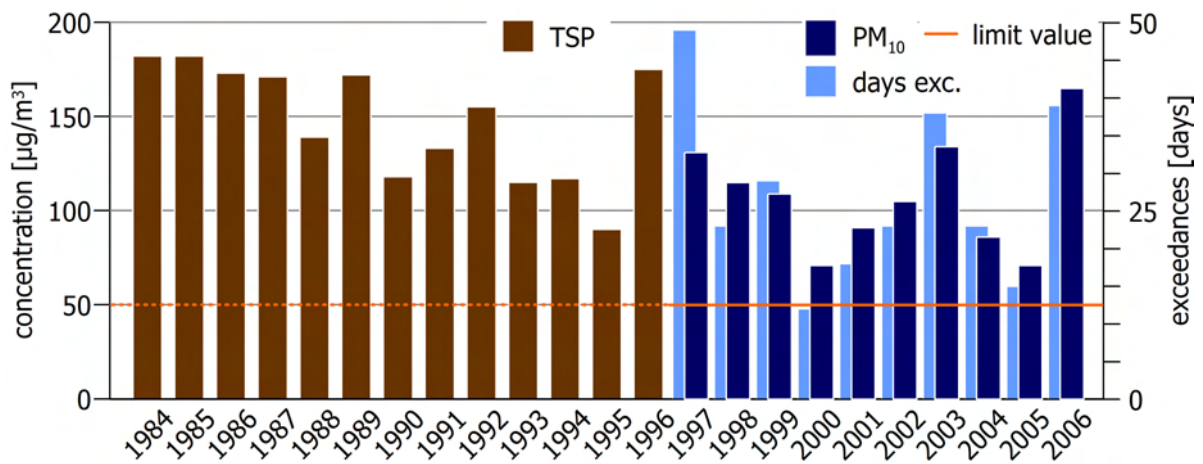


c) number of daily average exceedances (NO₂ > 80 $\mu\text{g}/\text{m}^3$, SO₂ > 100 $\mu\text{g}/\text{m}^3$, allowed at most once per year each)

Figure 2.6: Changes in the NO₂ and SO₂ concentrations at the NABEL station in Zürich from 1981 to 2006. The values for the year 2006 are preliminary. Source: [BAFU, 2006a] and NABEL (BAFU+EMPA). See also table 2.3.



a) annual average (the limit value for PM₁₀ is at 20 µg/m³)



b) maximum daily average (the limit value for PM₁₀ is at 50 µg/m³) and the number of exceedances (allowed at most once per year)

Figure 2.7: Changes in the TSP and PM₁₀ concentrations at the NABEL station in Zürich from 1984 to 2006. The values for TSP, which are plotted to scale with the PM₁₀ values, are deduced from the original TSP values. The values for the year 2006 are preliminary. Source: NABEL (BAFU+EMPA) and [BAFU, 2006a]. See also table 2.3.

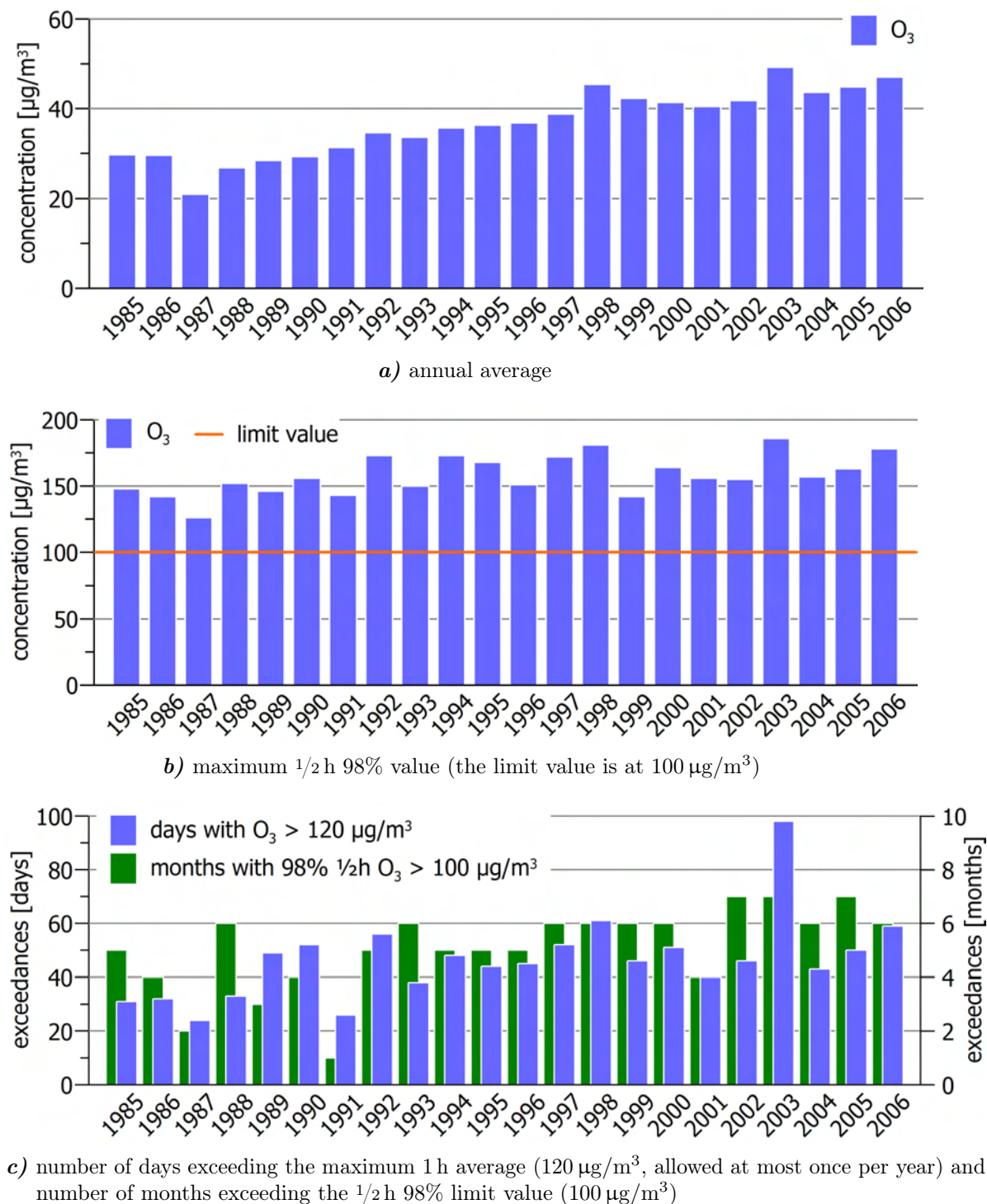


Figure 2.8: Changes in the O_3 concentrations at the NABEL station in Zürich from 1985 to 2006. The values for the year 2006 are preliminary. Source: NABEL (BAFU+EMPA) and [BAFU, 2006a]. See also table 2.3.

2.2 Global positioning system (GPS)

GPS is a satellite based and globally usable positioning system. Its full name is NAVSTAR-GPS which is the acronym for *navigation system with timing and ranging global positioning system*. It was developed by the United States for military purposes. In 1978 a first experimental satellite was launched and by 1985 several more satellites proved the applicability of the concept. It was decided that GPS would be made available for civilian use. The initial operational capability configuration was achieved in December 1993. The civil standard positioning service (SPS, [DoD, 1995a]) was made available to the general public. The SPS provides the exact position (longitude, latitude and height) and the precise time (universal time coordinated, UTC).

GPS can be divided into two segments: a space segment and a control segment. The latter consists of several ground stations distributed all over the world. The function of the control segment is to monitor and control the space segment.

Further detail on GPS can be found in various textbooks on the subject. A recommended reading for GPS novices, which provided valuable information for this chapter, are [Zogg, 2002] and [Zogg and Amman, 2001]. Further readings include [DoD, 1995a,b, 2001; Hofmann-Wellenhof et al., 2001].

2.2.1 GPS constellation

The space segment is formed by the GPS satellite vehicles (SV). A complete (or: nominal) GPS constellation consists of 24 satellites. The constellation is designed in order to provide a coverage of at least four satellites at any place (on Earth) at any time. The parameters of the nominal GPS constellation are described in table 2.4. Figure 2.9 shows a constellation of 24 satellites as a 2d diagram and as a 3d visualisation.

Today⁴ the GPS constellation consists of 31 operational satellites of three different generations (so called blocks):

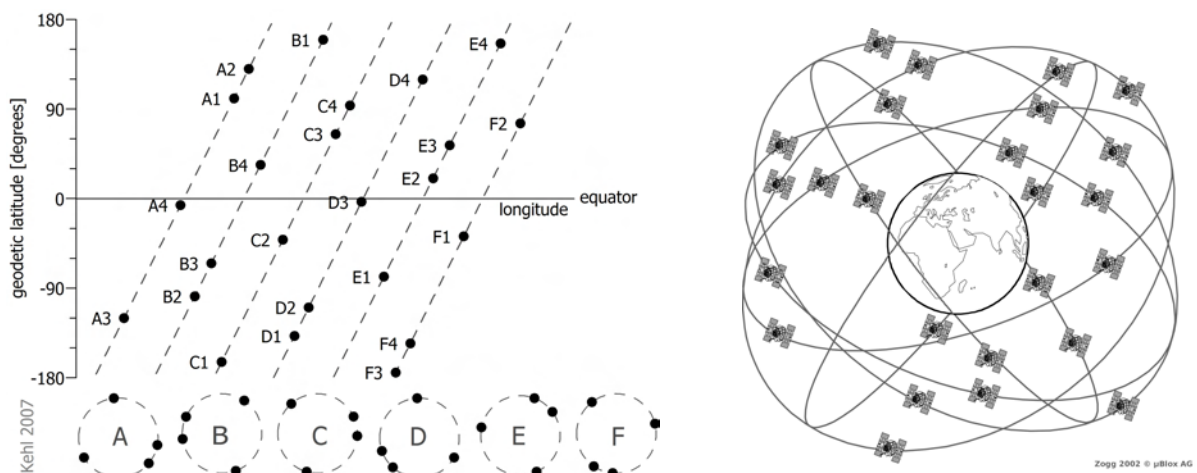
- * 14 block IIA, launched from 1991–1997
- * 12 block IIR, launched from 1997–2004
- * 5 block IIR-M, launched in 2005, 2006 (2) and 2007 (2)

In this constellation each orbital plane holds from four to six SV. The design life of the block IIA and IIR satellites, respectively, is 7.5 and 10 years. The status of constellation is continuously assessed to determine launch needs. The deployment of next generation GPS block IIF and later block III satellites is planned to start in 2008.

⁴Sources: <http://www.navcen.uscg.gov/navinfo/Gps/ActiveNanu.aspx> and <ftp://tycho.usno.navy.mil/pub/gps/gpsb2.txt>, retrieved January 17, 2008.

Parameter	Value
semi-major axis	: 26 000 km
eccentricity	: 0
period	: 11h 58''
inclination	: 55°
orbital planes	: 6 (60° separation)
satellites / plane	: 4

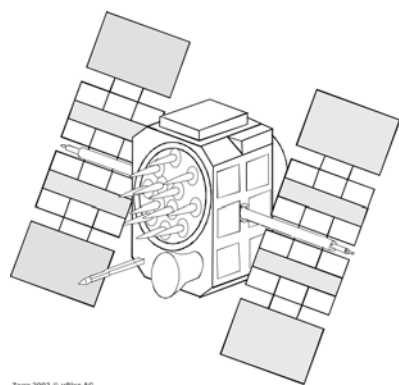
Table 2.4: Nominal GPS constellation parameters.



a) A diagram of the SV distribution on the orbital planes (top) and the same configuration displayed individually for each orbit (below). The constellation shows the epoch of July 1, 1990, 00:00:00 UTC.

b) A 3d visualisation of a nominal constellation as described in table 2.4.

Figure 2.9: Nominal GPS constellation with four SV in each of six orbital planes.



a) Block IIA (since 1990)



b) Block IIR (since 1997).

Figure 2.10: Illustrations of the GPS satellite vehicles (SV) currently in use.

2.2.2 Measurement principle

GPS positioning is based on measuring the transit time (Δt_i) of radio signals from the satellites to the receiver, i.e. the users position. Since radio signals travel at light speed ($c = 3 \cdot 10^8 \text{ m/s}$), the distance (R_i) to each satellite in view can be determined. The index i in the following corresponds to an individual satellite.

$$R_i = \Delta t_i \cdot c \quad (2.7)$$

The satellite's time reference are atomic clocks which are synchronised to each other and to UTC. So the time at which the signals is broadcasted by the satellite is known very precisely. But the receiver's clock is off by Δt_0 because it is not synchronised to UTC. This leads to errors in the measurement of the transit time. The resulting and inaccurate range is called a pseudo-range (PSR).

$$PSR_i = (\Delta t_i + \Delta t_0) \cdot c = R + \Delta t_0 \cdot c \quad (2.8)$$

Since the position of the receiver is the goal of the measurements we can introduce these variables and express R with the Cartesian co-ordinates of the receiver (user) and the satellite.

$$R_i = \sqrt{(X_i - X_{user})^2 + (Y_i - Y_{user})^2 + (Z_i - Z_{user})^2} \quad (2.9)$$

And with 2.9 in 2.8 we obtain:

$$PSR_i = \sqrt{(X_i - X_{user})^2 + (Y_i - Y_{user})^2 + (Z_i - Z_{user})^2} + \Delta t_0 \cdot c \quad (2.10)$$

2.10 contains the measured variable PSR_i , the known position of the satellite (X_i , Y_i and Z_i) and four unknown variables. These are the user's position (X_{user} , Y_{user} and Z_{user}) and the user's clock offset (Δt_0). Since the satellite clocks are synchronised, Δt_0 is common to all i .

This leads to the conclusion that four independent equations are needed to solve for the user's position and clock offset. Since 2.10 is true for any satellite, four satellites (or, more precisely, measurements from four satellites) are needed.

The approach used to solve the equation system incorporates the linearisation of the Taylor series approximation of the equation and then solving the system with linear algebra. If more than four satellites are available, the least-squares method is used to solve the linearised equation system. This reduces errors introduced through the measurements. See the next section on the sources of errors.

The result is the user's position and the offset of the user's clock to UTC.

2.2.3 Sources of errors and accuracy

There are six main effects that introduce errors to the positioning accuracy. The values given in this section are from [Zogg, 2002]. The effects are:

Two effects are related to the satellite. The *satellite clocks* are very precise atomic clocks. But since the signal travels at light speed (c) the error is 0.3 m/ns clock offset. The *satellite position in the orbit* is known within 1–5 m through the ephemeris data broadcasted by the satellite. The error introduced due to these effects is in the range of 2.1 m each.⁵

The radio signal travels through the atmosphere where two effects are dominant. In the *ionosphere* the speed of light and, therefore, the propagation speed of the signal slow down. The water vapour content of *troposphere* bends the signal path which lengthens the pseudo-range as well. The errors introduced by these effects are in the range of 4 m and 0.7 m, respectively.

At the receivers location another two effects cause errors. The receiver is only able to time the reception of the signal with a certain accuracy (≥ 10 ns). The effect on the positioning accuracy is approximately 0.5 m. Effects in the range of 1.4 m are introduced by multi-path effects. Multi-path is caused by the reflection of the signal at the ground, at buildings or at other surfaces near the receiver before it reaches the receiver's antenna.

The error of the navigation solution (i.e. the calculated position) also depends on the geometry of the satellites that are used in the measurement. A more or less collinear alignment of the satellites produces a large error in the orthogonal direction whereas an even distribution of the satellites in the sky lock the position more precisely. A geometrical explanation of this are poorly defined intersections at the users position of the spheres spanned around the satellites by the respective pseudo-range. The geometry is also the reason why the height error is larger than the 2d positional error (there are no signals from below the position). The measure for this effect is the dilution of precision (DOP). The mathematical definition of DOP is a function of the covariances of the navigation solution.

Four different DOP values are used to characterise a certain geometry and to quantify the effect on different values. GDOP is the geometrical DOP that refers to the 3d position in space and includes the time error. PDOP (positional DOP) refers to the 3d position. HDOP and VDOP respectively refer to the horizontal (2d position) and vertical DOP (height).

Figure 2.11 shows two examples of good and a bad geometry.

Zogg [2002] determines the following total errors under the assumption of average DOP values (VDOP = 2.5, HDOP = 2.0) and ranks these as not too optimistic.

<i>vertical error</i> (1σ , 68.3%)	: 12.8 m	<i>horizontal error</i> (1σ , 68.3%)	: 10.2 m
<i>vertical error</i> (2σ , 95.5%)	: 25.6 m	<i>horizontal error</i> (2σ , 95.5%)	: 20.4 m

⁵Until May 2, 2002 the so called selective availability intentionally degraded the users measurements by adding errors to the satellite's clock signal. Is was discontinued as the result of U.S. governmental order to push the civil GPS business and science. See also http://www.ostp.gov/html/0053_2.html.

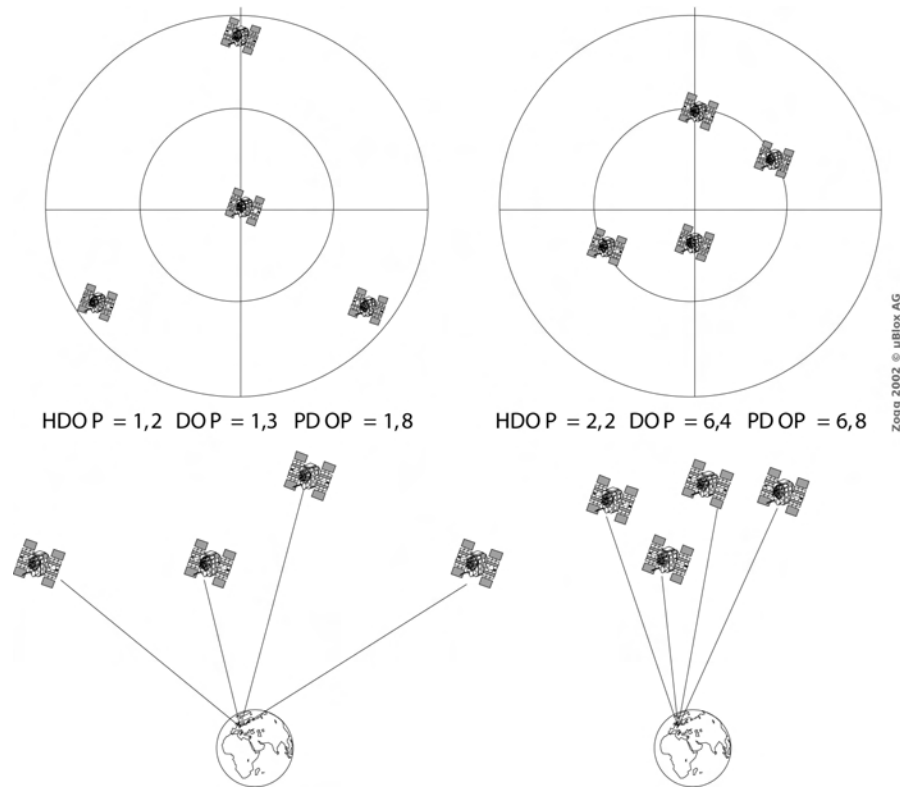


Figure 2.11: DOP as a GPS satellite coverage geometry qualifier (left good geometry/low DOP, right poor geometry/high DOP). The graphs at the top are sky plots with the zenith in the middle and the outer circle corresponding to the horizon. The graphs at the bottom visualise the above situation in 3d.

2.2.4 GPS in urban areas

Urban areas rise a challenge to GPS positioning. The horizon is generally limited from the receiver's point of view (see figure 2.12). Compared to locations with an unobstructed view like in a rural area or on a mountain top the visibility of GPS satellites is generally poor in urban areas. Buildings or trees block the available signals and only a part of the satellites in the sky are visible to the receiver. In street canyons this can mean a poor geometry (DOP) and as a consequence degraded accuracy of the navigation solution. In narrow streets and in streets lined with trees the visibility can degrade as far as that not enough satellites are received to obtain a position. GPS outages occur regularly in the urban area. They depend on the time or rather the satellite constellation and place.

Another effect that decreases the navigation accuracy is multi-path as defined in the previous section. In general there is increased multi-path in built-up areas. In urban areas multi-path can be very distinct. Often metal and coated glass is used as the materials for the fronts of office buildings. Both are good reflectors of electromagnetic waves. An actually shadowed signal can then still reach the receiver indirectly (see figure 2.12). This lengthens the pseudo-range of the observed satellite.

Figure 2.13 shows several typical location in the city of Zürich. Most locations are densely build-up and have limited sky visibility. There are pronounced street canyons and many streets lined with trees. Places with a less obstructed view, such as open squares, are less common.

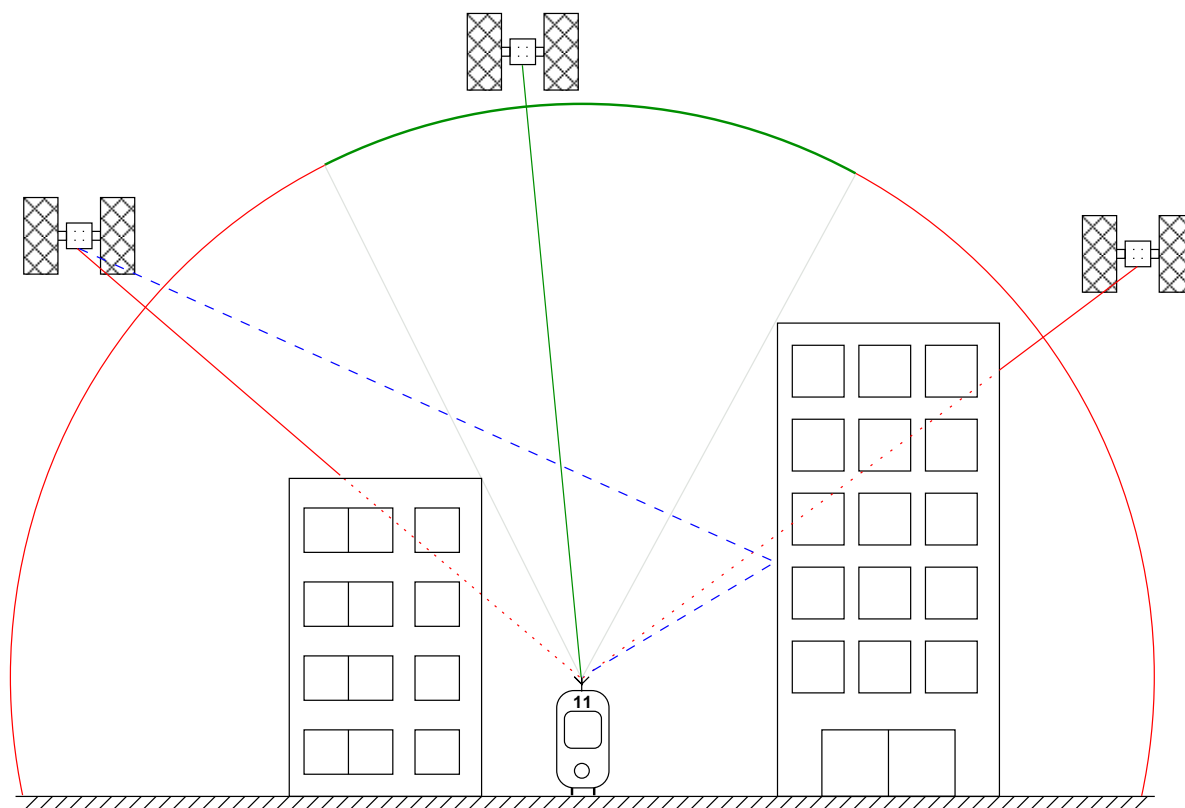


Figure 2.12: Schematic diagram of limited GPS visibility in a street canyon. Signals from satellites in the visible sky region (green arc) are directly received (green line). Signals from satellites in the shadowed sky region (red arcs) are blocked (red lines) and cannot be received (dotted red line). The buildings are an example for an obstruction. The topography and, to a lesser extent, trees have the same signal blocking effect. A blocked signal is sometimes received indirectly (multi-path) if it is reflected (blue line) at an appropriate surface. Metallic fronts and coated glass, which are often used in downtown office buildings, are good reflectors for radio signals.



a) Dense trees in Bahnhofstrasse.



b) Trees near the tram station Regensbergerbrücke.



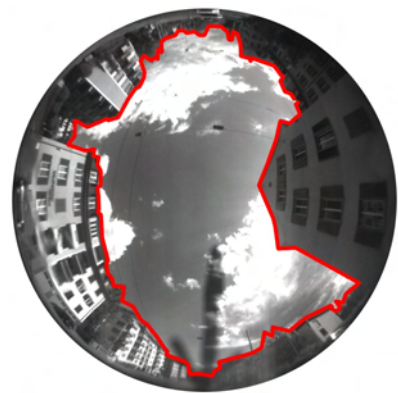
c) Less obstructive trees due to a broader street.



d) A deep street canyon (Stampfenbachstrasse).



e) A street canyon near tram station Walcheplatz.



h) A 180° fish-eye picture taken from the roof of a car. The image plane is approximately 1.7 m above the street. The driving direction and the street canyon orientation is downwards in the picture. The red line represents the horizon. 60% of the hemisphere are covered by buildings, trees and the topography.



f) Open space near the central railway station.



g) Open space on a bridge near Bellevue.

Figure 2.13: Typical urban situations in Zürich that challenge the GPS positioning. Many streets are lined with trees (*a*, *b*, *c*) and there are pronounced street canyons (*d*, *e*, *h*). Open squares (*f*) or streets with an unobstructed sight (*g*) are less common.

Source (a-g): [Forster and Landtwing, 2004].

2.2.5 Co-ordinate transformation

The navigation solution obtained through GPS are WGS-84 (world geodetic system 1984) co-ordinates. WGS-84 is an earth-centred and earth-fixed (ECEF) three-dimensional, right-handed and right-angled Cartesian co-ordinate system. The origin is at the Earth's mass centre (geocentric) and the X and the Y axis lie on the equatorial plane. The X axis goes through the Greenwich (0°) meridian (and, therefore, Y through 90° east and Z through the geographic north pole).

For further processing the GPS co-ordinates are transformed into the local land co-ordinate system used in Switzerland. This involves two steps.

1. Geodetic datum conversion The global geocentric (WGS-84) co-ordinates are converted into the local geocentric system (CH1903). This involves a shift, a rotation and an extension. The seven parameters are the definition of the Swiss geodetic datum CH1903. The Cartesian co-ordinates are converted into ellipsoidal (ϕ, λ, h) co-ordinates. CH1903 relies on the Bessel ellipsoid from 1841.

2. Projection An oblique conformal cylindrical projection is carried out. It involves the two steps outlined in figure 2.14. The ellipsoidal co-ordinates are projected onto a sphere. The sphere is then projected onto an obliquely positioned cylinder. The cylinder touches the sphere at the old astronomical observatory in Bern. The co-ordinates 600 000 / 200 000 (m) are given to this fundamental point. These offsets guarantee unique X and Y co-ordinates within Swiss territory.

The formulae for this process are described thoroughly in [Swisstopo, 2001b]. There are also direct approximation formulae available [Swisstopo, 2001a]. The latter are precise within a metre but must not be used for geodetic applications. The precise transformation was used in this project.

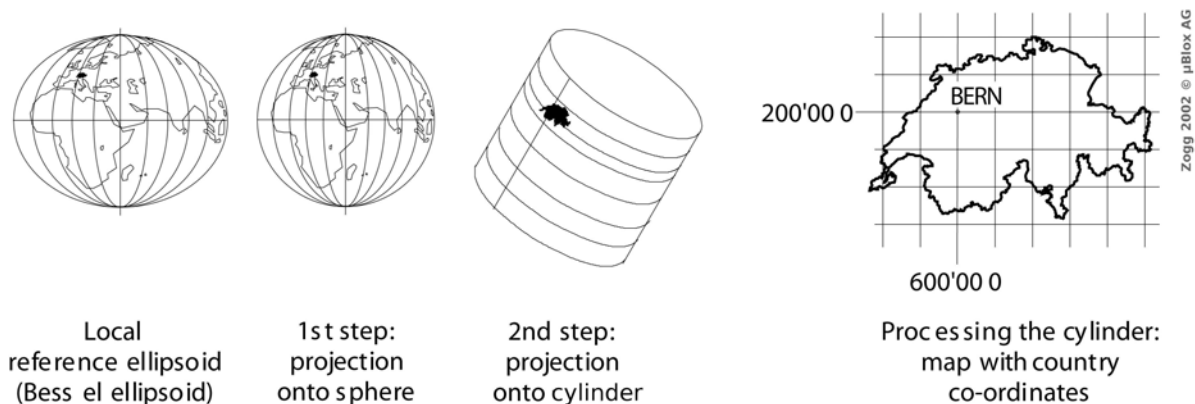


Figure 2.14: A scheme of the *Swiss projection*, which is used to transform co-ordinates from a local reference ellipsoid (the Bessel ellipsoid, see text) into the local co-ordinate system (country co-ordinates).

* * *

3

Measurement System

3.1 The measurement platform

To achieve the project goal of dynamic monitoring, a suitable mobile platform had to be found. A pilot survey had been carried out [Schneebeli and Wegmann, 2002] to investigate the technical and metrological demands for the mobile platform. To measure ambient air concentrations of nitrogen oxides (NO and NO₂), ozone, and particulates, the requirements are:

- * *space*, approximately 1 m³
- * *load capacity*, approximately 200 kg
- * *electrical power*, approximately 1000 W
- * *regular uptime* as long as possible, at least during daytime (covering morning and evening rush hours and the time between) for a longer time period (months or more)
- * the *platform* has to move along roads and aboveground covering many different places throughout the city
- * possibility to *position* the carrier
- * *no disturbance* of the sensors on the carrier by heat, exhausts or other sources of pollutants
- * reasonable *costs*

Since the technical demands made it impossible to use or build a dedicated vehicle, public transport vehicles were chosen. While busses were found unusable, certain types of trams met the requirements with respect to space, load capacity and electrical power as well as the demands for a regular uptime and the closeness to the traffic and the pollutants, respectively. The public transport of Zürich (Verkehrsbetriebe Zürich, VBZ) agreed to provide a suitable tram and to operate it on a regular basis on a desired line.

The chosen tram is a relatively modern one constructed in the year 1992/1993 (see figure 3.1. It is a *3. Serie Motorwagen Be 4/6*, or short a *Tram 2000 Serie III*. It is 21 m long and weights 26 t (figure 3.2a). The four motorised axis are powered by two 157 kW (213 PS) electric motors. The transport operator has carried out modifications to this tram in autumn 2006. A third element with low-floor entrances has been inserted. This

modified version is called *Sänfte Be 4/8*, is 28 m long and weighs 31 t (figure 3.2b). *Sänfte* is the German word for palanquin, hinting at the comfortably low doorsteps of the middle element.

The tram meets all of the above demands. Since it relies on semiconductor technology, there are no heat-producing breaking current resistors on the roof which might falsify the measurements. Of course the pantograph produces arcing and abrasion, but the placement of the sensors at the other end of the wagon minimises these influences. The weight of the tram itself is more than 26 tons and the roof construction already carries some other heavy technical equipment. Therefore the weight of the measurement system is not an issue. Even if there is almost infinite power on the overhead contact line, that power cannot be used directly. But there is a transducer on the tram with an energy reserve of about 1500 W which is enough to power the measurement system without disturbing the other electrical equipment used to drive the tram. A socket providing electrical power and mountings for the measurement system have been installed on the tram for easy setup and deinstallation.

For a description of the tram lines used for the measurements see section 4.1.



Figure 3.1: A slightly modified photo of a *Tram 2000 Serie III* tram.

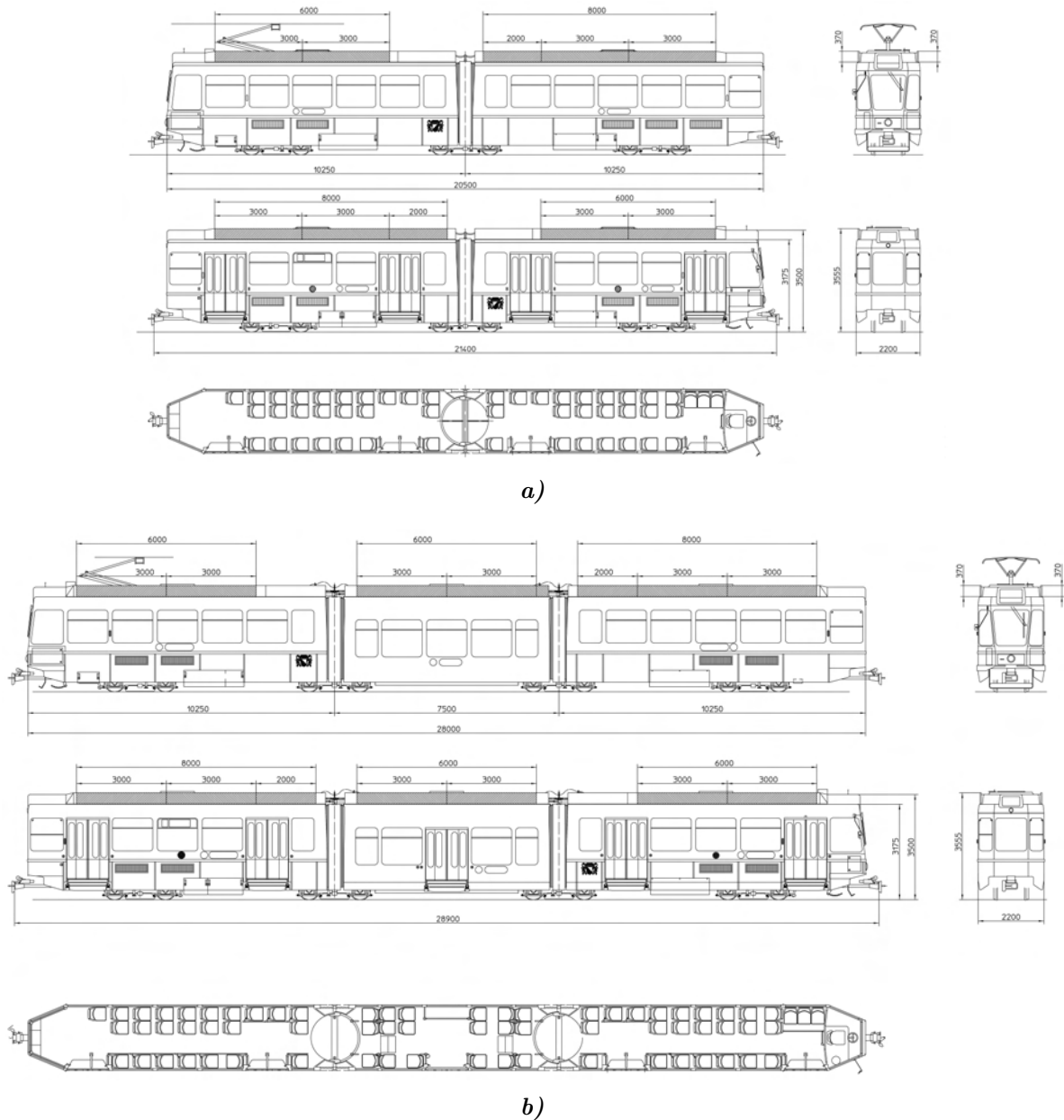


Figure 3.2: Blueprints of the *Tram 2000 Serie III* tram before (a) and after (b) the modification. Lengths are in [mm].

© VBZ

3.2 The measurement system

The measurement system (see figure 3.3) had been purpose-built to meet regulations, terms and metrological demands. The structure gage and the available space on the roof of the vehicle defined size and form of the box containing the measurement system. Because it is also exposed to atmospheric conditions, especially rainfall and radiation, the box has to be weather-proof. A commercially available roof box for cars has been chosen as the housing for the measurement equipment. To improve the stability and to provide mounts for the equipment, the box has been fortified. A high-grade steel framework has been assembled and fitted into the box. New mountings from the same steel have been added. On the tram itself supporting notches have been welded on the roof.

3.3 Environmental sensors & measurement principles

3.3.1 Nitrogen oxides sensor

The measuring principle of the nitrogen oxides sensor is chemiluminescence of NO formed by reactions with O₃. NO₂ is measured after conversion to NO. It has a measurement range of 0–200 ppb(v) with an averaging time of 10 seconds. The sample flow is nominally 1 litre per minute. The instrument, excluding the external vacuum pump, weights nearly 30 kg. The enclosure is 19 inch (43 cm) rack size in width, 22 cm height and 60 cm deep. The analyser operates at 230 VAC/50 Hz. The vacuum pump has been modified by the Swiss supplier of the analyser, Kull Instruments, in cooperation with KNF Germany, to operate at 24 VDC. The analyser has an internal ozone generator with permeation dryer at its input. The used instrument is a *Thermo Environmental Instruments Model 42C TL* (see figure 3.4).

The readings are available on analogue outputs as well as on a serial port. The latter can also be used to remotely control the unit. In this project, the readings are sampled from the analog output (0–10 V). The serial port is used to check the instruments status and alarms.

The manual [TEI, 2000, p.1-3] lists the following specifications.

<i>Zero noise</i>	: 25 ppt RMS (120 second averaging time)
<i>Lower detectable limit</i>	: 50 ppt (120 second averaging time)
<i>Zero drift (24h)</i>	: negligible
<i>Span drift (24h)</i>	: ± 1% full scale
<i>Response time</i>	: 60 s (10 s averaging time)

Precision or measurement accuracy is not specified in further detail. [BAFU, 2006b, p.28] specifies a measurement uncertainty of 7% for daily averages larger than 35 µg/m³ for this measuring method. An uncertainty in the same range, and possibly somewhat higher due to less stable measuring conditions, is expected for the tram measurements.

3.3.2 Ozone sensor

The ozone sensor measures the UV absorption of O₃ at the wavelength of 254 nm. It has one channel and an internal, replacable ozone scrubber to measure the zero point. The maximum measurement range is 0–100 ppm(v), although a narrower range of 0–250 ppb(v) is used. The minimum averaging time is 10 seconds. An external PTFE filter has been inserted into the sample line. The instrument operates at 12 VDC. It weights about 2 kg. The enclosure is 22 cm wide, 8 cm high and 28 cm deep. Recent versions of the instrument includes a Nafion tube for humidity control. At the time of purchase, this option was not available and the measurements have therefore been carried out without special humidity control. The used instrument is a *2b Technologies Ozone Monitor Model 202*.

The readings are available on an analog output (0–2.5 V). The device also has an internal logging memory which has not been used in this project.

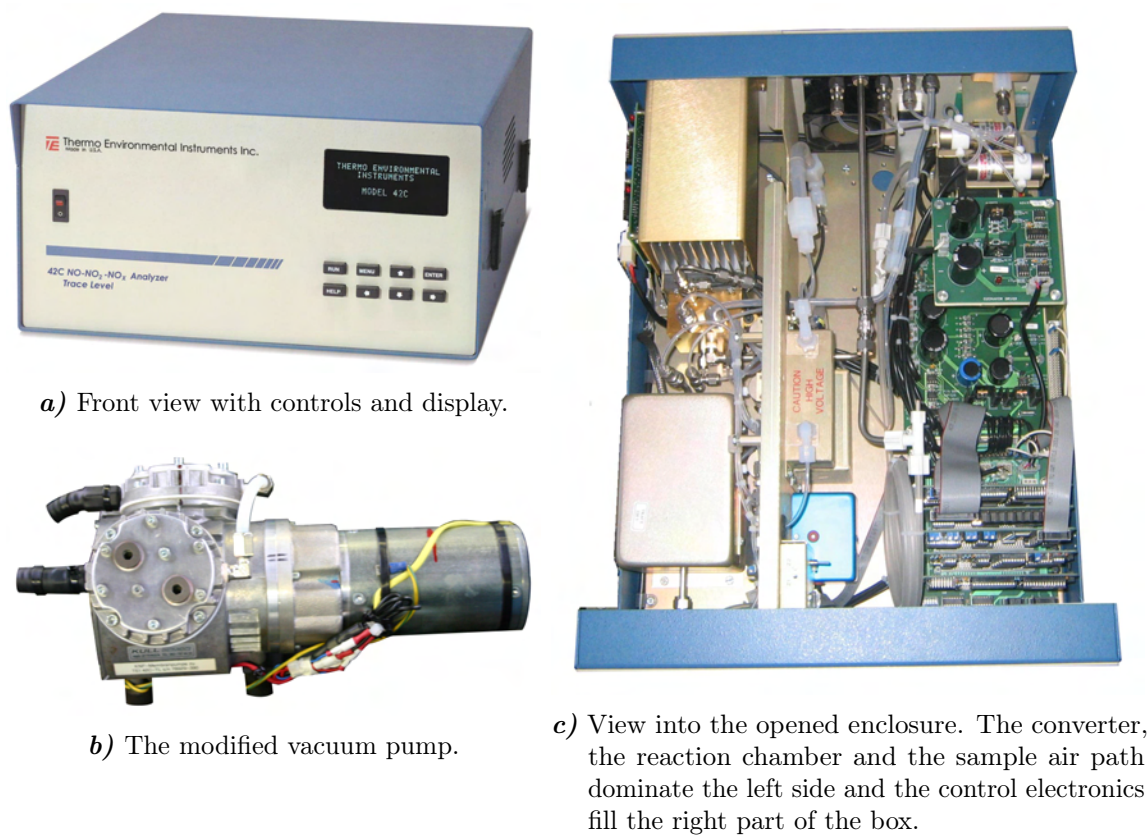


Figure 3.4: The Thermo Environmental Instruments Model 42C TL analyser.

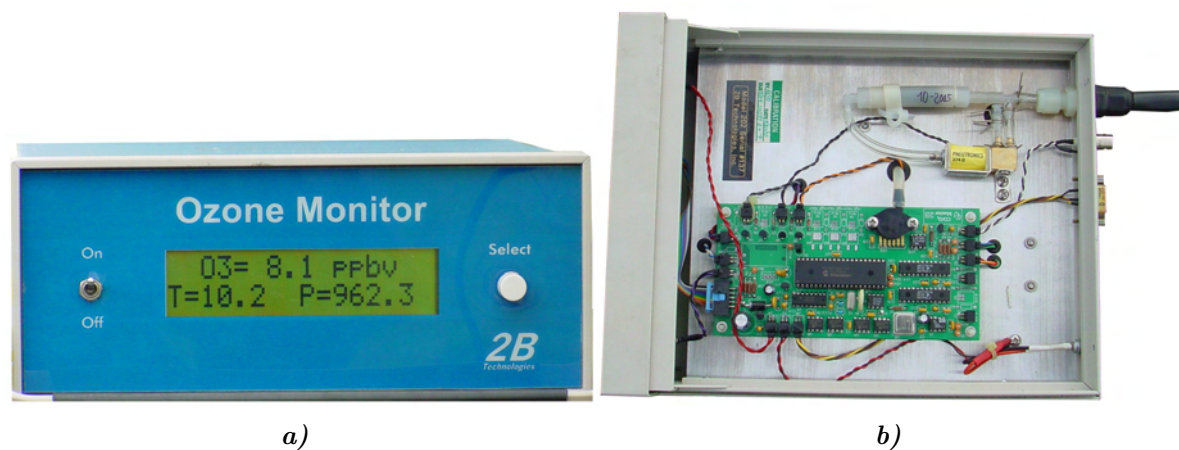


Figure 3.5: The 2b Tech. Ozone Monitor Model 202. Front view (a) and opened enclosure (b). The measurement chamber is under the electronics and is not visible here.

The manual [2bTech, 2001, p.4] lists the following specifications.

Precision : higher of 1.5 ppb(v) or 2%
Accuracy : higher of 1.5 ppb(v) or 2%

3.3.3 Particle sensor

Particulate matter is detected by a diffusion charging particle sensor. Unlike the traditional weighting of particles of a certain size class (e.g. $PM_{2.5}$ or PM_{10} , see section 2.1.4) this sensor determines the total active surface of all particles, the so called Fuchs surface [Matter et al., 1999; Pandis et al., 1991]. The device features a measurement range from $0-2000 \mu m^2 \cdot cm^{-2}$. The sensor reacts quickly on a change in ambient air concentration of particles). The sample flow is about 1.5 litres per minute. The instrument has digital inputs to control the pump and the corona discharge and digital outputs (alarms) to monitor the same. The instrument operates at 20 VDC/50 Hz. The enclosure is a 1/2-19 inch (22 cm), 15 cm height and 32 cm deep laboratory case. The used instrument is a *Matter Engineering Diffusion Charging Particle Sensor Type LQ 1-DC*.

The readings are available on an analogue output (0–5 V).

The manual [LQ1DC, 2001, appendix A] lists the following specifications.

<i>Resolution</i>	: $1 \mu m^2 \cdot cm^{-2}$
<i>Response time</i>	: approx. 15 s
<i>Accuracy</i>	: $\pm 15\% \pm 2 \mu m^2 \cdot cm^{-2}$
<i>Influence of humidity</i>	: $< 1\%$ (0–50% RH), $< 5\%$ (0–90% RH)



Figure 3.6: The Matter-Engineering LQ1-DC diffusion charge particle sensor. Photo: Matter-Engineering AG.

3.3.4 Meteorological sensors

Meteorological data of the ambient air are acquired as well. A combined sensor measures the temperature ($-30-+70^\circ C$) and the relative humidity (0–100%RH). A customised absolute pressure sensor measures the pressure in a range from 950–1020 hPa. The used sensors are a *Rotronic Hygroclip S3* (T, RH) and a *Keller Absolute Pressure Transmitter PAA-9-1.02* (p). Both sensors operate at 12 VDC. All three readings are available on analogue outputs (0–10 V and 0–1 V, respectively).

The specifications for the temperature and the humidity sensors are as follows.

<i>Response time</i>	: 12–15 s
<i>Accuracy</i>	: $\pm 1.5\%$, RH (at $23^\circ C$) $\pm 0.3 K$ (at $23^\circ C$)

The specifications for the pressure sensor are as follows.

Linearity : typical 0.25%, max. $\pm 1\%$

Hysteresis : $< 0.1\%$

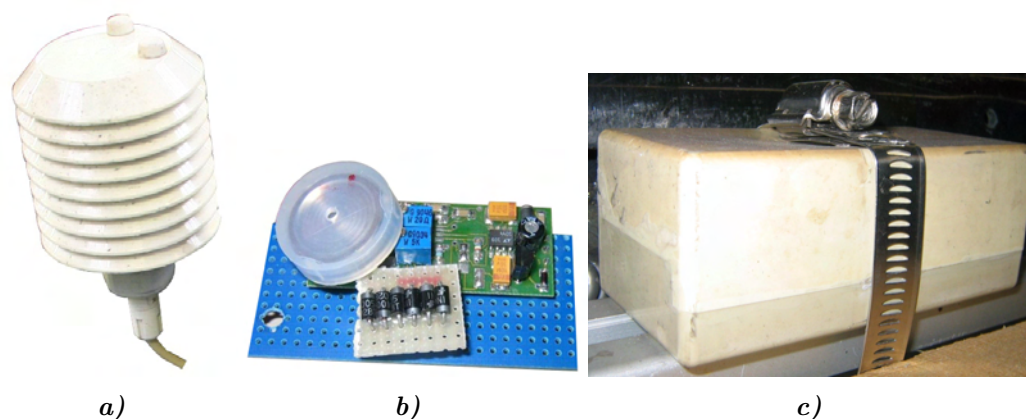


Figure 3.7: The meteorological sensors. The combined temperature and humidity sensor in a weather casing (a), the electronics of the pressure sensor (b) and its casing and installation outside of the measurement box (c). Note: the pictures are not to scale.

3.4 Positioning sensor & time reference

Positioning GPS has been chosen as a position and time reference. In an early stage of the project, investigations of the performance of various GPS receiver in urban areas were conducted [Heller, 2003]. It was shown that it is indeed possible to navigate in



Figure 3.8: The uBlox Antaris GPS receiver. The picture show the power supply and interface PCB (left) with the GPS module plugged on the left side of the board. The enclosure of the electronics is shown on the right. The patch antenna is shown in the foreground.

urban areas, even in pronounced street canyons with buildings of up to about 30 metres height, with a reasonable precision using certain receivers. The chosen receiver has been examined on the tram in further detail [Forster and Landtwing, 2004]. The results have shown the reliability of the receiver on most parts of the track.

The used sensor is a *uBlox Antaris EvalKit (SBR-LS)* with a standard active GPS patch antenna. The device operates at 12 VDC and outputs extensive navigation and performance information as *UBX* messages on a serial RS232 port [Vogel and Nigg, 2002]. For this project the receiver has been configured to output all relevant navigation, time and satellite information at a rate of 1 Hz (compare section 4.3.3). See section 5.4 for an analysis of the performance of this GPS receiver on the tram.

The precision of the position measurements depends on various factors (see section 2.2).

3.5 Power supply & control

The requirements for the power supply of the measurement system are multifaceted. The tram itself nominally provides 36 volts direct current which goes up to 42 VDC and might contain voltage peaks. The maximum power output is 1500 watts. This power source is not completely constant and may fail for short periods (seconds) due to the nature of the pantograph or for longer periods (minutes) due to re-starts of the street car which occasionally occurs.

Based on these facts the following specifications had been agreed upon. The current drawn from the tram may not exceed a certain amount in order not to disturb any electrically powered tram equipment. Then the voltage has to be regulated to remove the voltage peaks from the transformer and to provide the operating voltage of 26 volts direct

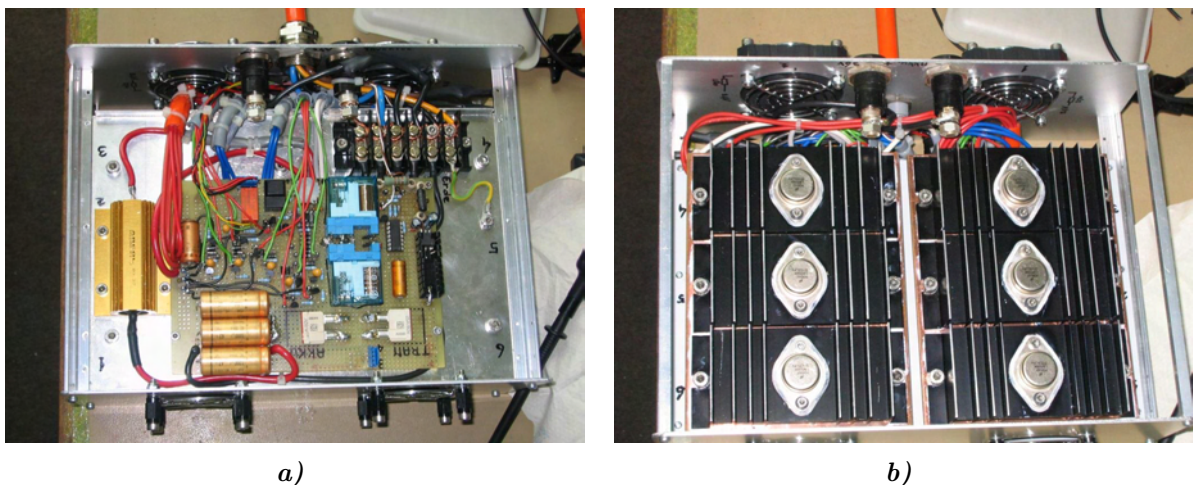


Figure 3.9: The purpose built power supply used in the measurement system. The top view (*a*) shows the control electronics that manages the power supply and the battery. The bottom view (*b*) shows the ventilated industry grade MOSFET-type power transistors .

current. In addition batteries had to be incorporated to bypass power outages. A charging circuit for the batteries had to be included as well. A custom-built uninterruptible power supply has been built [Sorber and Kehl, 2004] (see figure 3.9 and the schematics are shown in appendix A.2). Attached to this controlled power supply, different of-the-shelf converters had been installed to provide the various voltages needed for the sensors and other devices. Although many parts need a low direct current voltage, two devices require 230 volts alternating current (VAC). To power these, a high quality inverter had been installed as well. In total the complete measurement system draws between 400 and 750 watts, depending on the operation state of the sensors (normal operation versus heating/powering up).

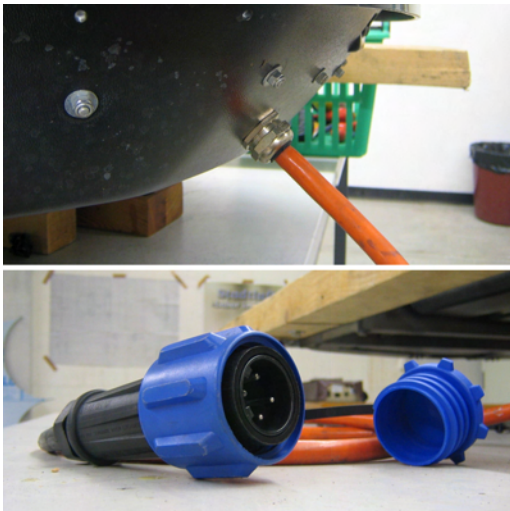
The power supply has a circuit to detect whether there is power from the tram or not.



a) The Buccaneer socket with a sealing cap.



b) Cables leading into the socket (view from inside the tram).



c) The cable from the measurement box and Buccaneer plug.



d) Contactor and fuse as a safety measure in the tram.

Figure 3.10: Photos of the electrical connection between the tram and the measurement system.

It also disconnects the measurement system from the tram's electrical system after an adjustable amount of time if the power has gone. This is a redundant safety measure to make the system shut down even if the computer failed to do so. To make the computer aware of the power status, a connector has been added to the power supply which outputs the power status and allows the computer to reset the timeout (see table A.3). The computer also monitors the battery and the power supply output voltages. The power supply has proven as very stable and 100% reliable.

For the electrical connectivity between the tram and the measurement system *series 900 Buccaneer* from *Bulgin* have been chosen for their IP68 rated properties which includes that they are environmentally sealed (see table A.2). On the roof of the tram a socket providing electricity for the measurement system was added. As protective measure it is connected to the tram's electrical system via a current limiting contactor. Since the socket is connected to the tram's direct current system and since this relays on batteries when the tram is disconnected from the overhead lines, a timer makes sure that the measurement system will be disconnected from the system after 20 minutes in any case. The power supply in the measurement system has never failed during the measurement campaigns and the current limiting contactor therefore has never been actually used. Refer to figure 3.10 and table A.1 on page 36) for photos and further details of this installation.

3.6 Computer & data logger

A low power and rugged industrial computer with passive cooling was selected to control the various sensors and devices as well as to log the data. The computer is a *MPL PIP7* (see figure 3.11) equipped with an Intel Pentium III CPU running at 400 MHz. It has an Intel 440BX chip set and the front-side bus (FSB) operates at 100 MHz. A 20 GB IDE hard drive was installed. The computer has several interfaces, including four opto-isolated RS232 ports, an IEE 1284 parallel port, a USB host controller, a 100BaseT network interface, an opto-isolated CAN bus interface, PS/2 and a PC104/104+ bus. The casing measures 25x16x7 cm³ and the system weights about 2.5 kg. It runs at 8–28 VDC and uses approximately 15 W. It was configured to power on automatically.

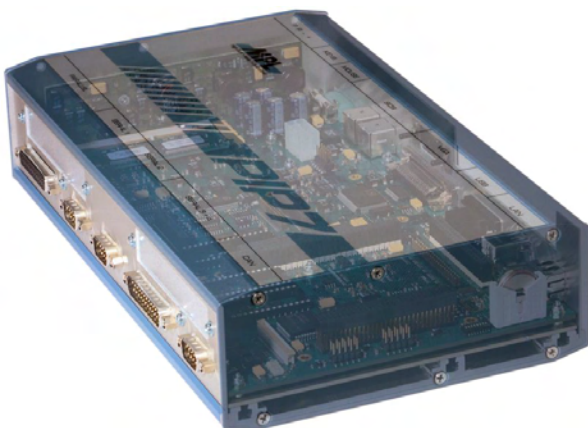


Figure 3.11: The *MPL PIP7* industrial computer.

Photo: MPI AG.

Debian GNU/Linux [Debian, 2002] was chosen as the operating system (OS) for the following reasons. It is customisable without constraints, including the possibility to

operate automatically and headless (i.e. without a monitor and a keyboard). It is furthermore well-established for systems where reliability and stability is critical. And last but not least the existing expertise of the OS at the GGL and the availability of free documentation allowed for the specialised setup used in this project.

The GNU compiler collection (GCC) [FSF, 2004] and related software was used to program low-level routines in the c programming language. These routines include relay control, signal input reading, serial communications, data logging and IP networking. Higher level programmes which control the measurement system were written in the Bash scripting language [FSF, 2002]. Many other tools available on Unix like operating systems were used as well.

Analog data were sampled by an A/D converter (*ICP Con Series 7000*) which had been connected to the computer by a RS232 interface. The resolution of the A/D converter is 1 mV. See table 3.1 for a list of the sampling range and the resulting sampling accuracy. A PC104 digital input/output board provided twenty opto-isolated inputs and twenty relay outputs. They were used to monitor signals and energise heavy duty industrial relays, respectively. The latter connected the sensors to the power supplies.

Sensor	Measurement range	Signal range	Accuracy
O ₃	1–250 ppb(v)	0–2.5 V	0.1 ppb (0.2 µg/m ³)
NO	0.001–200 ppb(v)	0–10 V	0.02 ppb (0.025 µg/m ³)
NO ₂	0.001–200 ppb(v)	0–10 V	0.02 ppb (0.038 µg/m ³)
particles	0–2000 µm ² · cm ⁻²	0–5 V	0.4 µm ² · cm ⁻²
temperature	-30–+70 °C	0–10 V	0.01 °C
humidity	0–100%	0–10 V	0.01 %
pressure	650–1020 hPa	0–1 V	0.37 hPa

Table 3.1: The sampling accuracy of the A/D converter depends on the measurement range used and the signal range output by the sensors. See also section 3.3 and compare table 2.1.

3.7 Telemetry

Since the street car has been in operational use, it was not possible to access the roof and the measurement system respectively on a regular basis. To monitor the measurement system and the measurements without interrupting the tram operation, remote access and telemetry devices had been installed. Two low-cost technologies had been chosen to provide remote access to the system. For short range, high-speed connections a commonly used wireless network technology (WLAN, IEEE 802.11b) had been chosen. The used device is a *Netgear ME103 WLAN AccessPoint*. Long distance connections are established by the means of mobile communication technology as used by mobile phones (GSM, global system for mobile communication). The data or internet service offered by most providers is used to establish a relatively slow internet connection. A GPRS-to-Ethernet bridge was installed. The used device is a *CabTronix NavComBox* (figure 3.12). The size of the enclosure is 12·14·3 cm³. These connections are used to

download the measurement data, to update the software and to transmit the readings and occasionally alarms in real time (see section 4.2.3). Ethernet networking inside the measurement system was established by *100BaseT Cat. 5*¹ cables and a *Netgear FS105 5 Port 10/100 Mbps Switch*.



Figure 3.12: The GSM communication system consists of a GPRS/GSM gateway (*a*) and an antenna (*b*).

* * *

¹ An abbreviation describing the type and quality of wires and connectors used and the nominal speed rating.

4

Measurement Campaigns & Data Processing

4.1 Tram operation and tram lines

Various tram lines were evaluated regarding their suitability for the project [Schneebeli and Wegmann, 2002]. The choice was limited because the suitable tram only circulates on certain lines. However, the demand for a long line covering many different places in the city had been met by one of these. The chosen line number 11 (see figure 4.1) is about 11 km long and extends across the city from north to south. The line is characterised by an interesting height profile and encounters various different traffic types. The tram and the measurement system, respectively, pass busy as well as downtown pedestrian areas (410 m above sea level) and cover higher altitudes (470 m up to 520 m above sea level) as well. Furthermore, this line does not pass any tunnels or high bridges lying above the usual traffic. Therefore, it is assumed that the resulting measurements represent the different situations in an urban area sufficiently well.

A first campaign was carried out done on tram running on this line. Thereafter the VBZ carried out modifications to the tram (see section 3.1). Due to the deployment concept of the VBZ the renovated tram operated on different lines after the modification. Nevertheless, the two new lines (10 and 6, see figure 4.1) satisfied our demands well enough and even shared parts of the track at the busy site around the Zürich central station. Figure 4.1 shows a map of Zürich with the three tram lines used in this project and 4.2 shows the height profile and the stop names of the tram lines. Figure 4.3 is a bird-eye perspective of the tram lines that emphasises the topography.

The tram tracks in Zürich mostly run in the middle of streets accompanied by lanes for private and commercial transport on each side. On straights the tracks in one and the opposite direction are separated by about 3.5 m. The separation is larger (about 4.5 m) in curves and at several places, for example at tram stations, at track intersections and branches or on squares, the separation is up to 10 m. At both ends of a tram track there are either end loops (diameter about 30–50 m) or, where the available space does not allow the latter, alternate routes to change to the opposite driving direction. Compare section 4.3.4).

A tram track for a certain line may change in length during the day for example if a part of the track is only serviced during the day. Another reasons for not changing the direction at an end loop include the changes in intervals of trams during the day (e.g. rush-hours versus late evening) and unplanned changes on the time table. Furthermore trams may return to a workshop for service, cleaning or repair according to schedule or unexpectedly in case of a failure. Figures 4.4 and 4.5 show the operating hours of the tram on the used tram lines.

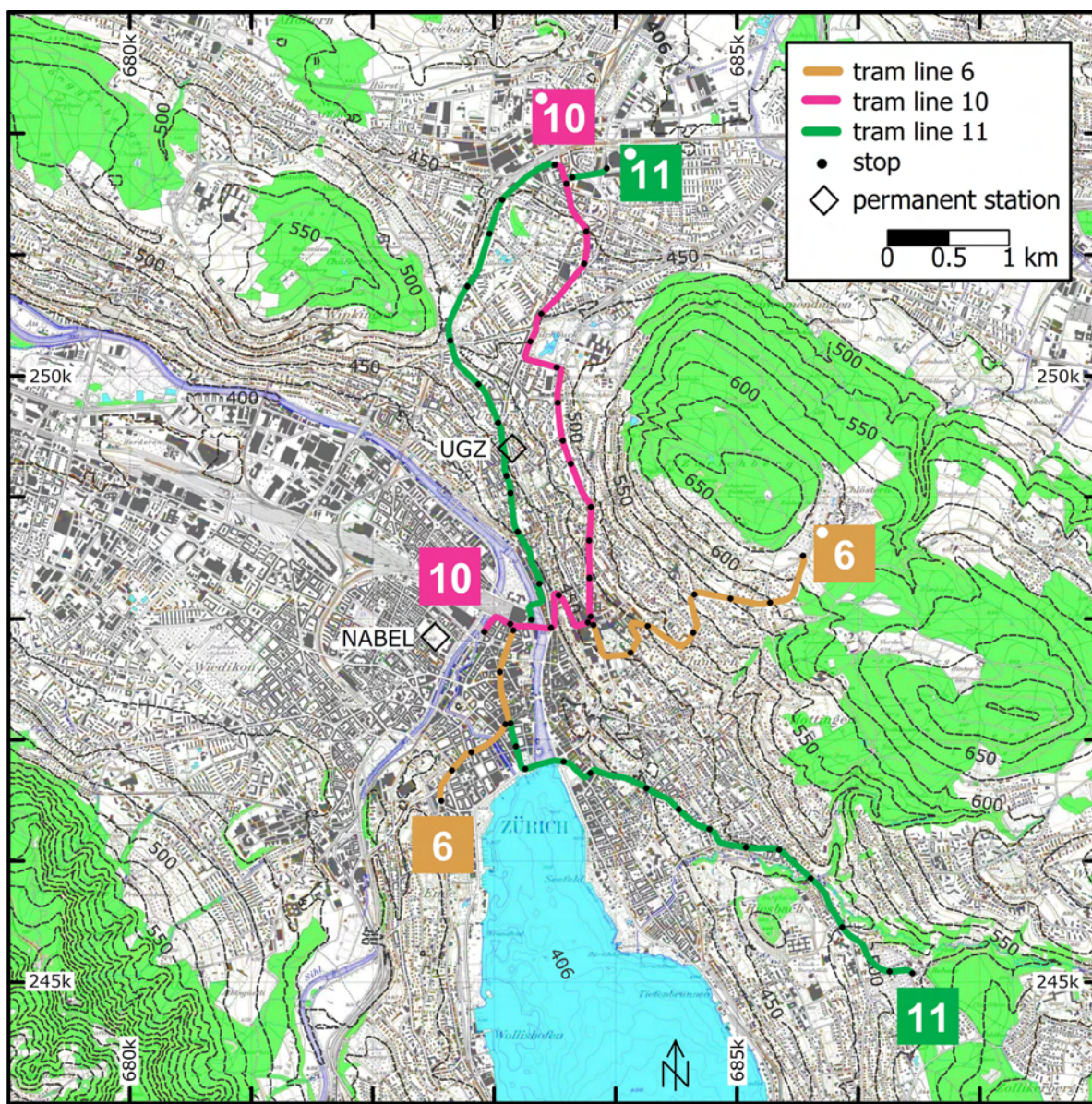
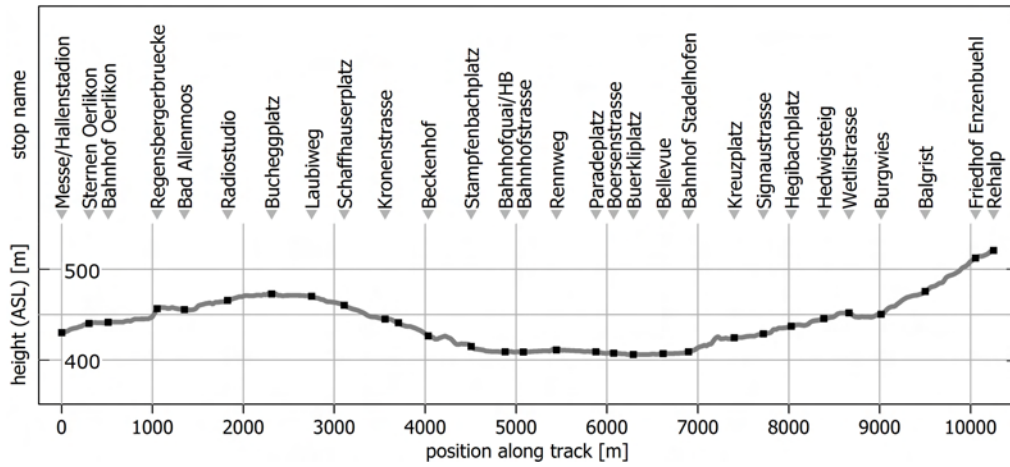
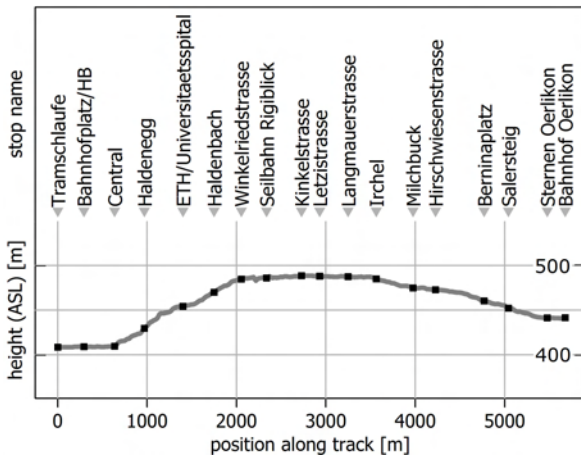


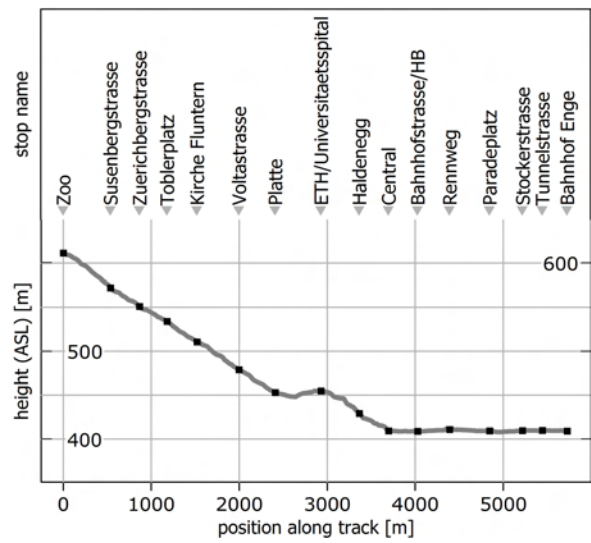
Figure 4.1: Map of Zürich with the tram tracks used in the measurement campaigns. The tram tracks are plotted in the official colours used by the public transport operator. Black points on the track represent stops (see figure 4.2 for the stop names). The numbered squares mark the ends of the tracks. The white points in the squares indicate the beginning of the track (position along track co-ordinate 0 m, compare figure 4.2). The diamonds mark the two permanent air quality monitoring stations from the NABEL network and communal environmental office (UGZ).



a) tram line 11



b) tram line 10



c) tram line 6

Figure 4.2: Tram lines track height profiles and station names. The position along the track is plotted versus the height above sea level (ASL) of the track (i.e. the terrain height). The station names correspond to the black squares on the height profile (compare figure 4.3).

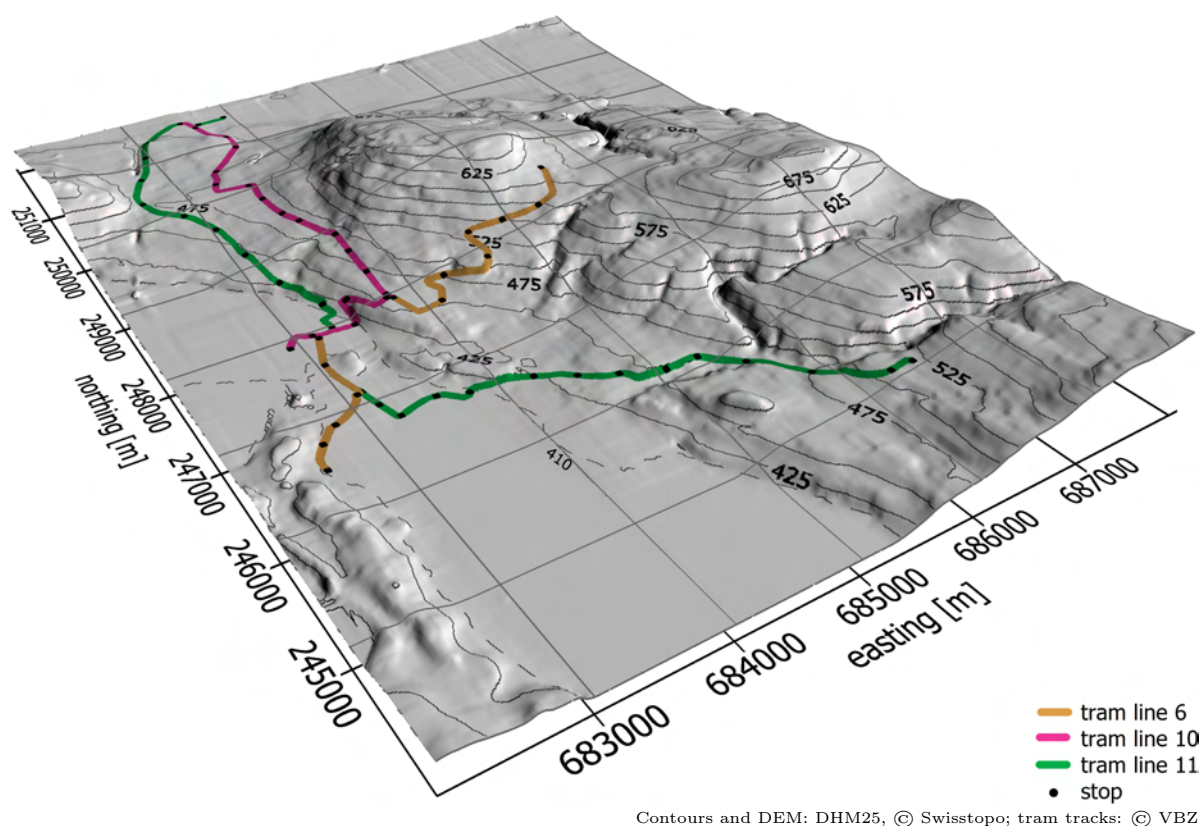


Figure 4.3: An extract from figure 4.1 rendered as a bird's eye perspective of the terrain with the tram tracks. The camera position is near south-west and the light source at south-east at 45° inclination. A 1 km grid and contour lines with 25 m equidistance are overlaid.

4.2 Measurement campaigns

4.2.1 Campaign #1

In 2005 the first campaign was carried out on the tram. The tram operated on line 11 (see section 4.1) during the whole campaign. Several technical difficulties not detected and corrected during the preceding testing at the laboratory caused some problems in data quality of the measurements. The difficulties included insufficient mechanical robustness, excessive heat in the measurement system, partly missing long-term experience with the operation of the environmental sensors, imperfect remote monitoring capabilities of the system and software problems (bugs).

A particular issue arose from the nitrogen oxide sensor (see section 3.3.1) or, more precisely, from its vacuum pump. The highly specialised pump was modified to DC. While the pump head remained original, the actuation had been replaced with a DC motor. This supposedly changed the heat tolerance characteristics of the pump (the original AC motor had different dimensions and included a ventilator). This was accompanied by the unexpected wear of the pump's membranes which made it impossible to obtain usable readings from the sensor. Later, and probably in correlation with the increasing ambient air temperatures, the pump's bearings failed and as a consequence

the motor broke down. A replacement had not been available off-the-shelf. Thus it was decided to stop the campaign and improve several technical aspects of the measurement system.

Another problem affected the GPS measurements. A software bug in the GPS data recording programme regularly caused corruption in the registered data. This error was not obvious from the positioning data transferred to the online visualisation (see section 4.2.3). It was until the end of the first measurement campaign when the problem which first had been related to the expected degraded navigation availability in urban areas (compare section 2.2.4) was identified and corrected. Nevertheless, enough GPS data was available to generate enough positions in order to georeference all the environmental measurements during (see section 4.3.4).

Usable data was collected on more than 82 days of the campaign (see figure 4.4). Because of the technical problems described above nitrogen oxide measurements are only available on a few days (see figure 5.4a/b on page 68).

4.2.2 Campaign #2

A second campaign was carried out from December 2005 to the beginning of June 2006. In the meantime the tram was converted to a longer tram with an added low-floor middle element (compare section 3.1). The installation of the measurement system had not been changed.

The time between the campaigns was used to improve the measurement system based on the experience made in the first campaign. The changes made to the system are as follows.

The overheating of the vacuum pump was improved. An additional ventilation was added in proximity to the pump. A thermostat was added to the main ventilation system and the maximal air flow through the system was increased. Nevertheless, over-heating became an issue with raising ambient air temperatures and insolation at the end of the campaign.

A nitrogen oxides sensor calibration equipment consisting of two flow controllers and gas bottles with zero air and NO calibration gas were acquired. Tests at the laboratory and occasional calibrations during the campaign showed a good stability of the calibration.

The real-time visualisation of the measurements was extended (see section 4.2.3). Routines to display the status of the sensors were added. Special attention was paid to the nitrogen oxides sensor. The extended version of the visualisation application provided an extensive display of the current condition of the sensor.

The sampling rate of the A/D converter was increased from 0.1 Hz to 0.5 Hz in order to meet the requirements of the sampling theorem. The oversampling factor is 2.5.

Several improvements to the software were added. These included the possibility to access the system from remote via GSM/GPRS (compare section 3.7), improved logging routines and additional signals (alarms) monitored.

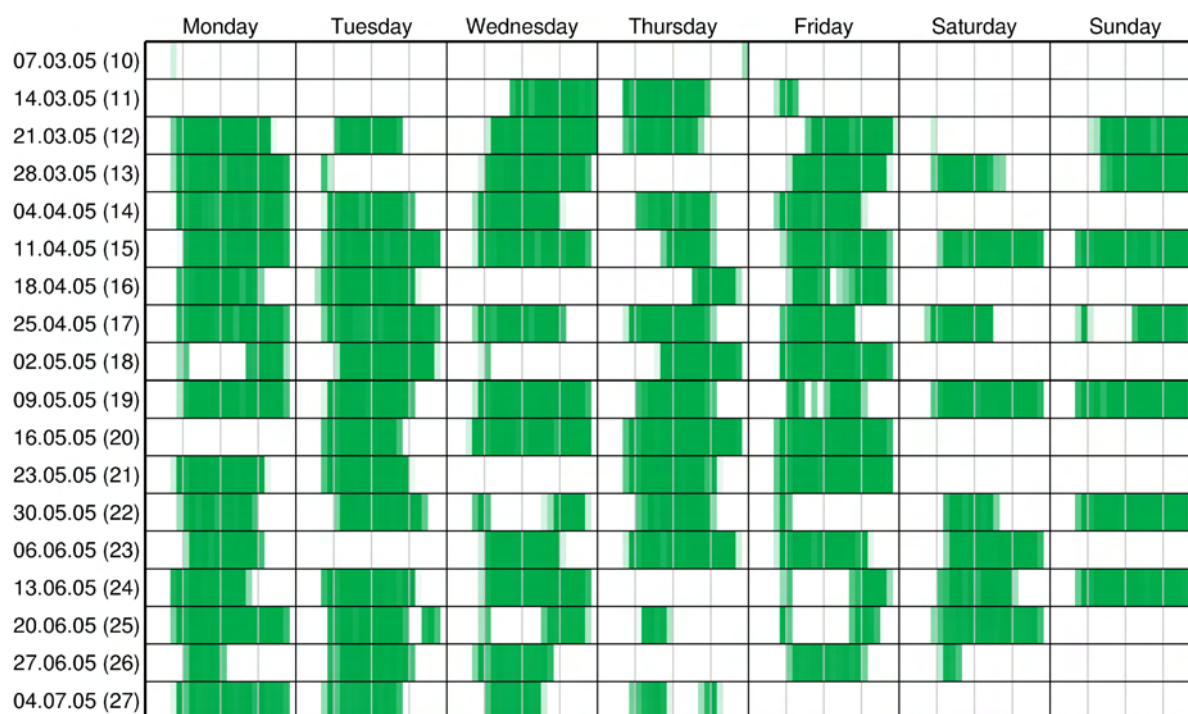


Figure 4.4: Summary of the data availability during campaign #1. The grid is arranged in columns for every day of the week. The lines correspond to the weeks. The labels on the left display the date of the respective Monday and the week number in parenthesis. The minor divisions (grey vertical lines) divide the day into four parts at 6, 12 and 18 o'clock UTC. Local time (central European time, CET) is one hour ahead of UTC. In addition daylight saving time (DST) was effective from March 25, 2005. The coloured areas (green for line 11, compare figure 4.1) reflect the hourly availability of data. Saturated green equals the total (100%) availability during the whole hour and a lighter green means that data is available only for a part of the respective hour (usually at the beginnings and ends of a measurement period). However, note that this availability does not include NO_x measurements (compare section 4.2.1).

The changes allowed for a successful second measurement campaign during winter 2005/06 and spring 2006. Since the conversion of the tram the concept of the public transport changed. Where a certain tram had been assigned to a certain line in the first campaign a more flexible system was introduced. It had been planned that the measurement tram operated on lines 6 and 10. The operator agreed to dispatch the tram with priority according to the projects demands. These were to minimise the changes of lines in order to obtain successive measurements on the same line (compare section 4.1). Figure 4.5 shows the availability of data on the lines 6 and 10 from the second measurement campaign. Data was collected almost consecutively on more than 67 and 43 days on line 10 and 6, respectively. A 15 days outage of the ozone monitor occurred in February 2006 due to a failure of the sensor's electronics (see figure 5.4c on page 68).

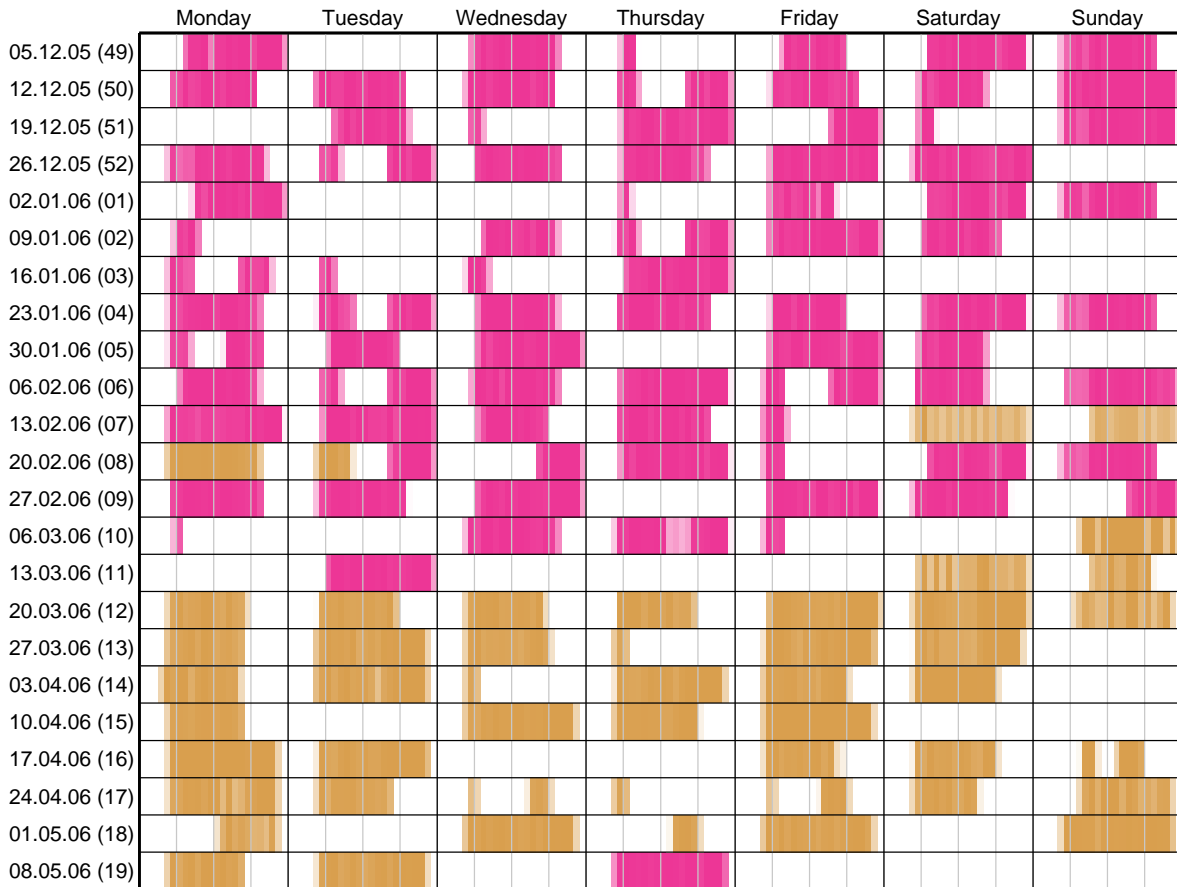


Figure 4.5: Summary of the data availability during campaign #2. The grid is arranged in columns for every day of the week. The lines correspond to the weeks. The labels on the left display the date of the respective Monday and the week number in parenthesis. The minor divisions (grey vertical lines) divide the day into four parts at 6, 12 and 18 o'clock UTC. Local time (central European time, CET) is one hour ahead of UTC. The coloured areas (pink for line 10 and orange for line 6, compare figure 4.1) reflect the hourly availability of data. Saturated colour equals the total (100%) availability during the whole hour and a lighter colour means that data is available only for a part of the respective hour (usually at the beginning and end of a measurement period). The first two third of the measurement campaign was carried out on line 10 (pink) and the last part was conducted on line 6 (orange).

4.2.3 Real-time visualisation of the measurements

An element of the project definition was to provide a real-time monitoring of the air quality. An Internet application was designed to visualise the measurement data as well as monitor the system performance [Kehl, 2005]. The data was transmitted by the measurement system by the means of mobile communication (see section 3.7). Several tasks on the computer, including the GPS data logger, the environmental sensors data logger and watchdog programmes, sent datagrams to a dedicated server at the laboratory (GGL). The user datagram protocol (UDP) which relies on the Internet protocol (IP) was chosen as the appropriate means to transport the data to the server. UDP is a connectionless protocol. Unlike the much more widely used transport control protocol

(TCP) UDP does not need any handshakes and transport control mechanisms. This is a great advantage on Internet connections with a low available transmission capacity (bandwidth). The drawback is that the sender does not know whether the datagram arrived at the destination and thus cannot decide to re-transmit in case of a failure. But the Internet connections used had proved very reliable as very few packet losses were encountered. Furthermore, a lost datagram would not be crucial to the real-time visualisation due to the frequent updates. The GPS positions, satellite information and the environmental measurements of the sensors were transferred at 0.1 Hz. The watchdog programmes sent status datagrams upon changes in the monitored states and regularly at intervals of 60 seconds. On the server (a Linux workstation at the GGL) a programme listened on incoming datagrams. It tested the validity of the data and stored valid datagrams into a log file & the latest readings and states into dedicated files. The latter were then used by the web application to update the visualisation.

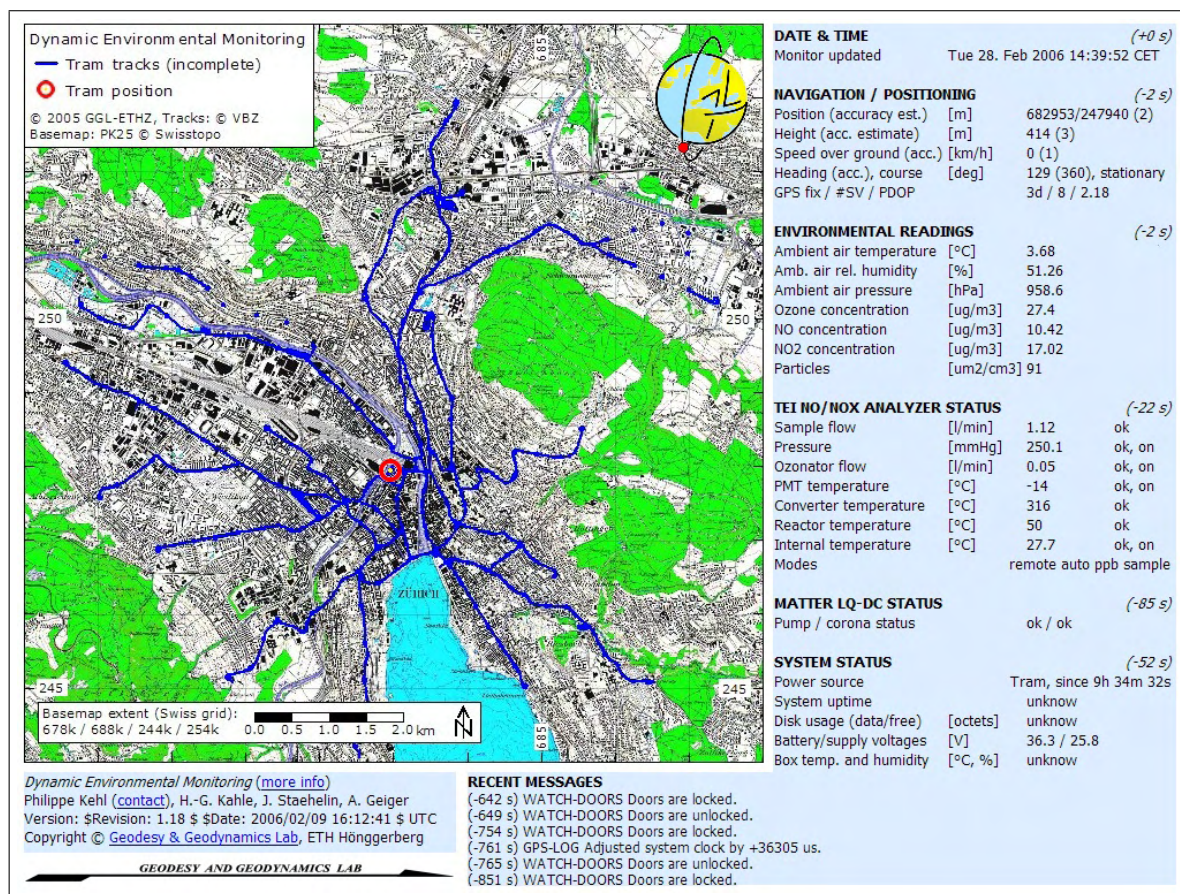


Figure 4.6: A screenshot of the real-time visualisation. The top left part of the screen is a map of Zürich with the tram tracks network (blue lines). The tram’s position is indicated by the red circle. The circle would pulsate on a computer screen for improved visibility. The blue area on the right and at the bottom right shows the latest readings, states and events from the measurement system. The times displayed in parenthesis determine the age of the respective information relative to the time stamp at the top of the blue box. The web page would automatically synchronise to the measurements and update every ten seconds.

The visualisation was available as a web page. It was compiled on demand by a PHP [PHP, 2002] programme using standard HTML [Le Hors et al., 1999] and CSS [Bos et al., 1998] markup language. The web page was optimised for a standard screen (XGA resolution of 1024 by 768 pixels) and worked in all common web browsers (preferably in full-screen mode). Figure 4.6 is a screenshot of the live visualisation web page. At an exhibition during the the 150th anniversary celebrations of the ETH Zürich in spring 2005 a special version of the real-time display was being presented to the public. The measurements were plotted along the tram track on a map and projected on a big screen. Furthermore, environmental sensors and background information were showed to the audience and speeches were held.

4.3 Data post-processing

The main goal of the data post-processing is to obtain a data set of georeferenced environmental measurements from the raw data. The raw environmental sensors readings were stored in flat ASCII files. The GPS measurements were stored in files in the receiver's native binary format. Each time the measurement system was started a new set of files was created. These files are the basis for the post-processing. Figure 4.7 shows the flow chart of this process.

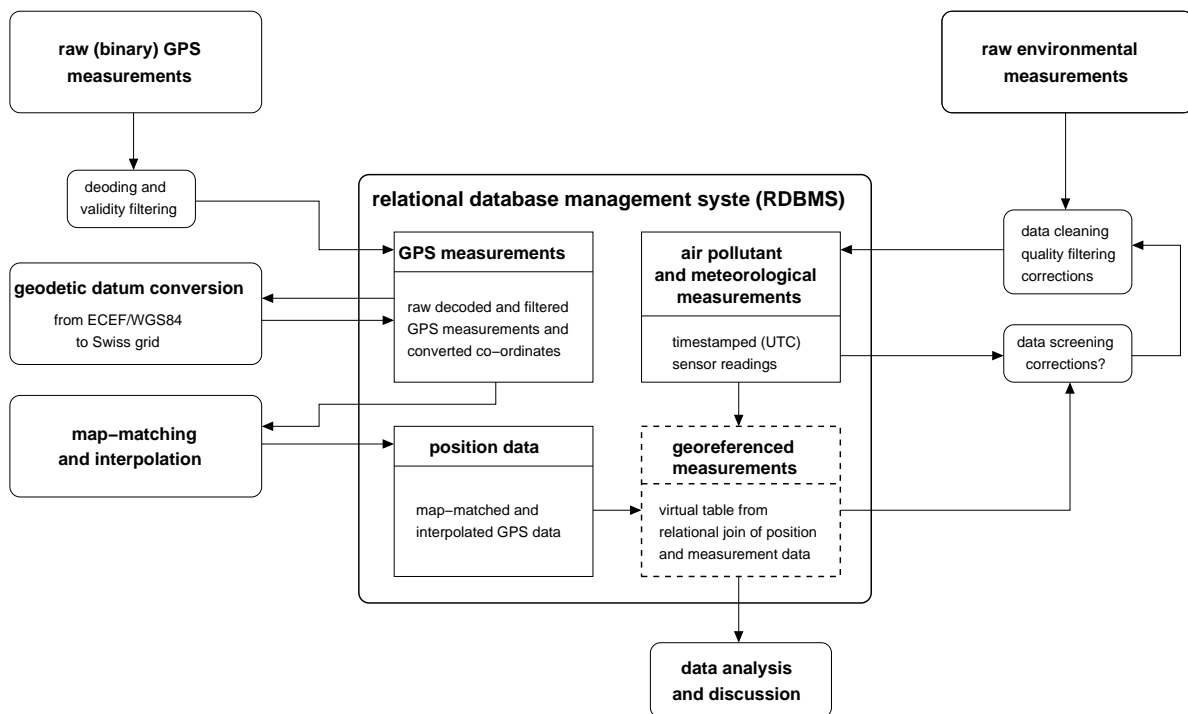


Figure 4.7: The data post-processing flow chart. The box in the centre represents the data repository in the relational database management system (RDBMS). It holds three tables for the quality filtered GPS and measurement data (top left and right) and a table with the calculated position data (bottom left). The virtual table at the bottom right is constructed from a relational join of the two adjacent tables. The left and right parts of the flow chart represent the raw data input and post-processing of the GPS and the environmental measurements, respectively.

4.3.1 Database

A relational database management system (RDBMS) was chosen as a repository for the measurement data. The RDBMS chosen is SQLite [Hipp, 2004]. As the name implies it is a lightweight SQL database. It implements most of the SQL-92 standard and allows most complex queries. The programme consists of a single binary (or a single programming library). The database is stored in a single file which makes it independent from large servers or sophisticated infrastructure. The database can be moved to and used on different computers or platforms without any difficulties.

The programming library has bindings to a large number of programming languages. In the post-processing shell scripts [FSF, 2002] and the interactive SQLite terminal were used to insert into, modify and extract from the database.

4.3.2 Environmental measurements

Figure 4.8 shows a time series of raw NO_x, O₃ and particulate matter measurements for one day (December 25, 2005). This day serves as an example to illustrate the post-processing procedure. The raw measurements were screened and filtered for errors (unreliable or wrong data) and then inserted into the database (table 4.1). The filtering included the clipping of readings from the warmup phase of the sensors and readings which were not in the measurement range (see table 3.1). Plots such as in figure 4.8 and, in a later stage of the post-processing, as in figure 5.1 (page 64) helped to identify further issues regarding the data quality. If a problem was detected, the data in the database was modified. Thanks to the RDBMS used as a data repository such changes immediately affected the output of the post-processing. It easily allowed for an iterative screening and filtering of the raw data. This proceeding proved to be advantageous for the spatial-temporal nature of the data for which significant plots are not trivial to create. The mass per volume concentrations were calculated from the raw number per volume readings according to the principle described in section 2.1.3.

4.3.3 GPS measurements

The GPS sensor (see section 3.4) was configured to fixed parameters which allowed the autonomous operation of the receiver. This includes fixed output rates of positions, navigation parameters and SV information at 1 Hz and UTC time at 0.2 Hz. The latter was used to keep the data logger's real time clock (RTC) and the time stamps of the environmental sensor readings in sync with UTC. Upon power on of the measurement system the receiver gets powered and starts to initialise itself. The time to the first (position) fix depends on the length of the off-time and the validity of the stored satellite orbits (almanac and ephemeris data). Theoretically the receiver is fully operable latest 15 minutes after the first satellite signal has been acquired. The trams are turned at least several minutes before they start operation so that the GPS was up before the tram went into service. Figure 4.9, detail A, exemplifies stationary GPS measurements for more than one hour at the workshop (depot) in the early morning. This is the common case.

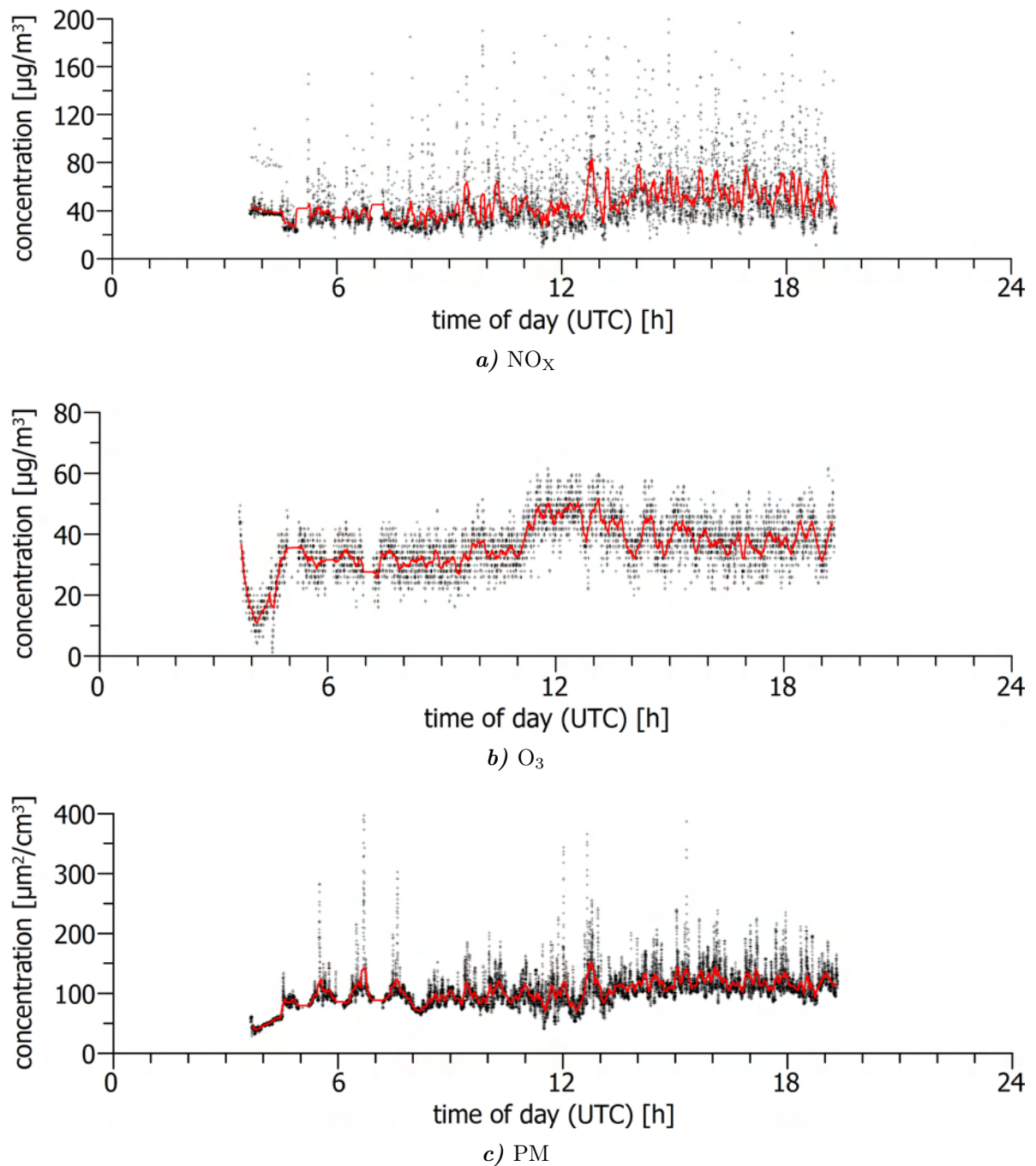


Figure 4.8: An example of the raw environmental measurements on one day (December 25, 2005) on tram line 10 (see figures 4.1). Outliers beyond the y axis limits are clipped in these plots. The red line is a running average with window size of approximately 1.5 min.

Attribute	Type	Description
timestamp	integer	POSIX timestamp [s]
mjd	real	MJD timestamp (UTC) [d]
datestring	text	timestamp in the form <i>DD.MM.YYYY HH:MM:SS</i> (UTC)
temp	real	temperature [°C]
rhum	real	relative humidity [%]
ahum	real	absolute humidity [g/m ³]
press	real	absolute pressure [hPa]
part	real	particles concentration [$\mu\text{m}^2 \cdot \text{cm}^{-2}$]
o3ppb	real	O ₃ concentration [ppb]
o3	real	O ₃ concentration [$\mu\text{g}/\text{m}^3$]
noppb	real	NO concentration [ppb]
no2ppb	real	NO ₂ concentration [ppb]
noxppb	real	NO _x concentration [ppb]
no	real	NO concentration [$\mu\text{g}/\text{m}^3$]
no2	real	NO ₂ concentration [$\mu\text{g}/\text{m}^3$]
nox	real	NO _x concentration [$\mu\text{g}/\text{m}^3$]
importid	integer	id which identifies the raw measurements file

Table 4.1: The *measdata* table in the relational database management system (RDBMS) used as a repository for the measurement data. This table hold the data obtained from the environmental sensors with timestamps (synchronised with the GPS data timestamps, see table 4.2). Missing data is marked by a NaN (not a number) value.

The GPS receiver (see section 3.4) has a built-in Kalman filter. The filter’s dynamic platform model was configured to “automotive” (other model options include “stationary”, “pedestrian” and “airborne”). This option matched the expected movements of a streetcar well [Forster and Landtwing, 2004]. The GPS sensor also features a receiver autonomous integrity monitoring (RAIM) which incorporates range checks, delta range checks and Doppler checks (all set to “on”). Further relevant parameters used are: static hold threshold (set to “off”), allow almanac navigation (set to “on”) and input and output filters (both left at defaults). The output from the GPS sensor, hereafter called raw GPS data, is actually the output of the on-board Kalman filter.

The raw binary GPS data was checked for validity and decoded into ASCII data according to the receiver’s manual [Vogel and Nigg, 2002] using a programme developed at the GGL. The values were stored in the database in the table *gpsdata* (see table 4.2). Further programmes (also proprietary GGL routines) were used to carry out the precise WGS-84 to Swiss grid co-ordinate transformation described in section 2.2.5.

4.3.4 Map-matching and interpolation

To overcome the often degraded navigation accuracy and availability in urban areas (compare section 2.2.4, see detail B in figure 4.9) a technique was developed to provide precise and reliable position data. Elements of this technique were studied and developed in [Forster and Landtwing, 2004; Bentz, 2005; Rossinelli, 2006]. The technique involves filtering and projective map-matching to exclude faulty positions and determine precise

Attribute	Type	Description
timestamp	integer	POSIX timestamp [s]
mjd	real	MJD timestamp (UTC) [d]
datestring	text	timestamp in the form <i>DD.MM.YYYY HH:MM:SS</i> (UTC)
tow	integer	time of GPS week [s]
week	integer	GPS week
lat	real	latitude (WGS-84) [°]
lon	real	longitude (WGS-84) [°]
hae	real	height above (WGS-84) ellipsoid [m]
hmsl	real	height above sea level [m]
x	real	easting in the Swiss grid [m]
y	real	northing in the Swiss grid [m]
z	real	height (Swiss height system) [m]
pdop	real	PDOP
pacc	real	position accuracy estimate [m]
numsv	integer	number of SV in view
svbitmask	integer	bitmask of SV used for navigation
svtext	text	comma separated list of SV used for navigation
speed	real	3d speed [m/s]
sog	real	speed over ground [m/s]
heading	real	heading [deg]
spdacc	real	speed accuracy estimate [m/s]
hdgacc	real	heading accuracy estimate [deg]
validtow	boolean	flag indicating a valid tow
validweek	boolean	flag indicating a valid week number
validutc	boolean	flag indicating valid UTC time (i.e. leap seconds known)
gpsfix	integer	type of position fix 3 = 3d, 2 = 2d, 0 = no fix
importid	integer	id which identifies the raw measurements file

Table 4.2: The *gpsdata* table in the relational database management system (RDBMS) used as a repository for the measurement data. This table holds the data obtained from the GPS receiver. It includes the geographic position, time information, satellite information, accuracy estimates and several validity flags. The Swiss grid co-ordinates are not obtained directly from the GPS receiver but are calculated from the WGS-84 co-ordinates.

positions. Furthermore standard position-time relations for the streetcars were determined to interpolate GPS outages. These last a few seconds up to a few dozens of seconds. The process transforms the GPS measurements into precise position data to georeference the environmental measurements. Figure 4.10 outlines this process.

The real tram track geometry was generalised to a one-dimensional line (**green line** in figure 4.10). The reason for this simplification was the ability to compare environmental measurements from the tram running in either direction easily. Therefore, a track geometry running in the middle of the two real tracks of each direction was defined. It was divided into elements of one metre length (**d_t**, **green markers**) which correspond to the (one-dimensional) position along the track (**green numbers**). This track is the position reference used in the map-matching and interpolation procedure discussed below

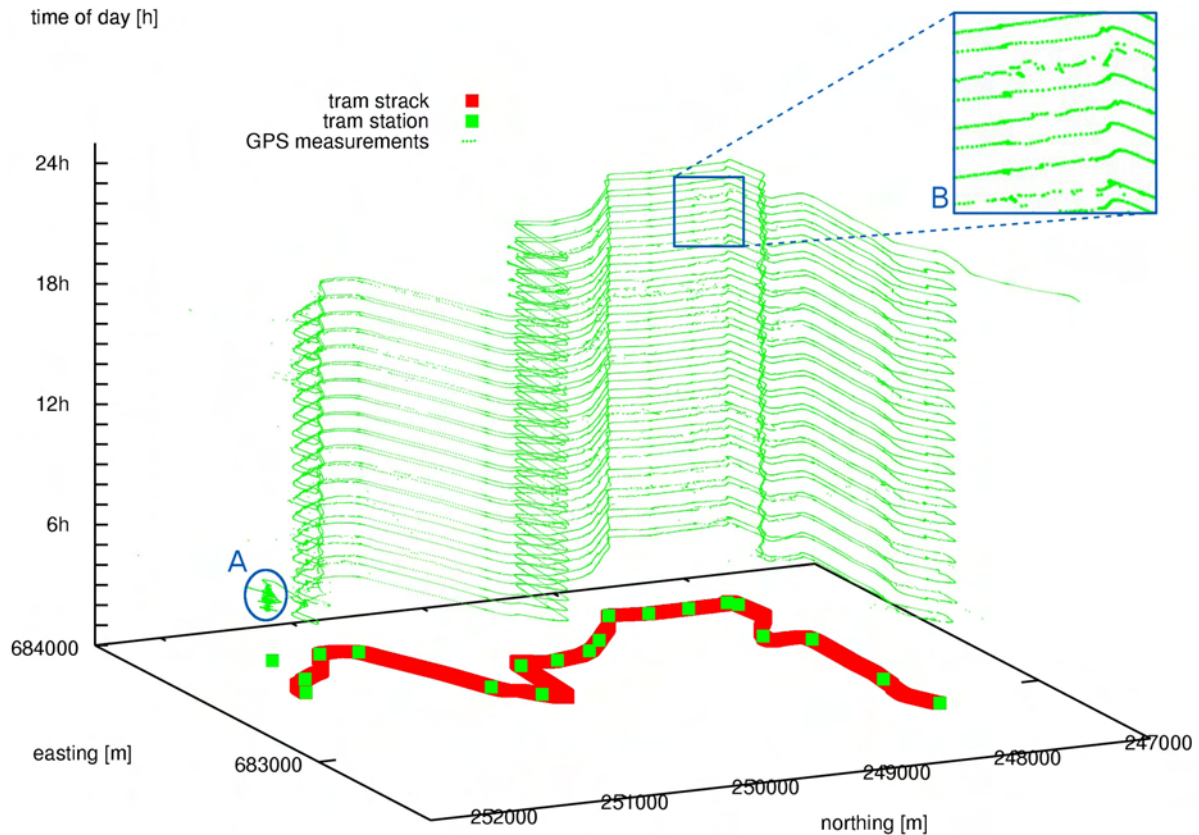


Figure 4.9: An example of measured GPS positions one day (December 25, 2005). The positions (green points) are Kalman-filtered and only good (3d navigation solutions) are depicted as a time series above the streetcar position (the vertical dimension shows the time of the measurements). The red line on the XY-plane corresponds to the tram track of line 10 (see figures 4.1 and 4.2). The stations (green squares) are plotted along it. The single green square off from the track corresponds to the depot where the tram starts in the morning. In the evening of this day the tram stopped in another depot from where it started again the next morning. Detail A shows stationary GPS measurements for more than one hour at the depot in the morning (compare section 4.3.3). Detail B magnifies an extract from the measurements which reveals degraded navigation accuracy and GPS outages.

as well as for the spatial data analysis in this report (chapter 5). The drawback is that the position along the track is slightly off from the real position. On most parts of the track (straights, curves) this error is below 2.5m and it usually stays below 10m (widening) (compare section 4.1 and the box in figure 4.10). At the end loops the error may be up to 25m. Then again, these errors are orthogonal to the driving direction whereas the variation of concentration along the track is of interest. For these reasons the generalisation of the real tracks to a one-dimensional geometry is considered adequate.

At most times (**A** in figure 4.10) the raw GPS positions would coincide with the tram's position except for a small error. A projective map-matching is done. The GPS position (**blue cross**) is projected onto the track geometry (**blue dotted lines**). If the deviation (**d**) is smaller than a certain maximal distance (**d_m**) it is assigned to the nearest track

point (red point). If the deviation is larger, the position is ignored (**D**). A value of 25 m was used for the maximum matching distance threshold d_m .

If the tram stops or moves very slowly the GPS positions start drifting (**B** in figure 4.10) as a result of the on-board filtering (compare section 4.3.3). The map-matching programme asserts that the tram does not move backwards (under normal conditions). It keeps track of the driving direction (**dd**) and only changes it if a certain threshold is exceeded.

Here (**B** in figure 4.10) the tram stopped and the positions drift backwards but the map-matched position stays at the same point. After some time and as the tram moves on, the positions and the GPS measured route (**blue line**) converge with the tram track and successive points are map-matched onto the track geometry.

The detection of a change in direction is done by looking ahead in the raw GPS data. The programme starts looking at the GPS position from t_r in the future of the currently processed position until it finds a position clearly ahead or behind on the track (with respect to the current driving direction). If that position lies ahead, a drift is assumed, otherwise the driving direction is changed. Then the map-matching algorithm continues.

The resulting map-matched positions are stored in the *gpsmatch* database table (see table 4.3).

At certain places GPS outages occur (compare section 2.2.4) and no positions are available by the sensor (**C** in figure 4.10). When the GPS reception begins again and positions are output, the map-matching continues.

Interpolation of missing positions (**C** and **D** in figure 4.10) was carried out on the map-matched position data in a separate programme. The routine finds the gaps in the data and interpolates the missing positions. For the interpolation standard position-time relations of the tram are used. These relations were determined for each track and each direction the measurement tram operated on [Rossinelli, 2006]. An extract from the corresponding curve that matches the start and end position of the gap is scaled to the missing period of time and the position at the missing times is determined. The interpolated positions were stored along the map-matched positions in the *gpsmatch* database table (see table 4.3).

The results of the map-matching and interpolation process were screened using plots analogue to figures 4.9 and 4.12. If a problem had occurred, manual corrections were applied where necessary and the process was re-run on the faulty part of the data.

4.3.5 Georeferencing

“To georeference” is a GIS term which means to geographically reference an object, often a raster map (e.g. an aerial image), to a co-ordinate system. Here the term means to establish a relation between the environmental measurements and the geographic position at which they were measured. The time stamps of the environmental measurements (table 4.1) as well as the time stamps of the position data (table 4.3) are synchronised to

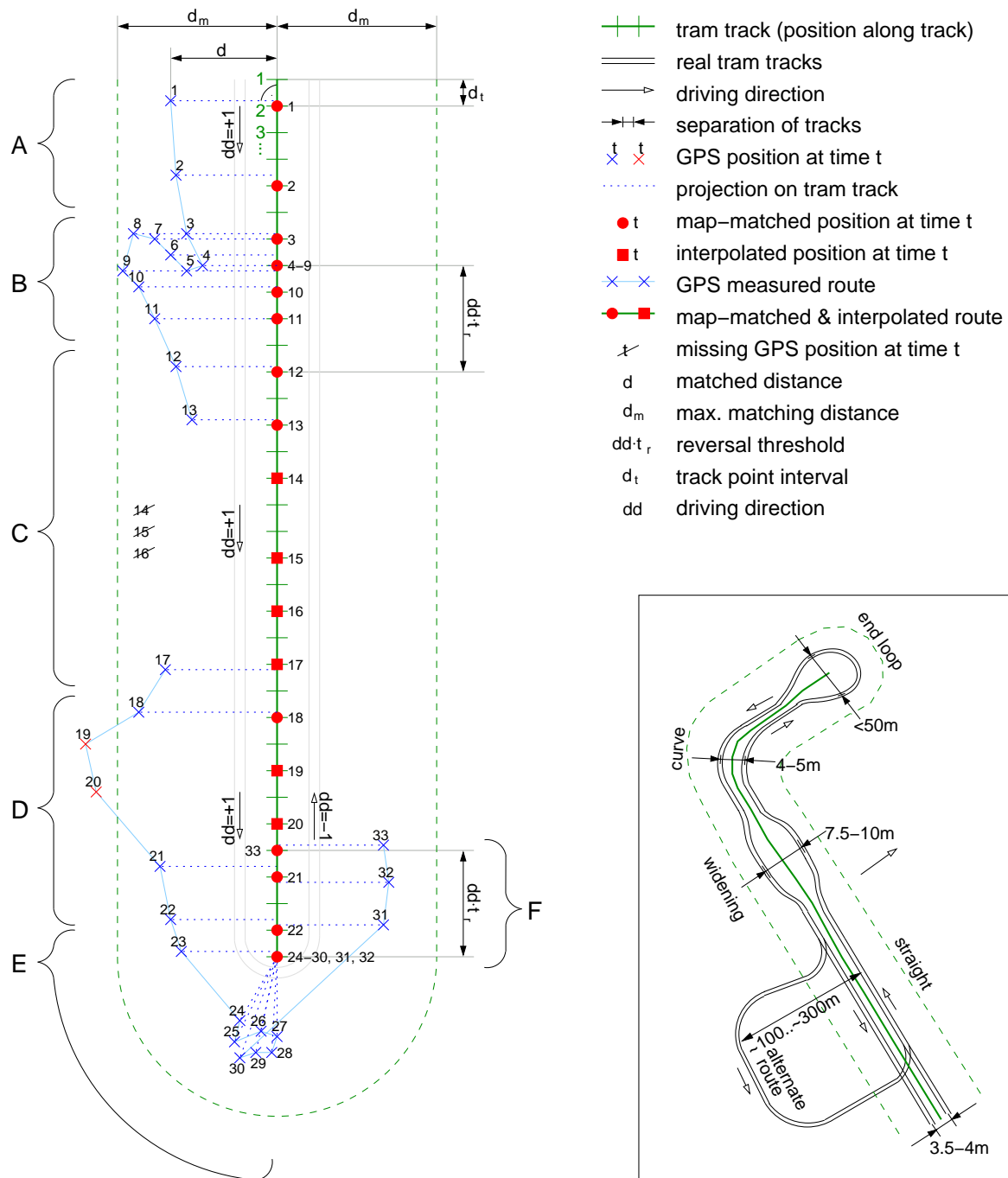
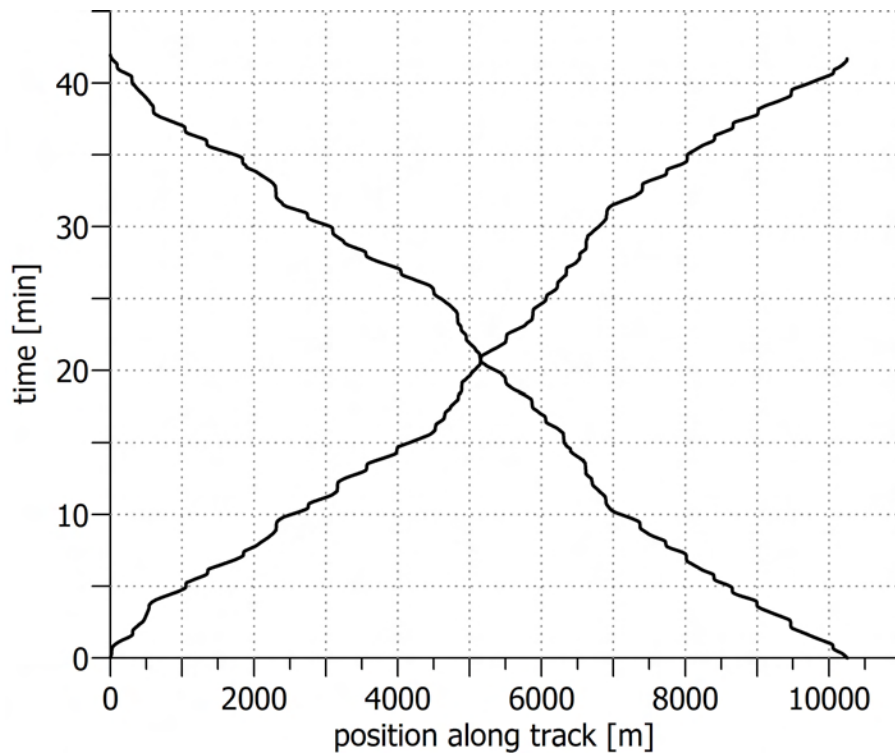
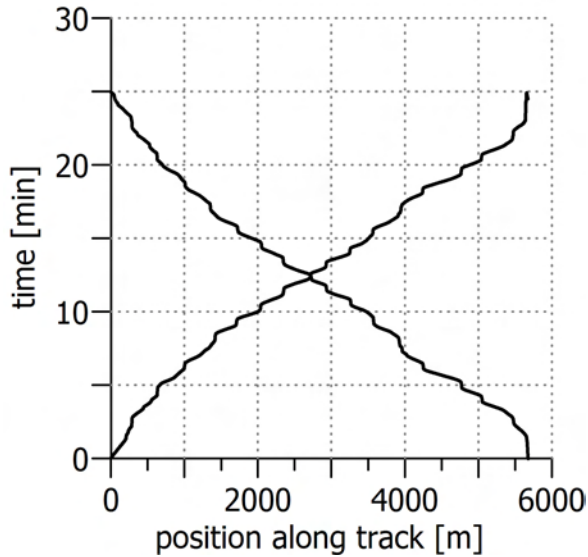


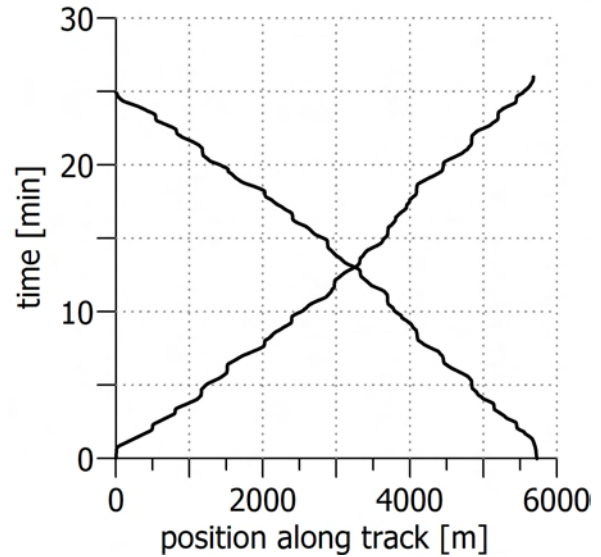
Figure 4.10: A schematic diagram of the GPS map-matching and interpolation process (left part, see section 4.3.4). The box at the bottom right is a generalisation of the common features of a tram track geometry (compare section 4.1).



a) tram line 11



b) tram line 10



c) tram line 6

Figure 4.11: The tram lines position time relations used for interpolation of missing positions. See section 4.3.4 and compare figure 4.2. The reasons for the differences in the shape of the curves between the runs in either direction include different traffic control, slopes and the generalisation of the tram track (see section 4.3.4).

Attribute	Type	Description
timestamp	integer	POSIX timestamp [s]
x	real	easting (Swiss grid) [m]
y	real	northing (Swiss grid) [m]
z	real	height (ASL, Swiss system) [m]
l	real	position along track [m]
line	text	id of the tram line
d	integer	direction, 1 = forward, -1 = backward
fillup	integer	flag, 0 = map-matched GPS measurement, 1 = interpolated
run	integer	enumeration of individual runs

Table 4.3: The *gpsmatch* database table contains the map-matched and interpolated positions (see section 4.3.4).

UTC. So they are used to establish the connection between measurements and positions, that is to georeference the measurements.

Thanks to the relational database management system, this was possible with a simple SQL query. It was defined as a virtual table (a view in SQL vocabulary) as follows.

```
CREATE VIEW v_meas AS
SELECT * FROM measdata JOIN gpsmatch USING (timestamp);
```

The resulting table contains all attributes from the joined tables of environmental measurements (table 4.1) and position data (table 4.3). It can be used (queried) like a normal table (e.g. *SELECT * FROM v_meas WHERE ...*).

Figure 4.12 is an example of the availability of georeferenced measurements. The overall availability of measurements is plotted in the figures 4.4 and 4.5 at the beginning of this chapter.

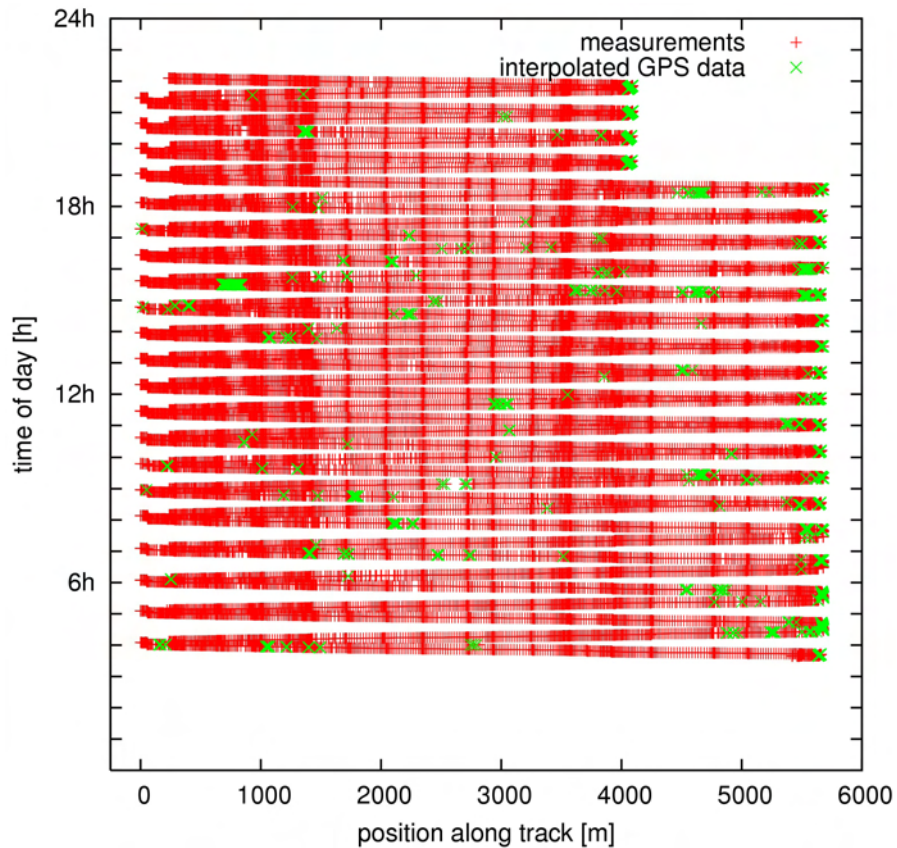


Figure 4.12: An example of the availability of georeferenced measurements one day (December 25, 2005) on tram line 10 (see figures 4.1). A cross is plotted for each georeferenced measurement. Red crosses represent map-matched positions and green crosses represent interpolated positions. The gap at the beginning of the ascending runs is due to the alternate route the tram travels to change the direction at this end of the track (compare section 4.1). Runs after 19 h (UTC) turn at the Milchbuck station (see figure 4.2. Due to the proximity of the loop to the track, the positions are interpolated rather than leaving a gap. The gap in the data at 2600 m / 9 h is due to an error in the data registration.

4.4 Permanent stations data

Data from two permanent measurement stations were used in this project. The stations are named NABEL and UGZ. NABEL is a station from the Swiss air quality monitoring network (see section 2.1.6) and UGZ a comparable communal station operated by the public authority of Zürich. The NABEL station is located in a park and is classified as an urban background station. The UGZ is located at a relatively busy street. Figure 4.1 shows the location of both stations. The data from the station were used for comparison and validation of the measurements from the tram (chapter 5) as well as for the dispersion modelling study (chapter 6).

Data for both stations was obtained from the respective authorities for the period from January 1 2005 until June 30 2006. The NABEL data is available as 10 minutes and 60 minutes averages (table 4.4) and the UGZ data is available as 30 minutes averages (table 4.5). The data was stored in a database using the system described in section 4.3.1.

The NABEL station is located at (Swiss grid): 682 515 / 247 850 / 409 [m].

The UGZ station is located at (Swiss grid): 683 150 / 249 400 / 457 [m].

Attribute	Type	Description
timestamp	integer	POSIX timestamp [s]
mjd	real	MJD timestamp (UTC) [d]
datestring	text	timestamp in the form <i>DD.MM.YYYY HH:MM:SS</i> (UTC)
no	real	NO concentration [$\mu\text{g}/\text{m}^3$]
no2	real	NO ₂ concentration [$\mu\text{g}/\text{m}^3$]
nox	real	NO _X concentration [$\mu\text{g}/\text{m}^3$]
o3	real	O ₃ concentration [$\mu\text{g}/\text{m}^3$]
pm10	real	PM ₁₀ concentration [$\mu\text{g}/\text{m}^3$]
noppb	real	NO concentration [ppb]
no2ppb	real	NO ₂ concentration [ppb]
noxppb	real	NO _X concentration [ppb]
o3ppb	real	O ₃ concentration [ppb]
timestamp	integer	POSIX timestamp [s]
mjd	real	MJD timestamp (UTC) [d]
datestring	text	timestamp in the form <i>DD.MM.YYYY HH:MM:SS</i> (UTC)
temp	real	temperature in [°C]
humid	real	relative humidity [%]
wspd	real	wind speed in [m/s]
wdir	real	wind direction in [°]
grad	real	global radiation [W/m^2]
brad	real	radiation balance [W/m^2]

Table 4.4: The *pollnabel* and *meteonabel* database tables, respectively, contain air quality and meteorological data from the NABEL permanent station. Each table is available for 10 and 60 minutes averages. The timestamps indicate the end of the averaging period. Missing values are marked as -9 999.

Attribute	Type	Description
timestamp	integer	POSIX timestamp [s]
mjd	real	MJD timestamp (UTC) [d]
datestring	text	timestamp in the form <i>DD.MM.YYYY HH:MM:SS</i> (UTC)
no	real	NO concentration [$\mu\text{g}/\text{m}^3$]
no2	real	NO ₂ concentration [$\mu\text{g}/\text{m}^3$]
nox	real	NO _X concentration [$\mu\text{g}/\text{m}^3$]
o3	real	O ₃ concentration [$\mu\text{g}/\text{m}^3$]
pm10	real	PM ₁₀ concentration [$\mu\text{g}/\text{m}^3$]
timestamp	integer	POSIX timestamp [s]
mjd	real	MJD timestamp (UTC) [d]
datestring	text	timestamp in the form <i>DD.MM.YYYY HH:MM:SS</i> (UTC)
temp	real	temperature in [°C]
humid	real	relative humidity [%]
wspd	real	wind speed in [m/s]
wdir	real	wind direction in [°]
press	real	absolute pressure [hPa]
grad	real	global radiation [W/m^2]
brad	real	radiation balance [W/m^2]

Table 4.5: The *pollugz* and *meteougz* database tables, respectively, contain air quality and meteorological data from the UGZ permanent station. The timestamps indicate the end of the averaging period. Missing values are marked as -9 999.

* * *

5

Data Analysis & Results

5.1 Overview over the available data

5.1.1 Raw time series

The data post-processing (see section 4.3) produced raw time series of the chemical species in a quasi two-dimensional way. The ambient air concentrations of the pollutants (the “sensor readings”) were referenced by an along track position (first dimension) and by the absolute time (second dimension). The along track position (in [m]) corresponds to the spatial position of the tram (see section 4.1).

The instruments provided mostly reliable measurements, which are compared with air pollutant measurements of two permanent monitoring stations in sections 5.3.1–5.3.4. A data quality assessment is discussed in section 5.2.

Figure 5.1 shows an example of post-processed pollutant measurements. A point is plotted for each measurement, coloured according to the ambient air concentration. Different colour scales (see scalebars below the plots) were used in order to visualise the highest measured values for each pollutant. Peak values beyond the scale are plotted in grey.

These raw time series reveal changes of ambient air concentration along the track as well as during the day. Places and times with high ambient air concentrations of nitrogen oxides (subfigures a–c) can roughly be identified. Particulates and ozone (subfigure d and e, respectively) show a more uniform distribution along the track and a smoother variability during the day. The raw measurements also reveal concentration peaks (purple and grey points), in particular for the particles measurements. The raw data needs further processing in order to be able to examine the temporal and spatial variability of the ambient air concentrations (see sections 5.3.5 and 5.3.6).

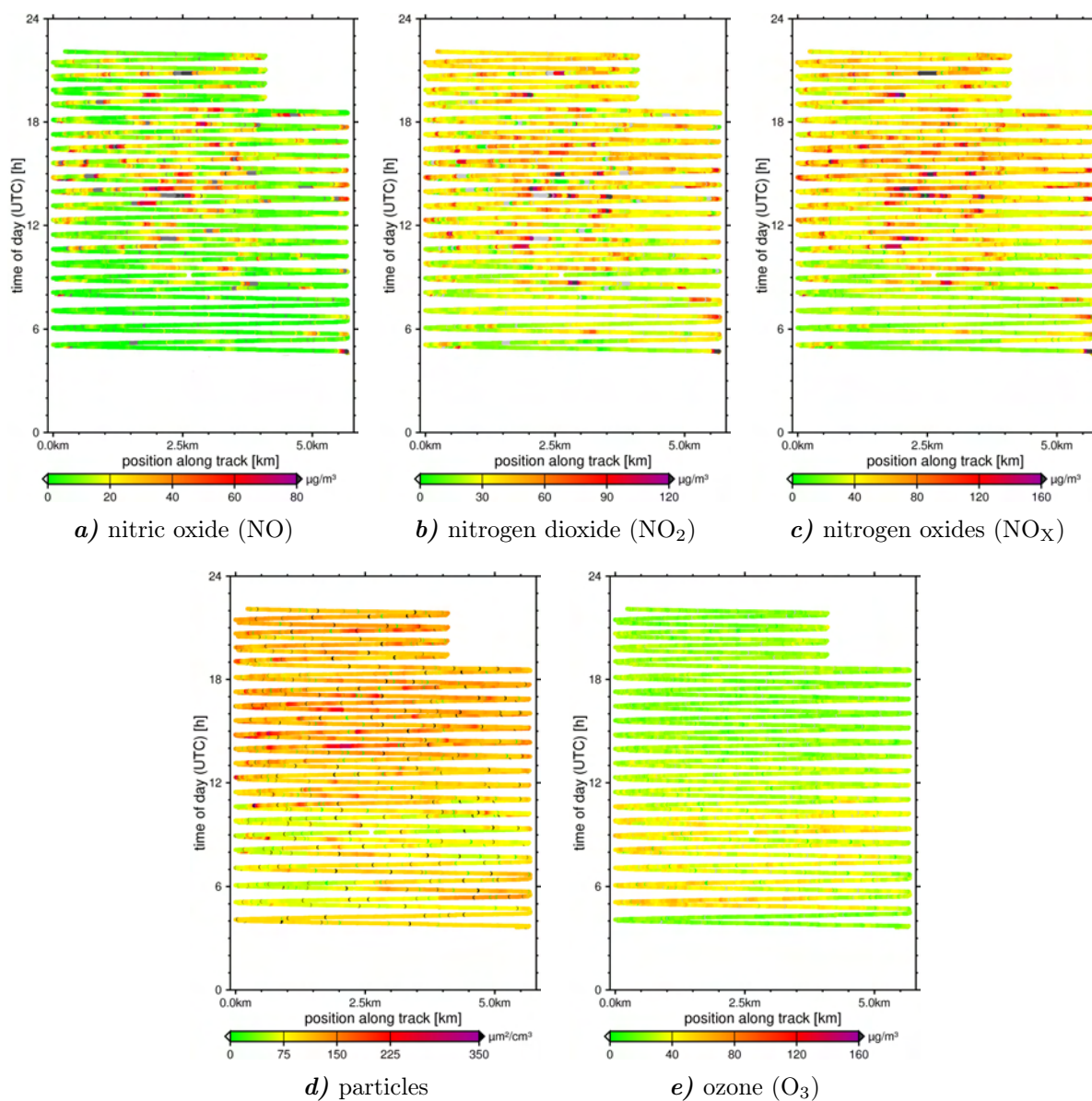


Figure 5.1: An example of the georeferenced environmental measurements on one day (December 25, 2005) on tram line 10 (see figure 4.1 on page 42). The plots are analogous to figure 4.12 (page 59) but show the measured values rather than only the availability. The colour bars are scaled individually for each plot in order to highlight the highest measured values.

5.1.2 Daily mean values

From the time series of measurements shown in the previous section (5.1.1) daily mean values were calculated in the following way for the whole data set from both campaigns (compare figures 4.4 and 4.5).

1. Hourly mean values were calculated from the raw measurements in the time domain (disregarding the positional dimension). No mean was calculated if less than half an hour of data was available.
2. Missing hourly mean values were then interpolated linearly. Gaps larger than 72 hours (3 days) were not filled and no extrapolation was done.
3. Daily mean values were then calculated from this data if twelve or more hourly mean values were available.

A similar processing was applied to the half-hourly and hourly values of the UGZ and NABEL, respectively, permanent monitoring stations. These stations, however, had only very little missing data, which was mostly connected to regular calibrations or maintenance of the instruments.

Figure 5.2 shows an example (four weeks in January/February 2006) of the daily mean values derived from the tram (subfigure a) and the permanent stations measurements (subfigures b and c). Note the four days ozone sensor outage on February 1–5, 2006, at the NABEL station (subfigure b) and the longer ozone sensor outage on the tram starting February 7, 2006 (compare section 5.2).

Figure 5.3 shows the same data as in figure 5.2, however, it is represented as comparisons of the tram measurements versus the permanent stations NABEL and UGZ (subfigures a and b, respectively) as well as the comparison between the two permanent stations themselves (subfigure c). The comparison indicate good agreement (compare section 5.3.1) between the three time series. This probably reflects, that the day to day variability of the two permanent stations and the tram measurements integrated along the tram track are basically determined by meteorology.

The complete time series of daily mean values (as in figures 5.2 and 5.3) are available in appendix B.1 (page 167ff).

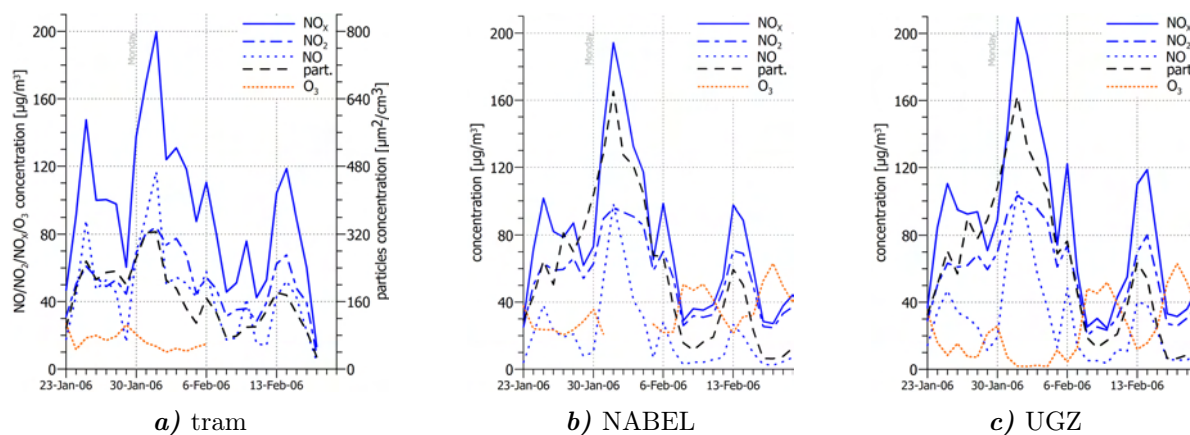


Figure 5.2: Example of the daily mean values time series derived from the tram measurements (a) and from the NABEL and UGZ permanent stations (b, c). The complete time series are available in appendix B.1 (page 167ff).

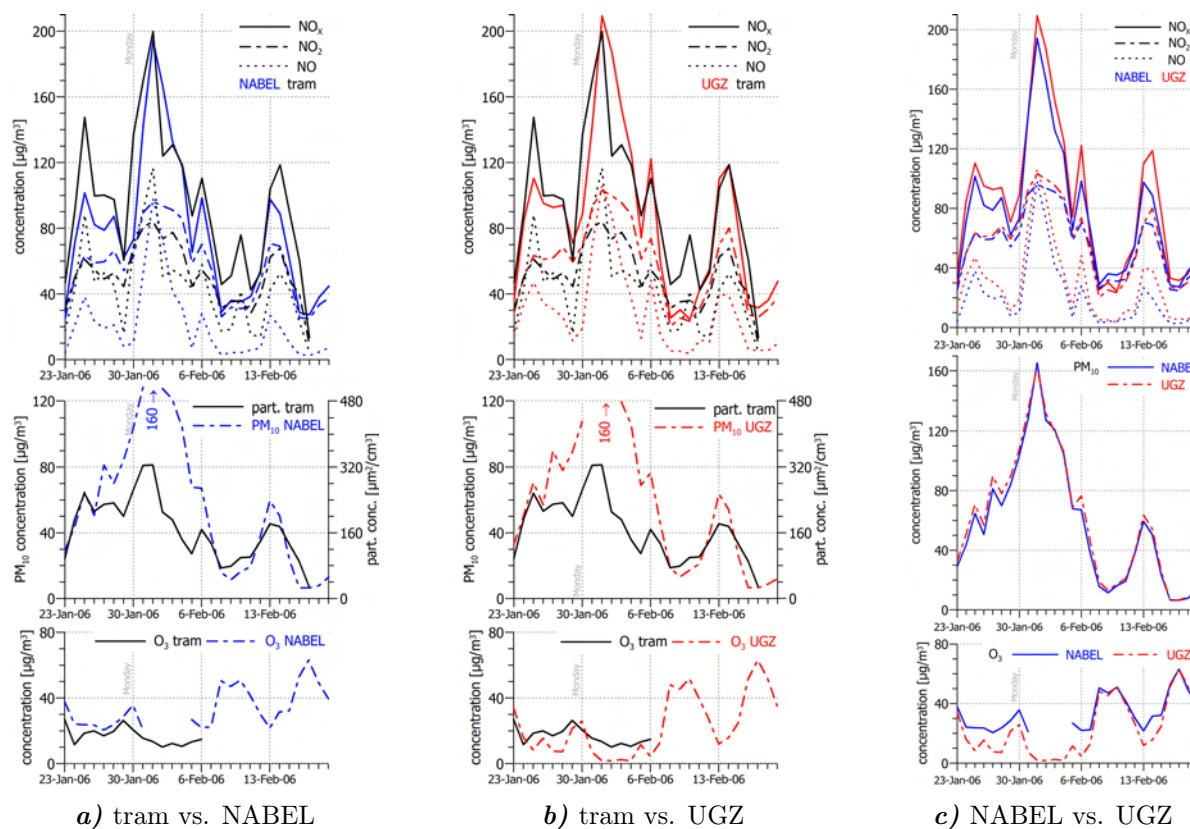


Figure 5.3: Example of the daily mean values time series comparison. The daily means derived from the tram measurements are compared with the daily means of two permanent stations (a, b). The comparison of the latter is shown in c. Note the outage of the ozone sensor on the tram on February 7–19 and the ozone sensor outage at the NABEL station on February 1–4. The complete time series are available in appendix B.1 (page 167ff).

5.2 Data quality assessment

The NO_x measurements of the tram suffered from technical problems in the first measurement campaign (see section 4.2.1). However, it was not an easy task to separate the suspicious measurements from the high quality measurements solely based on the documentation from the campaign. In order to make best use of the measurements the data quality of the NO_x measurements of the first campaign (spring/summer 2005) was assessed by comparison with the daily mean values of the permanent monitoring stations based on the data analysis presented in section 5.1.2.

Two periods with good NO_x measurements, which consist of several days of operation, were identified in the first campaign. They consist of:

1. 7 days from May 18–28, 2005 and
2. 10 days from June 23 – July 7, 2005.

The daily mean values derived from NO_x measurements during the second campaign in winter 2005/06 and spring 2006 are in good agreement with the daily mean values from the permanent stations. The correlation analysis revealed a correlation factor (r^2) of approximately 0.74 in the winter 2005/06 period (see section 5.3.1).

The daily mean values derived from the ozone measurements also shows a good agreement with the daily mean values from the permanent stations for certain periods. The agreement is best in the winter season and tends to be less obvious in the spring and summer seasons. The ozone sensor outage during the second campaign (compare section 4.2.2) affected 15 days from February 7–21, 2006 (see figure 5.4c).

The daily mean values derived from the particules sensor cannot be compared with the daily mean values from the permanent stations in the same way because two different measurement principles are involved and the values have different units “area per volume” and “mass per volume”, respectively (compare section 3.3.3), which cannot be converted to each other. However, the curves tend to follow a similar pattern over time.

See figures B.4–B.7 in appendix B.1 (page 167ff) for the complete time series of the comparison of the daily mean values.

See section 5.3.1 for a justification for this data quality assessment proceeding.

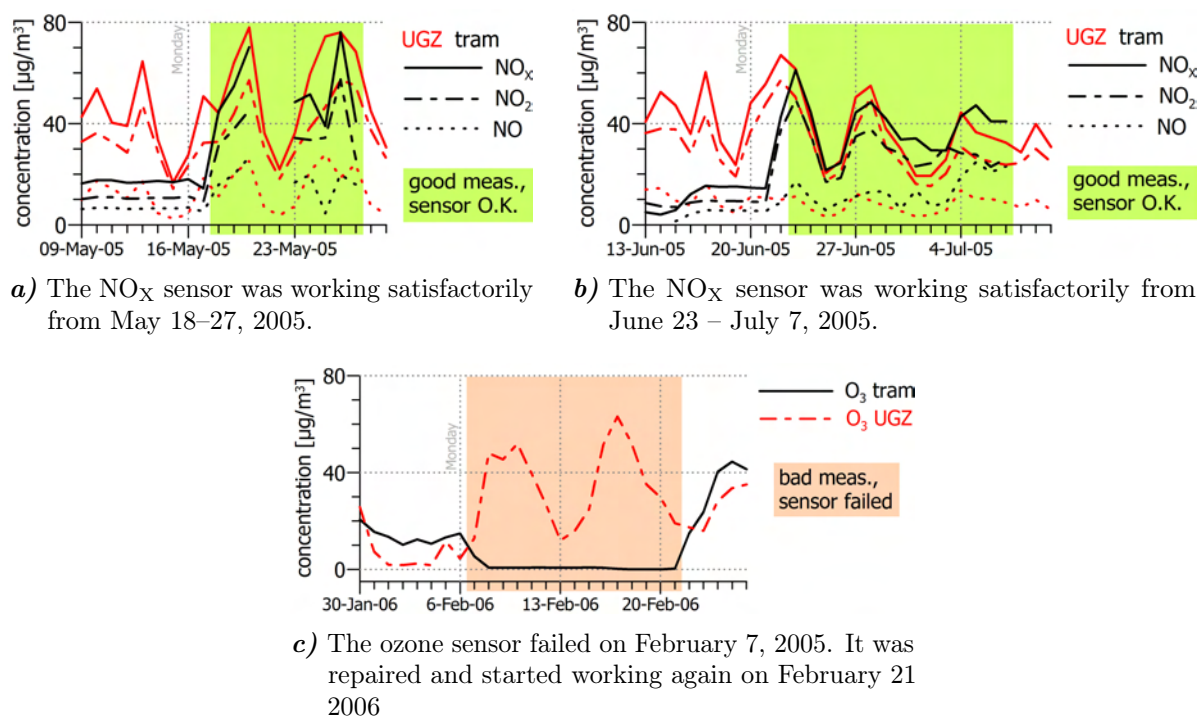


Figure 5.4: Days in the first campaign when the NO_x sensor worked satisfactorily (**a**, **b**, compare section 4.2.1). Days of an O_3 sensor failure in the second campaign (compare section 4.2.2).

5.3 Data analysis & discussion

5.3.1 Comparison of daily mean values

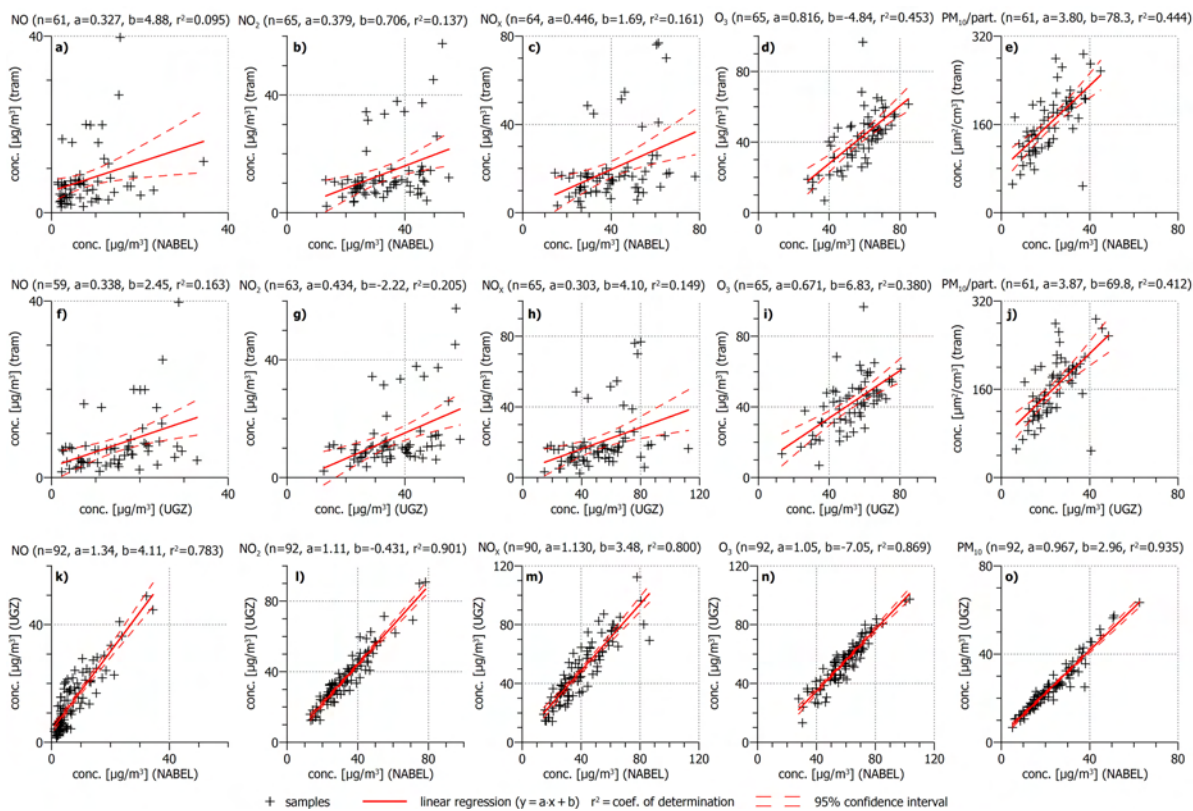
A correlation analysis of the daily mean values from the tram measurements and from two permanent stations (compare section 5.1.2) was carried out using scatter plots. The coefficients of determination (r^2) indicate the degree of agreement between the tram and either station. Figure 5.5 shows the scatter plots for each channel (columns) and each combination of the tram and permanent stations measurements (rows). The analysis was carried out for each season separately (subfigures a–d) and all daily mean values were considered. Table 5.1 summarises the coefficients of determination from all scatter plots.

The correlation of the tram's NO_x measurements is poor in the first campaign (spring and summer 2005, figure 5.5a and b) as expected due to the malfunction of the NO_x sensor during almost the whole campaign. It is significantly better ($0.612 \leq r^2 \leq 0.808$) in the winter period of the second campaign (figure 5.5c). The comparison of the NO_x measurements in spring 2006 show a less good determination ($0.207 \leq r^2 \leq 0.349$), possibly due to the fewer available data (approximately half as much as during winter 2005/06).

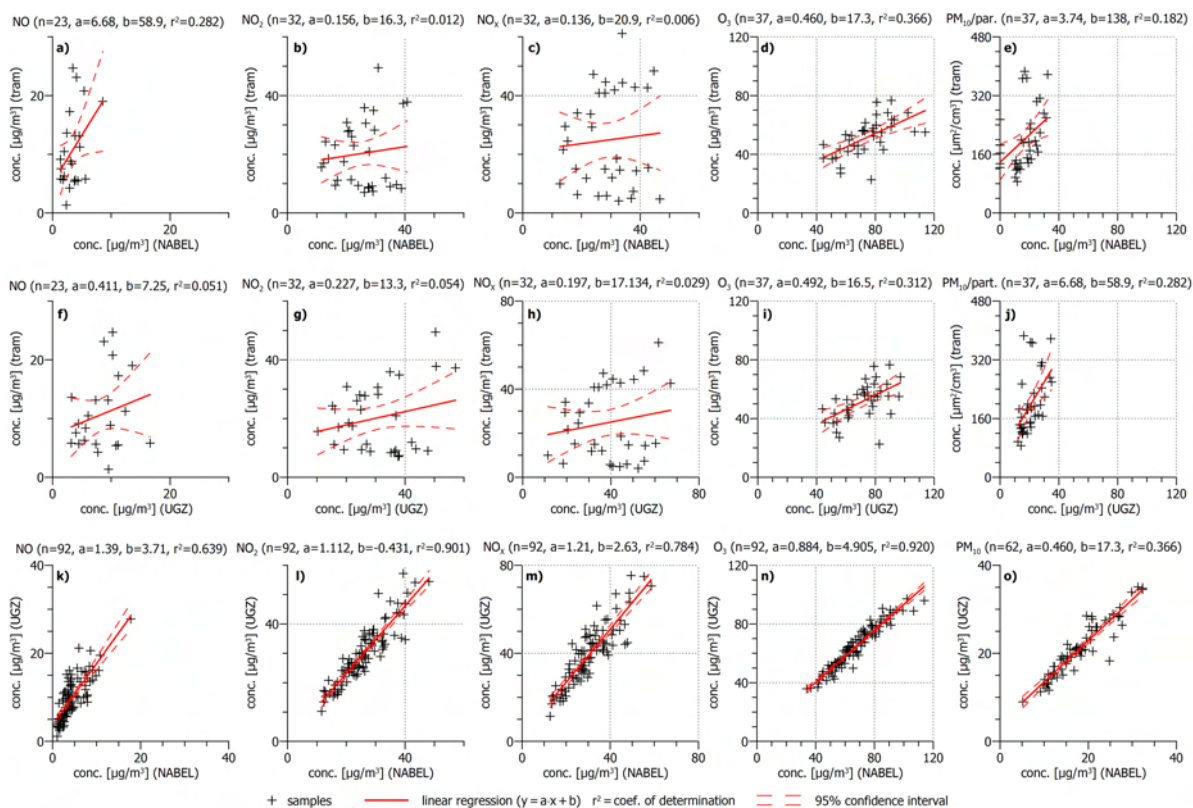
The comparison of the ozone daily mean values also shows the best agreement with the data from the permanent stations in the winter 2005/06 period ($0.473 \leq r^2 \leq 0.581$). During the first campaign the correlation is lower ($0.312 \leq r^2 \leq 0.453$). Again, the tram's daily mean values of the spring 2006 period show the poorest agreement with the daily means from the permanent station (see previous paragraph).

The tram's particulates daily mean values show an agreement to a certain extent with the PM_{10} daily means from the permanent stations despite the different measurement principles involved. A correlation factor of approximately 0.42 ($0.403 \leq r^2 \leq 0.444$) was found for the spring 2005 and the winter 2005/06 seasons. The correlation factor in summer 2005 is poorer ($0.182 \leq r^2 \leq 0.282$). There is almost no correlation in the spring 2006 period ($0.080 \leq r^2 \leq 0.088$).

One explanation for the generally poorer correlation in particles and PM_{10} is the different dimensions of the tram's and the permanent station's measurements ("area per volume" and "mass per volume", respectively). Another explanation is the occurrence of extraordinarily high peaks in the tram's measurements during all but the winter 2005/06 periods. In particular, the following outliers were identified: April 20/21 and May 5, 2005 (compare figures B.1a and B.4a/b); June 14/15 and July 26–29, 2005 (compare figures B.1b and B.5a/b); March 30 and April 9/10, 2006 (compare figures B.1d and B.7a/b).

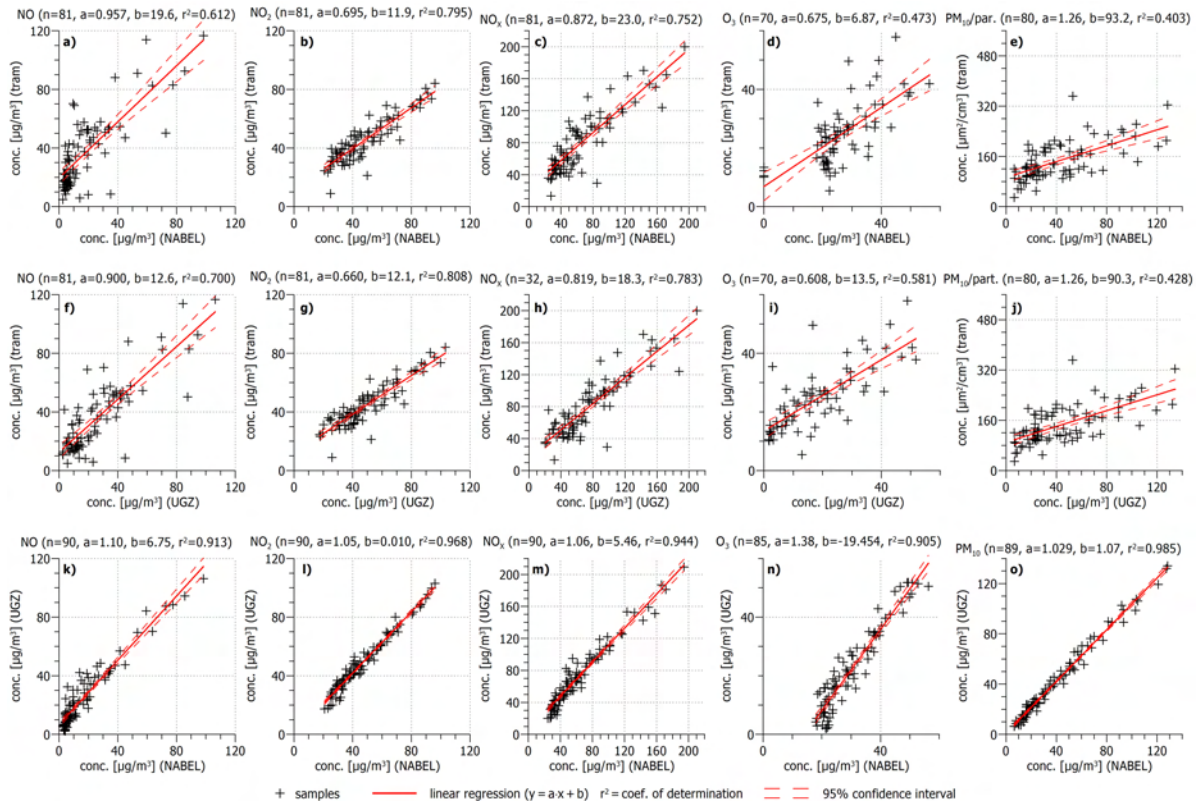


a) spring 2005

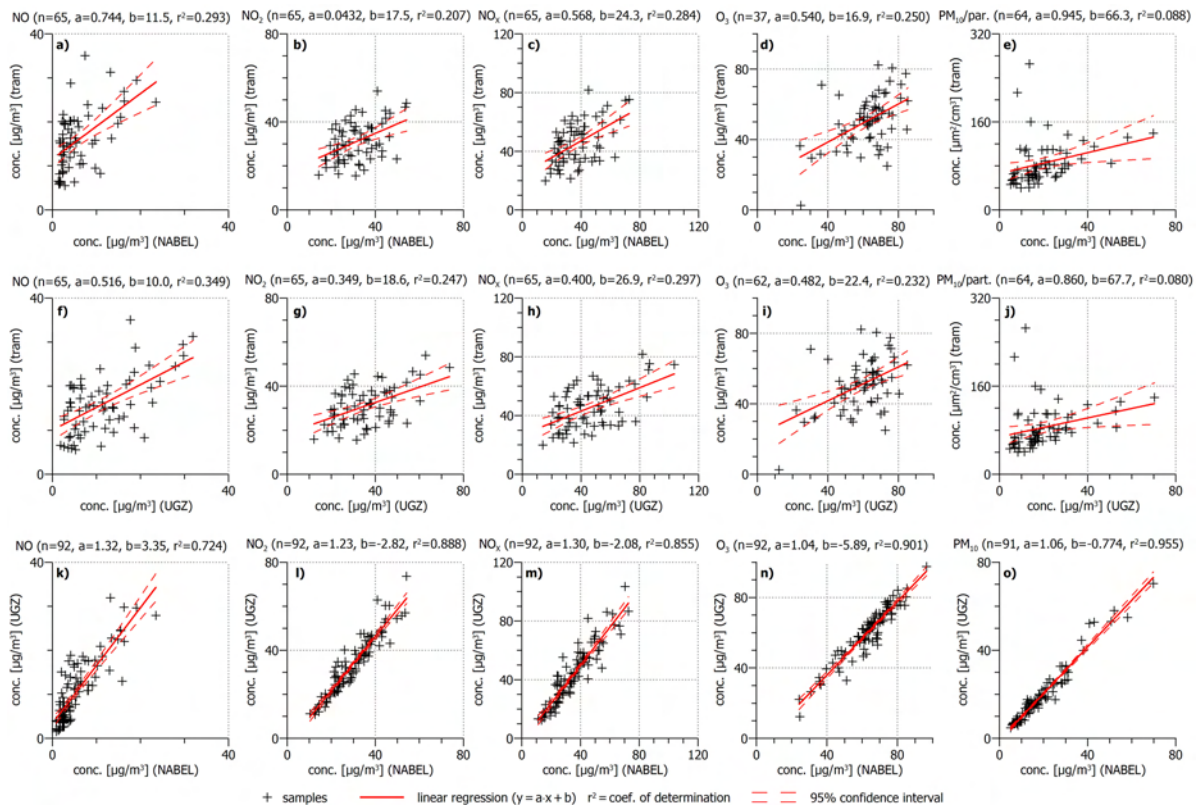


b) summer 2005

Figure 5.5: Scatter plots of the daily means of the tram and the permanent stations. All combinations of pollutants (columns) and measurement stations (rows) are plotted for four periods (“seasons”, subfigures a–d). (continued on next page)



c) winter 2005/06



d) spring 2006

Figure 5.5: (continuation from previous page) The plots in the first (a–e) and second (f–j) rows correlate the tram measurements against the NABEL and the UGZ permanent station, respectively. The two permanent stations are correlated in the third row (k–o).

season	measurements	coef. of determination (r^2) for...				
		NO	NO ₂	NO _x	O ₃	PM
spring 2005 (see fig. 5.5a)	NABEL vs. tram	0.095	0.137	0.161	0.453	0.444
	UGZ vs. tram	0.163	0.205	0.149	0.380	0.412
summer 2005 (see fig. 5.5b)	NABEL vs. tram	0.282	0.012	0.006	0.366	0.182
	UGZ vs. tram	0.051	0.054	0.029	0.312	0.282
winter 2005/06 (see fig. 5.5c)	NABEL vs. tram	0.612	0.795	0.752	0.473	0.403
	UGZ vs. tram	0.700	0.808	0.783	0.581	0.428
spring 2006 (see fig. 5.5d)	NABEL vs. tram	0.293	0.207	0.284	0.250	0.088
	UGZ vs. tram	0.349	0.247	0.297	0.232	0.080

Table 5.1: Coefficients of determination of the fits to the daily means scatter plots (figure 5.5).

5.3.2 Comparison of monthly mean values

Similarly to the daily mean values, monthly mean values were derived from the integrated tram measurement's daily means. Table 5.2 lists the tram's monthly means along the monthly mean values derived from the NABEL and UGZ permanent stations. Figure 5.6 represents the same data in a bar plot. Figure 5.7 shows scatter plots for each pollutant species (columns) and the combination of the mean values derived from the tram and the UGZ and NABEL permanent stations (rows).

Even though only between five and nine monthly mean values are available, a correlation analysis was carried out. It reveals the following correlations:

- * The NO₂ monthly mean values derived from the tram measurements agree well with the monthly means of the NABEL and UGZ permanent stations. The correlation factors (r^2) are 0.908 and 0.950, respectively. The absolute mean values from the tram are 1% \pm 8% higher than the NABEL values and 7% \pm 6% lower than the UGZ values (mean difference and 95% confidence interval).
- * The NO monthly mean values derived from the tram measurements also show a high correlation factor with the mean values of the NABEL and the UGZ permanent stations. The factor (r^2) is 0.939 and 0.954, respectively. The absolute values of the tram are 62% \pm 9% higher than the NABEL values and 35% \pm 5% higher than the UGZ values (mean difference and 95% confidence interval).
- * The O₃ monthly mean values derived from the tram measurements agree well with the monthly means of the NABEL and UGZ permanent stations. The correlation factor (r^2) is 0.840 and 0.822, respectively. The absolute values from the tram are 21% \pm 14% lower than the NABEL values and 5% \pm 32% lower than the UGZ values (mean difference and 95% confidence interval).
- * The particles monthly mean values derived from the tram measurements show a significant correlation to the PM₁₀ monthly mean values of the NABEL and UGZ permanent station in the second campaign only. The correlation factor (r^2) is 0.670 and 0.661, respectively. A comparison of the absolute values is not possible due to the different dimension of the measurements ("area per volume" and "mass per volume", respectively).

Pollutant Unit Station	NO [$\mu\text{g}/\text{m}^3$]			NO ₂ [$\mu\text{g}/\text{m}^3$]			O ₃ [$\mu\text{g}/\text{m}^3$]			PM ₁₀ [$\mu\text{g}/\text{m}^3$]		Part. [$\mu\text{m}^2 \cdot \text{cm}^{-2}$]
	N	U	T	N	U	T	N	U	T	N	U	T
March 2005	9	17	n/a	39	43	n/a	51	47	29	28	32	175
April 2005	8	15	n/a	34	37	n/a	58	53	43	22	24	185
May 2005	5	11	n/a	29	32	n/a	68	65	51	18	20	187
June 2005	4	9	n/a	26	32	n/a	79	75	54	20	22	206
July 2005	4	9	n/a	25	28	n/a	66	64	n/a	n/a	21	n/a
August 2005	5	11	n/a	27	29	n/a	56	54	n/a	17	20	n/a
December 2005	14	23	34	38	41	40	29	21	29	26	26	145
January 2006	21	30	53	53	56	56	27	17	27	52	57	176
February 2006	17	25	35	49	51	47	32	28	25	46	48	135
March 2006	4	11	17	31	36	34	62	58	47	24	27	93
April 2006	7	12	18	33	36	30	61	58	53	18	17	82
May 2006	5	9	n/a	25	28	n/a	67	65	n/a	16	15	n/a

Key: N = NABEL, U = UGZ, T = Tram, n/a = no (or too few) measurements available

Table 5.2: Monthly mean values from the two permanent stations NABEL and UGZ and the tram measurements for nitrogen oxides, particulates and ozone. See also figure 5.6 and table 5.3. N.B. The NABEL and UGZ values were calculated from the respective raw data and are not necessarily in perfect agreement with the official values.

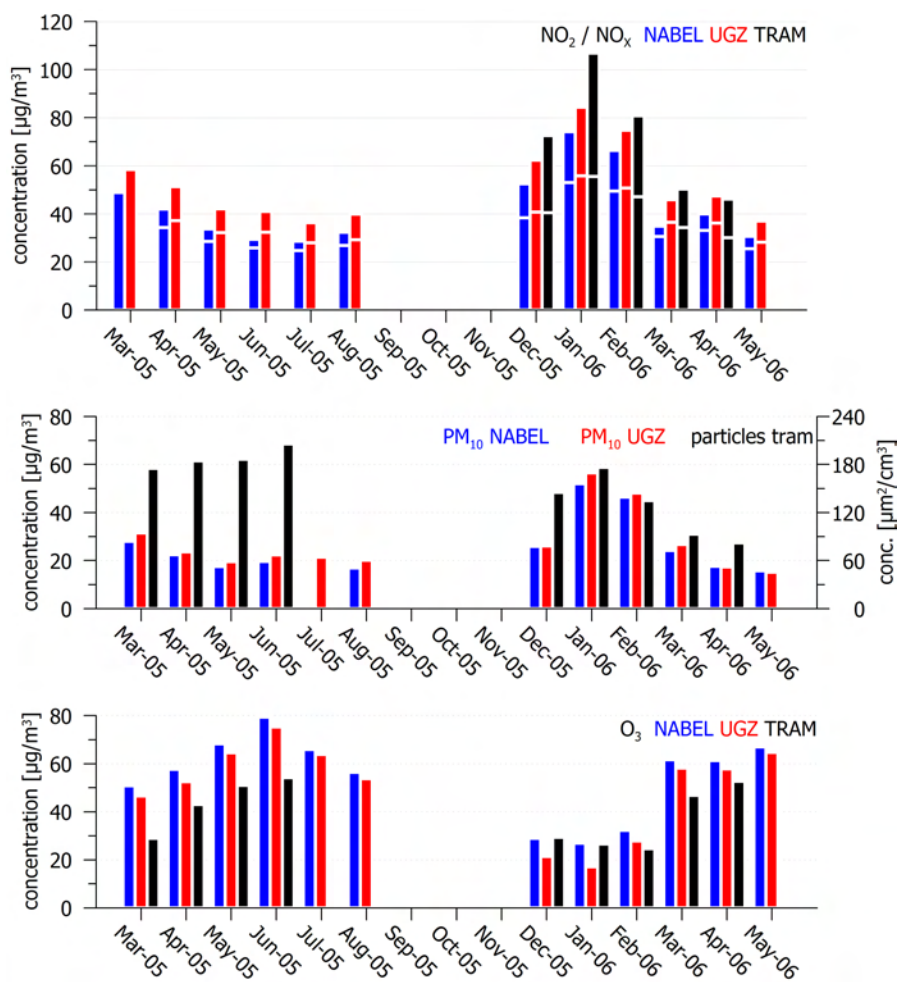


Figure 5.6: Monthly mean values from the two permanent stations NABEL (blue) and UGZ (red) and the tram measurements (black) for nitrogen oxides (top), particulates (middle) and ozone (bottom). See also table 5.2. N.B. The NABEL and UGZ values were calculated from the respective raw data and are not necessarily in perfect agreement with the official values.

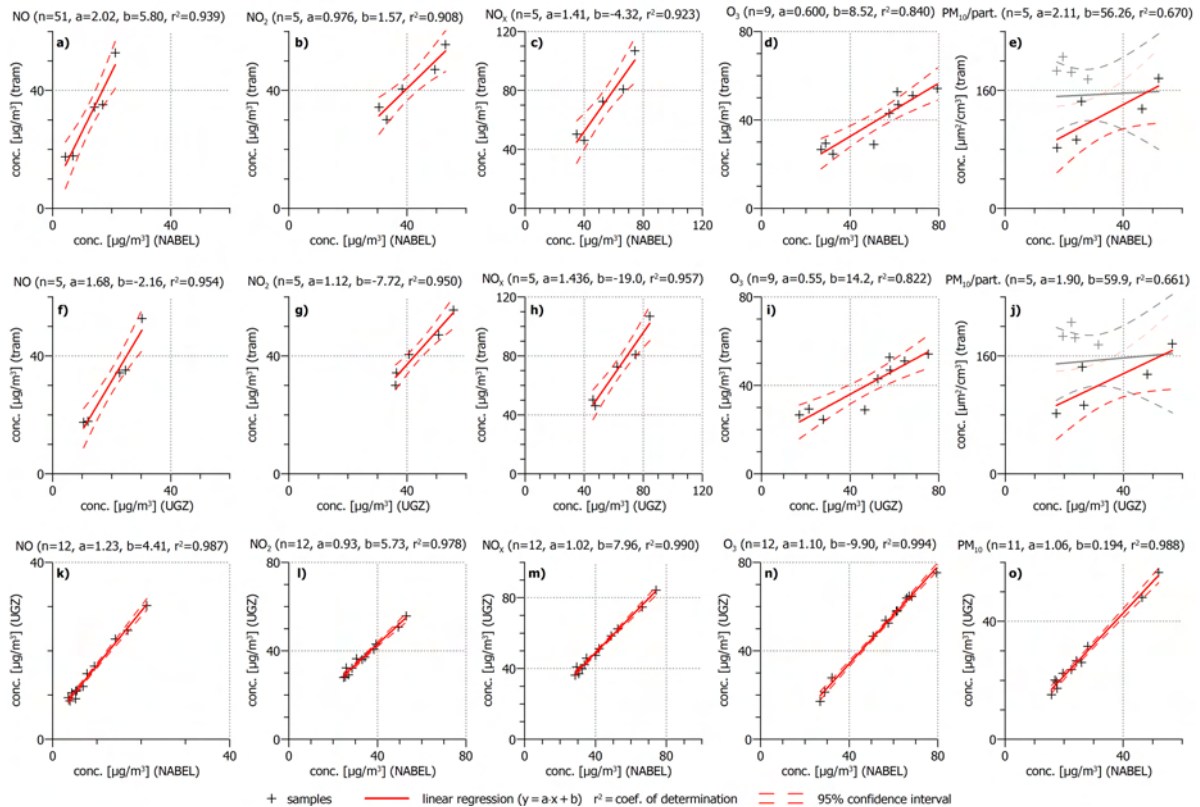


Figure 5.7: Scatter plot of the monthly mean values. Each combination of the mean values derived from the tram measurements and the two permanent stations (NABEL and UGZ) for each pollutant species is plotted. A linear fit to the data was added to each plot. For plots e and j two fits were applied. The first fit (plotted in grey) includes all available data and the second fit (plotted in red) only contains the data derived from second measurement campaign.

5.3.3 Limit value exceedances

The daily and hourly mean values introduced in section 5.1.2 were used to identify limit values exceedances for NO₂ and O₃, respectively. Table 5.3 shows the number of limit values exceedances at the NABEL and UGZ permanent stations along the number identified in the tram measurement's daily and hourly mean value data.

The comparison of the numbers reveals that only a fraction of the limit values exceedances was detected using the daily and hourly mean values derived from the tram measurements. Therefore, it is not feasible to use this measurement concept to determine the limit value exceedances with a high success rate. Even though the limit values exceedances occur during daytime and the measurement system operated on daytime, it has not covered all times when limit values exceedances occurred. However, given that the daily mean values of the tram and the permanent stations correlate reasonably well (see section 5.3.1) it would be possible to increase the success rate if the measurements would fully cover the period of interest. This could be achieved by increasing the availability of measurements. The operating time of a single measurement system could be extended or several measurement systems could be operated.

Limit Station	NO ₂ ≥ 80 µg/m ³			O ₃ ≥ 120 µg/m ³			PM ₁₀ ≥ 20 µg/m ³	
	N	U	T	N	U	T	N	U
2005-03	0	2	n/a	0 / 0	0 / 0	0 / 0	3	4
2005-04	0	0	n/a	14 / 5	9 / 3	12 / 6	0	0
2005-05	0	0	n/a	45 / 7	40 / 6	46 / 6	0	0
2005-06	0	0	n/a	106 / 17	79 / 13	11 / 4	0	0
2005-07	0	0	n/a	51 / 8	39 / 6	n/a	0	0
2005-08	0	0	n/a	7 / 2	5 / 1	n/a	0	0
2005-12	0	0	0	0 / 0	0 / 0	0 / 0	2	2
2006-01	5	5	2	0 / 0	0 / 0	0 / 0	17	18
2006-02	4	5	2	0 / 0	0 / 0	0 / 0	11	11
2006-03	0	0	0	0 / 0	0 / 0	7 / 4	5	7
2006-04	0	0	0	17 / 5	11 / 2	14 / 5	0	0
2006-05	0	0	n/a	24 / 6	10 / 3	n/a	0	0

Key: N = NABEL, U = UGZ, T = Tram, n/a = no or too few measurements available

Table 5.3: Limit exceedances for the two permanent stations NABEL and UGZ and the tram measurements for nitrogen oxides, particulates and ozone. For O₃ n/m means that the limit was exceeded for n hours and on m days. See also tables 5.3 and 2.3. N.B. The NABEL and UGZ values were calculated from the respective raw data and are not necessarily in perfect agreement with the official values.

5.3.4 Comparison of tram measurements at the UGZ permanent station

The tram line 11, where the measurement system operated on during the first campaign, drives past the UGZ permanent. The inlets of the UGZ sensors are mounted in a window of a building which borders the street. The measurement system's inlet passed them a couple of metres below and aside in the middle of the street. There is one lane, and in one direction also a tram track, in between.

A comparison of the measurements at this site (± 50 m) for the two periods with satisfactory NO_x measurements (compare section 5.2) is presented here.

Figures 5.9 and 5.8 show the $\text{NO}/\text{NO}_2/\text{NO}_x$ time series at the UGZ permanent station and the measurements from the tram at the corresponding point in the plot for each period. The photo-stationary state (K, equation 2.5 on page 6) was calculated, too.

The plots show the following features:

- * Some tram measurements match the UGZ measurements fairly well for $\text{NO}/\text{NO}_2/\text{NO}_x$ as well as O_3 (e.g. May 19, 2005 in figure 5.9 or July 5, 2005 in figure 5.8). This could be explained by a relatively stable state of the air masses and the ambient air concentrations in the street canyon.
- * Some tram measurements show higher $\text{NO}/\text{NO}_2/\text{NO}_x$ values than the UGZ in connection with lower O_3 measurements but similar values vor K (e.g. May 23, 2005 in figure 5.9 or July 1, 2005 in figure 5.8). In this case, high local NO emissions used O_3 to form NO_2 (see equation 2.4 in section 2.1.2, page 5). This short-term effect was evened out in the $1/2$ h averages of the UGZ measurements.
- * Many of the tram measurements do not agree well with the UGZ measurements. This is probably attributed to two circumstances. The averaging times of the instruments on the tram and at the UGZ station differ widely (10 s vs. 0.5 h) and turbulences in street canyons can lead to a very irregular distribution of ambient air concentrations with large variability in close proximity.

A correlation analysis of the data was carried out (figures 5.11 and 5.10). It reveals insignificant to poor correlation for $\text{NO}/\text{NO}_2/\text{NO}_x$ and particulate matter. This is due to the dominating disagreement of the tram's measurements with the UGZ measurements due to the large variability of primary pollutant concentration in street canyons induced by turbulence (compare the third point above). Ozone, however, shows a high correlation in both examined periods. The correlation factor is 0.815 and 0.803, respectively.

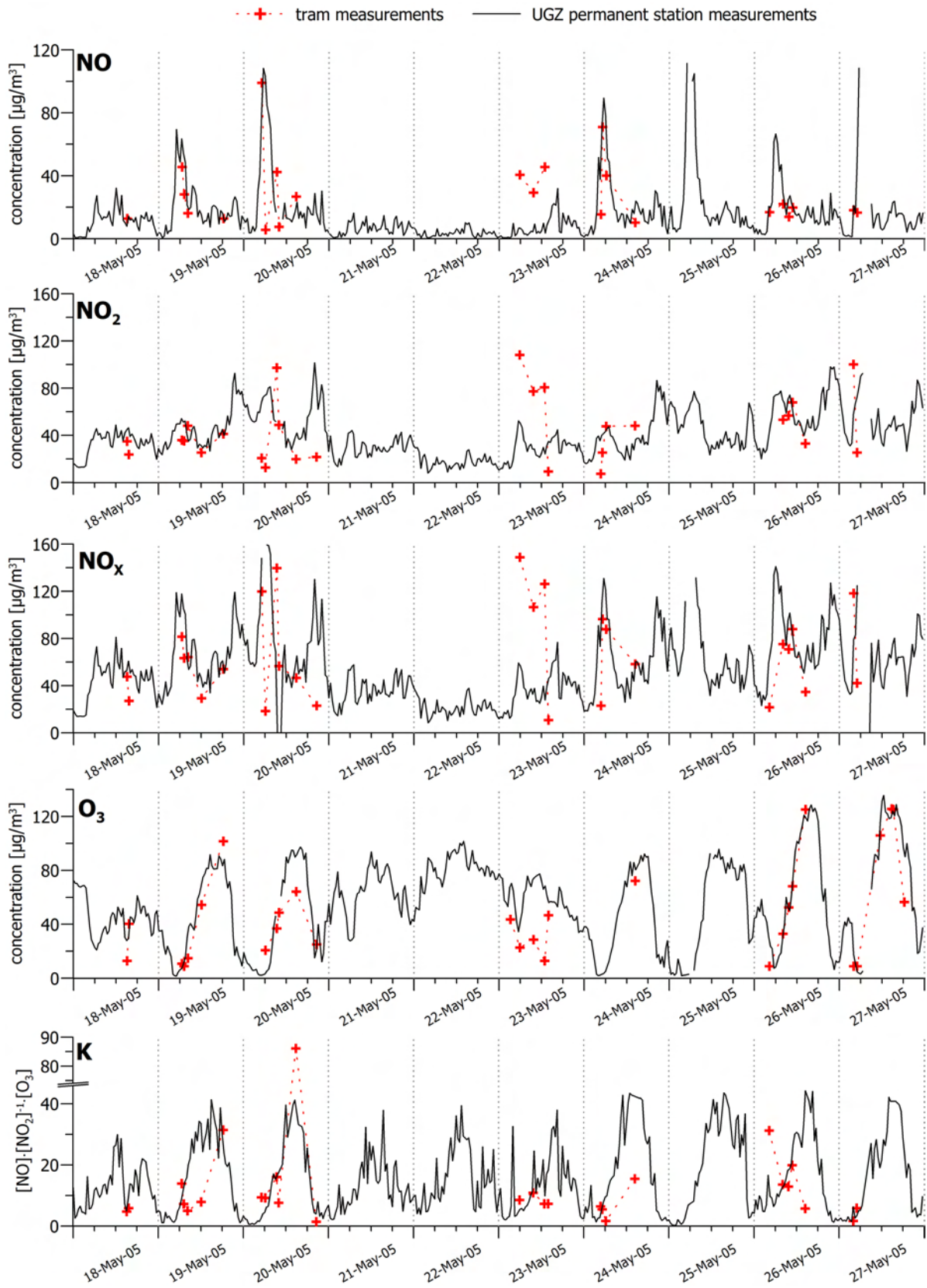


Figure 5.8: Comparison of the tram measurements with the measurements from the UGZ permanent station in May 2005 (compare figure B.4b).

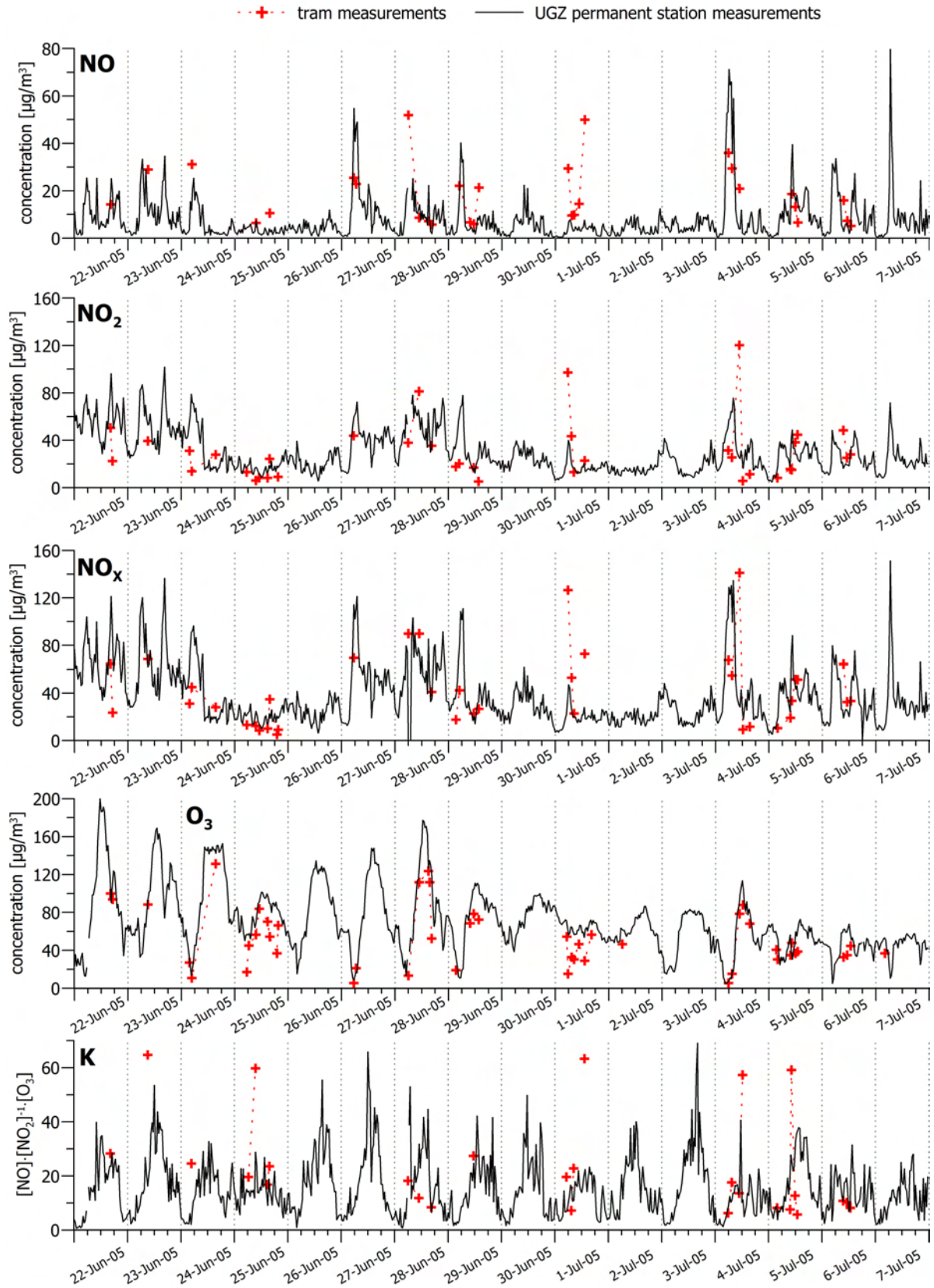


Figure 5.9: Comparison the tram measurements with the measurements from the UGZ permanent station in June/July 2005 (compare figure B.5b).

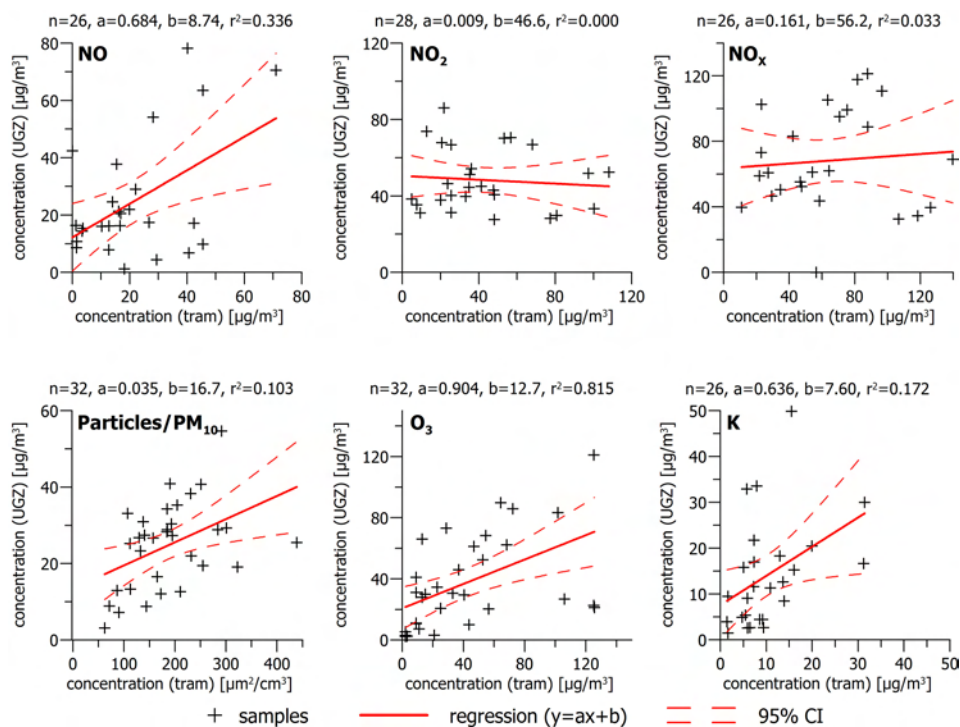


Figure 5.10: Statistics of the comparison of the tram measurements with the measurements from the UGZ permanent station in June/July 2005 (see figure 5.8).

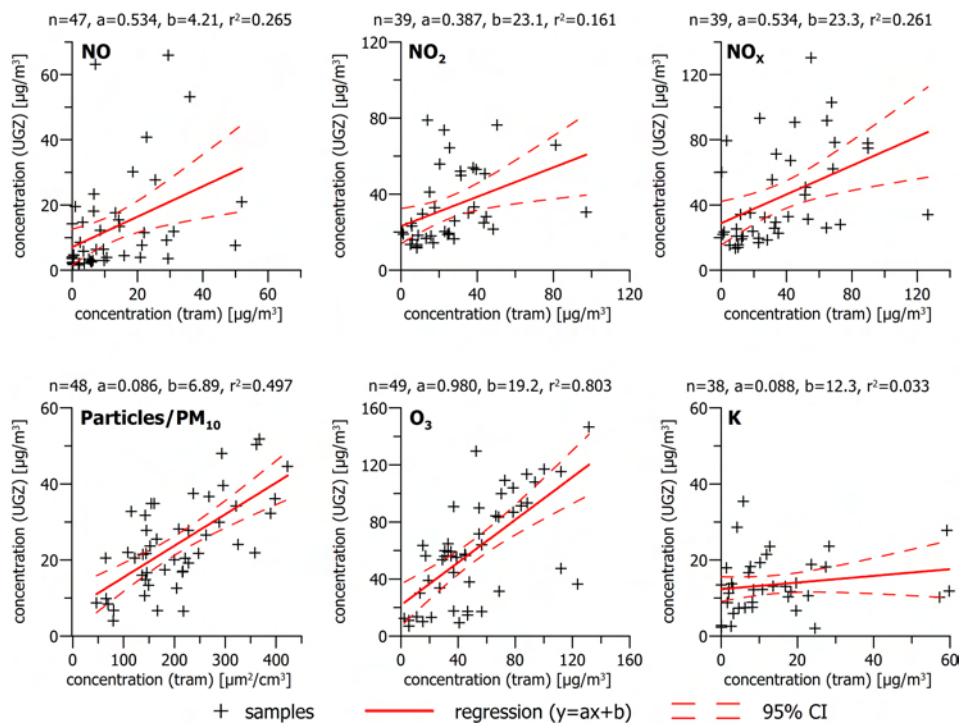


Figure 5.11: Statistics of the comparison of the tram measurements with the measurements from the UGZ permanent station in June/July 2005 (see figure 5.9).

5.3.5 Summer 2005

Methodology

The collocation method will be used in this and the next section (5.3.5 and 5.3.6) to interpolate the measurements in the position–time domain. The method allows to concurrently fit a deterministic and stochastic model to the irregularly spaced (in position and time) measurements in order to obtain the most likely results (plots). The method is also known as kriging. Further details can be found in textbooks on statistics or data processing, such as [Moritz, 1980]. The covariance function used is:

$$f(\Delta t, \Delta s) = \frac{e^2}{\frac{\Delta s^2}{\sigma^2} + \frac{\Delta t^2}{\tau^2} + e^2} \quad (5.1)$$

Where:

- Δs : distance between two measured sites (position along track domain)
- Δt : time difference between tow measurements (time domain)
- σ : correlation length in position domain
- τ : correlation length in time domain
- e : smoothing factor

Overview of available measurements

A period in summer 2005 which contains typical hot summer days as well as summer days with adverse weather was used for this analysis. This period also coincides with the period of satisfactory NO_x measurements (compare section 5.2) so that data from all sensors is available for this analysis. Besides of limit value exceedances, the average daytime radiation (see figure B.12, page 180) and the “meteo archive” (http://www.sf.tv/sfmeteo/diverses_archiv.php) proved useful.

Figure 5.12 shows the measurements at the NABEL permanent station for the selected period. A photochemical smog period (compare section 2.1.5) starts to develop from June 18. Caused by sunny weather with stable atmospheric conditions and lots of sunshine (hereafter called “fair weather”) the peak ozone concentrations increased from day to day. The limit values were exceeded for several hours every day until June 24, when the smog period was interrupted by a storm on June 25. Another three days of fair weather again caused limit value exceedances on June 26–28. On June 29 to July 8 stormy and unsettled weather with low solar radiation dominated (hereafter called “adverse weather”).

The days where tram measurements are available are marked with horizontal bars in figure 5.12 (compare figure 4.4). Yellow bars denote days with fair weather and blue bars denote days with adverse weather. Data is available during five days and six days, respectively. They are:

fair weather : June 22, 23, 24, 27 and 28

adverse weather: June 25 and July 1, 4, 5, 6 and 7

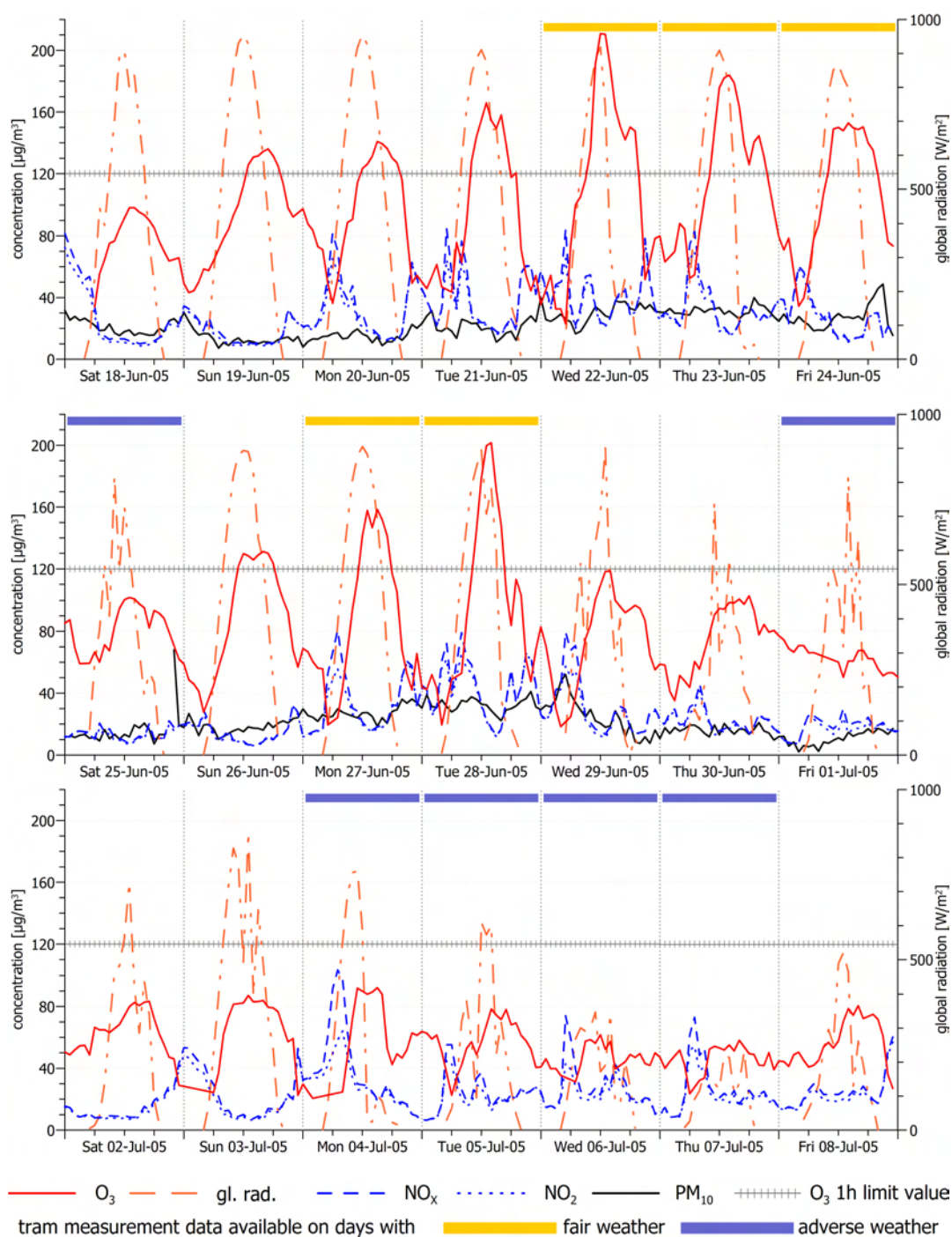


Figure 5.12: A photochemical smog period in June/July 2005 observed at the NABEL station in Zürich (see figure 4.1 on page 42). From June 19–24 and again from June 26–28 the ozone one hour limit value ($120 \mu\text{g}/\text{m}^3$, compare table 2.3 on page 14) was exceeded for several hours every day. A storm on June 29 ended the ozone period. Unsettled and stormy weather dominated the following days. The yellow and blue bars indicate the availability of tram measurements on days with fair and adverse weather, respectively. Note: PM_{10} measurements are not available on July 2–8, 2006, at the NABEL station.

Data processing

The following processing was applied to the fair weather days (five days), the adverse weather days (six days) and the combination of fair and adverse weather (i.e. all eleven) days:

1. Each day was interpolated to a regular grid using the collocation method described above. All single day collocation plots can be found in appendix B.2.
2. The group of days was combined. Due to restrictions in computation time and processing capacity, the combined measurements were filtered by a median filter. The filtered data was then interpolated using the collocation method (figures 5.13, 5.17 and 5.21).
3. Average along track concentrations were derived from the collocated data (figures 5.14, 5.18 and 5.22). The corresponding mean values at the UGZ permanent stations (same days and same averaging intervals) were added to the plot.
4. Average along track concentrations for five three-hours intervals (6–9, 9–12, 12–15, 15–18 and 18–21 h) were derived from the collocated data (figures 5.15, 5.19 and 5.23).
5. Cross-sections at twelve places along the track were extracted from the collocated data (figures 5.16, 5.20 and 5.24).

The grid spacing used for the interpolation was 50 m in the along track dimension and 0.5 h in the time dimension. The parameters used for the covariance function were:

$$\begin{aligned}
 \sigma_m &= 100 \text{ [}\mu\text{g/m}^3\text{]} && \text{measurement noise} \\
 \sigma_n &= 10 \text{ [}\mu\text{g/m}^3\text{]} && \text{signal noise} \\
 e &= 3.3 && \text{smoothing factor} \\
 \sigma &= 50 \text{ [}m\text{]} && \text{correlation length in position domain} \\
 \tau &= 8 \text{ [}h\text{]} && \text{correlation length in time domain}
 \end{aligned}$$

The following pages contain the mentioned plots. The discussion of the results starts on page 96

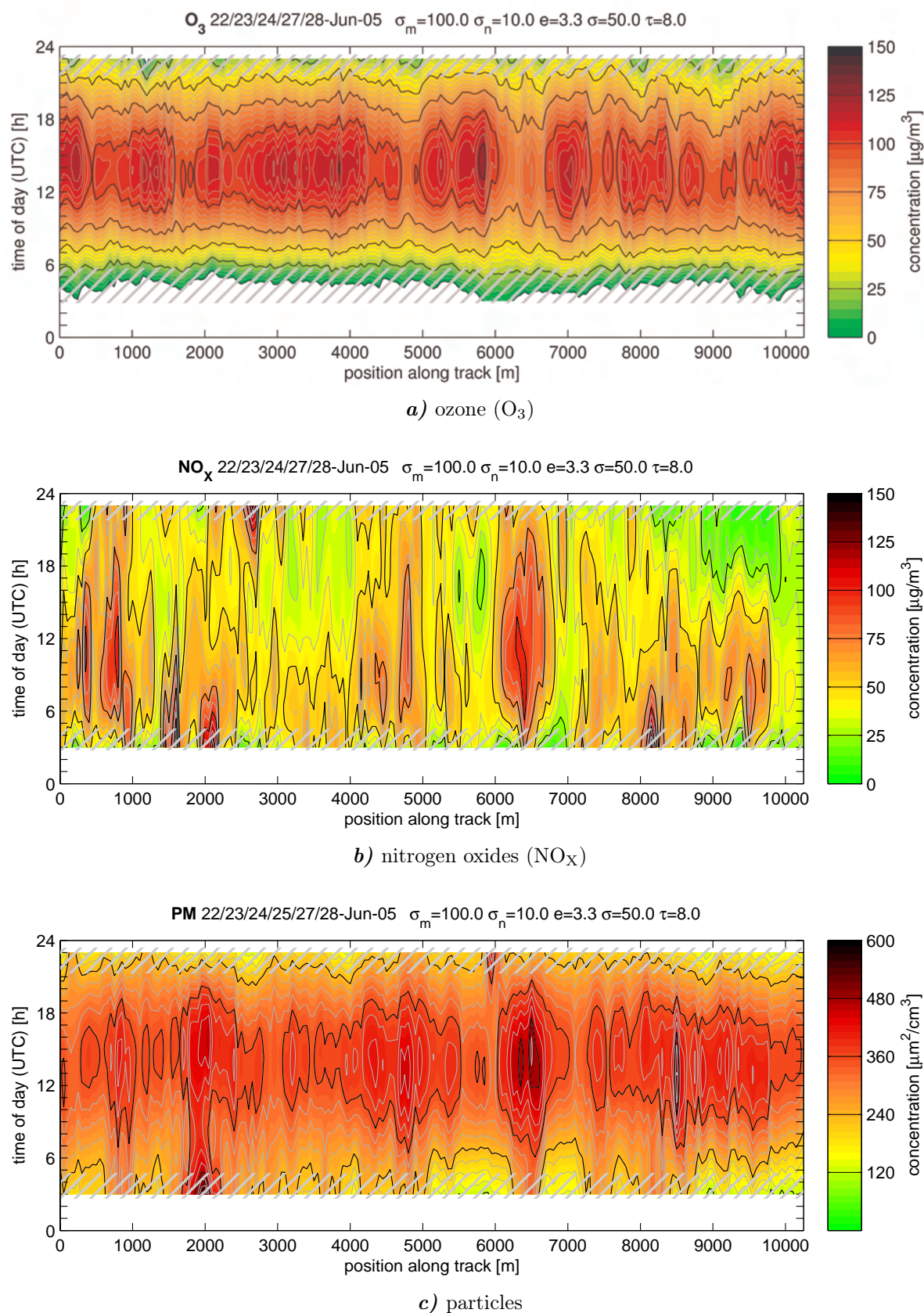


Figure 5.13: Spatial and temporal distribution of pollutant concentrations during fair weather (photochemical smog period) in June 2005 (collocated average of five fair weather days).

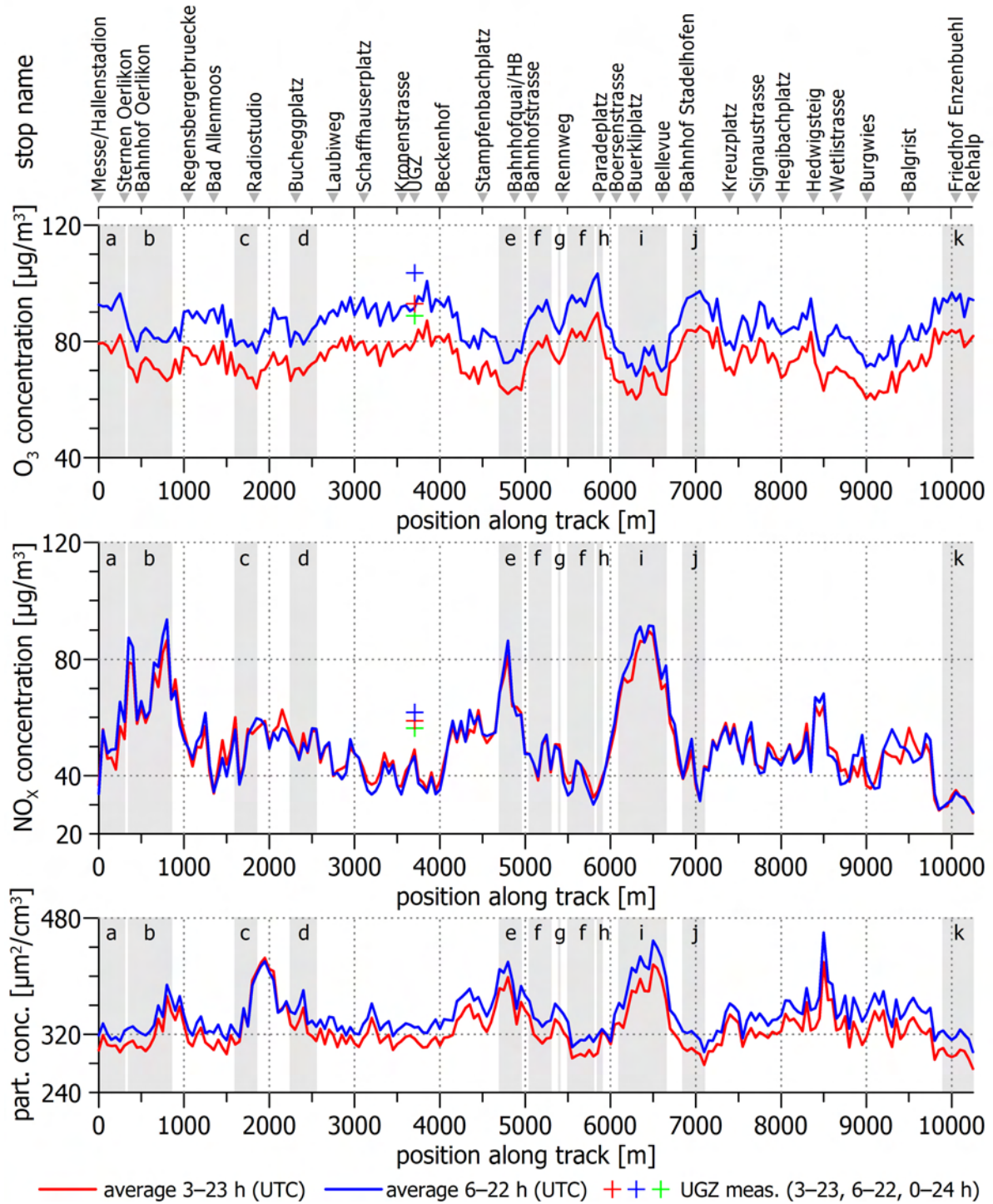


Figure 5.14: Average concentrations along track during fair weather (photochemical smog) in June 2005. Compare figure 5.13. The grey bars correspond to the places used in figure 5.16.

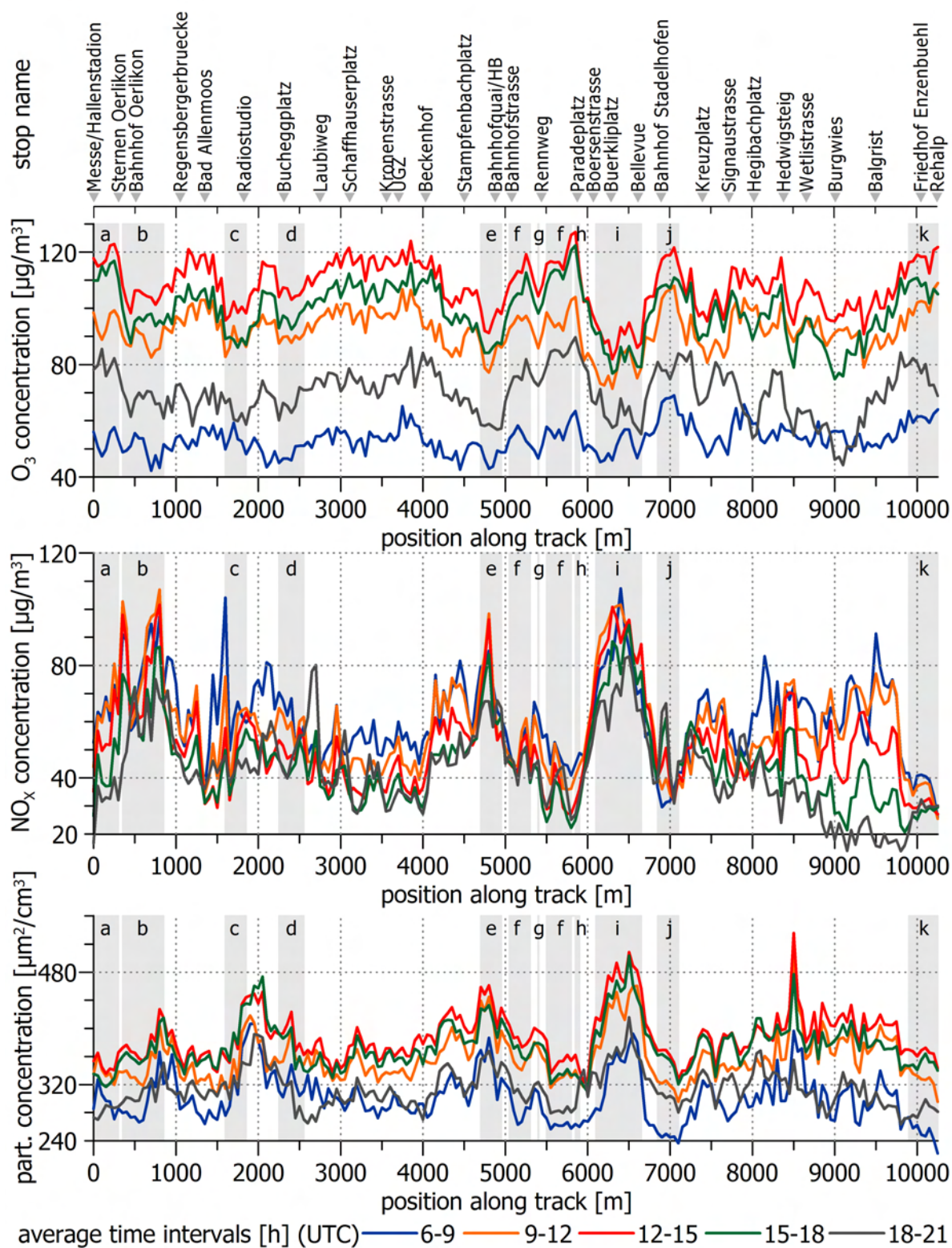


Figure 5.15: Average concentrations along track during fair weather (photochemical smog) in June 2005. Compare figure 5.14. The grey bars correspond to the places used in figure 5.16.

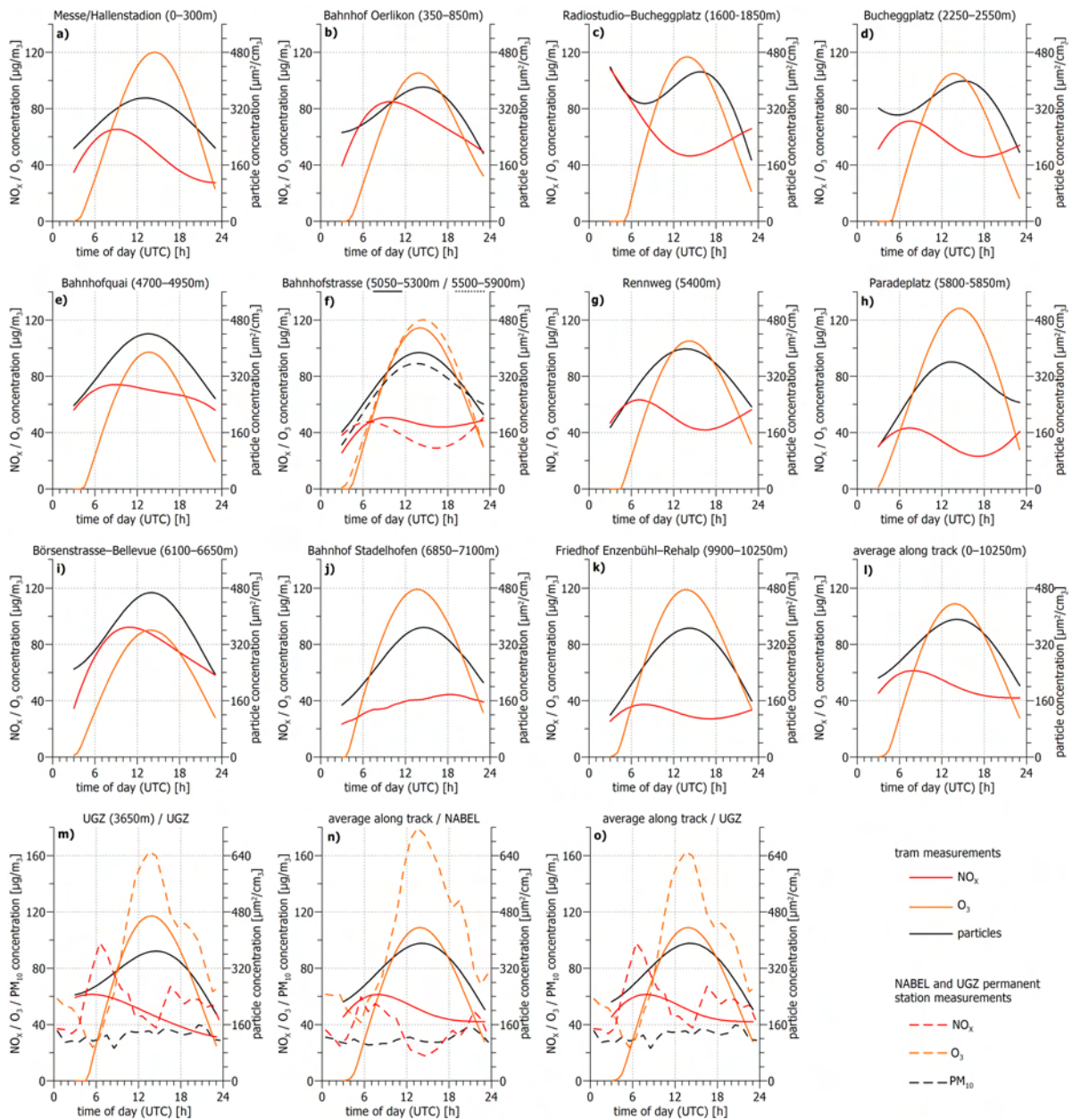


Figure 5.16: Diurnal variations at certain sites during fair weather (photochemical smog) in June 2005. Compare figures 5.13 and 5.14.

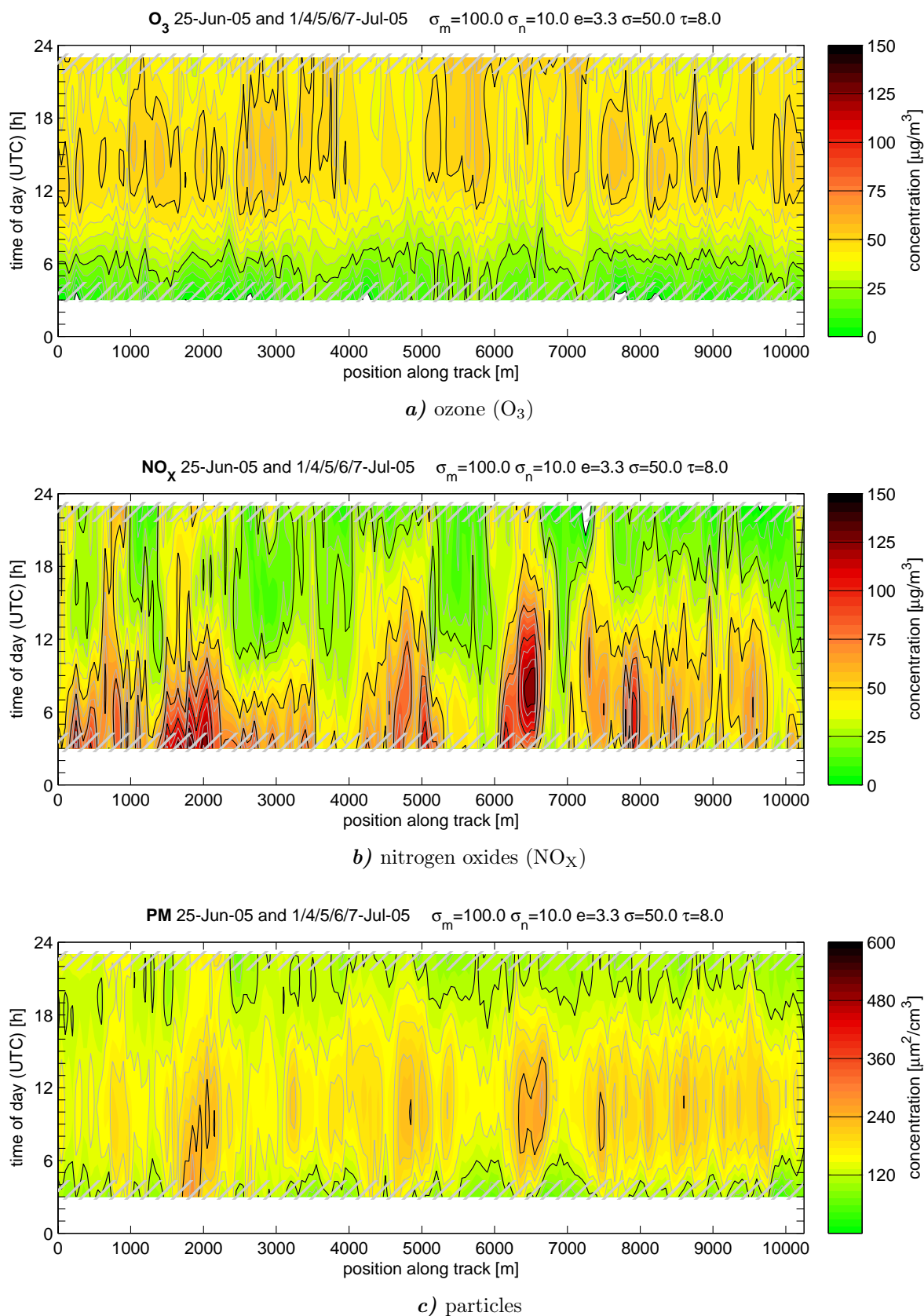


Figure 5.17: Spatial and temporal distribution of pollutant concentrations during adverse weather (unsettled and stormy) in June/July 2005 (collocated average of six adverse weather days).

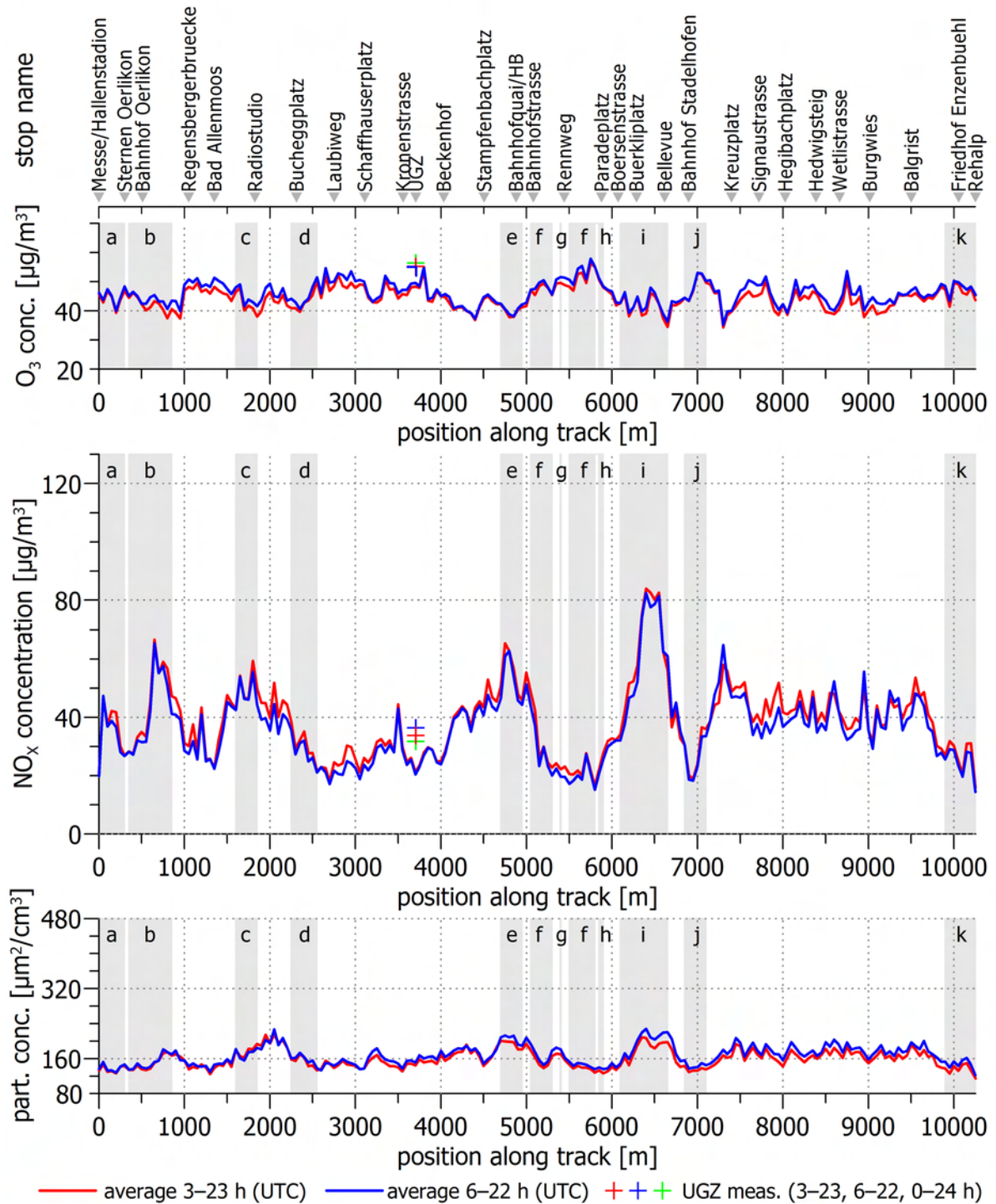


Figure 5.18: Average concentrations along track during adverse weather (unsettled and stormy) in June/July 2005. Compare figure 5.17. The grey bars correspond to the places used in figure 5.20.

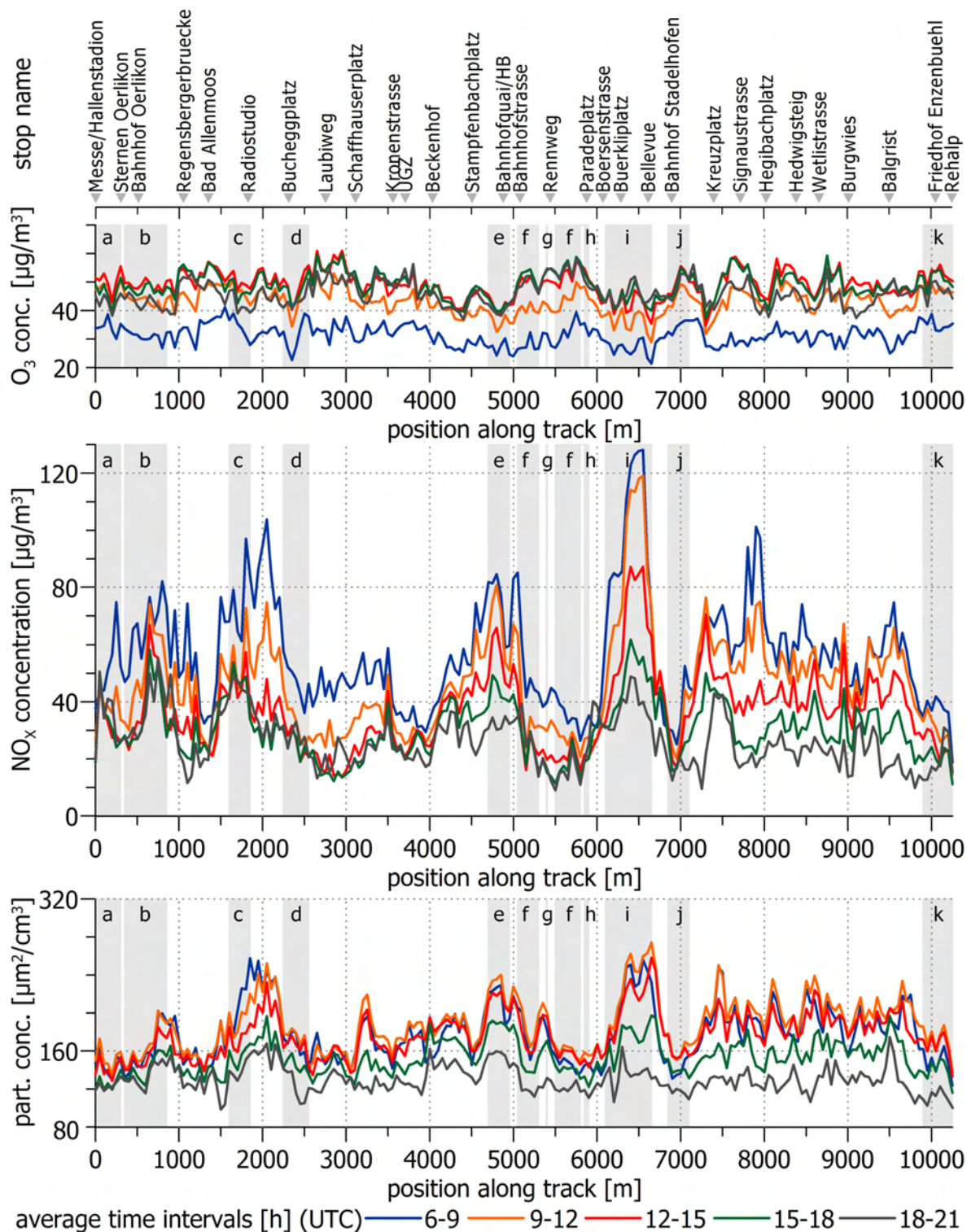


Figure 5.19: Average concentrations along track during adverse weather (unsettled and stormy) in June/July 2005. Compare figure 5.18. The grey bars correspond to the places used in figure 5.20.

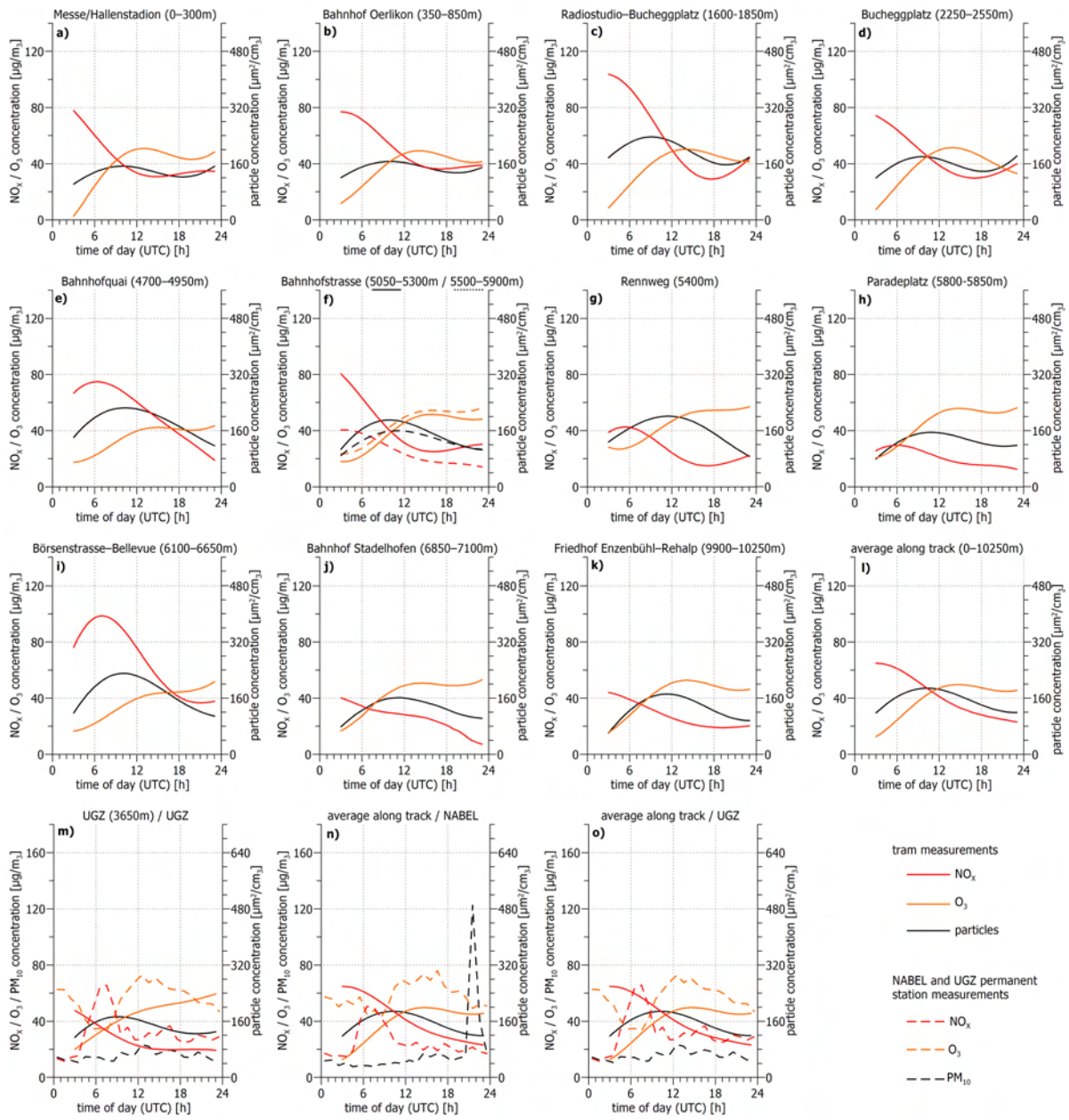


Figure 5.20: Diurnal variations at certain sites during adverse weather in June/July 2005. Compare figures 5.17 and 5.18.

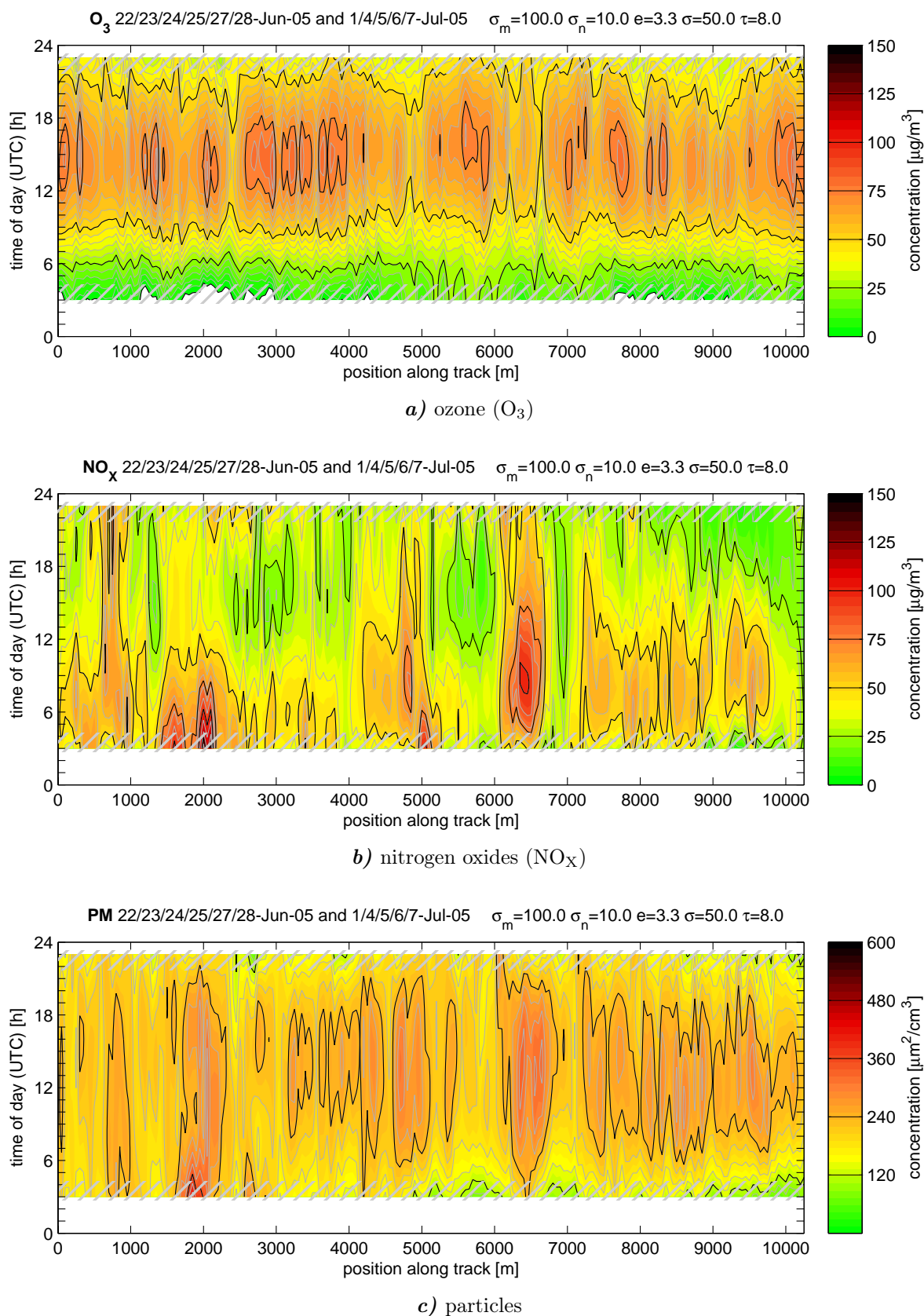


Figure 5.21: Spatial and temporal distribution of pollutant concentrations for the combination of fair and adverse weather in June/July 2005 (collocated average of eleven days).

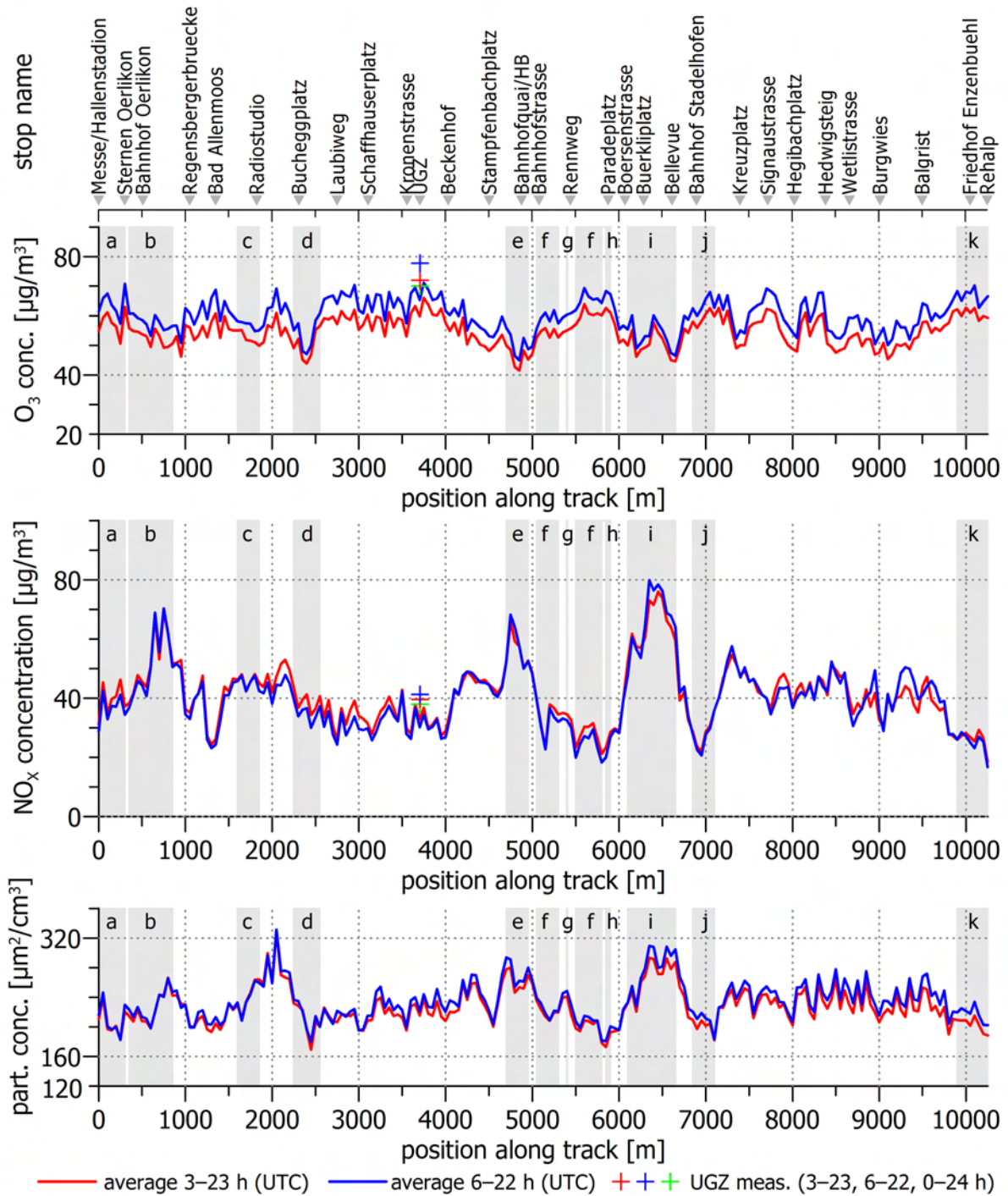


Figure 5.22: Average concentrations along track for the combination of fair and adverse weather in June/July 2005. Compare figure 5.21. The grey bars correspond to the places used in figure 5.24.

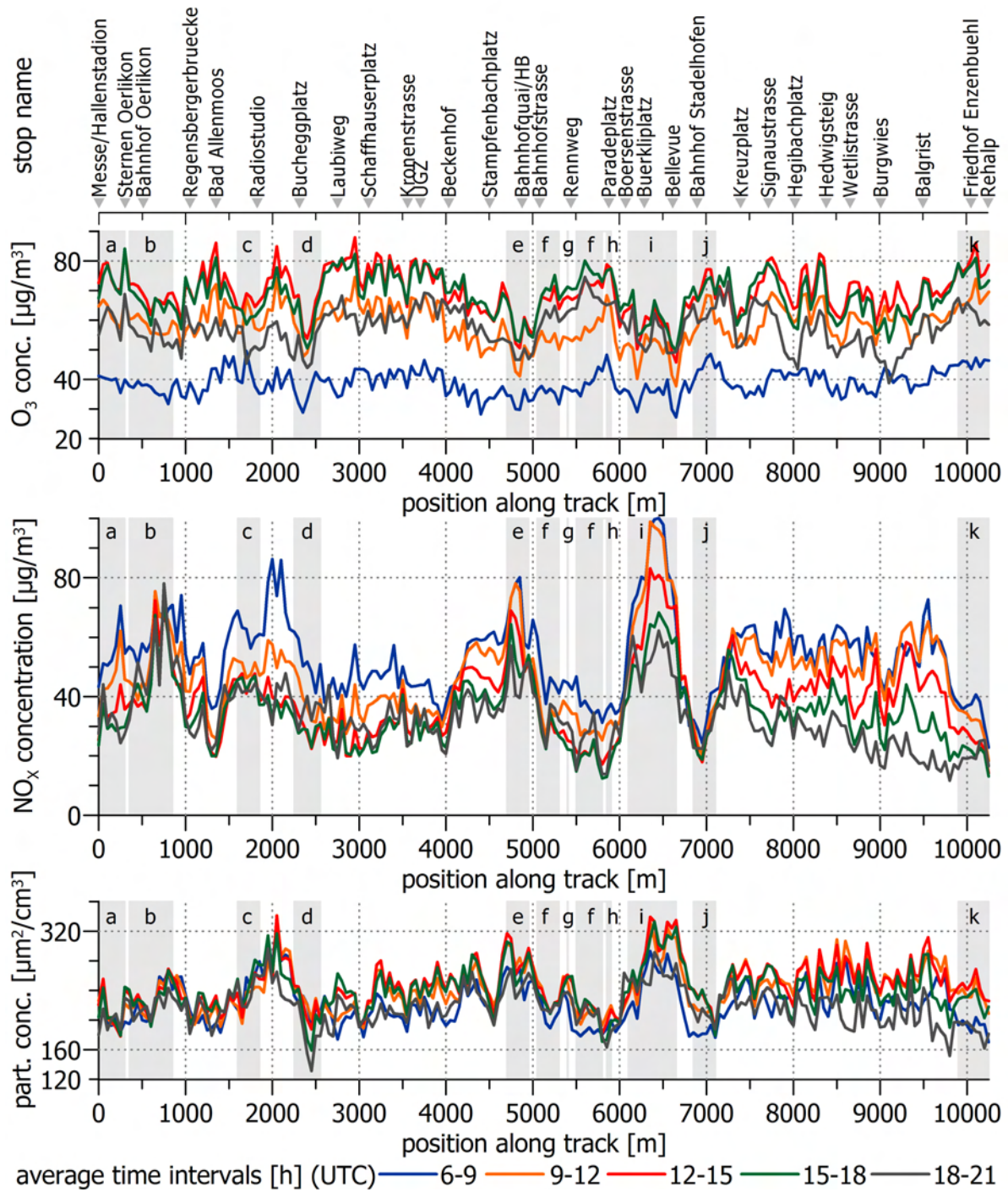


Figure 5.23: Average concentrations along track for the combination of fair and adverse weather in June/July 2005. Compare figure 5.22. The grey bars correspond to the places used in figure 5.24.

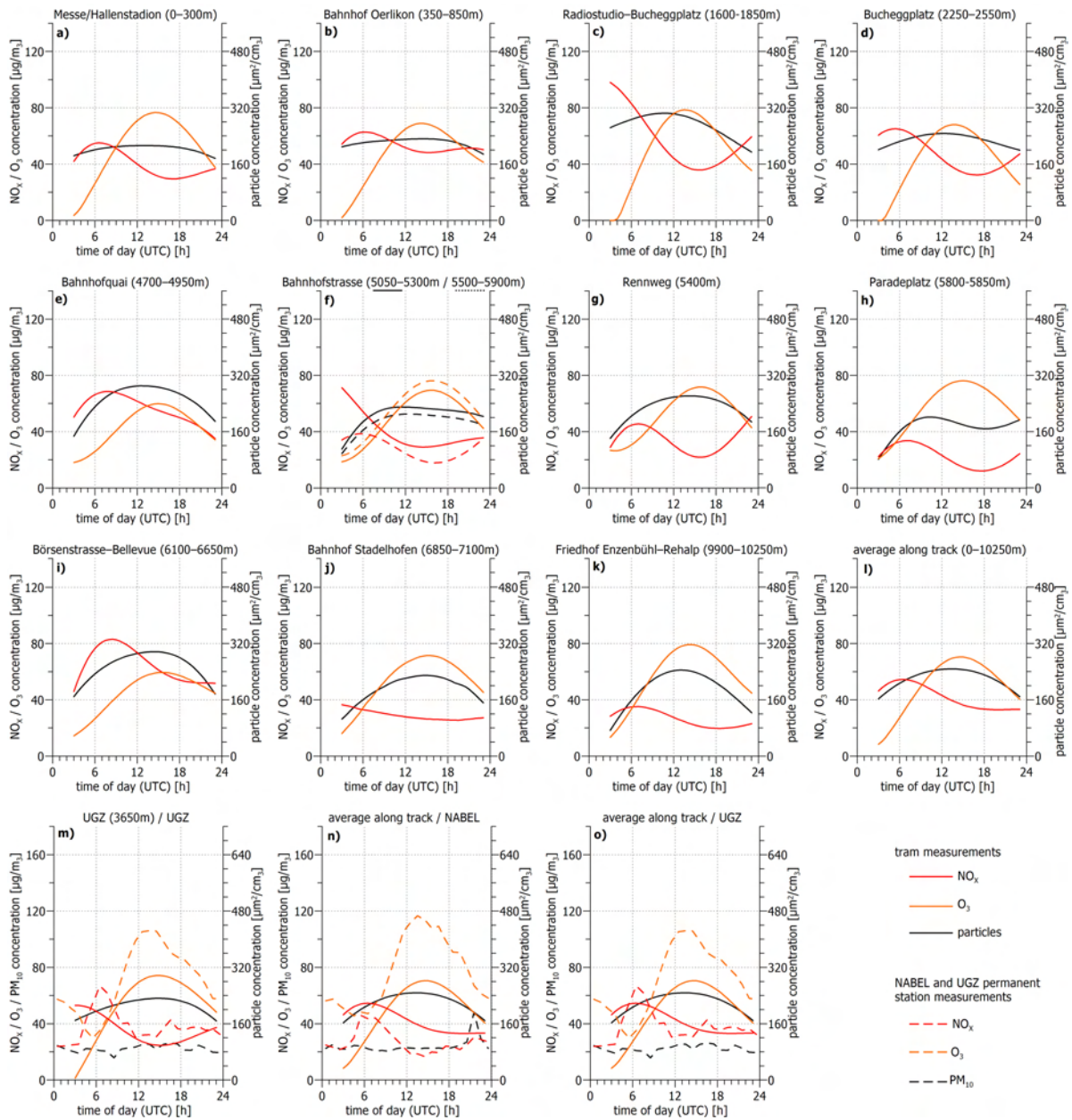


Figure 5.24: Diurnal variations at certain sites during the combination of fair and adverse weather in June/July 2005. Compare figures 5.21 and 5.22.

Discussion

The different types of plots showed on the previous pages are all made from three data set. Certain features of the data are more pronounced in one plot than in the other plots. In order to keep “see figure so-and-so” clutter in the discussion low, the plots will be referred to as follows.

	<i>fair weather...</i>	<i>adverse weather...</i>	<i>combined...</i>
<i>... collocation plot</i>	fig. 5.13	fig. 5.17	fig. 5.21
<i>... along track plots</i>	fig. 5.14 and 5.15	fig. 5.18 and 5.19	fig. 5.22 and 5.23
<i>... diurnal variation plot</i>	fig. 5.16	fig. 5.20	fig. 5.24

Therefore, for example, the *adverse weather collocation plot* would be figure 5.17 or the 9–12 h curve in the *combined along track plot* could be found in figure 5.23.

The grey bars added to the along track plots labelled a–k correspond to the places a–k in the diurnal variations plots.

The collocation plots show the average ambient air concentrations during the day (y axis) and along the tram track (x axis) for fair and adverse weather days as well as for the combination of fair and adverse weather days. The along track plots and the diurnal variations plots are extracts from the collocation plots.

The analysis reveals several features of the spatial and temporal distribution of the ambient air concentration. They include:

- * A high variability of the ambient air concentration exists for all pollutants. It is more pronounced for the primary pollutants NO_x and particulate matter, which are directly linked to the emissions sources.
- * Since the emissions mainly originate from road transport, busy places can be clearly seen in the data. The most distinctly busy section along the tram line 11 is from *Börsenstrasse* via *Bürkliplatz* to *Bellevue* (position 6100–6650 m in the collocation plots, “i” in the other plots). The multi-lane roads handle large amounts of inbound and transit traffic and transport throughout the day.
- * Further well-known busy places include the sites around *Messe/Hallenstation* and *Bahnhof Oerlinkon* (0–850 m, “a/b”) as well as around the main station (4700–4950 m, “e”). They also show high ambient air concentrations of NO_x and particulate matter throughout the day.
- * The ambient air concentration of ozone correlates less with the traffic (and accordingly the position along the track). The ozone concentrations increase with the position of the sun and reach the maximum in the afternoon. The diurnal variation is significantly less pronounced during adverse weather, where far less solar radiation reaches the ground than during fair weather (compare figure 5.12). The afternoon peak is roughly half as high during adverse weather compared to the photochemical smog during fair weather.
- * A meteorological effect can be identified during fair weather. In the morning hours the NO_x concentrations are generally highest. When the inversion dissolves in the later morning the concentrations generally decrease but at busy places. Compare the blue (6–9 h) and the orange and red (9–12 h and 12–15 h, respectively) curves in the second position along track plot for fair weather at *Burgwies/Balgrist* (9000–9800 m)

or at *Schaffhauserplatz–Beckenhof* (3100–4000 m). The integrated average along the track also shows this effect (see sub-figure l in the diurnal variation plot).

- * A similar diurnal variation for NO_x can be seen during adverse weather (see the second position along track plot and sub-figure l in the diurnal variation plot). Here, the effect is probably due to the morning rush hour and the weather conditions (rain, wind).
- * The titration of O_3 by NO (a chemical effect) below the inversion layer can be seen. It is best visible at busy places, such as from *Börsenstrasse* to *Bürkliplatz* (6100–6650 m) or around the main station (4700–4950 m).

The interpolation of the irregularly distributed data (compare section 5.1.1) generally produces meaningful plots which are valuable to assess the temporal and spatial distribution of the pollutant concentrations. However, a drawback of the collocation modelling seems to exist in the time domain. The diurnal variations for obtained through this interpolation method do not show the irregularity in the diurnal variations which are seen in the data from the permanent stations (compare sub-figures m–o in the diurnal variations plots). Furthermore, there is a boundary value deficiency for the interpolation of ozone where the curves tend to start at zero and quickly increase to a reasonable value in the morning and throughout the day. The variations of the concentration along the tram track are very pronounced and busy places can be clearly seen. This enables temporal-spatial air quality assessments which would not be possible with conventional monitoring stations.

5.3.6 Winter 2006

General situation

In winter 2005/06 several smog situations developed in January and February, 2006 (compare figures B.2c and B.3c), during which the limit values for NO_2 and PM_{10} were exceeded for several days.

Figure 5.25 shows the daily averages for NO/NO_2 , O_3 and PM_{10} at the NABEL and the UGZ permanent monitoring station during a 25 days period. It starts on January 23 and ends on February 16, 2006. The daily limit value for PM_{10} is exceeded on during almost two weeks at both stations. The NO_2 limit is exceeded during five days. On February 6–7 the daily means fall below the limits and the situation normalises. A short and less distinct period of high pollutant concentrations occurs on February 13–14. The daily mean values derived from the tram measurements (see section 5.1.2) are plotted in the background of figure

During this 25 days period high quality measurements from the tram line 10 are available on 23 days which cover at least the morning and early afternoon hours (compare figure 4.5, page 47).

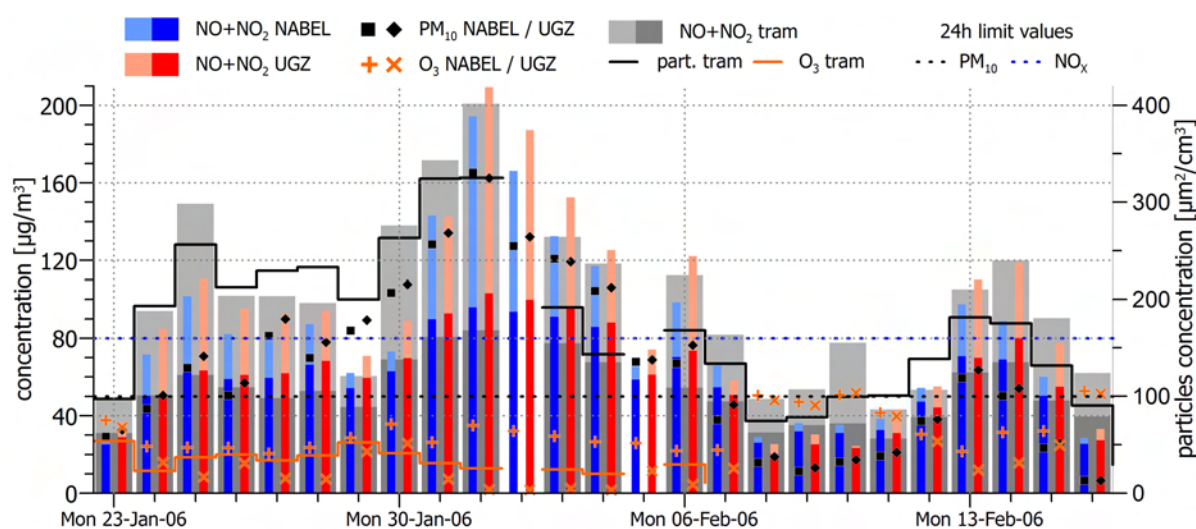


Figure 5.25: General situation during twenty-five days in winter 2006 (January 23 to February 16, 2006). A smog period lasting almost two weeks develops on January 24–25 during which the PM_{10} limit value was exceeded constantly. The maximum daily mean concentration of PM_{10} on February 1 was more than three times the limit value at two permanent stations (NABEL and UGZ, see figure 4.1) in the city of Zürich. The NO_2 limit was exceeded during five days (January 31 – February 4). The grey bars in the background are the daily means derived from the tram measurements (see section 5.1.2).

Average ambient air concentration

The data from the 23 days of tram measurements were interpolated using the collocation method (compare section 5.3.5). Figure 5.26 shows the collocated combination of all measurements (23 days) for each chemical species. The data is plotted along the track (x axis) versus the time of the day (y-axis). The collocated plots for each day can be found in appendix B.3 (page 186).

Figure 5.27 shows the mean concentration along the track for five 3-hours intervals (6–9 h, 9–12 h, 12–15 h, 15–18 h and 18–21 h) as well as the 4–18 h average.

The plots reveal generally higher primary (NO and particles) pollutant concentrations in the morning (figures 5.26a and d, respectively). The variation of the ambient air concentration is most distinct for these species in the morning. Very high concentrations can be seen from the main station to the *Central* place (0–650 m) and in the section from *Haldenbach–Letzistrasse* (1650–2850 m). On these parts of the tram track the tram runs in the middle of very busy places and streets. The streets around the main station as well as the *Central* place are multi-lane traffic junctions. In the second section the tram runs in busy street canyons (*Universitäts-/Winterthurerstrasse*). The last part of the track from *Irchel* (4750) to *Oerlikon* consists of less busy and wider streets. The NO₂ concentrations only show this pattern to a certain extent. This is probably due to the accumulation and dispersion of the secondary pollutant NO₂. However, the correlation between traffic and primary pollutants can be clearly identified.

Due to the high concentrations of NO_x and the weak solar radiation in winter, the ozone concentrations are relatively low. A weak ozone maximum is visible in the afternoon (5.26e and the red curve for O₃ in figure 5.27).

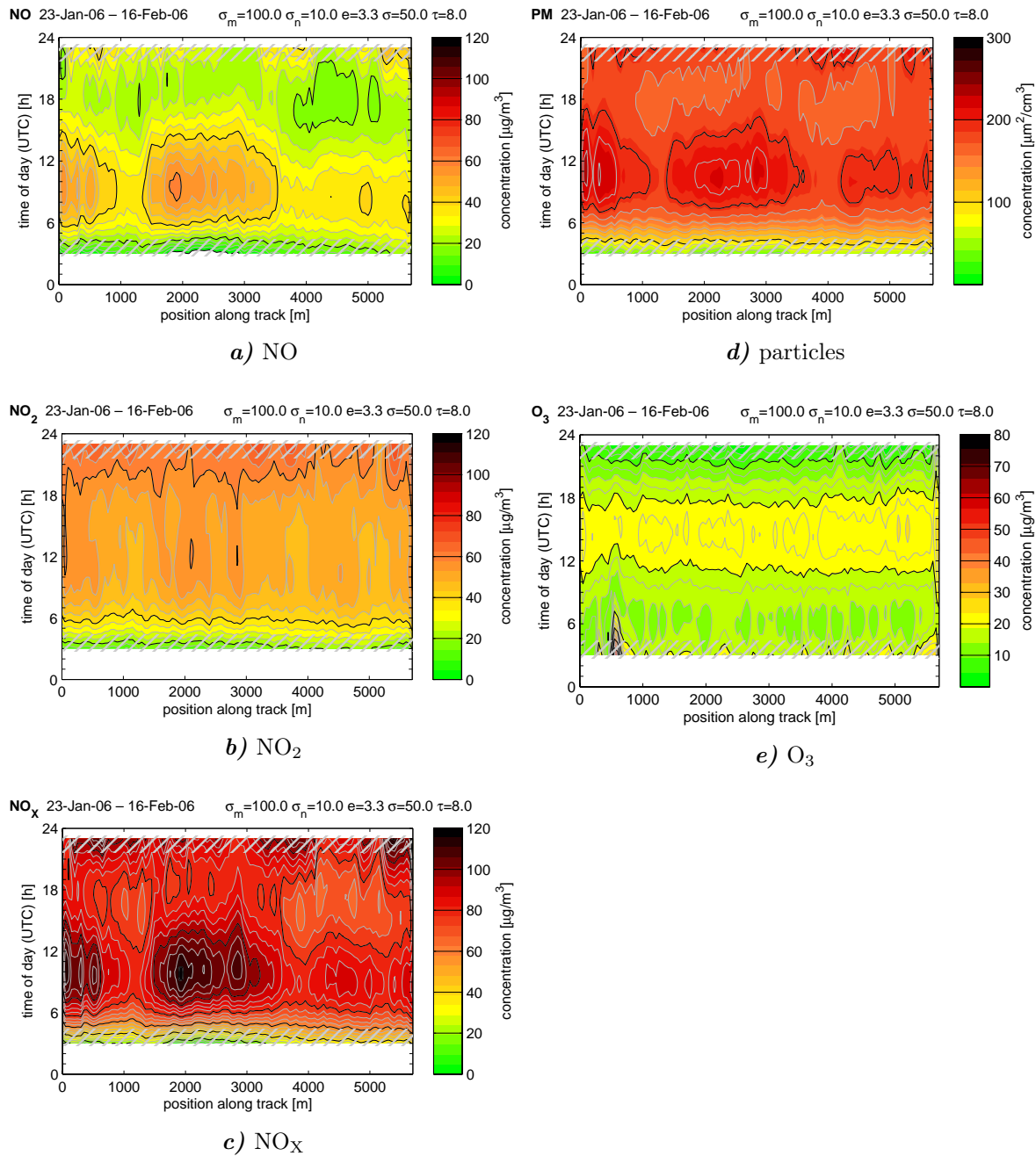


Figure 5.26: Spatial and temporal distribution of pollutant concentrations in winter 2006 (collocated average of 23 days in the period of January 23 – February 16). Two sections of the track with above-average ambient air concentrations in the morning to the early afternoon can be seen for the primary pollutants NO (**a**) and particles (**d**). They correlate with the busy streets and places at the main station and the *Central* place (0–650 m) and the section along *Universitäts-* and *Winterthurerstrasse* (1650–2850 m). The secondary pollutant NO₂ (**b**) shows this pattern only weakly due to the accumulation during the period. The ozone concentrations (**e**) are generally low due to the high NO_x concentrations and the weak solar radiation in winter. A low peak in the afternoon can still be identified.

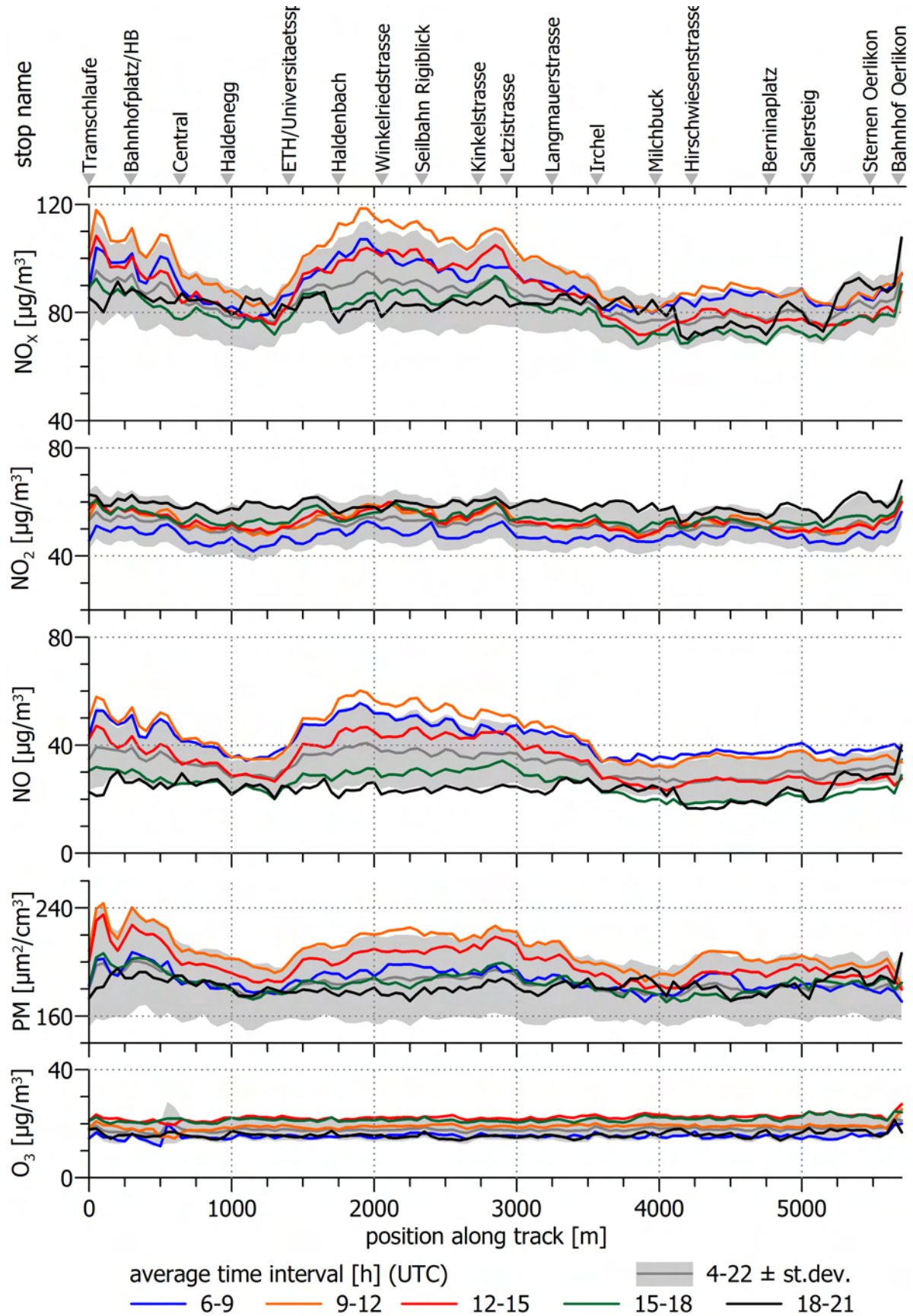


Figure 5.27: Average ambient air concentrations along the track during 23 days in winter 2006 (January 23 – February 16). Selected time intervals are plotted for each chemical species. Compare figure 5.26.

Accumulation

During smog period the pollutants accumulate and the ambient air concentrations increase from day to day. The 9–14 h (UTC) averages for every day in the period introduced above were extracted from the daily collocation results (see appendix B.18).

The left column in figure 5.28 shows the 9–14 h mean concentrations time series (y axis) along the tram track (x axis). Missing data (February 2 and 5) was interpolated linearly. Three accumulation periods can be identified for NO/NO₂/NO_x and particles. They are:

1. January 23–25
2. January 29 – February 2
3. February 11–14

The right column in figure 5.28 shows the day-to-day difference in ambient air concentration. The plots reveal that the difference for the primary pollutants is virtually constant along the track (sub-figures a and

During the selected interval (9–14 h) the accumulation of NO and particles is stronger in the section from *Haldenbach* to *Letzistrasse* (1650–2850 m) than on other parts of the tram track.

Figure 5.29 shows the absolute values and the day-to-day differences at selected sites and sections of the track along the values and differences derived from the measurements at the UGZ permanent station. The interpolation of the missing tram measurements fits well into the time series on February 2 (green marks). On February 5, however, the interpolation does not agree with the measurements at the UGZ permanent station. This leads to errors in the day-to-day difference on this and the following day (red marks).

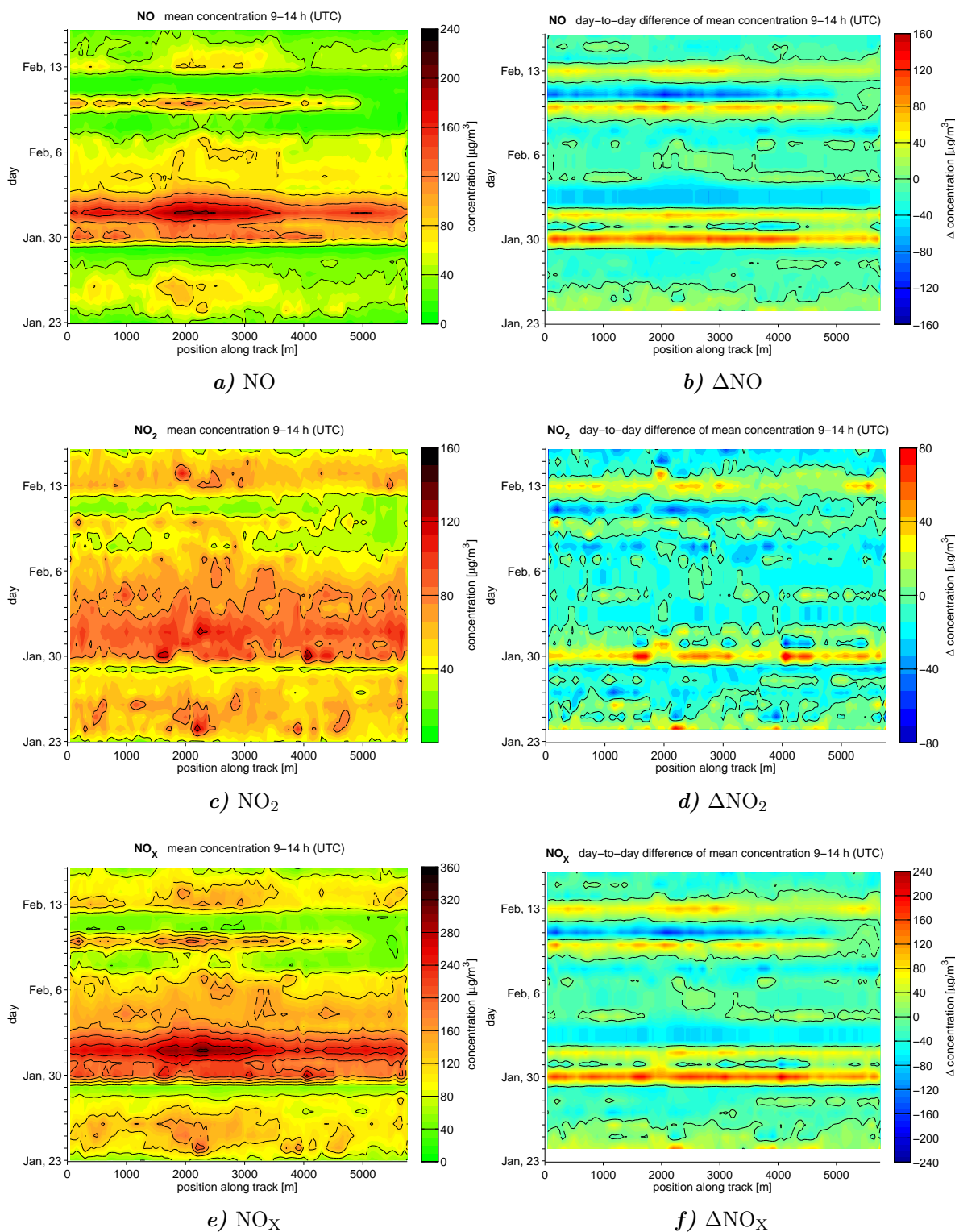


Figure 5.28: Mean ambient air concentrations during the period from 9 to 14 h (UTC) (left column) and the day-to-day change in the ambient air concentration (right column). The data for the days where no measurements are available (February 2 and 5) were interpolated linearly. The contour lines in the plots in the left column are according to the grid lines in the scale bar. In the day-to-day differences plots (right column) the contour lines separate negative and positive values. (continued on next page)

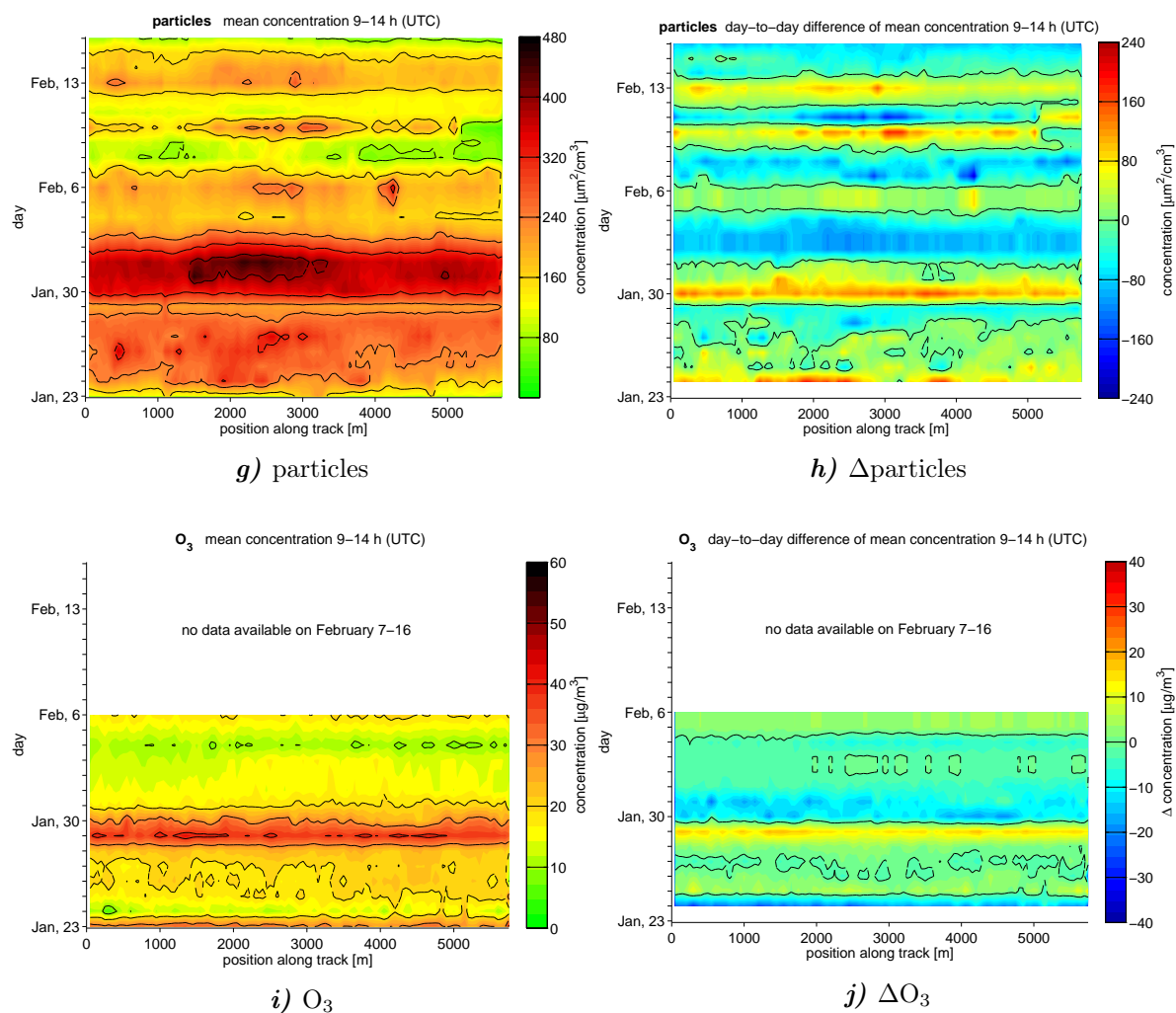


Figure 5.28: (continuation from previous page)

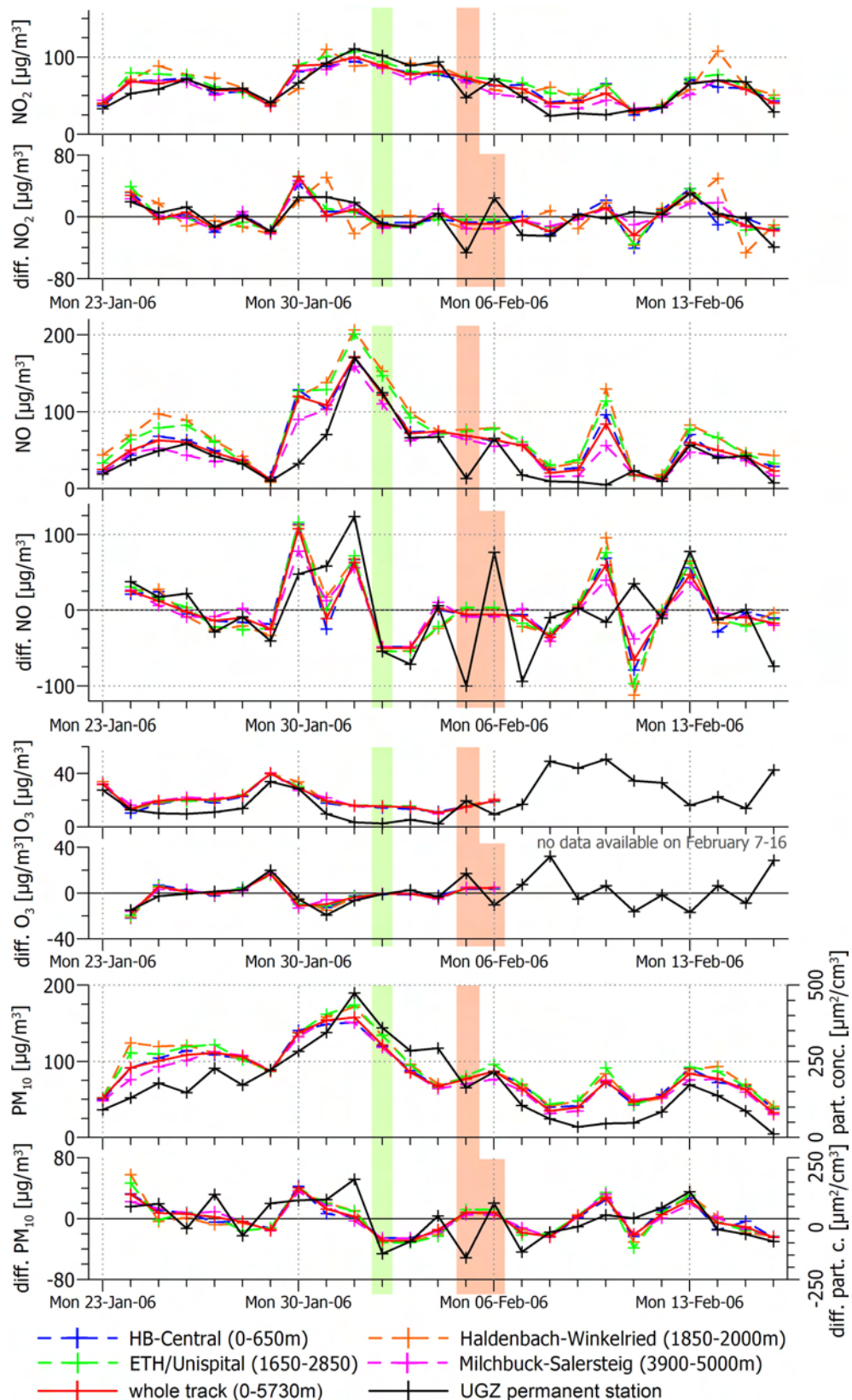


Figure 5.29: Time series of the average 9–14 h ambient air concentrations and their day-to-day differences for selected parts of the tram track along the corresponding time series derived from the measurements at the UGZ permanent station for each chemical species. The red and green marks denote the influence of a good and a poor interpolation of missing data, respectively (see text).

5.4 GPS performance analysis

A general analysis of the GPS performance during the two campaigns was carried out for the quality-filtered GPS measurements (i.e. those measurements which were used in the post-processing). Figure 5.30 shows two properties which characterise the performance of the GPS receiver in terms of the PDOP value (see section 2.2) and the number of available satellites. Sub-figures a–c show the histogram of the number of satellites available on each tram track used during the measurement campaigns. Statistical properties of the distribution (mean, median, standard deviation, minimum and maximum) are given in the title of each plot. In average 6–7 GPS satellites were visible in positions which met the quality requirements for the post-processing (compare section 4.3.3 and 4.3.4). Sub-figures d–f show the distribution of PDOP values and its statistical properties. The mean PDOP was 5.1–5.5 on all three tram lines. This is a relatively poor PDOP in comparison what one would get in an unobstructed environment. However, the chosen receiver proved to be capable of producing reliable and accurate positions in urban areas and pronounced street canyons of up to approximately 20–30 metres height ([Heller, 2003; Forster and Landtwing, 2004; Rossinelli, 2006]). This is probably due to the sophisticated Kalman filter engine in the receiver which was tuned to the expected movement of vehicles running on streets. Subfigures g–i plot the number of used satellites versus the observed PDOP with error bars. The two variables correlate strongly in all three data sets. The correlation coefficient is between 0.833 and 0.989. The PDOP value decreases by approximately 0.35–0.40 with each additional satellite.

The ratios of GPS outages along the tram tracks was calculated and analysed. Figure 5.31a–c shows the ratio of GPS outages individually per driving direction for all three tram tracks used during the measurement campaigns. The distinct peaks seen in these plots are due to the simplification made regarding the tram track geometry (compare section 4.1). At a few sites the offset of the real tram track and the tram track geometry used was larger than a threshold radius and the possibly good GPS measurements were discarded and later interpolated during the map-matching process. This produced the peaks at approximately position 500 m (*Bahnhof Oerlikon*) on line 11 in both directions (sub-figure a) and at approximately position 1500 m (*Kirche Fluntern*) on line 6 in the backward direction (sub-figure c). The peaks on line 10 (sub-figure b) have other reasons. The peak at approximately position 5400 m (*Oerlikon*) in the backward direction is probably due to the pronounced street canyon at this site and the peak at approximately position 4100 m (*Milchbuck*) corresponds to the turning in a loop at this site in the evenings (compare figure 4.12).

Figure 5.31d shows scatter plots of the GPS outage ratios for the tram lines 11, 10 and 6. They reveal that there is no correlation between the outage ratio of either driving direction. The outage ratios on tram line 11, which are between 13 and 18% in average, are significantly higher than the outage ratios on lines 10 and 6 (between 2.2 and 3.5% in average). The difference of the ratios observed on line 11 to the ratios seen on the other lines is probably due to the software problems during the first measurement campaign (see section 4). Therefore, it is assumed that 2.2–3.5% is the average ratio of GPS outages which can be expected on a tram driving through the city of Zürich.

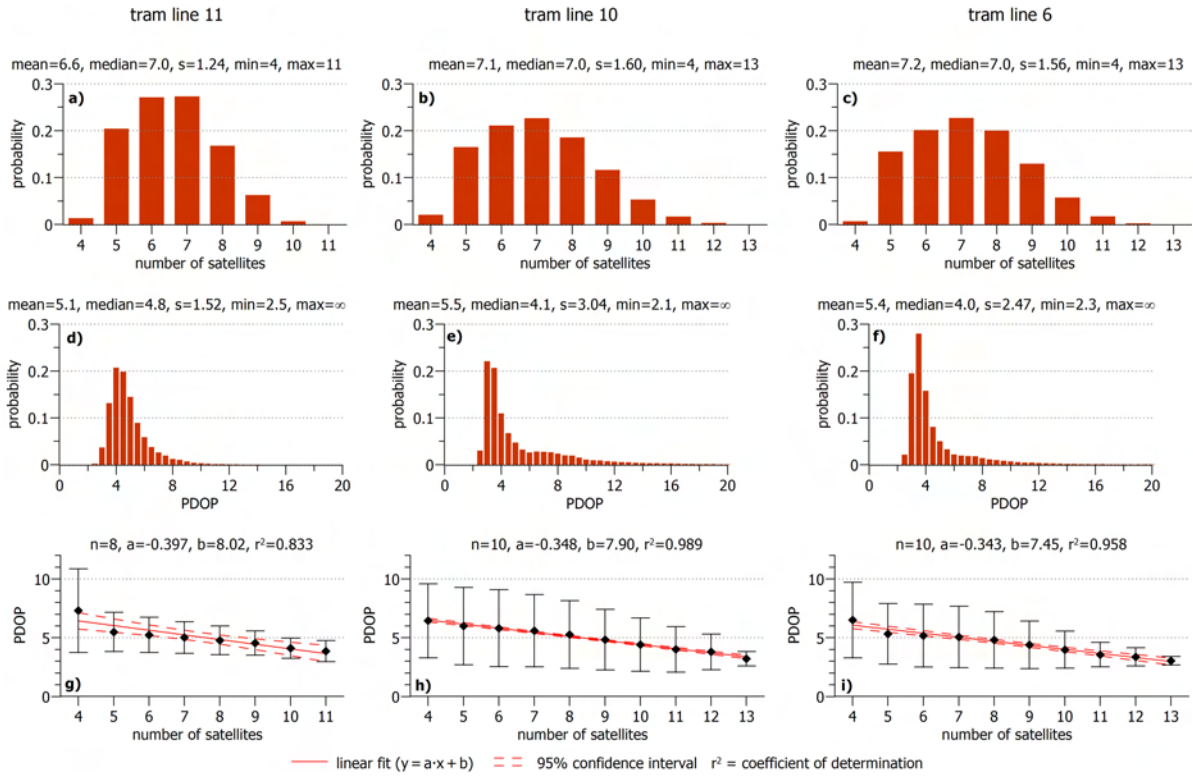


Figure 5.30: General statistical analysis of the GPS performance on the three tram lines (columns) used during the measurement campaigns. All GPS measurements which were used in the post-processing are included in the data set. The first row of plots (a, b and c) show the histogram of the number of satellites. The plots d, e and f show the histogram of the PDOP values in each data set. The last row of plots (g, h, i) analyse the correlation between the number of satellites and the PDOP value. Statistical properties of each plot are given above it.

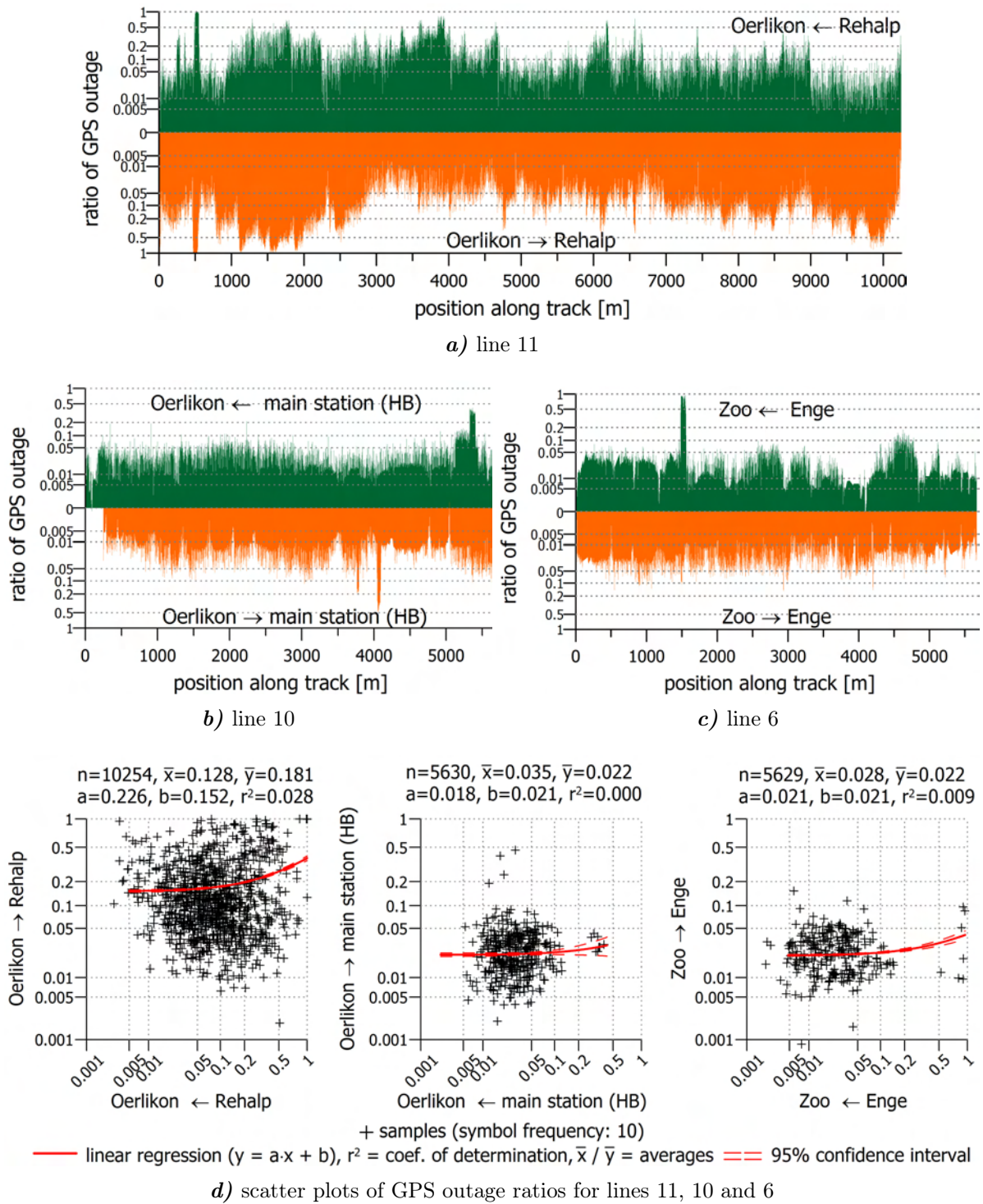


Figure 5.31: GPS outage ratios per driving direction for the tram lines 11 (a), 10 (b) and 6 (c). Distinct peaks are due to the post processing of the GPS data (see text). Scatter plots (c) of the outage ratios show the distribution of the outage ratios and reveal that outages in either driving direction does not correlate with outages in the other direction.

A detailed analysis of the GPS performance and the map-matching accuracy was carried in [Rossinelli, 2006] for selected days in the first campaign. This analysis was partly reproduced using the complete data set of GPS measurements obtained during the first campaign. The data set consists of approximately $3.5 \cdot 10^6$ GPS measurements. The matched distance, i.e. the distance between the (Kalman filtered) position obtained from the GPS receiver and the corresponding position determined on the tram track (compare figure 4.10), was examined.

Figures 5.33 and 5.33 show the results of this analysis.

The mean PDOP values in each driving direction at a certain position along the track only correlate weakly ($r^2=0.542$, figure 5.32c). The number of satellites, however, shows a correlation coefficient of 0.699 (sub-figure d). The mean matched distance in each driving direction do not correlate ($r^2=0.046$, sub-figure e).

Figures 5.32a and e show the histograms of the mean matched distance in each direction and the statistical properties of the distribution.

Figures 5.32a–d and f–h show scatter plots of the mean number of satellites, the mean PDOP and the mean matched distance for each driving direction. There is no significant correlation between any of the variables.

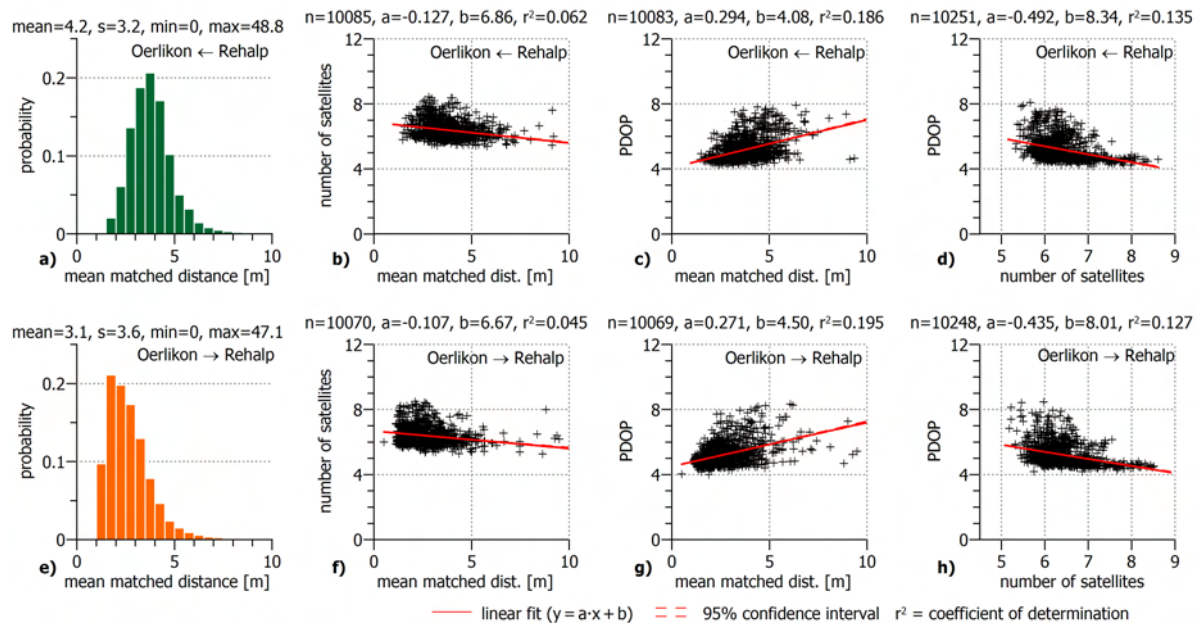


Figure 5.32: Histograms of the mean matched distance for each driving direction and the statistical properties of the distribution (**a** and **e**). Scatter plots of the three variables “number of satellites”, “mean matched distance” and “PDOP” in all combinations separately for each driving direction (**b–d** and **f–h**).

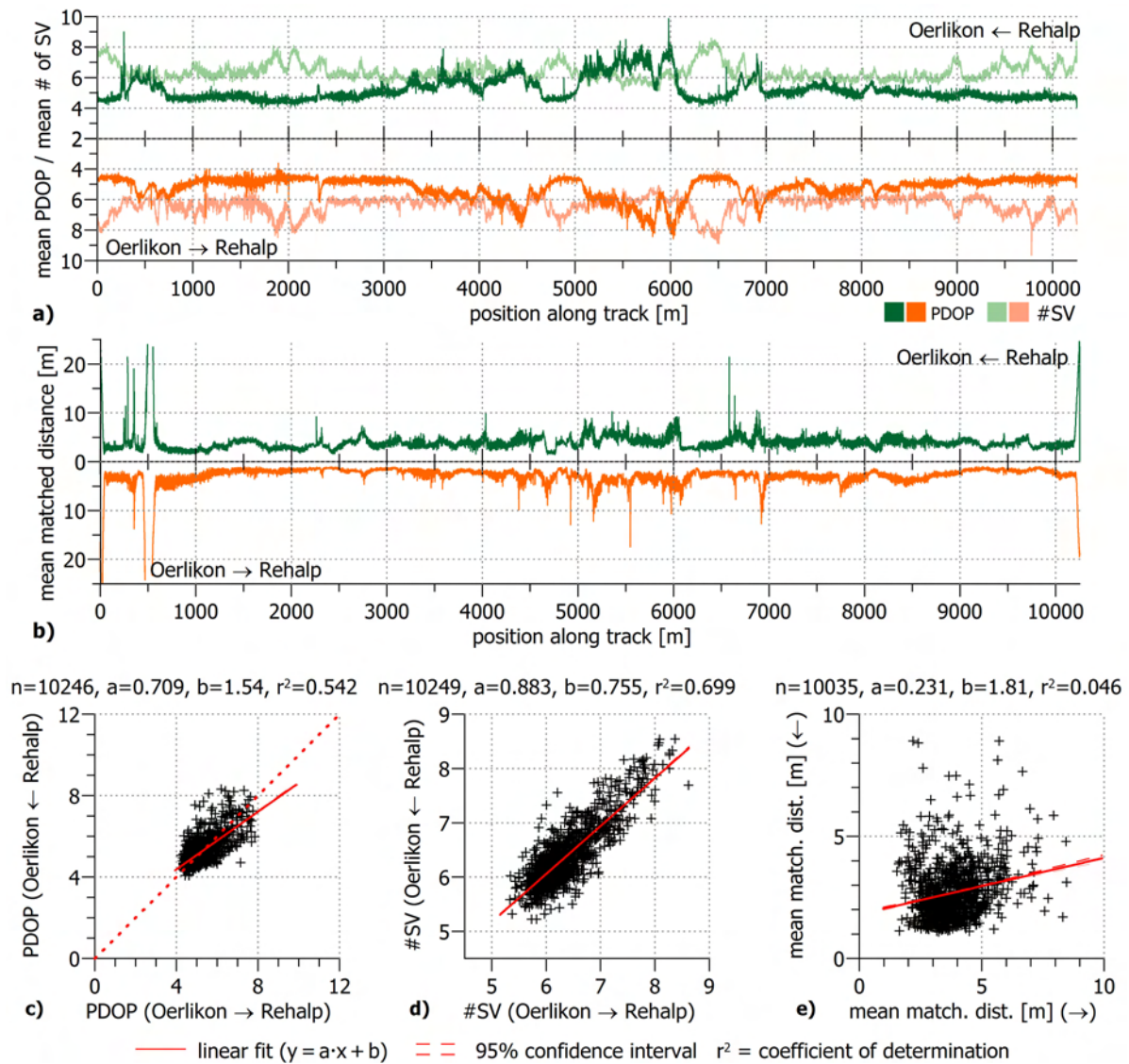


Figure 5.33: The mean number of satellites and the mean PDOP value is plotted along the track for each driving direction (**a**). Sub-figure **b** shows the mean matched distance along the track individually. A certain symmetry can be seen in **a** and **b**. The scatter plots reveal a correlation for PDOP and the number of satellites (**c** and **d**, respectively). There is no correlation for the mean matched distance (**e**).

* * *

6

Emission & Dispersion Modelling

6.1 Introduction

At ground level in a city most pollutants originate from road traffic. The emission sources are mainly internal combustion engines used in cars, trucks, busses, motorbikes and scooters. They together build line sources along the road network. The pollutants then disperse into the city. Depending on the weather situation (wind, radiation, precipitation) they accumulate, degrade or react to other compounds. Urban areas are a complex terrain with a rough surface where wind induces turbulence in the street canyons. This influences the dispersion of the emissions. To determine the spatial distribution of the mean concentration of a pollutant in a city many parameters have to be taken into account. In this chapter the modelling approach is described. The steps involved to obtain the spatial distribution of the major air pollutant NO_x in the inner city of Zürich is detailed. The results obtained from the dispersion modelling are compared with measurements conducted in this project.

This chapter has been done with great support of Mr. Dietmar Oetl of the *Institute of Internal Combustion Engines and Thermodynamics* of the *Graz University of Technology*. The necessary models and software to carry out the calculations were provided by him. References based on personal communication with Mr. Oetl is hereafter indicated by the citation [Oetl].

The study area extents over 3.3 km^2 in the inner city of Zürich (figure 6.2). It was chosen with respect to available measurement data, both from the tram measurements and an established reference station (see also figure 4.1), as well as its urban character covering busy places and streets without private road traffic and computational limits. The dispersion calculations were carried out for a period of one year (June 1, 2005 until May 31, 2006).

6.2 Modelling approach

The modelling approach involves three models. These are:

- NEMO** – The road traffic emission model (*Network Emission Model*) which allows the calculation of traffic emissions on road networks [Rexeis and Hausberger, 2005; Rexeis et al., 2007]. It relies on the handbook of emission factors for road traffic (HBEFA) [UBA/BUWAL, 2004].
- GRAMM** – The 3d wind field model (*Graz Mesoscale Model*) [Oettl, 2000].
- GRAL** – The dispersion model (*Graz Lagrangian Model*) [Oettl et al., 2001a,b,c, 2002, 2003, 2004].

Figure 6.1 provides a general overview of the complete modelling and calculation process. Basically, meteorological, geometrical and emission data is needed to carry out the final dispersion calculations. The steps to generate this input data is detailed in the following sections of this chapter.

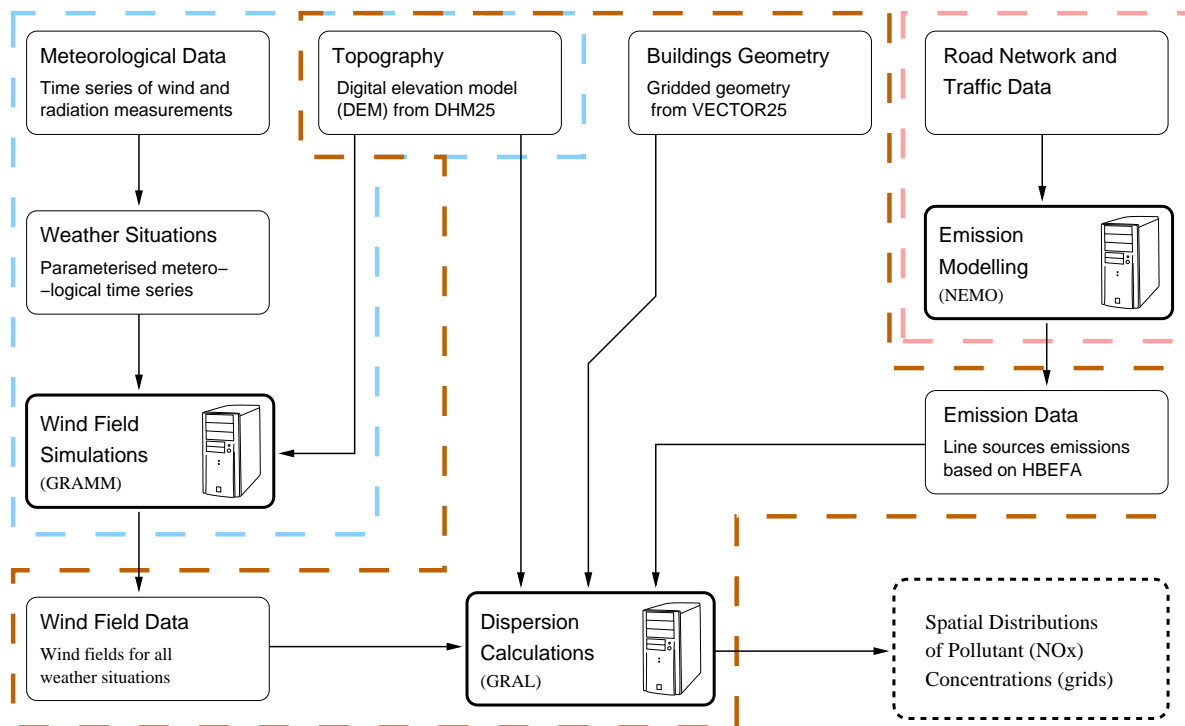


Figure 6.1: General flow chart of the dispersion modelling. The four boxes at the top correspond to the input data. The bold framed boxes represent the three modelling/simulation programmes. The other framed boxes correspond to pre and post processing. The final result are represented by the bottom right box. See also sections 6.3–6.6 and figures 6.8 and 6.18

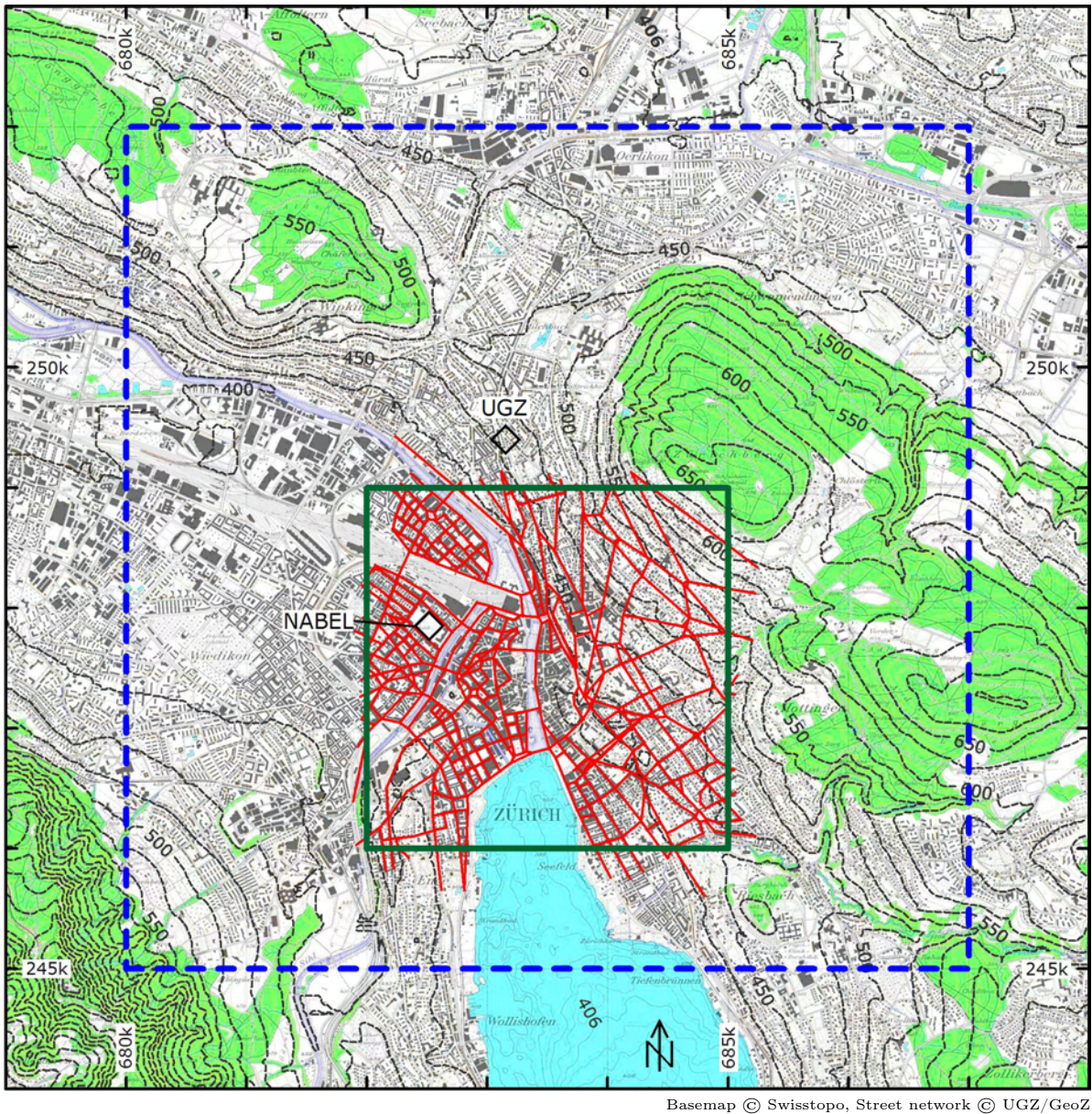


Figure 6.2: Study area for the dispersion modelling. The wind field was calculated for the larger 7.7 km^2 extent (dashed line). The dispersion has been modelled on the smaller 3.3 km^2 extent taking into account the road network (red). The location of two reference stations (NABEL and UGZ) are marked with diamonds. The base map has been lightened and contour lines with 25 m spacing were added.

6.3 Geometrical data

6.3.1 Topography (elevation model)

The wind field calculations (see section 6.5) and the dispersion calculations (see section 6.6) take the terrain into account. This is available for Switzerland in the digital elevation model DHM25 (*Digitales Höhenmodell 25 m*) data set from Swisstopo (Federal Office of Topography). The basis model consists of digitised contour lines and spot heights from the Swiss topographic maps (1:25 000). The available model is an interpolated grid with 25 m, mesh width and a vertical accuracy better than 2 m [Swisstopo, 2005a]. It represents the form of Earth's surface without vegetation or buildings. An extract from this data set covering the 7.7 km² study area (figure 6.2) was converted to the binary format used in the calculations (file GGEOM.DAT) [Oettl].

6.3.2 Buildings

The dispersion calculations (see section 6.6) need the geometry of the buildings in order to take street canyon effects into account. Such data is available in the VECTOR25 data set from Swisstopo [Swisstopo, 2005b]. The layer *geb* (*Gebäude*, buildings) contains digitised geometrical data of all buildings from the Swiss topographic maps (figure 6.3 left). Scripts using the Shapefile C library [Warmerdam et al., 2002] and GNU awk [FSF, 2006] was written to extract the contour of the buildings within the area of investigation (fig 6.2). The data from this region was updated to the year 2000. The gridding routines of the *Surfer* computer programme was used to create a grid of the



Figure 6.3: The building geometry in the 3.3 km² study area (**a**) were extracted from the VECTOR25 data set. The vector data was gridded with 5 m mesh width (**b**) and included in the dispersion calculations.

VECTOR25 © Swisstopo

buildings at 1 m resolution. Due to computational limits, particularly memory limits but also acceptable calculation time, it was re-sampled to a grid with 5 m mesh width (figure 6.3 right). Building heights had to be assumed due to the lack of corresponding data. An average building height of 20 m was chosen and openings through (passages) or within (courtyards) buildings were disregarded. This data served as basis file `GEBAEUDE.DAT` for the dispersion calculations.

The file has the following format: 8 bit (ASCII) text with coma separated values. Each line corresponds to one grid cell and consists of the four values x , y , z_0 and z_1 where x and y is the position, z_0 is the lower edge of the building (in this study: 0.0) and z_1 is the upper edge of the building (in this study: 20.0).

6.4 Emission modelling

6.4.1 Overview

Emission modelling is based on traffic data and emission factors for road transport, the handbook of emission factors for road traffic (HBEFA) [UBA/BUWAL, 2004]. This calculations was kindly carried out by [Oettl] using the *NEMO* model (Network Emission Model). Figure 6.4 shows the flow chart of the calculations in the model. Rexeis and Hausberger [2005] and Rexeis et al. [2007] describe the model in detail.

This section describes the input data created for the study area (figure 6.2) and the output data received for further processing within the dispersion calculations (section 6.6).

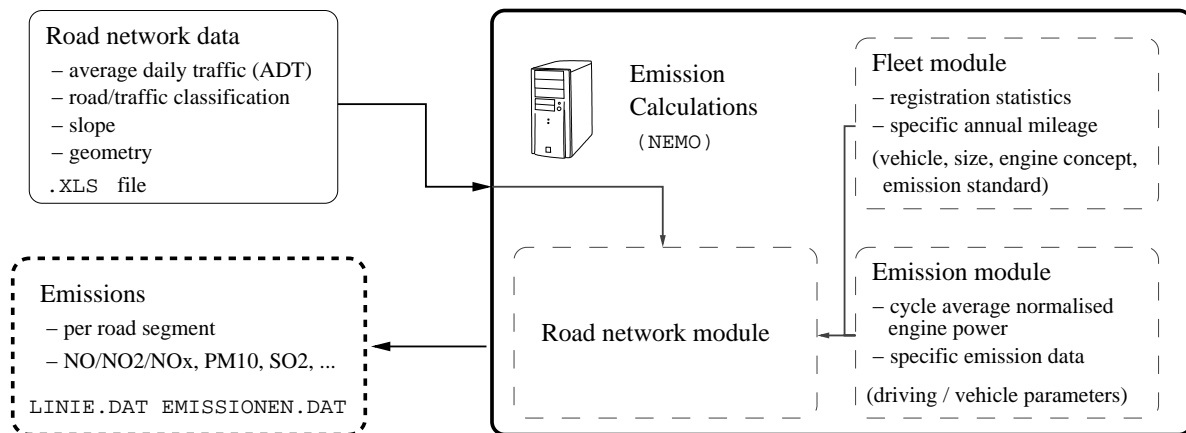


Figure 6.4: Flow chart of the emission calculations using the *NEMO* model.

6.4.2 Input data

The input data is an Excel file containing road network data. The road network consists of individual lanes. Each lane has a number of attributes. Table 6.1 lists the attributes which have to be given as the input.

The road network geometry, the street classification and the other attributes was extracted from a data set used by and obtained from the UGZ (*Umwelt und Gesundheitsschutz Zürich*, office for environment and health protection of Zürich). The data set is part of study about emissions of road traffic in the city of Zürich [Leuenberger et al., 2004] and contains traffic data determined for the year 2004. The report projects the data to the future in different scenarios. These depend on the growth of traffic in general on the growth of the diesel engine fraction. For this study the so called basis scenario for the year 2005 was chosen. It has a diesel engines fraction according to the HBEFA (estimated 38% in the year 2020) and a slight growth of traffic (1.12%/a). The heights of the lane segment nodes were extracted from the digital elevation model introduced above. The yearly average daily traffic (ADT) is visualised in figure 6.5.

attribute	unit	description
Kürzel VS	text	traffic situation identifier (see table 6.2)
Strassenname	text	street name ¹
Abschnittsnr	text	segment number ¹
L	km	length of the lane segment ¹
Stg	%	average slope of the lane segment
Strassentyp	int	street type (1: urban, 2: rural, 3: highway)
JDTV	n/day	yearly average daily traffic (JDTV, ADT)
Ant. LNF	–	fraction of JDTV of light-duty commercial vehicles ²
Ant. SNF	–	fraction of JDTV of heavy-duty commercial vehicles ³
Ant. Solo LKW	–	fraction of SNF of solo heavy-duty comm. vehicles ²
Ant. LSZ	–	fraction of SNF of trailer trucks ²
Ant. Rb	–	fraction of SNF of overland busses ²
Ant. Libus	–	fraction of SNF of public transport busses ²
QGr	int	emission layer ⁴⁵
xvon	m	easting of start node of the lane segment ¹
yvon	m	northing of start node of the lane segment ¹
zvon	m	height of start node of the lane segment ¹
xbis	m	easting of end node of the lane segment ¹
ybis	m	northing of end node of the lane segment ¹
zbis	m	height of end node of the lane segment ¹
StrBreit	m	width of the lane segment ⁵
LSW	m	height of noise barrier ⁶

¹ value is passed to the output file⁴ feature not used in this study² determined by NEMO⁵ input for dispersion calculations³ input data available⁶ not applicable in this study (=0)

Table 6.1: Street network attributes used as input for the emission modelling.

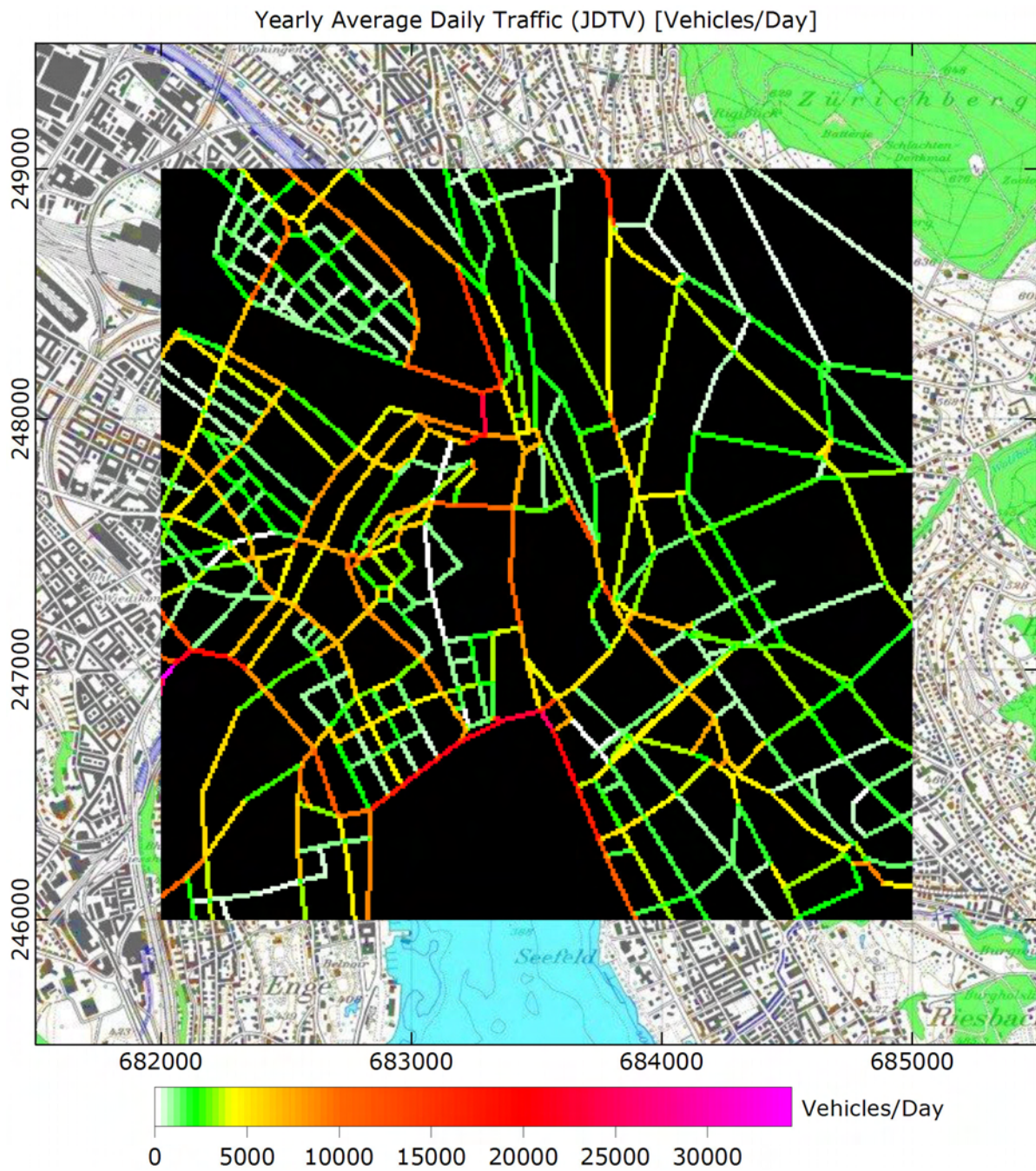


Figure 6.5: Yearly average daily traffic (JDTV, ADT).

identifier	description	mean speed
AB_80	highway, speed limit 80 km/h, traffic < 1500 vehicles/h per lane	n/a
IO_HVS1	urban, main street, has right of way, little jamming	53 km/h
IO_HVS2	urban, main street, has right of way, medium jamming	42 km/h
IO_HVS3	urban, main street, has right of way, strong jamming	31 km/h
IO_LSA1	urban, main street, with traffic lights, little jamming	34 km/h
IO_LSA2	urban, main street, with traffic lights, medium jamming	28 km/h
IO_LSA3	urban, main street, with traffic lights, medium jamming	21 km/h
IO_Kern	urban, downtown street	21 km/h
IO_Nebenstr_dicht	side street in dense urban area	21 km/h
IO_Nebenstr_locker	side street in loose urban area	31 km/h
IO_Stop+Go	rural street with stop-and-go traffic	5 km/h

Table 6.2: Traffic situations used, according to [UBA/BUWAL, 2004].

6.4.3 Results

The results consist of the road network data with added emission parameters for various substances. These are NO, NO₂, NO_x, HC, CO, PM₁₀ (non-exhaust), PM₁₀ (exhaust), CO, CO₂, SO₂, N₂O, NH₃, CH₄, NMHC, benzene, toluene and xylene. In this study only NO_x is being used for the dispersion calculations. The data is stored in a coma separated ASCII file named LINIE.DAT containing the street network geometry, the traffic data and the emission factors. Furthermore a file EMISSIONEN.DAT is produced which contains the diurnal variations of the normalised emission rate (figure 6.6). It is a 24 lines long white space separated ASCII file with the following columns:

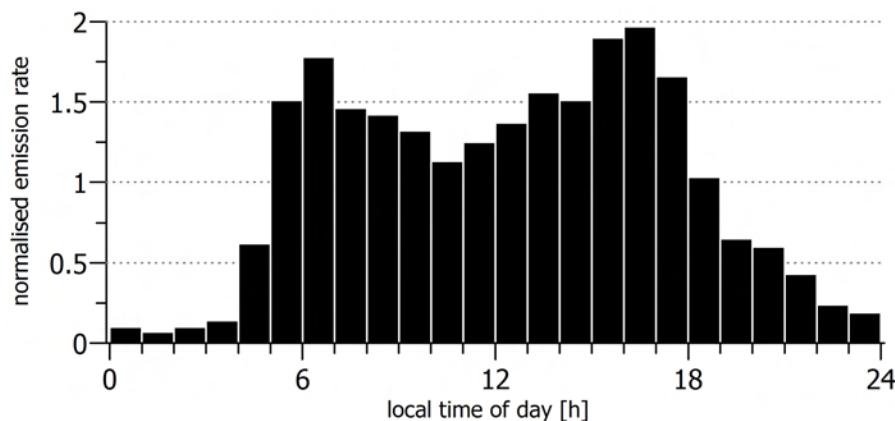


Figure 6.6: Diurnal variation of the normalised emission rate of an average day used in the dispersion calculations.

1. Time of day (integer hour).
2. Normalised emission rate for each hour of the day.
3. Normalised emission rate for each month (only first 12 lines, here always 1).

The diurnal variation of the normalised emission rate (figure 6.6) reflects an average day. There is no differentiation of weekdays and weekends.

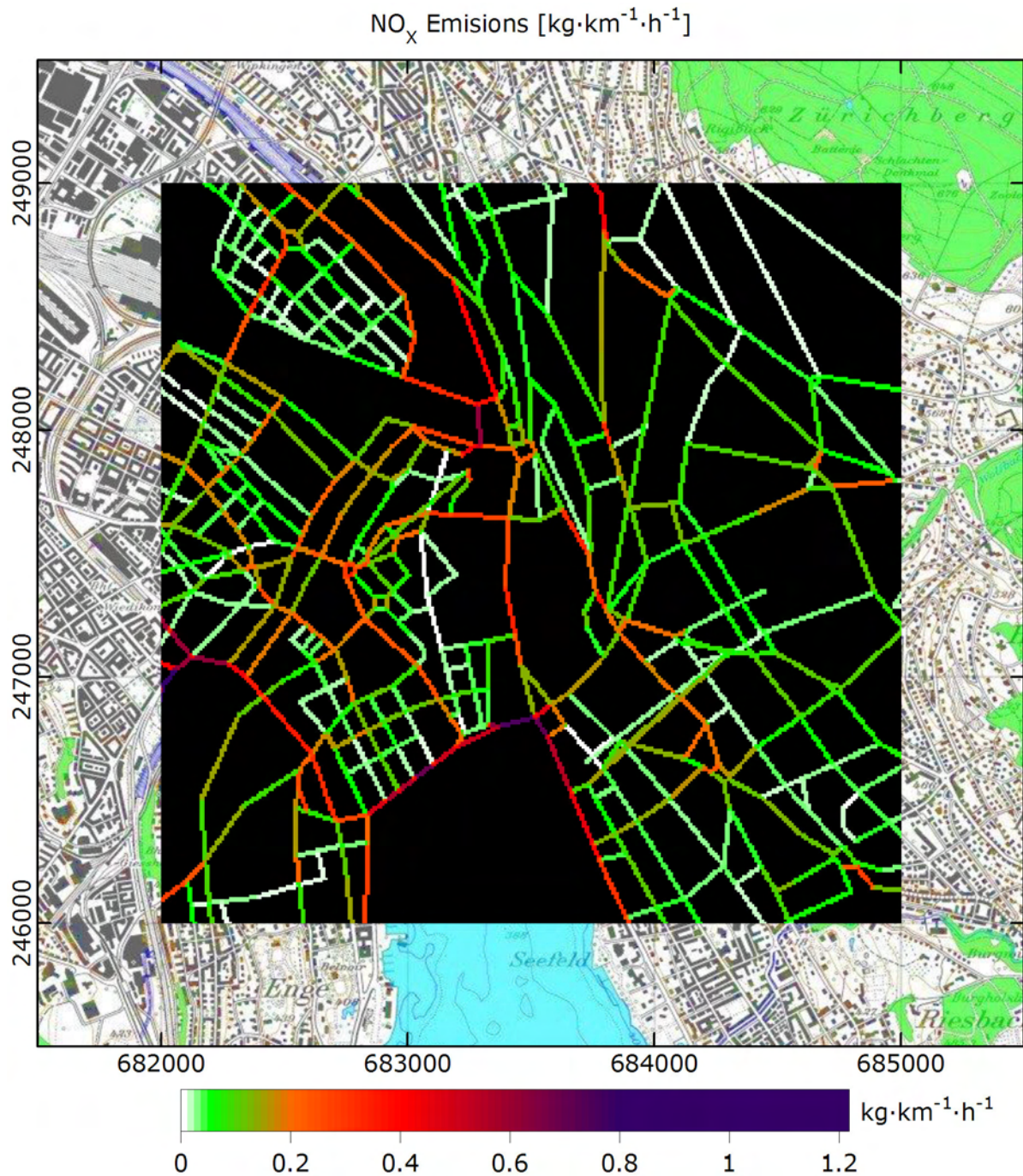


Figure 6.7: NO_x emissions on the street network used for the dispersion calculations. See appendix C.2 for plots for other substances.

6.5 Meteorological modelling (wind field simulations)

6.5.1 Overview

The dispersion calculations require an input of a one year time series of meteorological data. Since measurements on the tram had been carried out in winter and spring 2005/2006 on the period for the calculations was chosen to start June 1, 2005 and end May 31, 2006.

The wind field modelling and calculation were done by means of the *GRAMM* model and program (Graz Mesoscale Model). It simulates steady-state wind fields for parameterised meteorological situations based on measurements at a point within the area of investigation. The model is described by Oetl [2000] in detail. It is a computationally time-consuming process which needs a calculation time of several days and a huge amount of resources (memory) to work. Figure 6.8 shows the flow chart from the input data to the final product consisting of an aggregated data set of wind fields used in the dispersion calculations (6.6).

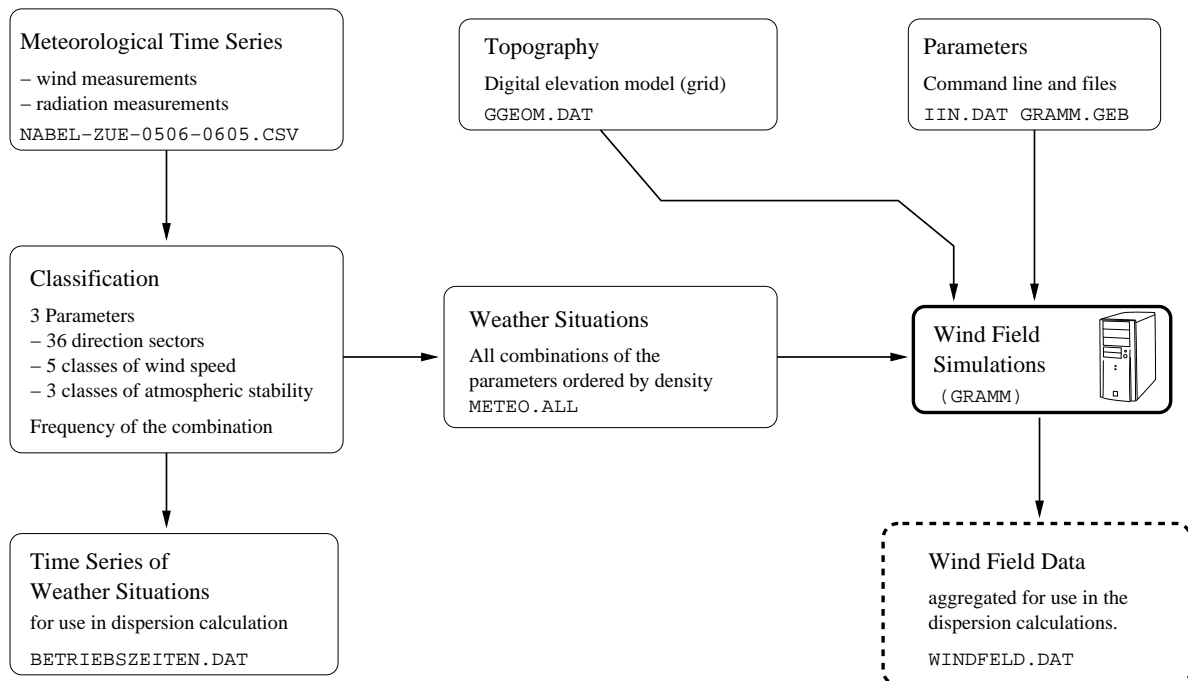


Figure 6.8: Flow chart of the wind field simulations process.

6.5.2 Classification of weather situations

The time series of wind and radiation measurements were obtained from the NABEL (*Nationales Beobachtungsnetz Luft*, national air monitoring network) station ZUE (Zürich) which lies inside the study area (see 6.2). Hourly mean values from this station have kindly been provided by the BUWAL (now BAFU, *Bundesamt für Umwelt*, federal office for environment).

The meteorological modelling is based on statistical wind field data. To reduce the computation time, the one-year time series of wind data is classified using three parameters. These are a classification of the wind direction, speed and a classification of the atmospheric stability condition (amount of atmospheric turbulence) based on radiation measurement and wind speed [Oettl].

The classification of the wind direction d in $[\circ]$ into 36 sectors is as follows (6.1).

$$c_{sector} = int(d \div 10) + 1 \quad (6.1)$$

The wind speed in v [m/s] is classified into five classes c_{speed} as follows (6.2).

$$c_{speed} = \begin{cases} 0.8 & v \leq 1 \\ 1.5 & 1 < v \leq 2 \\ 2.5 & 2 < v \leq 3 \\ 3.5 & 3 < v \leq 4 \\ 4.9 & 4 < v \end{cases} \quad (6.2)$$

The determination of the stability (or: dispersion) class c_{AKLA} depends on the wind speed d [m/s] and the net radiation r [W/m^2] (6.3–6.6).

For $0 \leq v \leq 1.9$:

$$c_{AKLA} = \begin{cases} 1 \text{ (convective)} & 55 < r \\ 2 \text{ (neutral)} & -7 < r \leq 55 \\ 3 \text{ (stable)} & r \leq -7 \end{cases} \quad (6.3)$$

For $1.9 < v \leq 2.9$:

$$c_{AKLA} = \begin{cases} 1 \text{ (convective)} & 109 < r \\ 2 \text{ (neutral)} & -7 < r \leq 109 \\ 3 \text{ (stable)} & r \leq -7 \end{cases} \quad (6.4)$$

For $2.9 < v \leq 6.9$:

$$c_{AKLA} = \begin{cases} 1 \text{ (convective)} & 109 < r \\ 2 \text{ (neutral)} & -28 < r \leq 109 \\ 3 \text{ (stable)} & r \leq -28 \end{cases} \quad (6.5)$$

For $6.9 < v$:

$$c_{AKLA} = 2 \text{ (neutral)} \quad (6.6)$$

The wind and radiation time series were classified using the above rules and the frequency of the occurrence of each combination was calculated (figure 6.10). Of the theoretical 540 ($36 \cdot 5 \cdot 3$) combinations 488 have occurred in the time series. Each combination of parameters corresponds to a certain weather situation. See appendix C.1 for a complete list of all weather situations and their frequency. The list of the 488 weather

situation were stored the tab separated ASCII file METEO.ALL which has the following columns:

1. Wind direction class c_{sector} .
2. Wind speed class (c_{speed}).
3. Stability class (c_{AKLA}).
4. Frequency in 1/1000.

A second file (BETRIEBSZEITEN.DAT) containing the time series of the weather situations had been created. Figure 6.9 shows the time series of the stability class. This data is used in the dispersion calculations. The file is a comma separated ASCII file with the following columns:

1. Date in the format *day.month*.
2. Hour (integer).
3. Wind speed class (c_{speed}).
4. Wind direction class (c_{sector}).
5. Stability class (c_{AKLA}).



Figure 6.9: Time series of the stability class. The plot has a “calendar style” layout, starting June 2005 (top) and ending May 2006 (bottom). The stability class c_{AKLA} is plotted as a step plot for each month (from left to right, offset to the weekday the month starts with). The three states stable (s), neutral (n) and convective (c) are indicated to the left.

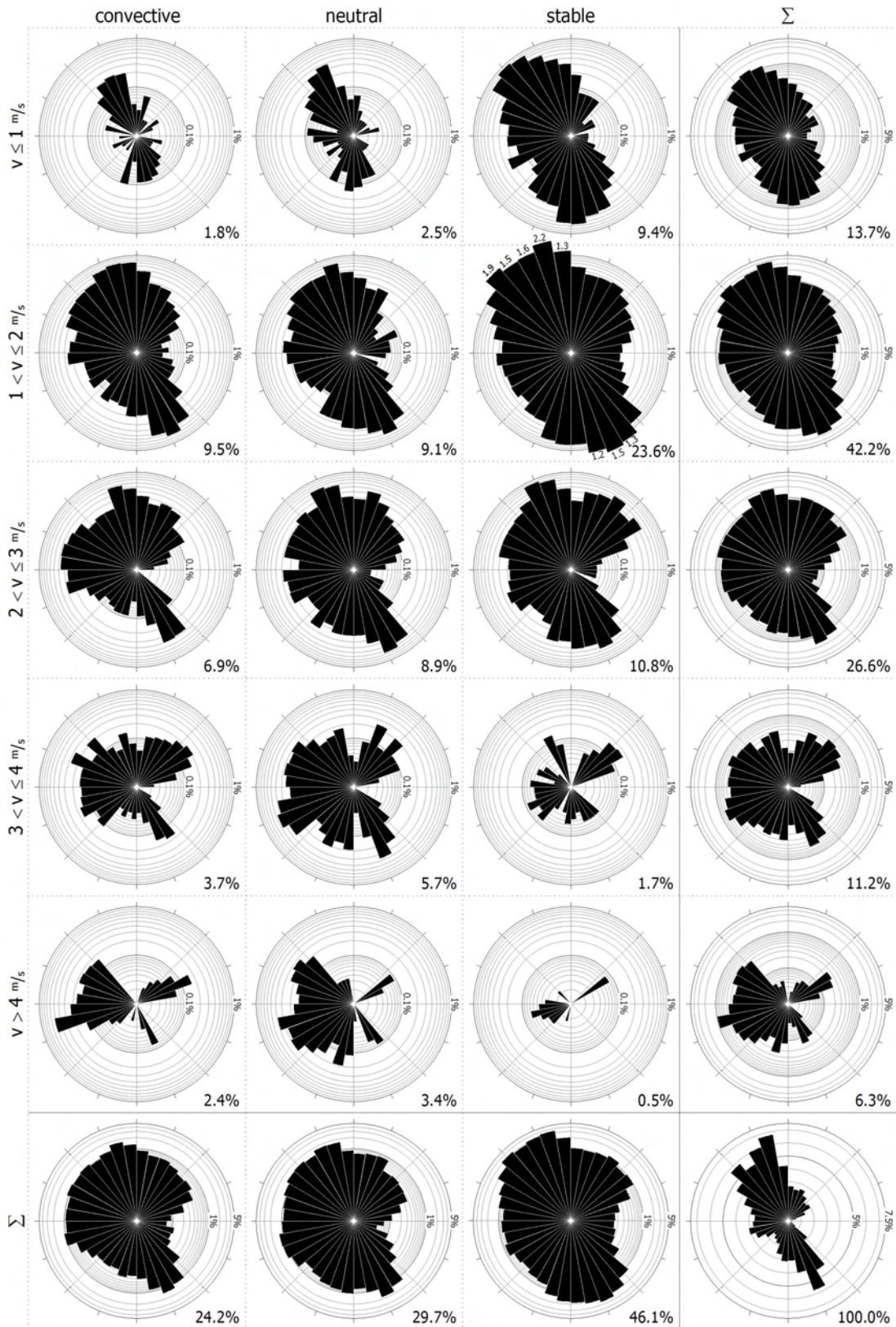


Figure 6.10: Analysis of weather situation parametrisation. For every combination of stability class (c_{AKLA}) and wind speed class (c_{speed}) a rose diagram with a logarithmic radial axis is plotted with the density for each sector (c_{sector}). The most right column and the bottom row represent the sum of each row and column, respectively. The diagram at bottom right is the total for all combinations (linear radial axis). The total density for each diagram is indicated beneath.

6.5.3 Calculation

The calculation program `GRAMM.EXE` takes four input files:

`GGEOM.DAT` – Topography as discussed in section 6.3.1.

`METEO.ALL` – Parameterised weather data, i.e. the weather situations as discussed in the previous section.

`GRAMM.GEB` – Defines the spatial extent and the grid parameters for the wind field calculations (figure 6.12). It defines a grid of 7.7 km² with a horizontal (square) mesh width of 100 m and 15 vertical layers. The lowest cell's height is 10 m and increases with the height above ground (see figures 6.16 and 6.17).

`IIN.DAT` – Further parameters for the wind field simulations (figure 6.13). These defaults were recommended by the producers of the program [Oettl].

Furthermore two parameters have to be given to the program on the command line. The first specifies the height of the anemometer over ground. For the measurement station used in this study (see section 6.5.2) this height has been estimated to be 25–30 m.¹ Therefore, a height of 27.5 m was used.

The second parameter specifies the roughness length to be used. The roughness of Earth's surface influences the wind blowing along it. The roughness length is a measure for the extent of the slowdown effect the surface has on the wind. Water or other smooth surfaces (e.g. concrete runways on airports) have little influence on the wind. Trees and bushes have a considerable slowdown effect on the wind. Cities are even rougher and have roughness lengths from 0.4 m (villages, small towns) to 1.6 m (very large cities with tall buildings and skyscrapers). Larger cities with tall buildings have a roughness length of about 0.8 m [Troen and Petersen, 1991]. This is consistent with the references of the program's maker who recommends a value between 0.5 and 1.0 m. For this study a roughness length of 0.75 m was used.

The calculation program (`GRAMM.EXE`) is a 32bit console-based Windows application. These calculations are very time-consuming (many days, see table 6.3) and the available computers were needed for other tasks as well. The `SRVANY.EXE` utility from the Windows NT Resource Kit was used to establish the calculation task as a low-priority background process. This allowed for use of the workstation as usual with little interference of users. A single command prompt window (`CMD.EXE`) and rarely a little sluggish reaction of the user interface were the only noticeable effect.

The calculation can be started at any weather situation number. This allows for continuation of an interrupted calculation, for example due to the need to apply patches and reboot or for the reason of investigation the so far calculated data. The weather situations are ordered by their frequency of occurrence (density) starting at the most common weather situation. Figure 6.11 shows the density and probability curves. The first 78 weather situations cover 50% of the time horizon (one year) used here. 266 calculated weather situations cover 90% of the period and would be sufficient to obtain meaningful results with the dispersion calculation. Nevertheless, a total of 438

¹Personal communication (email) with Dr. Christoph Hüglin, Air Pollution / Environmental Technology Lab., EMPA - Materials Science & Technology, Dübendorf, Switzerland (December 2006).

weather situations were calculated representing 99.5% of the period in survey. Table 6.3 summarises the computational aspects of this calculation. In total it took about 44 days to calculate 438 weather situations. In average, 10 weather situations were calculated per day. The computer used was a Pentium 4 with 1 GB of RAM running at 2.8 GHz.

The result of these calculations is a file WINDFELD.DAT. It is used in the dispersion calculations described in the next section of this chapter.

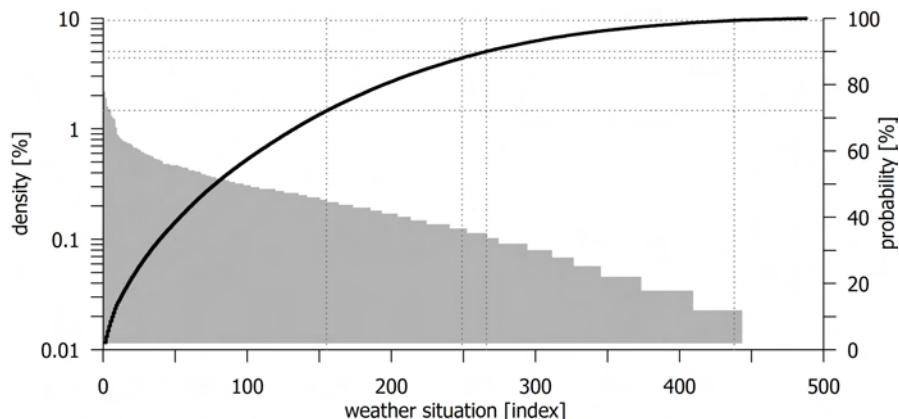


Figure 6.11: Density (logarithmic scale) and probability of the weather situations. Some percentiles are 50%: 78, 60%: 108, 70%: 146, 80%: 194, 90%: 266 and 95%: 325.

[n]	%	file size	n	days	n/day
155	72.2	133 MB	155	16	9.7
249	88.1	213 MB	94	9	10.4
266	90.0	228 MB	17	3	5.7
438	99.4	375 MB	172	16	11.5
Totals			438	44	10.0

Table 6.3: Number of weather situations calculated ([n]), probability in % and the output file size in MB (2^{20} bytes). Each line represents an interruption of the calculation. After each interruption the time (days) needed to calculate a number (n) of weather situations were recorded and their ratio been calculated. An Intel Pentium 4 with 1 GB of RAM running at 2.8 GHz was used.

```

70      !Anzahl Zellen im Auszaehlgitter GRAMM in x-Richtung
70      !Anzahl Zellen im Auszaehlgitter GRAMM in y-Richtung
15      !Anzahl Zellen im Auszaehlgitter GRAMM in z-Richtung
680000 !Westgrenze des Gebiets [m]
687000 !Ostgrenze des Gebiets [m]
245000 !Suedgrenze des Gebiets [m]
252000 !Nordgrenze des Gebiets [m]

```

Figure 6.12: The file GRAMM.GEB defines the spatial extent and the grid parameters for the wind field calculations.

BERECHNUNGSDATUM	(TTMM)	:	0103
BERECHNUNGSBEGINN	(hhmm)	:	1500
ZEITSCHRITT DT	[s]	:	1
ZEITDAUER TLIMIT[s]/Durchstroemung[%]		:	0.1
ZWISCHENSPEICHERN NACH JE ? ZEITSCHRITTEN		:	10
MAX. ZULAESSIGE W-ABWEICHUNG OBEN < 1 [mm/s]		:	0.01
RELATIVE FEUCHTE DER ATMOSPHAERE [%] GT.0!		:	0.01
SEEHOEHE DER UNTERSTEN BERECHNUNGSHOEHE [m]		:	0.0
BEZUGSTEMPERATUR DER LUFT AM BODEN [K]		:	290.0
GRADIENT DER TEMPERATUR [K/100m] (U -> 0)		:	-0.7
NEUTRALE SCHICHTUNG BIS ZUR HOEHE UEBER GRUND		:	0.0
BEZUGSTEMPERATUR DER BODENOBERFLAECHE [K]		:	290.0
TEMPERATUR DES BODENS IM ERDINNEREN [K]		:	290.0
GEORAPHISCHER BREITENGRAD (NORDEN)		:	47
NEUE STRAHLUNGSDATEN NACH JE ? ZEITSCHR.		:	1
ZEITLICHE AENDERUNG AM RAND LINEAR=1 COSINUS=0:		:	0
BERECHNE U V W PN T PH FO	JA=1	:	1111100
BERECHNE BR PR QU PSI TE TB STR	JA=1	:	1000000
ANFANGSBEDINGUNGEN DIAGNOSTISCH	JA=1	:	1
EXPLIZIT ODER IMPLIZIT IM = 1	EX = 0	:	1
RELAXATIONSFAKTOR GESCHWINDIGKEIT		:	0.3
RELAXATIONSFAKTOR TEMPERATUR		:	0.3
DRUCKGLEICHUNG MIT TDMA (0) ODER GCCG (1)		:	0
NUDGING (=1) ODER GROSSKALIGER ANTRIEB (=0)		:	1
BOUNDARY CONDITION (1,2,3,4)		:	5

Figure 6.13: The file IIN.DAT specifies parameters for the wind field simulations.

6.5.4 Analysis

Two post-processing tools to analyse the calculated wind field data (`windfeld.dat`) are available.

The program `WINDSTAT.EXE` takes a location (x/y co-ordinates) and a crop height above ground level (AGL). It outputs two files.

`WINDSTAT.DAT` – First part consists of two values per weather situation. Second part is 16 lines with two values each.

`MEANWIND.DAT` – Contains a grid of the yearly average wind speed. Three columns: x , y and v . See figure 6.14 for an example.

The program `POSTGRAMM.EXE` takes a weather situation (i.e. its index number), a crop height above ground and x and y co-ordinates to define a north-south slice and a west-east slice, respectively. It outputs three files.

`HORIZONTAL.DAT` – Horizontal vector field that defines the wind flow conditions. Six columns: x , y , z , u , v , w . (u , v , w) define the wind vector at position (x , y , z). See figure 6.15 for an example.

`VERTIKAL-WO.DAT` – West-east cross-section. See figure 6.16 for an example.

`VERTIKAL-NS.DAT` – North-south cross-section. See figure 6.17 for an example.

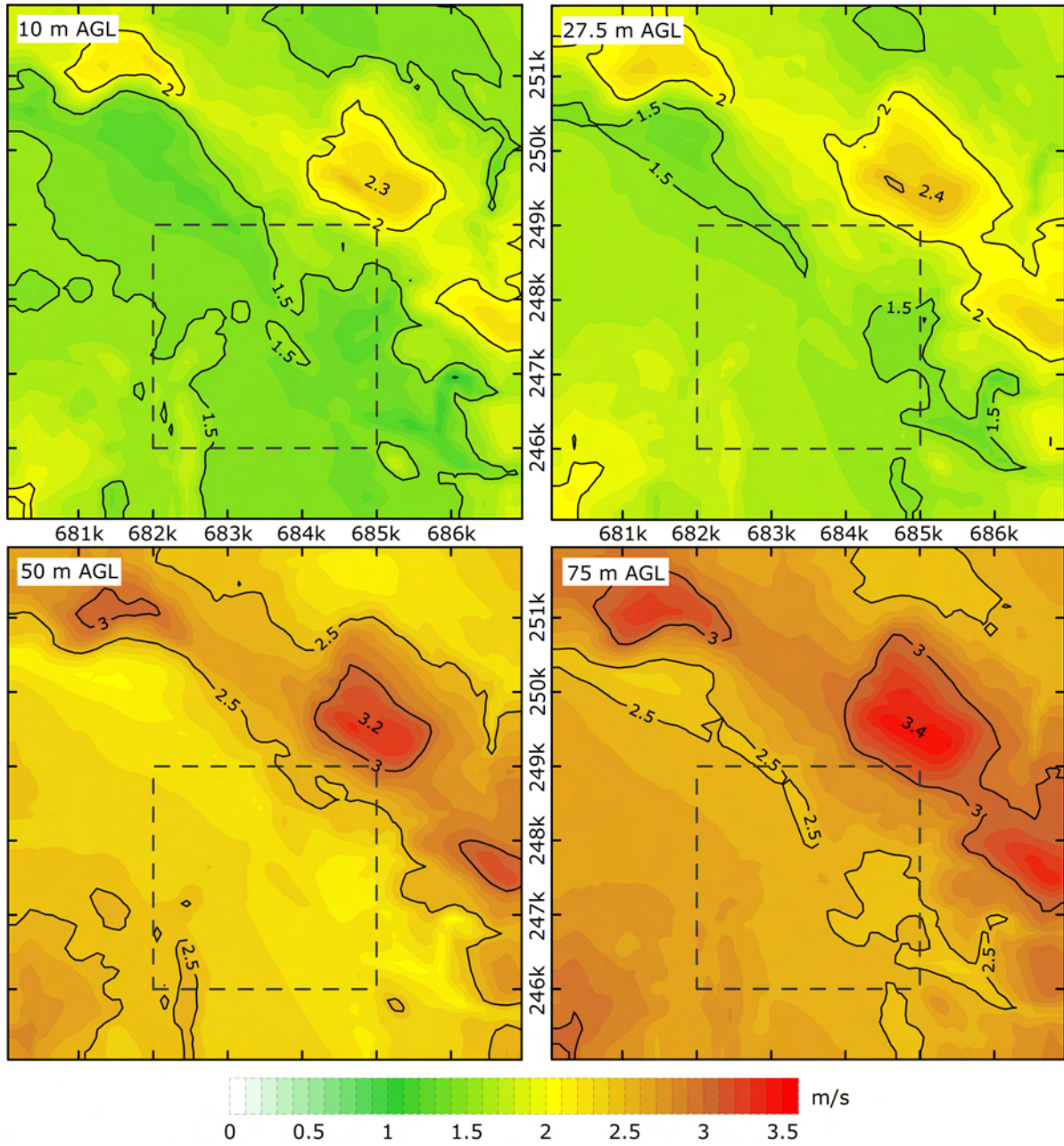


Figure 6.14: Yearly average wind speed at different heights above ground level (AGL). The dashed square represents the GRAL simulation area. See also figure 6.2.

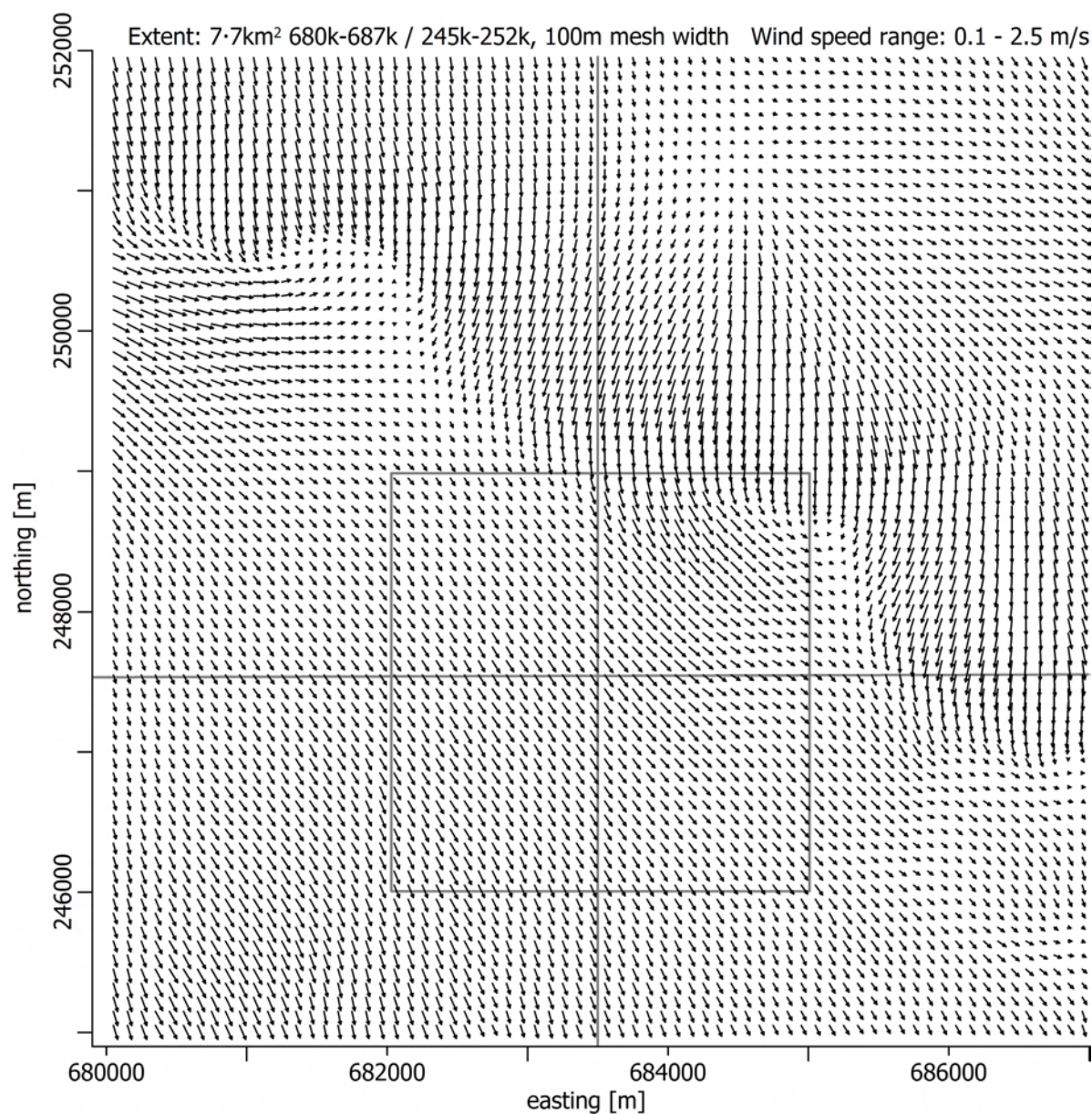


Figure 6.15: Wind flow conditions at 27.5 m above ground level for weather situation #1 ($c_{speed} = 1.5$, $c_{sector} = 35$, $c_{AKLA} = 3$, probability 21.8%). Prevailing wind is along the Limmat valley and the sea basin. The gray square indicates the extent for which the dispersion calculations were done. The gray lines indicate vertical cross-sections (see figures 6.16 and 6.17).

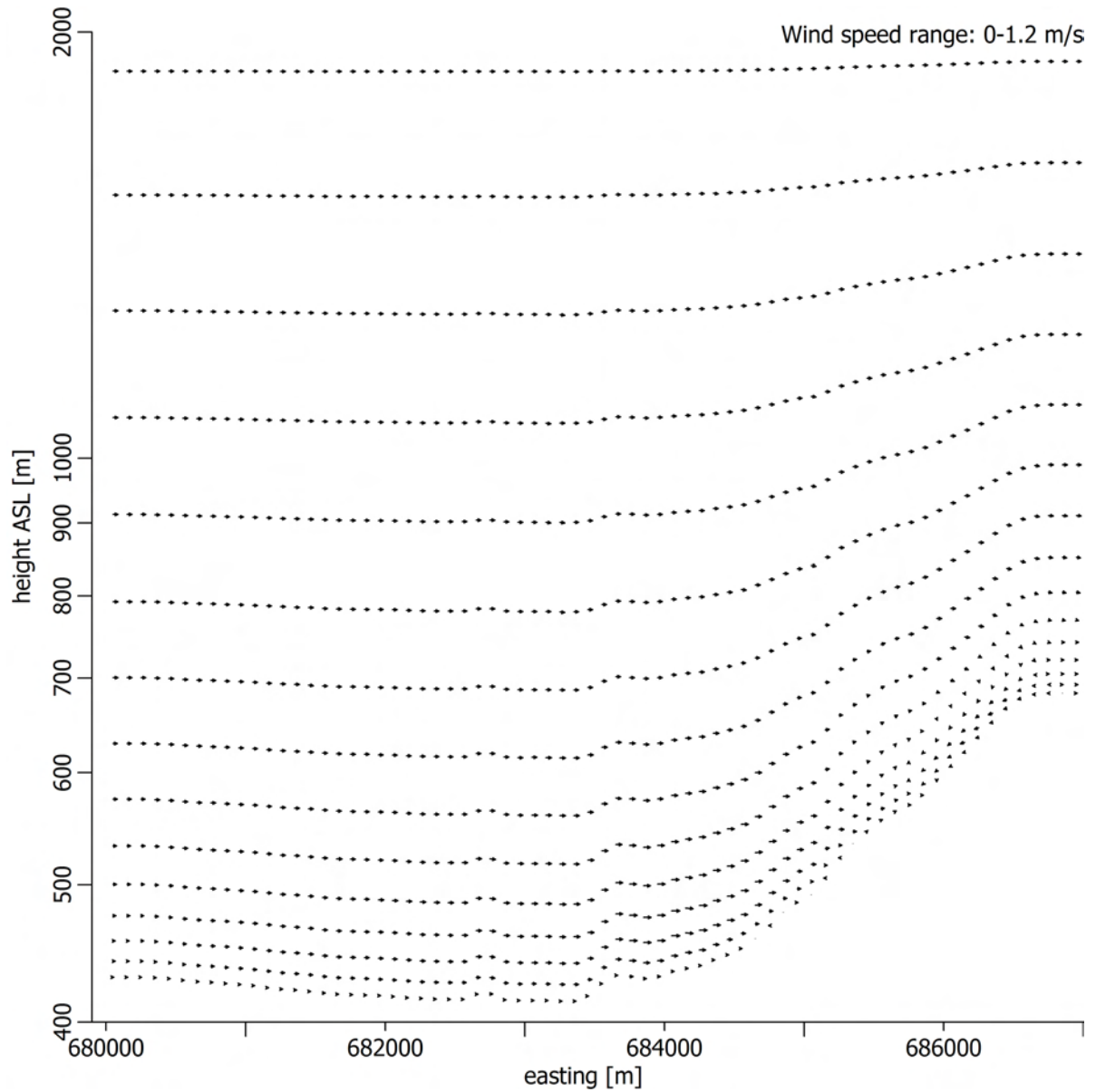


Figure 6.16: West-east cross-section for weather situation #1 ($c_{speed} = 1.5$, $c_{sector} = 35$, $c_{AKLA} = 3$).

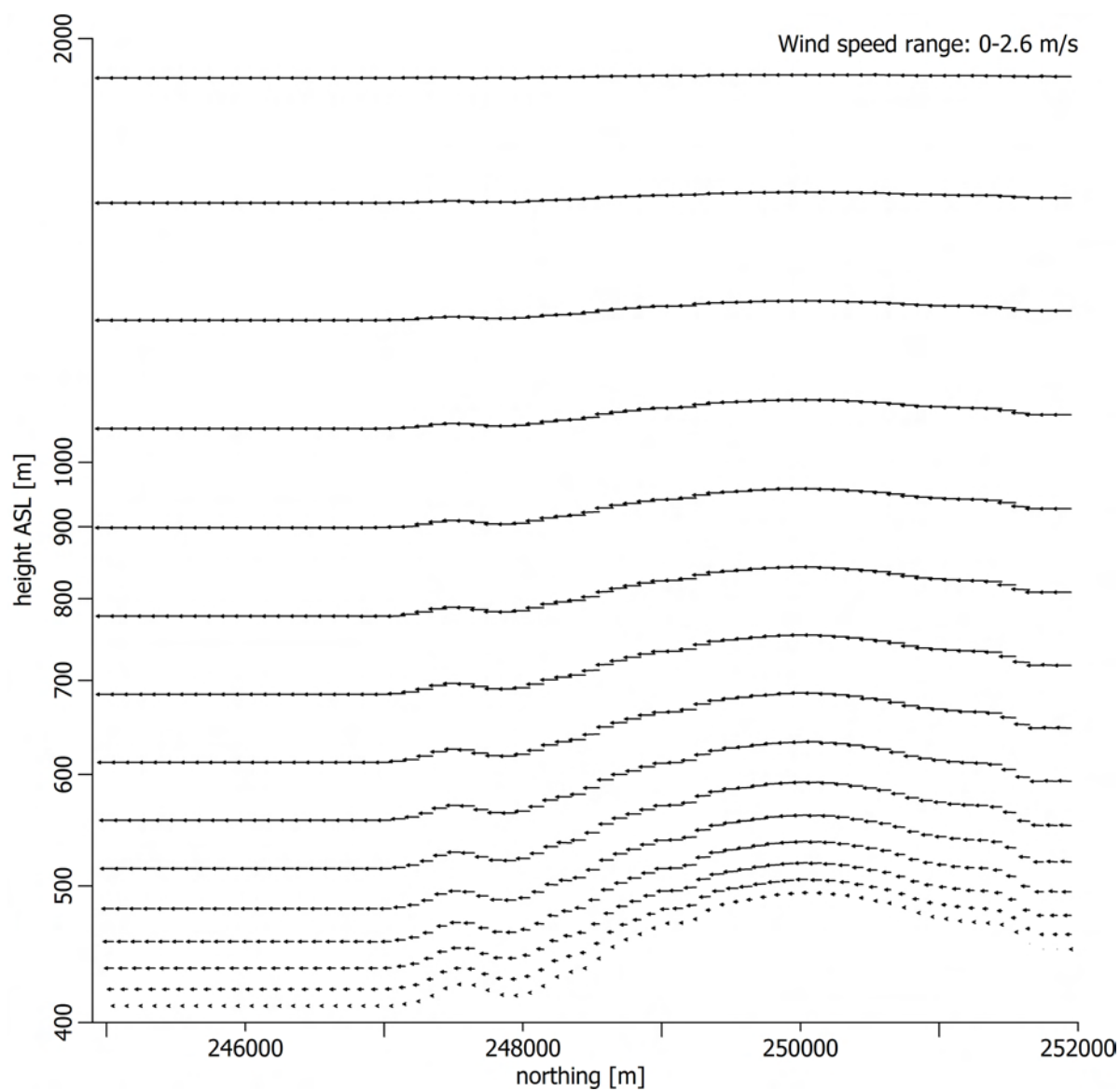


Figure 6.17: South-nord cross-section for weather situation #1 ($c_{speed} = 1.5$, $c_{sector} = 35$, $c_{AKLA} = 3$).

6.6 Dispersion modelling

The dispersion modelling and calculations were carried out using the *GRAL* (Graz Lagrangian model) model and program [Oettl et al., 2001a,b,c, 2003, 2004].

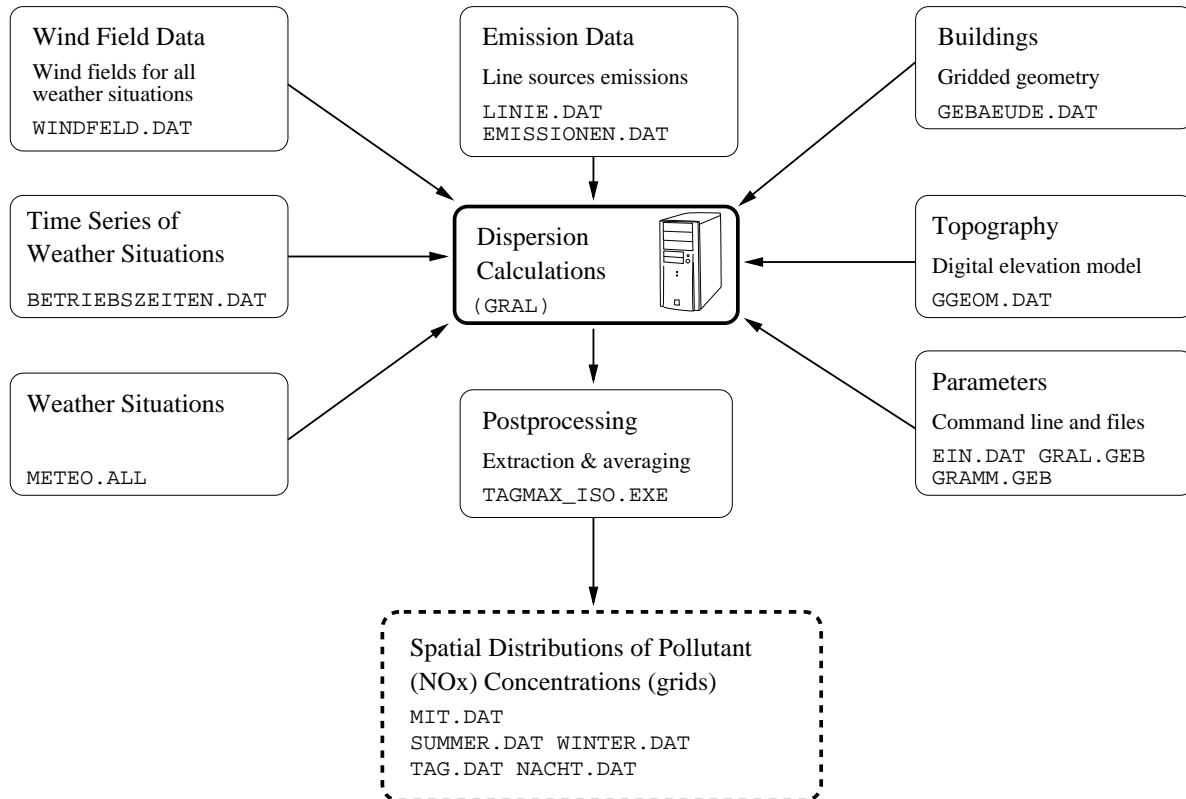


Figure 6.18: Flow chart of the dispersion calculations process using the *GRAL* model.

6.6.1 Calculation

The calculation program (*GRAL.EXE*) is a 32bit console-based Windows application. The calculations are time-consuming and take hours to days. The calculations were carried out on a workstation in the same fashion as the wind field simulations were done. See section 6.5.3 for more details on this. Table 6.4 summarised the computational aspects of this calculations. In total it took about 111.5 hours (4.6 days) to calculate 438 weather situations. In average, 3.9 weather situations were calculated per hour (94 per day).

The post-processing program *TAGMAX_ISO.EXE* takes roughly 2 hours to generate the output grids from the calculated data. It has been run interactively at normal priority.

The file *EIN.DAT* (figure 6.19) specifies parameters for the dispersion calculation programm *GRAL.EXE*. These include the number of particles, the dispersion time, layer definitions, calculation domain and other parameters [Oettl]. The file *GRAL.GEB* defines the grid parameters for the wind field data (mesh width 5 m), the spatial extent (3·3 km²) and the dispersion grid resolution (mesh width 3 m).

```

60      !Teilchen pro Sekunde
3600    !Ausbreitungszeit
1       !Stationaere Berechnung=1,Einzelfall=0,Instationaere B.=2
1       !Eingabe Meteorologie: ZR=0,AK=1,ELI=2,SONIC=3
0       !Eingabe Rezeptoren Ja=1
.1      !Bodenrauhigkeit
47      !Breitengrad
N       !Standardmodell=J
NOx     !Schadstoff: NOx,CO,PM,HC
3.5     !Horizontale Schnittebene
2       !Vertikale Gitteraufloesung
1       !Wetterlage mit der Berechnung beginnen soll

```

Figure 6.19: The file EIN.DAT defines parameters for the dispersion calculations.

```

5       !Zellgroesse fuer kartesisches Windfeld in GRAL in x-Richtung
5       !Zellgroesse fuer kartesisches Windfeld in GRAL in y-Richtung
5       !Zellgroesse fuer kartesisches Windfeld in GRAL in z-Richtung
1000    !Anzahl Zellen im Auszaehlgitter GRAL in x-Richtung
1000    !Anzahl Zellen im Auszaehlgitter GRAL in y-Richtung
1       !Anzahl der horizontalen Schnitte
1       !Anzahl der Quellgruppen
682000  !Westgrenze des Gebiets [m]
685000  !Ostgrenze des Gebiets [m]
246000  !Suedgrenze des Gebiets [m]
249000  !Nordgrenze des Gebiets [m]

```

Figure 6.20: The file GRAL.GEB defines the spatial extent and the grid parameters for the dispersion calculations.

[n]	%	data size	n	hours	days	n/hour	n/day
155	72.2	962 MB	155	39.9	1.7	3.9	93
249	88.1	1 549 MB	94	23.4	1.0	4.0	96
266	90.0	1 658 MB	17	3.5	0.1	4.9	117
438	99.4	2 704 MB	172	44.7	1.9	3.8	92
Totals			438	111.5	4.6	3.9	94

Table 6.4: Number of weather situations calculated ([n]), probability in % and the total size of data files in MB (2^{20} bytes). Each line represents an interruption of the calculations. After each interruption the time (hours) needed to calculate a number (n) of weather situations were recorded and their ratio was calculated. An Intel Pentium 4 with 1 GB of RAM running at 2.8 GHz was used.

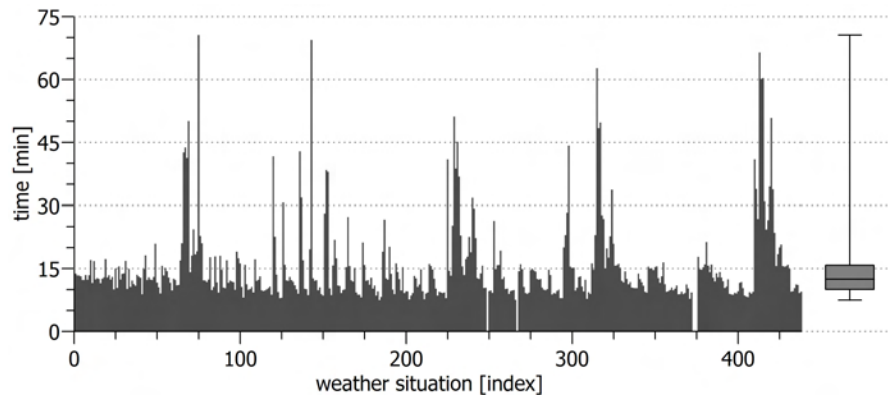


Figure 6.21: Dispersion modelling calculation time (minutes) needed for every weather situation. The box plot on the right indicates the minimum at 7.6, the maximum at 70.6, the mean at 15.5 and the standard deviation of 9.8.

6.6.2 Results analysis

The post-processing routine `TAGMAX_ISO.EXE` generates several files. Each file is a grid with a mesh-width of 3 m (defined in `GRAL.GEB`) which contains the spatial distribution of NO_x concentrations (in $\mu\text{g}/\text{m}^3$). The periods are taken from the meteorological time series described in section 6.5. The files are as follows.

`MIT.DAT` – Annual mean concentrations.

`WINTER.DAT` – Wintertime (December–February) daily mean concentrations.

`SUMMER.DAT` – Summertime (June–August) daily mean concentrations.

`TAG.DAT` – Daytime (08–16 h) yearly mean concentrations.

`NACHT.DAT` – Night-time (16–08 h) yearly mean concentrations.

See figures 6.22 – 6.26 for the plotted results of the dispersion calculations for the above periods.

The calculations were done for a number of weather situations (see section 6.6.1) and they were interrupted at certain stages. The more weather situations considered, the preciser the results will be. To obtain reliable result, a minimal amount of weather situations covering about 70% of the meteorological time series should be considered [Oettl]. This corresponds to the 155 weather situations (72.2%) when the calculations were interrupted the first time. The calculations were finally stopped at 438 weather situations which makes 99.4% time series (see figure 6.11). Statistics over the differences between the grids resulting from 155 weather situations and those resulting from 438 weather situations were calculated. They show very little differences (figure 6.28). A plot of a cross-section (6.27) at the mentioned two stages of calculation confirms these differences to be insignificant (figure 6.29). This cross-section was selected because of the large emission strength occuring at the Bellevue place, which is one of the most busy places in Zürich. The main feature of the data include higher concentrations during daytime than during night-time as expected from the traffic frequency.

The same cross-section was used to compare the various calculated grids (figure 6.30).

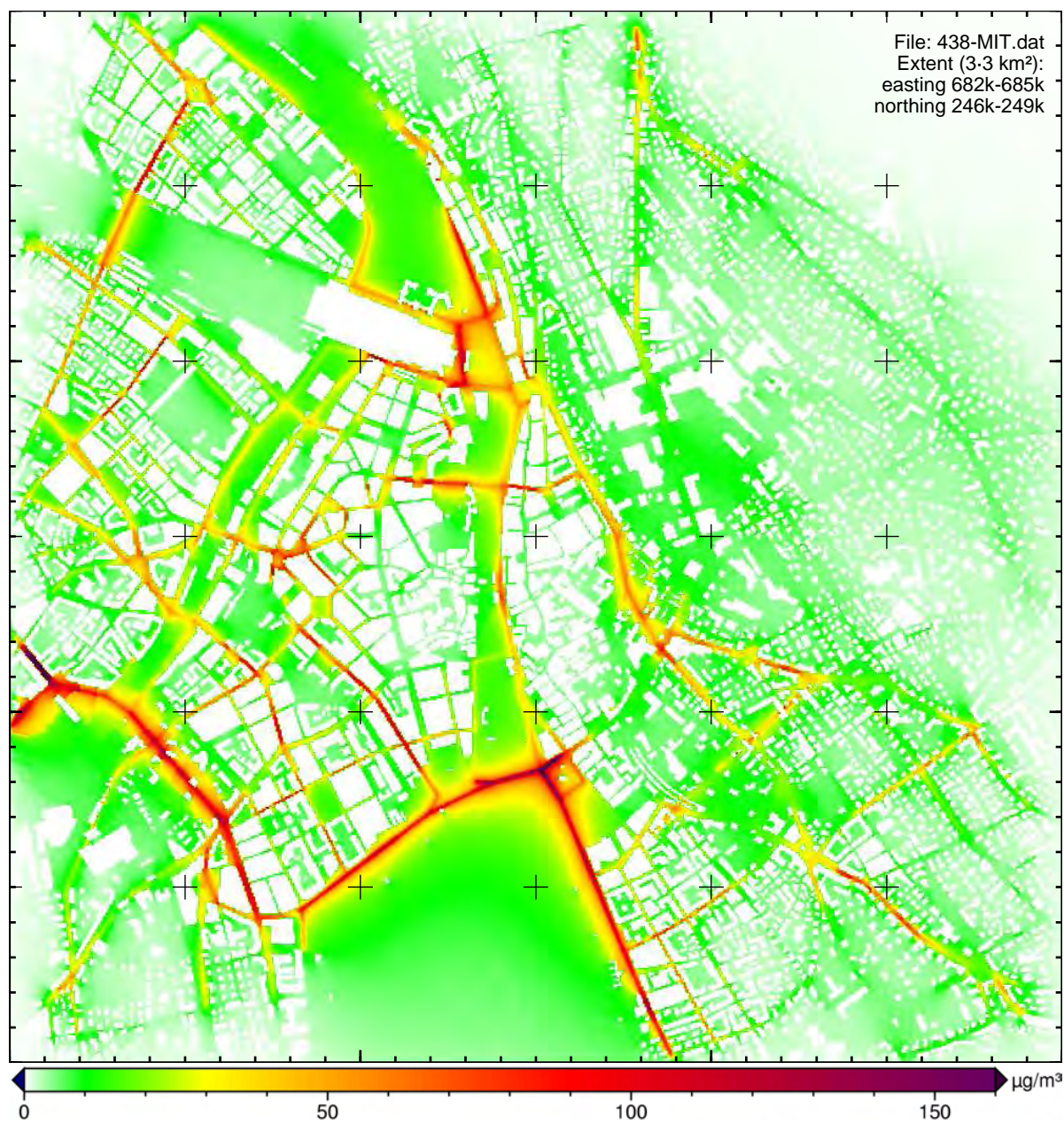


Figure 6.22: Annual mean concentrations of NO_x.



Figure 6.23: Daytime (08–16 h) mean concentrations of NO_x.

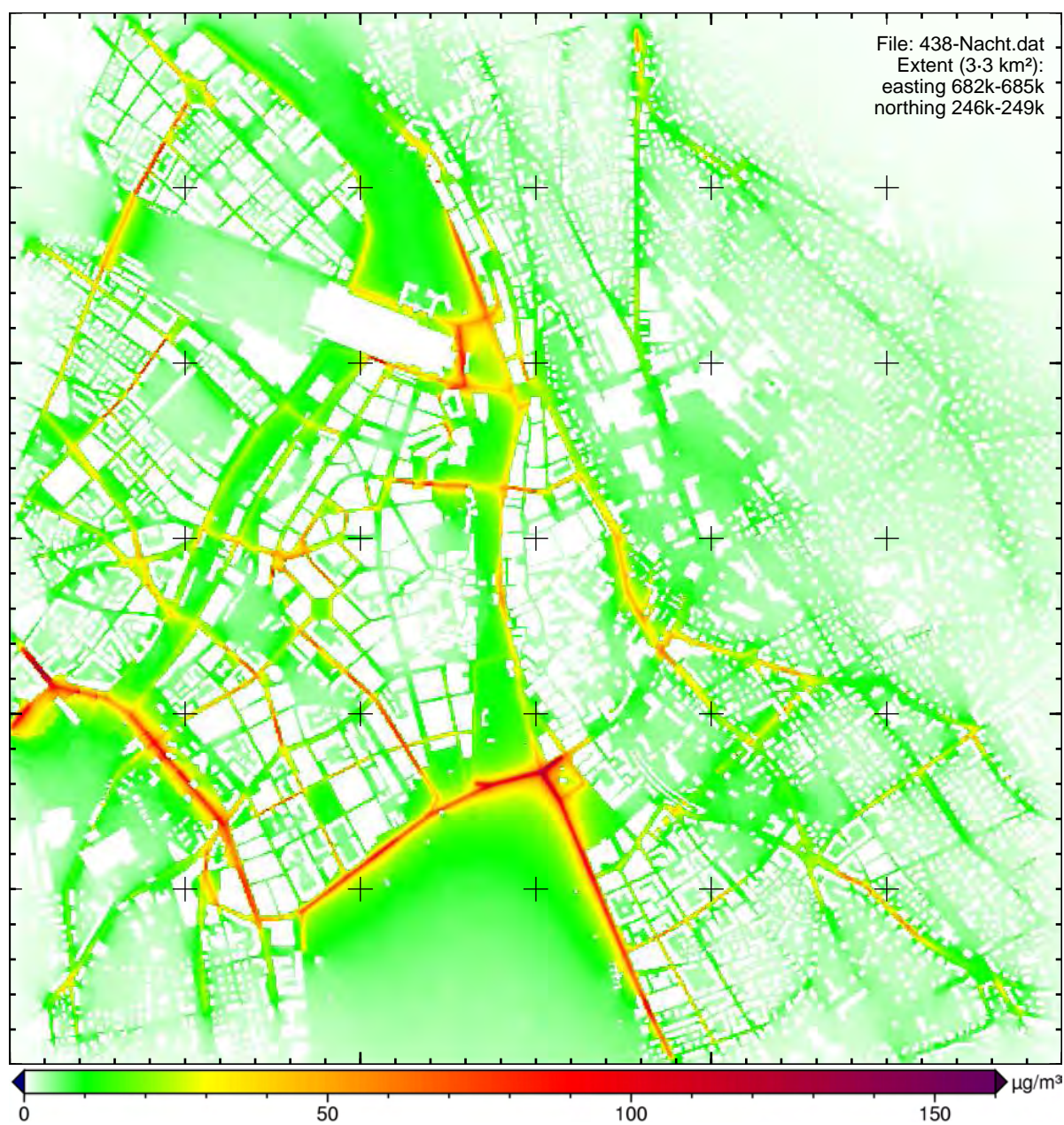


Figure 6.24: Night-time (16–08 h) mean concentrations of NO_x.

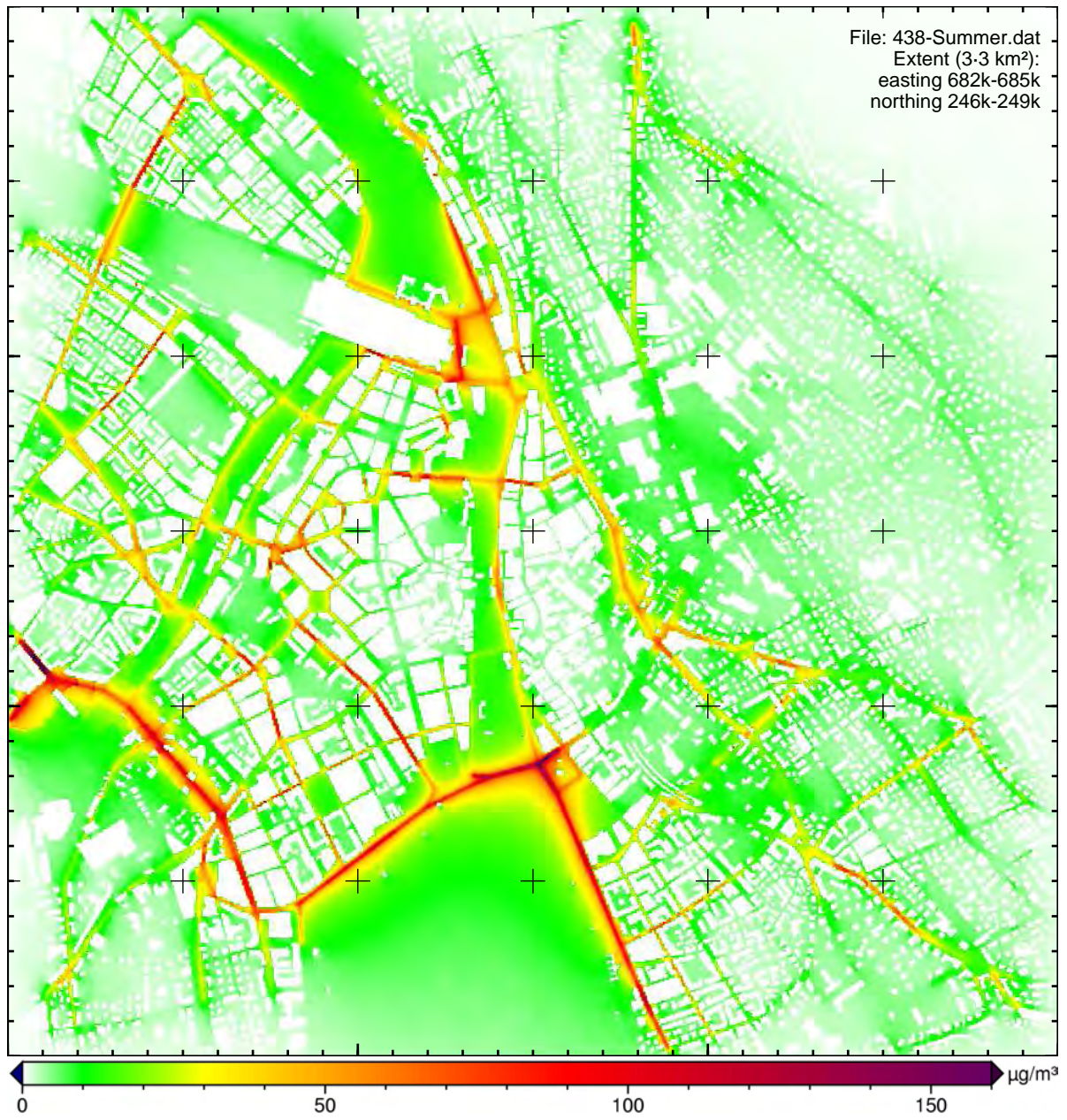


Figure 6.25: Mean concentrations during summer period (June-August) of NO_x.

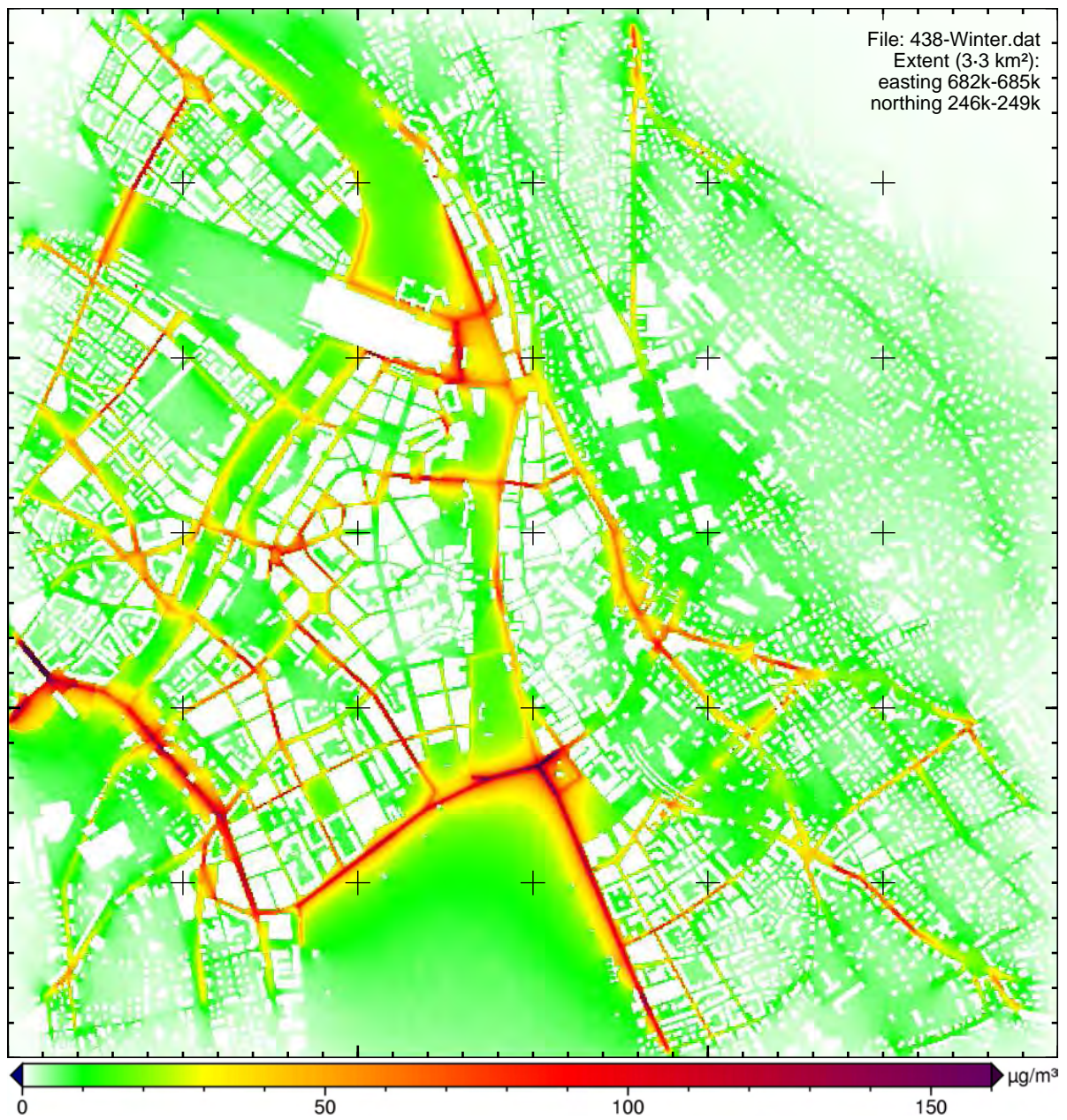


Figure 6.26: Mean concentrations during winter period (December-February).

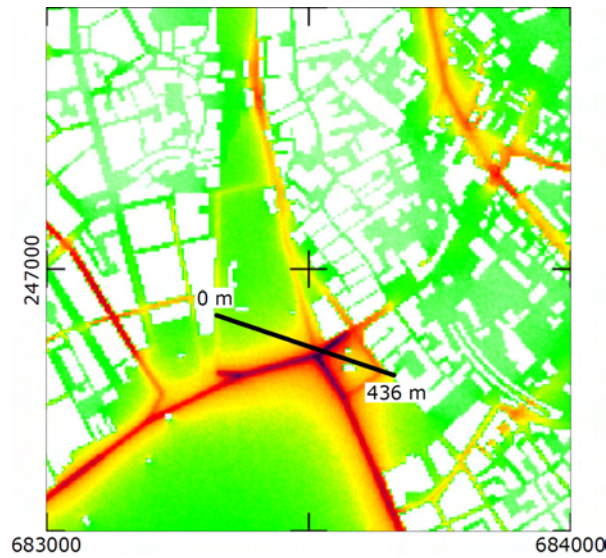


Figure 6.27: Cross-section over the Bellevue place.

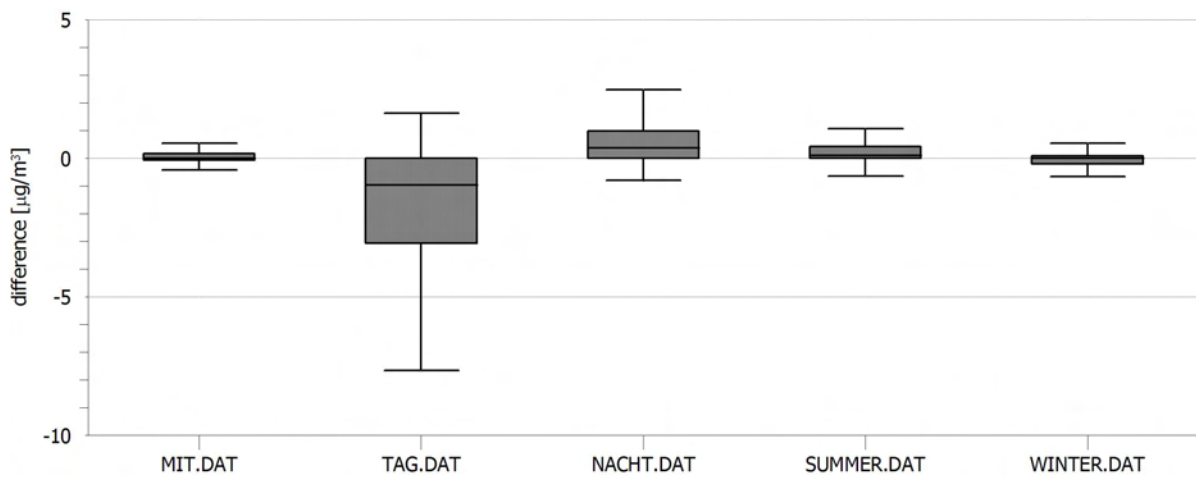


Figure 6.28: Statistics of the differences between the grids resulting from 155 weather situations (72.2%) and those resulting from 438 weather situations (99.4%) were calculated and plotted as box-plots. Outliers are not plotted.

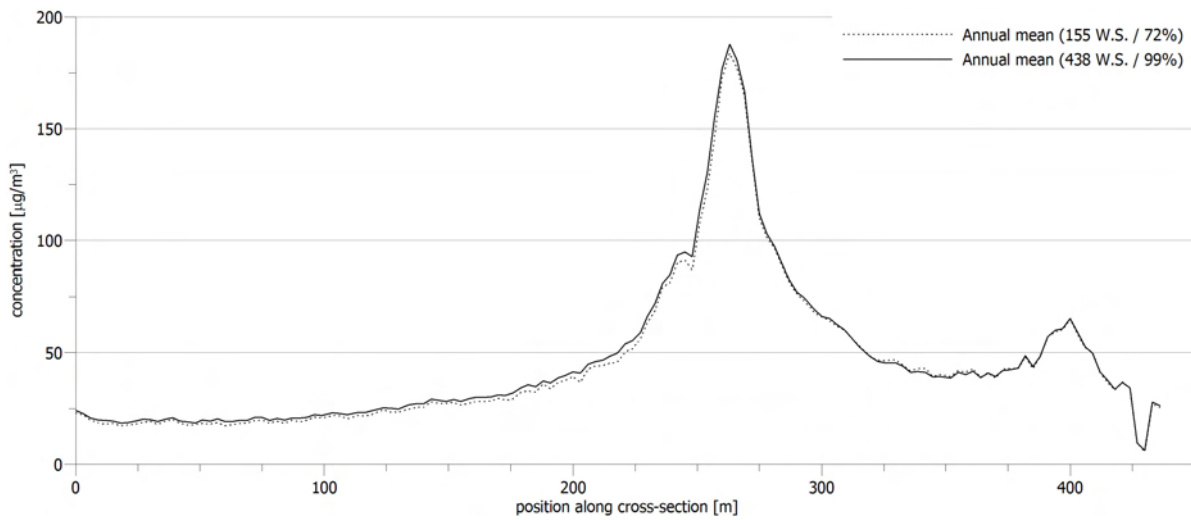


Figure 6.29: Comparison of the dispersion calculations results at two stages of calculation. The plot shows the cross-section from figure 6.27 over the annual mean at two stages of the calculations. The dotted line represents the results including 155 weather situations (72%) and the stroke-through line represents the results at 438 weather situations (99%).

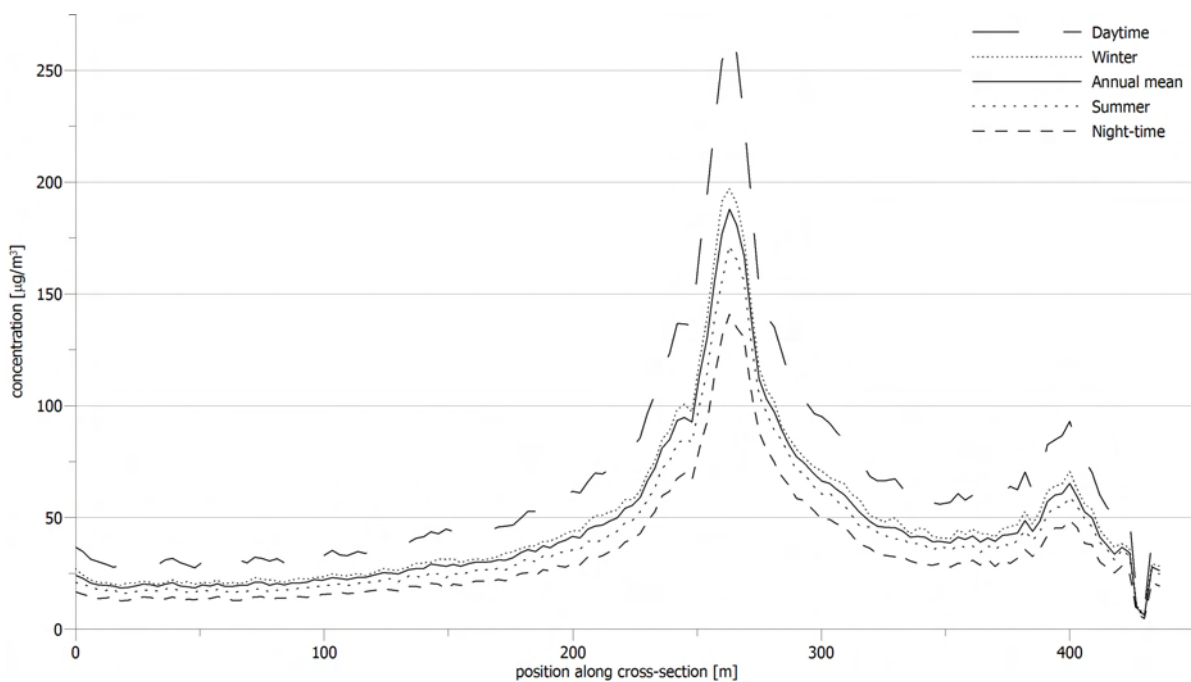
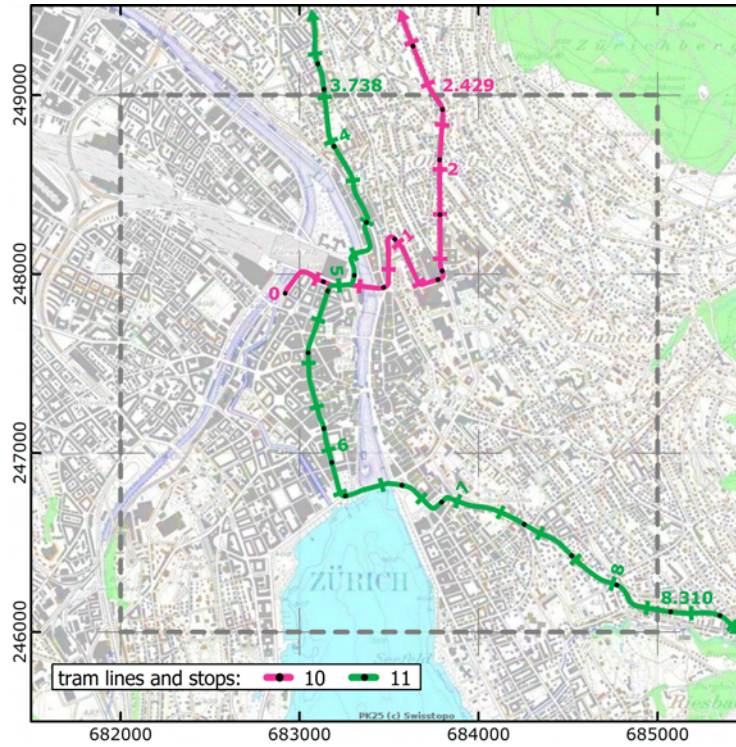
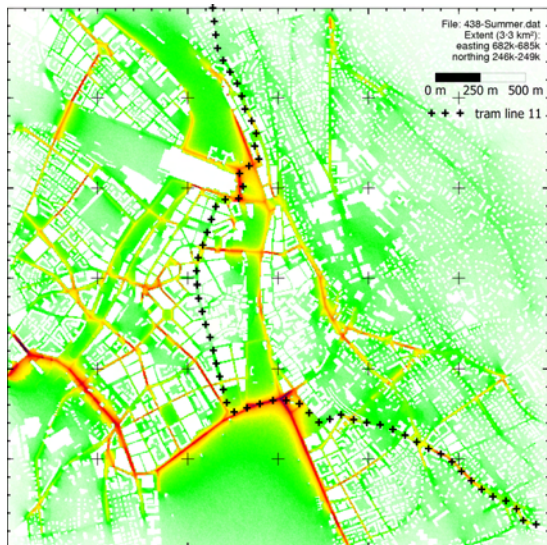


Figure 6.30: Comparison of the different dispersion calculations results. The plot shows the cross-section from figure 6.27 over the various calculated grids.

6.7 Comparison with measurements



a) tram tracks in the GRAL study area



b) cross-section along tram track 11 in the GRAL "summer" results



c) cross-section along tram track 10 in the GRAL "winter" results

Figure 6.31: Maps of the comparison of the GRAL results with the tram measurements. The tram tracks considered in this analysis are plotted with stops and indicators of the position along the track (a). The numbers indicate the position along the track in [km] and marks are set every 250 m. Cross-section along the tram tracks are also plotted on the corresponding GRAL results grid (b, c).

6.7.1 Summer 2005

Figure 6.32 shows the comparison of the GRAL “summer” results with tram “summer” measurements. The latter are the interpolated summer measurements for fair and adverse weather introduced in section 5.3.5. The combination of fair and adverse weather days (compare figure 5.21) should represent average “summer” days sufficiently well. The plotted curves are: the mean (black line) \pm standard deviation (grey area), the median (blue line) and the early morning (6–9 h UTC) mean.

The GRAL measurements were sampled along a cross-section which corresponds to the tram line 11 (figure 6.31b). Several sampling radii were used (5–25 m) and the mean value of all grid points within the radius (excluding buildings) was calculated. This results in different curves. The difference is marginal at low concentrations and increases with the concentration. The smaller the sampling radius, the larger the peaks in the resulting curve turn out. The maximum difference can be seen at the section from *Bürkliplatz* to *Bellevue* place (approx. position 6300–6600 m). At this site the values obtained with a 5 m sampling radius is approximately 30–45% then the values obtained with a 25 m sampling radius.

The concentrations sampled from the GRAL “summer” grid generally agree with the tram measurements. The qualitative agreement of the simulation and the measurements seem to be reasonable. Significant differences seem to exist where GRAL shows low concentrations. In this study only traffic emissions were used as input into the dispersion calculation. However, they should be the main emission source in summer (no domestic heating, which would be another main contributor in winter).

A correlation analysis of the mean tram measurements along the track and the GRAL cross-sections of different sampling radii was carried out (figure 6.33). It shows significant to good correlation coefficients (0.666–0.834). It quantifies the offset of the GRAL simulation results from the measurements (at places where GRAL shows very low values) at approximately $30 \mu\text{g}/\text{m}^3$.

Besides of missing emissions and the dominance of air pollution which originates from traffic there could still be missing background concentrations. Further reasons which could play a role in the discrepancies might come from inaccuracies in the input data, which includes traffic densities, street network geometry, emission factors, buildings geometry and meteorological data.

The GRAL simulation results agree best with the measurements at busy places (main station / *Bahnhofquai/HB*) and between *Buerkliplatz* and *Bellevue*.

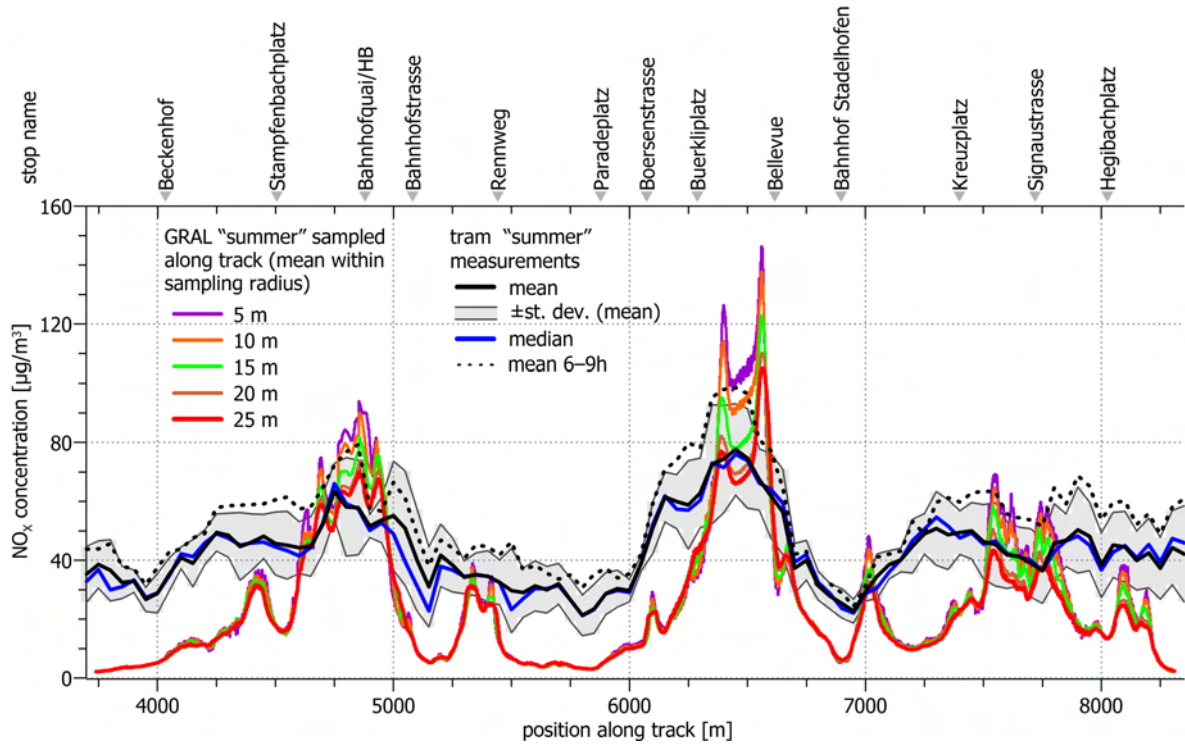


Figure 6.32: Comparison of measured average NO_x concentration along the tram line 11 in summer 2005 (see section 5.3.5) with the GRAL “summer” results.

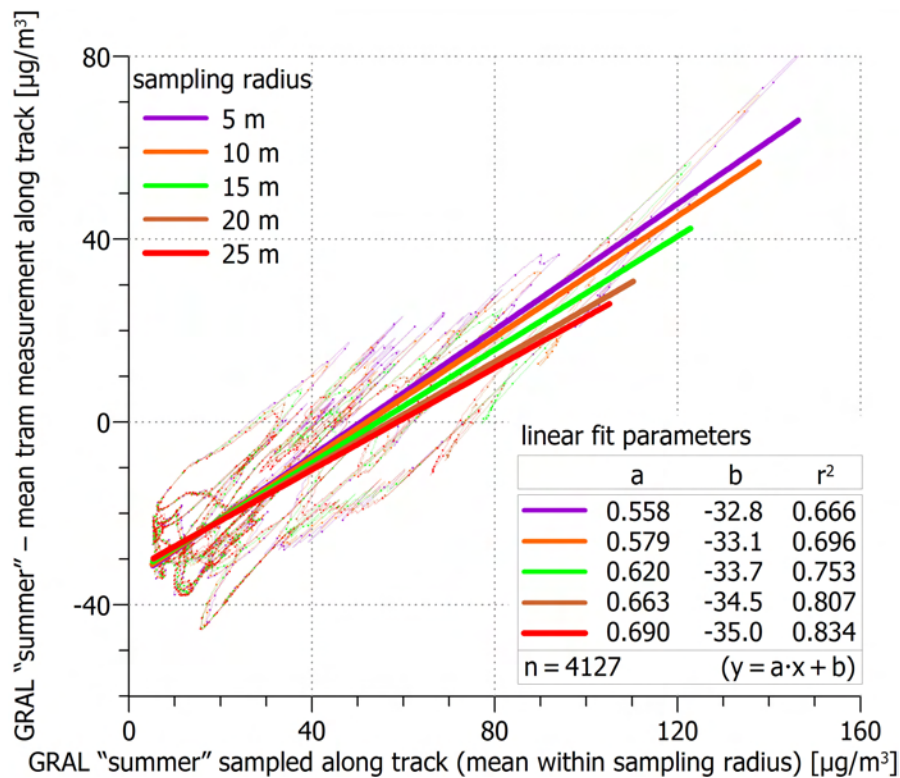


Figure 6.33: Correlation analysis of the GRAL “summer” results with measured average NO_x concentration in summer 2005. Compare figure 6.32

6.7.2 Comparison with the NABEL permanent station

In order to examine the accuracy of the GRAL results at places with low traffic densities, and, therefore, low emissions, mean values from the GRAL results were compared with the measurements at the NABEL permanent station. Figure 6.34 shows three places at and near the NABEL station. Values at these places were extracted from the GRAL grids using the mean of all grid points (excluding buildings) within a sampling radius of 25 m. Table 6.5 shows the values calculated from the measurements at the monitoring station along the values extracted from the GRAL grids. GRAL underestimates the concentrations significantly during all periods.

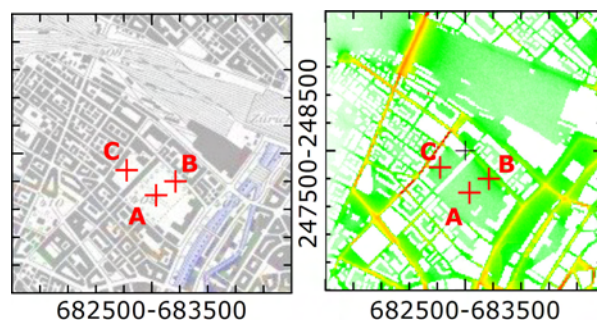


Figure 6.34: Location of the NABEL permanent station (A, compare figure 6.2) on a map (left) and in the GRAL “summer” grid (right). Place B is on the same open space near to the adjacent street (*Militärstrasse*) and place C is in the courtyard of the old barracks.

period	NABEL	A	B	C
annual mean	48.56	4.54	11.45	5.77
summer mean	30.12	4.15	10.37	5.38
winter mean	64.30	4.78	12.04	5.95
daytime mean	46.33	6.96	16.74	8.27
night-time mean	49.67	3.09	8.29	4.28

Table 6.5: Comparison of the GRAL results with the NABEL permanent station (in $\mu\text{g}/\text{m}^3$) for the GRAL results periods (see section 6.6.2). The GRAL measurements were sampled at the permanent station’s location and at two nearby places (see figure 6.34). The comparison shows large differences between simulated and measured concentrations.

6.7.3 Winter 2006

Figure 6.35 shows the comparison of the GRAL “winter” results with measurements made in winter 2005/06. The plot is analogous to figure 6.32. In winter 2005/06 tram measurements are available on 71 of 90 days. In the interpolated average of all measurements (black line and grey area) very little variation along the track can be seen. GRAL, however, shows distinct variations along the track with steep gradients. The offset to the measurements at the lowest GRAL values is larger than in the summer results. This is probably due to added emission from domestic heating in winter. The dashed black line is the 9–14 h average from the winter smog period analysis introduced in section 5.3.6. It features more pronounced variations along the track than the whole winter average. It doesn’t correlate with the GRAL curves (correlation factor of approximately 0.1).

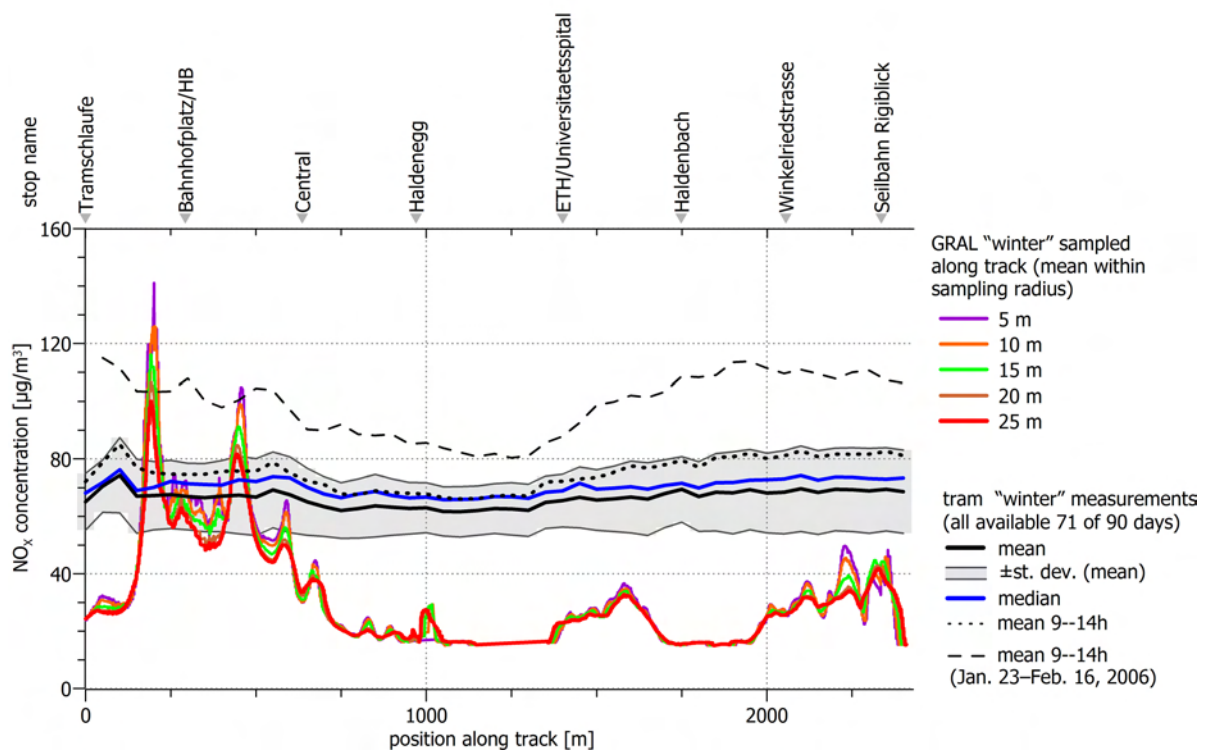


Figure 6.35: Comparison of measured average NO_x concentration along the tram line 10 in winter 2005/06 (see section 5.3.6) with the GRAL “winter” results.

* * *

7

Conclusions

In urban areas ambient air concentrations of air pollutants largely depend on emissions of road transport (internal combustion engines), domestic heating and local industry. Cities consist of different types of urban sites, such as busy places, pedestrian areas with low to no traffic and quarters of different site density. The variation of ambient air concentration is furthermore influenced by meteorological processes such as surface inversions, wind, precipitation and solar radiation. Elevated ambient air concentrations have a negative effect on life on Earth in general and on human health in particular. The high-resolution assessment of the temporal and spatial variability of ambient air concentration is, therefore, of great interest.

The overall goal of this research project was to assess the feasibility of dynamic monitoring of air pollutants in Zürich, Switzerland. The effort for developing and operating should be kept low while maintaining high spatial and temporal resolution and coverage. Means for precise and reliable positioning in an urban environment had to be found and implemented. Furthermore, it was specified to monitor air quality on-line and in real-time, and to investigate the correlation between traffic and ambient air concentration. The measurement system had to be designed and built, and suitable post-processing and analysis methods had to be developed.

A dedicated mobile and autonomous measurement system has been developed. A tram was found to be a suitable platform for mobile air pollution measurements in Zürich for several reasons. It operates on a regular basis throughout the day, which enables spatially and temporally extensive measurements. The chosen lines cross the city and represent the various urban characteristics described above. A fully autonomous measurement system was built into a single box of approximately $2.1 \cdot 0.4 \text{ m}^3$ volume and 150 kg weight. The box is mountable on the roof of a tram and, besides the mechanical connection consisting of four bolts, only needs to be connected to the tram's internal power supply. The measurement system powers up and shuts down automatically. It has an uninterruptible power supply, which includes a fail-safe backup shutdown procedure in case the control computer fails. Software was developed on a Linux basis which controls the instruments, logs the data and transmits measurements and status information in real-time using mobile communication technology.

Two measurement campaigns were carried out. The first campaign on tram line 11 lasted from March 7 to July 7, 2005 during which data was collected on 82 days. The second campaign lasted from December 5, 2005 to May 11, 2006. Data is available on 67 and

43 days on lines 10 and 6, respectively. During the campaigns an Internet application (web page), which visualised the measurements and the system performance in real-time, was publicly available. A special version of the visualisation and general information on air pollution was presented to the public during the 150 years ETH Zürich exhibition (“Welten des Wissens”) in April and June 2005.

GPS was chosen as a position and time reference. A suitable GPS receiver capable of providing precise positions in urban areas with pronounced street canyons of up to 20–30 m height was determined and used in the measurement system. The receiver’s Kalman filter engine was tuned to the expected movement of a vehicle running on city streets. This and the receiver’s optimisation for vehicle navigation provided precise measurements even under difficult conditions (high PDOP, few satellites) most of the time. The average ratio of GPS outages, either due to no availability or due to unsatisfactory accuracy (quality filtering), was between 2.2 and 3.5%. At certain sites along the track the outage ratio increased to 5–10%. There are few places where it is larger than 20%. On average 6.6–7.2 satellites were visible (median: 7) and an average PDOP value of 5.1–4.4 (median: 4.0–4.8) was observed. The PDOP decreased by approximately 0.35 per additional satellite in view. The minimal average PDOP at any point along the track is approximately 4.

A projective map-matching technique was developed to transform the measured position to the position of the tram on the track. 95% of the positions obtained from the GPS receiver were 6.7–7.4 or less metres off from the used geometry of the tram track. A technique was developed to generate accurate positions during periods of GPS outages, which in general lasted a few seconds up to a few dozens of seconds. The method relies on the track geometry and the characteristics of the movement of the tram.

The combination of the GPS measurements and the interpolation of missing positions enabled a precise and reliable referencing of the environmental measurements in space and time. A data post-processing procedure was developed which produces raw time series in a quasi tow-dimensional way. The ambient air concentrations of the pollutants (the “sensor readings”) are referenced by an along-track position (first dimension) and by the absolute time (second dimension). High spatial and temporal resolution of the measurements has been achieved and it has been shown that a single mobile measurement system adds a spatial component to ambient air concentration time series. The post-processed data has been analysed in various ways. The feasibility if dynamic monitoring has been shown.

Suitable data preparation and interpretation methods were identified to discuss the measurements as well as to compare them with data obtained from permanent air quality monitoring stations and results from a modelling study.

Daily mean values were derived from the tram measurements by integration in the time domain (and, therefore, neglecting the position dimension) and interpolation of missing (nocturnal) measurements. These values generally agree well with the daily means observed at the NABEL and UGZ permanent stations, two monitoring sites in the city of Zürich. The correlation factor for ozone measurements are between 0.403 and 0.444. In winter 2006, where high-quality measurements are available on 71 of 90 days, the daily means of NO and NO₂ correlate with factors of 0.612–0.700 and 0.795–0.808, respectively, with the mean values observed at the permanent stations. The particle measurements

also show a correlation, despite the fact that different quantities were measured (surface versus mass). This correlation factor is 0.403–0.428.

Monthly mean values were derived from the integrated daily means of the tram measurements. They agree very well with the monthly mean values observed at the permanent stations. The correlation factors are 0.909–0.954 for NO and NO₂, 0.822–0.840 for O₃ and 0.661–0.670 for particulates/PM₁₀. Furthermore, the analysis of the monthly mean values also reveals that the tram measurements show significantly higher NO values than what has been observed at the permanent stations (62% ±9% and 35% ±5% compared to the NABEL and UGZ sites, respectively). On the other hand, the tram's O₃ monthly means are 21% ±14% and 5% ±32% lower than the values observed at the NABEL and UGZ sites, respectively. Obviously the tram encounters most of the traffic (and therefore the primary pollutant NO). This is also witnessed by the lowest O₃ concentrations due to titration of O₃ by NO.

The correlation analysis of the daily and monthly mean values probably reflect, that the day to day (and to a larger extent the month to month) variability at the permanent stations and integrated along the tram track are basically determined by meteorology. The number of times limit values have been exceeded is a quantity the tram measurements cannot reproduce well. Even though single (daily or hourly) exceedances are clearly visible in the data, a permanent monitoring station is superior for long term assessments of air quality standards.

During the first campaign on tram line 11 the measurement system passed the UGZ permanent station within a distance of a few metres. A correlation of mobile measurements at this site with the UGZ measurements revealed an insignificant to poor correlation for NO/NO₂ and particulate matter. This is probably due to a large variability of primary pollutant concentrations in street canyons induced by turbulence. The secondary pollutant O₃ does not show these pronounced gradients and, hence, shows a significant correlation factor of >0.8.

A typical summer period consisting of a photochemical smog period followed by days with unsettled and stormy weather was analysed. The collocation method was used to obtain the spatial-temporal distribution of pollutant concentrations during the photochemical smog period, during adverse summer weather as well as for the combination of both. The main findings in this analysis are: A high variability of the ambient air concentration exists for all pollutants. It is more pronounced for the primary pollutants NO and particles, which are directly linked to emission sources. Since emission in summer and in a city mainly originate from road transport, busy places can be clearly seen in the data. The correlation of traffic and air pollution is best visible at two well-known busy places: Bürkliplatz/Bellevue and the main railway station. They show high concentrations of NO_x and particulates throughout the day. During the photochemical smog period the titration of O₃ by NO is clearly seen at these places. Furthermore, a meteorological effect, the dissolving of the inversion layer, can be seen in the data.

A distinct (winter) smog period in January/February 2006, during which the limit values for PM₁₀ and NO₂ were exceeded on several days, was measured on tram line 10. The analysis shows high concentrations of primary pollutants (NO and particles) as well as two sections of the tram track with concentrations above the average. They correlate with busy streets (main station and Universitäts-/Winterthurerstrasse). However, the variations along the track are less pronounced than in the “summer analysis” (see previous

paragraph). The accumulation phases were analysed as well. They reveal that the day-to-day difference in the mean (primary) pollutant concentration is uniform along the track. A comparison of the accumulation phases with measurements at the UGZ permanent station shows some agreement.

A state-of-the art dispersion model was used to produce seasonal and yearly mean distributions of NO_x for a 3.3 km^2 area in Zürich downtown. The area includes the main station, Bürkliplatz and the Bellevue place. All tram lines used in the measurement campaigns cross this area. The dispersion modelling involved the models NEMO (traffic and emissions), GRAMM (meteorology) and GRAL (dispersion) of the Institute of Internal Combustion Engines and Thermodynamics of the Graz University of Technology.

The NO_x measurements were compared with the results from the dispersion calculations, the “GRAL results”. The average concentration along the track for the combined (fair and adverse weather) and collocated summer measurements was compared with the GRAL “summer” results. The curves correlate well (correlation factor of 0.666-0.834) and the absolute values agree at busy places. However, the GRAL results show concentrations strongly correlated with the traffic and, therefore, rather low values at places without traffic. At these places the GRAL results are approximately $25\text{--}30 \mu\text{g}/\text{m}^3$ off compared to the measured values. The discrepancies are believed to mainly come from missing background concentrations in the model. Further reasons which could play a role might come from inaccuracies in the input data (traffic data, street network geometry, emission factors, buildings geometry or meteorological data).

A comparison of the GRAL results at and near the NABEL permanent station, which lies within the GRAL simulation area, show a similar effect. The NABEL station is characterised as an urban background station. It is located in a park surrounded by low to medium busy streets. The comparison of the NABEL summer mean and the GRAL summer mean at this site shows similar differences than mentioned in the previous paragraph.

The GRAL winter results were compared with the winter measurements. Here, GRAL also shows distinct variations along the tram track. The average concentration derived from the winter measurements (where 71 of 90 days of measurements are available) shows very little variation along the track. The discrepancies are larger than in the summer comparison. This is probably also due to the missing background concentration as well as additional emission sources not present in summer (mainly domestic heating).

This research project has proved the feasibility of dynamic monitoring of air pollutants in a city and its limitations have been identified. A single measurement system has provided measurements with high temporal and spatial resolution. Techniques based on GPS measurements and post-processing routines to provide a reliable and precise position and time reference for the environmental measurements have been developed and demonstrated. The analysis of spatio-temporal distribution of air quality and its modelling have clearly revealed that the research conducted in this thesis provides a solid basis for advanced interpretation of air quality.

* * *

Bibliography

- 2bTech (2001). *Ozone Monitor Model 202 Operation Manual (Rev. B)*. 2B Technologies, Inc., U.S.A.
- BAFU (2006a). *Datenbank Immissionswerte Schweiz*. Schweizerische Gesellschaft der Lufthygieniker (Cercl’Air) and BAFU, http://www.bafu.admin.ch/luft/luftbelastung/blick_zurueck/01694/index.html, May 29th 2007.
- BAFU (2006b). *Luftbelastung 2005 – Messresultate des nationalen Beobachtungsnetzes für Luftfremdstoffe*. Bundesamt für Umwelt (BAFU) & eidg. Materialprüfungs- und Forschungsanstalt (EMPA). <http://www.umwelt-schweiz.ch/luft/>.
- Batta, G., Firket, J., and Leclerc, E. (1933). *Les problèmes de pollution de l’atmosphère*. Thone, G., Liège.
- Bentz, F. (2005). GPS Sensoren zur genauen Navigation und Fahrtenkontrolle im öffentlichen Verkehr. Technical report, Geodesy and Geodynamics Lab, Institute for Geodesy and Photogrammetry, ETH Zürich.
- Bos, B., Lie, H. W., Jacobs, and Lilley, C. (1998). *Cascading Style Sheets, level 2 (CSS2) Specification*. W3C recommendations, the World Wide Web consortium, <http://www.w3.org/TR/1998/REC-CSS2-19980512>.
- BUWAL (2004). *Empfehlungen Immissionsmessungen von Luftfremdstoffen*. Bundesamt für Umwelt, Wald und Landschaft. <http://www.umwelt-schweiz.ch/buwal/de/fachgebiete>.
- Debian (2002). *Debian GNU/Linux (release 3), the universal operating system*. The Debian project, <http://www.debian.org>.
- DoD (1995a). *Global Positioning System, Standard Positioning Service, Signal Specification, 2nd ed.* Department of Defence, United States of America.
- DoD (1995b). *Navstar GPS user equipment introduction*. Department of Defence, United States of America.
- DoD (2001). *Global Positioning System, Standard Positioning Service, Performance Standard*. Department of Defence, United States of America.
- Firket, J. (1936). Fog along the meuse valley. *Trans. Faraday Soc.*, 32:192 – 1196.
- Forster, M. and Landtwing, S. (2004). GPS-Sensoren im öffentlichen Verkehr - Map Matching und Extrapolation zur Verbesserung der Positionszuverlässigkeit. Technical report, Geodesy and Geodynamics Lab, Institute for Geodesy and Photogrammetry, ETH Zürich.
- FSF (2002). *GNU Bash*. The Free Software Foundation, <http://www.gnu.org/software/gawk/>.

- FSF (2004). *The GNU Compiler Collection (release 3.4)*. The Free Software Foundation, <http://www.gnu.org/software/gcc/>.
- FSF (2006). *GNU awk*. The Free Software Foundation, <http://www.gnu.org/software/gawk/>.
- GNUFDL (2002). *The GNU Free Documentation License*. The Free Software Foundation. <http://www.fsf.org/licensing/licenses/fdl.html>.
- Haldane, J. (1931). Atmospheric pollution and fogs. *British Medical Journal*, 1:336–7.
- Heller, O. (2003). Low-Cost GPS im städtischen Raum. Technical report, Geodesy and Geodynamics Lab, Institute for Geodesy and Photogrammetry, ETH Zürich.
- Hipp, R. D. (2004). *SQLite SQL database engine*. <http://www.sqlite.org/>.
- Hofmann-Wellenhof, B., Lichtenegger, H., and Collins, J. (2001). *Global Positioning System (GPS) Theory and Practice*. Springer-Verlag, fifth, revised edition edition.
- Hueglin, C., Buchmann, B., and Weber, R. O. (2006). Long-term observation of real-world road traffic emission factors on a motorway in Switzerland. *Atmospheric Environment*, 40(20):3696–3709.
- Kehl, Ph. (2005). Internet Live-Visualisierung «Labor im Tram». <http://www.laborimtram.ethz.ch/live/>.
- Kehl, Ph. (2007). «Labor im Tram» Luftmessungen auf dem 2120. *Regenbogen*, 58(1):22–24. Personalzeitschrift der VBZ Züri-Linie.
- Kehl, Ph., Geiger, A., Kahle, H.-G., and Stähelin, J. (2006a). «Labor im Tram» Dynamische Umweltmessungen zur Erfassung der Luftverschmutzung in Zürich mit GPS als Positionssensor und Zeitreferenz. *Geomatik Schweiz*, 2006(11):602–607.
- Kehl, Ph., Stähelin, J., Braun, C., Kahle, H.-G., and Geiger, A. (2005). Monitoring of air pollutants in Zürich (Switzerland) using a streetcar as measuring platform. In Eichsleder, U.-P. D. H., editor, *14th Symposium Transport and Air Pollution*, volume 85/II, pages 53–58. Institute for Internal Combustion Engines and Thermodynamics, Graz University of Technology.
- Kehl, Ph., Stähelin, J., Geiger, A., and Kahle, H.-G. (2006b). Air quality monitoring in Zürich using a streetcar as measuring platform. In ProClim, editor, *7th Swiss Global Change Day*. ScNat. Poster.
- Kehl, Ph., Stähelin, J., Geiger, A., and Kahle, H.-G. (2007). Dynamic monitoring of air pollutants in Zürich (Switzerland) using a streetcar as measuring platform. In *Abstracts of the 6th International conference on Urban Air Quality*, volume 6, page 145. University of Hertfordshire. Full paper only on CD-ROM.
- Krzyzanowski, M., Kuna-Dibbert, B., and Schneider, J., editors (2005). *Health effects of transport-related air pollution*. World Health Organization, Regional Office for Europe.
- Le Hors, A., Raggett, D., and Jacobs, I. (1999). *HTML 4.01 Specification*. W3C recommendations, the World Wide Web consortium, <http://www.w3.org/TR/1999/REC-html401-19991224>.

- Leuenberger, C., Schletti, B., and C., B. (2004). Emissionen des Strassenverkehrs in der Stadt Zürich. Technical report, Umwelt und Gesundheitsschutz Zürich (Abteilung Umwelt).
- Logan, W. P. D. (1952). Mortality in the london fog incident. *Lancet*, 1:336–338.
- LQ1DC (2001). *Diffusion Charching Particle Sensor Type LQ 1-DC operating instructions*. Matter Engineering AG, Switzerland.
- LRV (1985). *Luftreinhalte-Verordnung*. Schweizerische Eidgenossenschaft. Stand am 23.08.2005, SR 814.318.142.1, http://www.admin.ch/ch/d/sr/c814_318_142_1.html.
- Matter, U., Siegmann, H., and Burtscher, H. (1999). Dynamic Field Measurement of Submicron Particles from Diesel Engines. *Environ. Sci. Technol.*, 33:1946–1952.
- Moritz, H. (1980). *Advanced physical geodesy*. Wichmann / Abacus Press.
- Nemery, B., Hoet, P. H., and Nemmar, A. (2001). The meuse valley fog of 1930: an air pollution disaster. *Lancet*, 357:704–708.
- Oetl, D. (2000). *Weiterentwicklung, Validierung und Anwendung eines Mesoskaligen Modells*. PhD thesis, Universitaet Graz, Naturwissenschaftliche Fakultae, Institut fuer Geographie und Raumforschung.
- Oetl, D., Almbauer, R., and Sturm, P. (2001a). A new method to estimate diffusion in stable, low wind speed conditions. *J. of Appl. Meteor.*, 40:259–268.
- Oetl, D., Almbauer, R., Sturm, P., Piringer, M., and Baumann, K. (2001b). Analysing the nocturnal wind field in the city of graz. *Atmos. Environ.*, 35:379–387.
- Oetl, D., Kukkonen, J., Almbauer, R., Sturm, P., Pohjola, M., and Härkönen, J. (2001c). Evaluation of a gaussian and a lagrangian model againmst a roadside data set, with emphasis on low wind speed conditions. *Atmos. Environ.*, 35:2123–2132.
- Oetl, D., Sturm, P. J., and Almbauer, R. (2004). Evaluation of GRAL for the pollutant dispersion from a city street tunnel portal at depressed elvel. *Environmental Modelling & Software*, 20:499–504.
- Oetl, D., Sturm, P. J., Bacher, M., Pretterhofer, G., and Almbauer, R. A. (2002). A simple model for the dispersion of pollutants from a road tunnel portal. *Atmos. Environ.*, 36:2943–2953.
- Oetl, D., Sturm, P. J., Pretterhofer, G., Bacher, M., Rodler, J., and Almbauer, R. (2003). Lagrangian dispersion modeling of vehicular emissions from a highway in complex terrain. *J. of the Air and Waste Management Association*, 5:5165–5175.
- Ordóñez, C., Brunner, D., Staehelin, J., Hadjinicolaou, P., Pyle, J. A., Jonas, M., Wernli, H., and Prévôt, A. S. H. (2007). Strong influence of lowermost stratospheric ozone on lower tropospheric background ozone changes over europe. *Geophysical Research Letters*, 34:L07805.
- Ordóñez, C., Mathis, H., Furger, M., Henne, S., Hüglin, C., Staehelin, J., and Prévôt, A. S. H. (2004). Changes of daily surface ozone maxima in Switzerland in all seasons from 1992 to 2002 and discussion of summer 2003. *Atmospheric Chemistry and Physics Discussions*, 4:7047–87.

- Oxford University Press (1999). *The Oxford American Dictionary of Current English*. Oxford Reference Online (April 25th 2007, <http://www.oxfordreference.com>).
- Oxford University Press (2006a). *The Concise Oxford English Dictionary, eleventh edition revised*. Oxford Reference Online (April 25th 2007, <http://www.oxfordreference.com>).
- Oxford University Press (2006b). *The Concise Oxford English Dictionary, eleventh edition revised*. Oxford Reference Online (May 22nd 2007, <http://www.oxfordreference.com>).
- Pandis, S., Baltensperger, U., Wolfenbarger, J., and Seinfeld, J. (1991). Inversion of Aerosol, Data from the Epiphaniometer. *Aerosol Sci.*, 22:417–428.
- PHP (2002). *The PHP hypertext preprocessor (release 4)*. The PHP Group, <http://www.php.net>.
- Rexeis, M. and Hausberger, S. (2005). Calculation of vehicle emissions in road networks with the model NEMO. In Eichsleider, U.-P. D. H., editor, *14th Symposium Transport and Air Pollution*, volume 85/II, pages 118–127. Institute for Internal Combustion Engines and Thermodynamics, Graz University of Technology.
- Rexeis, M., Hausberger, S., Zallinger, M., and Kurz., C. (2007). PHEM and NEMO: Tools for micro and meso-scale emission modelling. In *Abstracts of the 6th International conference on Urban Air Quality*, volume 6, page 109. University of Hertfordshire. Full paper only on CD-ROM.
- Rossinelli, S. (2006). GPS Sensoren zur genauen Navigation und Fahrtenkontrolle im öffentlichen Verkehr. Technical report, Geodesy and Geodynamics Lab, Institute for Geodesy and Photogrammetry, ETH Zürich.
- Schneebeli, H. and Wegmann, M. (2002). Dynamisches Verkehrs- und Umweltmonitoring. Technical report, Geodesy and Geodynamics Lab, Institute for Geodesy and Photogrammetry, ETH Zürich.
- Sorber, P. and Kehl, P. (2004). Konzept und Schaltplan für die Stromversorgung des «Labor im Tram». Technical report, Geodesy and Geodynamics Lab, Institute for Geodesy and Photogrammetry, ETH Zürich. interner Bericht.
- Staehelin, J. (1999). Einführung in die Atmosphärenchemie. Technical report, IAC. Vorlesungsskript.
- Staehelin, J. (2003). Atmosphärenchemie quo vadis? *GAiA*, 12(3):181–6.
- Staehelin, J., Prevot, A., and Barnes, J. (2000). *Photochemie der Troposphäre, Handbuch der Umweltveränderungen und Ökotoxikologie, Band IA: Atmosphäre*. Guderian, R. (ed.), Springer Verlag.
- Swisstopo (2001a). *Approximate solution for the transformation CH1903–WGS84*. Federal Office of Topography. <http://www.swisstopo.ch/en/basics/geo>.
- Swisstopo (2001b). *Formulas and constants for the calculation of the Swiss conformal cylindrical projection and for the transformation between coordinate systems*. Federal Office of Topography. <http://www.swisstopo.ch/en/basics/geo>.

- Swisstopo (2005a). *DHM25: Das digitale Höhenmodell der Schweiz, Produktinformation*. Bundesamt für Landestopographie. <http://www.swisstopo.ch>.
- Swisstopo (2005b). *VECTOR: Das digitale Landschaftsmodell der Schweiz, Produktinformation*. Bundesamt für Landestopographie. <http://www.swisstopo.ch>.
- TEI (2000). *Model 42c Trace Level Chemiluminescence NO-NO₂-NO_x Analyzer Instruction Manual*. Thermo Environmental Instruments Inc., Massachusetts, U.S.A.
- Troen, I. and Petersen, E. L. (1991). *European Wind Atlas*. Risoe National Laboratory, Risoe, Denmark. ISBN 87-550-1482-8.
- UBA/BUWAL (2004). *Handbook Emission Factors for Road Transport (HBEFA) version 2.1*. Umwelt Bundesamt Berlin (UBA) and Bundesamt für Umwelt, Wald und Landschaft (BUWAL). CD-ROM.
- USG (1983). *Bundesgesetz über den Umweltschutz (Umweltschutzgesetz)*. Schweizerische Eidgenossenschaft. Stand am 4. Juli 2006, http://www.admin.ch/ch/d/sr/c814_01.html.
- Vogel, M. and Nigg, T. (2002). *ANTARISTM EvalKit GPS Receiver Evaluation Kit, User's Guide*. document #GPS.G3-EK-02003, uBlox AG, Switzerland, <http://www.u-blox.com>.
- Warmerdam, F., Anderson, C., Giacomelli, A., et al. (2002). *The shapefile C library*. <http://shapelib.maptools.org>.
- WHO, editor (2004). *Health aspects of air pollution*. World Health Organization, Regional Office for Europe.
- Zogg, J.-M. (2002). *GPS Basics, Introduction to the System, Application overview*. uBlox AG, Switzerland, http://telecom.tlab.ch/~zogg/Dateien/GPS_basics_u_blox_en.pdf.
- Zogg, J.-M. and Amman, D. (2001). *The GPS dictionary, Acronyms, abbreviations and glossary related to GPS*. uBlox AG, Switzerland, http://telecom.tlab.ch/~zogg/Dateien/the_gps_dictionary.pdf.

